OFDM Based T-transform for Wireless Communication Networks

by

Mohammed Shweesh Ahmed

A thesis submitted to the School of Electrical Electronic & Computer Engineering

in partial fulfilment of the requirements for the degree of

Doctor of Philosophy

Faculty of Science, Agriculture and Engineering

Newcastle University, June 2012

Abstract

The prominent features associated with orthogonal frequency division multiplexing (OFDM) have been exploited in the area of high-speed communication networks. However, OFDM is prone to impairments such as frequency selective fading channel, high peak-to-average power ratio (PAPR) and heavy-tailed distributed impulsive noise, all of which can have negative impacts on its performance. These issues have received a great deal of attention in recent research.

To compensate for these transmission impairments, a T-OFDM based system is introduced using a low computational complexity T-transform that combines the Walsh-Hadamard transform (WHT) and the discrete Fourier transform (DFT) into a single fast orthonormal unitary transform. The key contribution in this thesis is on the use of the T-transform along with three novel receiver designs. Additionally, new theoretical bit error rate (BER) formulae for the T-OFDM system are derived over communications channels using zero forcing (ZF) and minimum mean square error (MMSE) detectors, that are validated via simulation and shown to have close performance with the obtained performance results. It has been found that the T-OFDM outperformed the conventional OFDM based systems in the investigated channel models by achieving a signal-to-noise ratio (SNR) gain range of between 9dB and 16dB measured at 10^{-4} BER.

In addition, the sparsity and block diagonal structure of the T-transform, along with its lower summation processes are exploited in this study to reduce the superposition of the subcarriers, leading to reduce the peak of the transmitted signals by a range of 0.75 to 1.2 dB with preserved average power. Furthermore, these attractive features of T-transform are employed with the conventional selective mapping (SLM) and partial transmitted sequences (PTS) schemes to propose three low cost novel techniques; T-SLM, T-PTS-I, and T-PTS-II. Compared to the conventional schemes, the T-SLM and T-PTS-I schemes have achieved a considerable reduction in both computational complexity and in PAPR, further increasing multipath resilience, even in the presence of high power amplifier (HPA). Whereas using the T-PTS-II scheme, the complexity ratio has been significantly reduced by approximately 80%, as well as reducing the SI bits further by two, with negligible PAPR degradation.

Moreover, the effect of the independent sections of T-transform on the performance of T-OFDM system over the impulsive channel is addressed in this work, by deriving a new theoretical BER formula over such a transmission media. Furthermore, two novel

schemes WHT-MI-OFDM and WHT-MI-OFDM incorporating nonlinear blanking, both of which utilise the WHT and a matrix interleaver (MI) with the OFDM system, are proposed to suppress the deleterious effects of a severe impulsive noise burst on the T-OFDM system performance. Comparing with the traditional MI-OFDM system, the proposed schemes are much more robust to disturbances arising from the impulsive channel.

Acknowledgements

Firstly, I thank **ALLAH** for all the things that have happened to me in my life. It would be selfish not to acknowledge the people who have helped me in numerous ways. First of all my supervisor Prof. Said Boussakta who has encouraged, guided and supported me to complete this project. He has always taught me to aim for the best. I would like to thank my second and third supervisors, Prof. Bayan Sharif and Dr. Charalampos Tsimenidis from whom I learnt many things either directly or indirectly by sharing their great knowledge about practical systems. These people have gone through the pain of answering my questions. For all their valuable comments, hints, and suggestions that inspired this work remarkable I wish to express my appreciation. I have grown to respect them; not only for their great intuition and intellect, but also, for the dedication they show to their students. I would like to thank Mrs. Gillian Webber for her support and help.

My deep thanks to my sponsor (Ministry of Higher Education and Scientific Research/IRAQ) for offering me this great opportunity. I also would like to thank Iraqi Cultural Attache/London for the appreciated support and help throughout my PhD study.

My gratitude is also extended to the School of Electrical, Electronic and Computer Engineering for giving me the opportunity to undertake this memorable learning experience. I would also like to thank my friends Salah, Muayad, Moneer, Ebrahim, Ahmed, Omer, Abdulrahan, Sabah, Emad, Chintan, Ammar and many others for being a lively and entertaining part of the journey.

My special gratitude is due to my father, my mother for always being there when I needed them most. They deserve far more credit than I can ever give them. I could not imagine the level that I have reached without their warm-heartedness, support and help. Also, I dedicate this research to my brothers, and my sisters, who have supported me throughout my life. Finally, I owe my thanks to my wife and my children. They have lost a lot due to my research abroad. Without their encouragement and understanding it would have been impossible for me to finish this work.

Mohammed Shweesh Ahmed
June 2012

Declaration

I declare that this thesis is my own work and it has not been previously submitted, either by me or by anyone else, for a degree or diploma at any educational institute, school or university. To the best of my knowledge, this thesis does not contain any previously published work, except where another person's work used has been cited and included in the list of references.

Mohammed Shweesh Ahmed
June 2012

Contents

List of Tables

List of Figures

List of Abbreviations and Symbols

List of Abbreviations

16-QAM	Sixteen-Quadrature Amplitude Modulation
3G LTE	Third Generation Long Term Evolution
ACE	Active Constellation Extension
ADSL	Asymmetric Digital Subscriber Lines
AM	Amplitude Modulation
AWGN	Additive White Gaussian Noise
BCH	BoseChaudhuri-Hocquenghe)
BER	Bit Error Rate
CCRR	Computational Complexity Reduction Ratio
CIR	Channel Impulse Response
CP	Cyclic Prefix
CSI	Channel State Information

DAB	Digital Audio Broadcasting
DAC	Digital-to-Analog Converter
DFE	Discrete Fourier Transform
DMT	Discrete Multitone
DSI	Dummy Sequence Iteration
DVB	Digital Video Broadcasting
DVB-S2	Second Generation Digital Video Broadcasting and Satellite
DVB-T	Digital Video Broadcasting-Terrestrial
FEC	Forward Error Correction
FFT	Fast Fourier Transform
FLO	Forward Link Only
FS	Frequency Selective
FTT	Forward T-Transform
HD	Heavy distribution
HDSL	High-bit-rate Digital Subscriber Lines
HDTV-TB	High-Definition Television Terrestrial Broadcasting
HIPERLAN/2	High Performance LAN type 2
HPA	High Power Amplifier
ICI	Inter-Carrier Interference
IDFE	Inverse Discrete Fourier Transform
IEEE	Institute of Electrical and Electronics Engineers
IFFT	Inverse Fast Fourier Transform

ISI	Intersymbol Interference
ITT	Inverse T-Transform
ITU	International Telecommunication Union
LAN	Local Area Network
LDPC	Low-Density Parity-Check
M-PSK	M-array Phase Shift Keying
M-QAM	M-array Quadrature Amplitude Modulation
MC	Multicarriers
MC-CDMA	Multi-Carrier Code Division Multiple Access
MD	Medium distribution
MI	Matrix Interleaver
MIMO	Multiple-Input and Multiple-Output
ML	Maximum Likelihood
MMSE	Minimum Mean Square Error
MSE	Mean Square Error
OFDM	Orthogonal Frequency Division Multiplexing
PAPR	Peak-to-Average Power Ratio
PDF	probability density function
PIC	Parallel Interference Cancellation
PM	Phase Modulation
PTS	Partial Transmitted Sequence
QPSK	Quadrature Phase Shift Keying

SC	Single Carriers
SC	Subcarrier
SI	Side Information
SIC	Successive Interference Cancellation
SLA	Soft Limiter Amplifier
SLM	Selective Mapping
SNR	Signal-to-Noise Ratio
SSPA	Solid State Power Amplifier
STC	Space Time Coding
T	T-transform
TR	Tone Reservation
TWTA	Travelling-Wave Tube Amplifier
VDSL	Very-high-speed Digital Subscriber Lines
WD	Weak distribution
WHT	Walsh-Hadamard Transform
WiMAX	Worldwide interoperability for Microwave Access
WLANs	Wireless Local Area Networks
ZF	Zero Forcing

List of Symbols

λ	Received SNR
$(.)^H$	Hermitian operator

$(.)^T$	Transpose operation
$(.)^*$	Complex conjugate operation
$*$	Linear convolution operation
β	Impulsive noise burst
$\circledast$	Circular convolution operation
ϵ	The ratio of $\mathbf{\Omega}$ over $\mathbf{Q}$
η	CCRR value
Γ	The probability of $\zeta_n = 1$
γ	The number of samples hit by each individual burst
$\hat{\Gamma}$	The probability of $\zeta_n = 0$
$\hat{\mathbf{A}}'''$ and $\hat{\mathbf{B}}'''$	Sub-matrices of the matrix $\hat{\mathbf{B}}'$
$\hat{\mathbf{A}}'$ and $\hat{\mathbf{A}}''$	Sub-matrices of the matrix $\hat{\mathbf{A}}$
$\hat{\mathbf{A}}$ and $\hat{\mathbf{B}}$	Sub-matrices of the IDFT matrix $\hat{\mathbf{F}}$
$\hat{\mathbf{B}}'$ and $\hat{\mathbf{B}}''$	Sub-matrices of the matrix $\hat{\mathbf{B}}$
$\hat{\mathbf{C}}'''$ and $\hat{\mathbf{E}}'''$	Sub-matrices of the matrix $\hat{\mathbf{B}}''$
$\hat{\mathbf{C}}$ and $\hat{\mathbf{C}}'$	Sub-matrices of the matrix $\hat{\mathbf{A}}'$
$\hat{\mathbf{E}}$ and $\hat{\mathbf{E}}'$	Sub-matrices of the matrix $\hat{\mathbf{A}}''$
$\hat{\mathbf{F}}$ or $\mathbf{F}^H$	IDFT matrix
$\hat{\mathbf{R}}$	Received signal in Frequency-domain
$\hat{\mathbf{T}}$	ITT matrix
$\hat{\mathbf{X}}'$	The output of the interleaver on the transmitter side
$\hat{\mathbf{X}}$	Equalised data sequence

$\hat{a}^{'}$, $\hat{b}^{'}$, $\hat{c}^{'}$, $\hat{d}^{'}$, $\hat{e}^{'}$, $\hat{f}^{'}$, $\hat{g}^{'}$, $\hat{h}^{'}$, $\hat{l}^{'}$, $\hat{m}^{'}$, $\hat{n}^{'}$, $\hat{o}^{'}$, $\hat{p}^{'}$ and $\hat{q}^{'}$	Elements of ITT matrix $\hat{\mathbf{T}}$
$\hat{d}$	The resultant data sequence of the PTS scheme in the time-domain
$\hat{L}$	Number of the channel paths
$\hat{m}$	Data index in Walsh-domain
$\hat{m}_{\hat{r}}$	Bit representation of index $\hat{m}$
$\hat{w}^{n}$	The twiddle factor of the T-transform
$\hat{y}_{n}$	The output of the nonlinear blanking scheme on the receiver side
$\Im\{.\}$	Imaginary part of complex value
λ_0	SNR of transmission
$\hat{\mathbf{Q}}$	Equaliser sequence in the Walsh-domain
$\hat{\mathbf{q}}$	The disjoint subblocks of the PTS scheme
$\hat{\mathbf{S}}$	The blanking threshold
$\mathbf{\Psi}$	Total noise vector, i.e. AWGN plus impulsive noise
$\mathbf{A}$ and $\mathbf{B}$	Sub-matrices of the FFT matrix $\mathbf{F}$
$\mathbf{A}^{'''}$ and $\mathbf{B}^{'''}$	Sub-matrices of the matrix $\mathbf{B}^{'}$
$\mathbf{A}^{'}$ and $\mathbf{A}^{''}$	Sub-matrices of the matrix $\mathbf{A}$
$\mathbf{B}^{'}$ and $\mathbf{B}^{''}$	Sub-matrices of the matrix $\mathbf{B}$
$\mathbf{C}$ and $\mathbf{C}^{'}$	Sub-matrices of the matrix $\mathbf{A}^{'}$
$\mathbf{C}^{'''}$ and $\mathbf{E}^{'''}$	Sub-matrices of the matrix $\mathbf{B}^{''}$
$\mathbf{D}$	Circulant channel matrix
$\mathbf{d}^{(u)}$	The uth disjoint subblocks in SLM and PTS schemes
$\mathbf{E}$ and $\mathbf{E}^{'}$	Sub-matrices of the matrix $\mathbf{A}^{''}$

$\mathbf{F}$	DFT matrix
$\mathbf{G}$	A new normalized symmetrical matrix used with the proposed T-PTS-I scheme
$\mathbf{h}$	Vector of the CIR
$\mathbf{I}$	Identity matrix
$\mathbf{P}$	A new matrix derived from the WHT matrix
$\mathbf{Q}$	Equaliser diagonal matrix
$\mathbf{q}$	The oversampled vector of the T-SLM scheme
$\mathbf{R}$	Received data sequence in frequency-domain
$\mathbf{r}$	Received data sequence in time-domain
$\mathbf{s}$	Phase rotation vector of the SLM scheme
$\mathbf{T}$	FTT matrix
$\mathbf{v}$	The phase optimised vector in SLM and PTS schemes
$\mathbf{W}$	WHT matrix
$\mathbf{X}$	Discrete frequency-domain sequence
$\mathbf{x}$	Discrete time-domain sequence
$\mathbf{X}'$	The output of the WHT on the transmitter side
$\mathbf{Y}$	Output signals of the FTT block
$\mathbf{y}$	The output of WHT with SLM scheme
$\mathbf{Z}$	Frequency-domain sequence of the AWGN
$\mathbf{z}$	Time-domain sequence of the AWGN
μ	The ratio of the man-made noise variance, σ_v^2, over the AWGN variance, σ_z^2

Ω_k	The quantity that equivalent to $Q_k H_k$
$\oplus$	Bit-by-bit modulo 2 sum of the integers
$\otimes$	The tensor or Kronecker product operation
$\overline{\otimes}$	Dyadic convolution operation
ϕ_m	Phase of the signal
$\Re\{.\}$	Real part of complex value
ρ	Gaussian noise in Walsh-domain
σ_X^2	Desired signal average power
σ_Z^2	White Gaussian noise average power
σ_φ^2	Impulsive noise average power
X1 and **X2**	Random variable in frequency-domain
x1 and **x2**	Random variable in time-domain
ε	The average number of nearest neighbour signal points
φ	Impulsive noise sequence
ζ	A Bernoulli process
ζ_{ave}	The average power of the transmitted signal
$\zeta_{\max}$	The peak power of the discrete-time signal
a	The quantity that equivalent to $\frac{1}{N}\sum_{k=0}^{N-1}\Omega_k$
B''	Alternative representations for the symbol with the proposed T-PTS-II scheme
B'	Alternative representations for the symbol in the PTS scheme
$b^{(u)}$	Weighting phase factors of the PTS scheme
C_A	The number of complex additions

C_M	The number of complex multiplications
$D^{'}$	The complexity required for PAPR calculation and phase optimisation processes in the PTS scheme
e	MSE parameter
$E[.]$	Expectation operator
f	Real additions in each real multiplication
h_l	CIR of the lth path
i	Frame index
i_1 and i_2	The input data to each individual butterfly of the T-transform
J	An integer valuer
k	Data index in frequency-domain
$k_{\hat{r}}$	Bit representation of index k
L	Oversampling factor
l	Channel path index
M	Number of constellation points
m	Number of information bits carried by a constellation
$max\{.\}$	Maximum value of elements
N	Number of the subcarriers
n	Data index in time-domain
N_g	CP length
N_t	Total length of symbol, i.e. $N_t = N + N_g$
o_1 and o_2	The output data from each individual butterfly of the T-transform
p	HPA smoothness parameter

$p(x(t))$	The output of the HPA
P_e	Probability of error
$Q(x)$	The Q-function of variable x
$Q_{1,1}$	Equaliser elements at row 1 and column 1
R_{A}	The number of real additions
R_{M}	The number of real multiplications
R_{Total}	Total real additions
S_0, S_1, S_2, and S_3	Sections of the 16-points T-transform
S_{HPA}	The threshold of clipping of the HPA
t	Time instance
U	The number of phase rotation vectors
$U^{'}$	Effective disjoint subblocks in the proposed T-PTS-II scheme
w	FFT twiddle factor base
$a^{'}$, $b^{'}$, $c^{'}$, $d^{'}$, $e^{'}$, $f^{'}$, $g^{'}$, $h^{'}$, $l^{'}$, $m^{'}$, $n^{'}$, $o^{'}$, $p^{'}$ and $q^{'}$	Elements of FTT matrix $\mathbf{T}$

CHAPTER 1

Introduction

Due to its attractive features, broadband (wideband) technology is widely employed efficiently in the modern technologies of the wireless network industry instead of narrowband technology [4], [5]. The key concept of broadband is the utilisation of a wide range of frequencies to transmit a signal. The core of the orthogonal frequency division multiplexing (OFDM) system is based on this technology. The basic principle of OFDM is to split a high data rate stream into a number of lower rate streams that are transmitted simultaneously over a number of subbands or subcarriers occupying high spectral efficiency [6]. In this chapter the a brief historical overview and the basic principal of OFDM system are presented. Moreover, some applications that has been utilised OFDM as the transmission technique in their physical layer are illustrated.

1.1 A Brief Historical Overview of OFDM

At the end of the fifth decade of the twentieth century, the demand for fast and reliable transmission techniques for military communications became crucial. Therefore, this led to the conception of OFDM as a multicarrier transmission technique for this purpose [7], [8]. In multicarrier transmission, a single data stream is transmitted over a number of lower-rate subcarriers (SCs). One of the main reasons for using OFDM is to increase robustness against frequency-selective fading or narrowband interference. In a single-carrier system, a single fade or interferer can cause the entire link to fail; but in a multicarrier system only a small percentage of the SCs will be affected. However, high implementation complexity was the main limitation of widely using OFDM. The first employment of discrete Fourier transform (DFT) as a multicarrier modulator and demodulator was done by Weinstein and Ebert in 1971 [9]. During the start of the following decade the performance of OFDM was studied for high-speed modems, digital mobile communications and high-density recording. Additionally, the OFDM technique has been exploited in the wideband data communications over mobile radio frequency modulation (FM) channels, digital audio broadcasting (DAB) and high-definition television terrestrial broadcasting (HDTV-TB) [6]. Furthermore, due to the development of modern networks (wired or wireless), OFDM became popular for practical applications. Due to its spectral efficiency and robustness against frequency-selective multipath fading propagation, OFDM has been adopted by various high data rate wireless communication systems, including wireless local area network (WLAN) (802.11a/g/n) in the United States of America (USA); high performance

LAN type 2 (HIPERLAN/2) in Europe; worldwide interoperability for microwave access (WiMAX); flash-OFDM; third generation long term evolution (3G LTE) and fourth generation (4G) cellular systems [10].

In addition, in wired technologies including the asymmetric digital subscriber line (ADSL), high bit rate DSL (HDSL) and very high speed DSL (VDSL), OFDM based on discrete multitone (DMT) terminology is utilised as an excellent method to deliver high speed data to customers at a low cost [11] [12].

1.2 Basics of OFDM

Multicarriers (MC) modulation is the key concept of OFDM techniques; whereby high bit-rate data is transmitted by dividing the stream into several parallel lower bit-rate streams and modulating each of these data streams on separate subcarriers [10]. The entire allocated channel is simultaneously occupied through the transmission of carriers. Due to the parallel transmission of several symbols, the duration of the symbol is increased leading to a reduction in the effects of intersymbol interference (ISI) arising from the dispersal of multipath propagation. Moreover, OFDM essentially converts a frequency selective channel into a number of subchannels that exhibit approximately flat fading. In simple terms, the symbol duration is made longer than the delay spread of the channel. In addition, the spacing between adjacent subcarriers is adjusted as an integer multiples of the inverse of symbol duration of the parallel bit streams. Thus, they are all orthogonal to one another within the entire symbol duration. This technical issue can be provided with OFDM owing to the use of an inverse fast Fourier transform (IFFT) on the transmitter side of such a system. The size of the IFFT should be chosen carefully where the OFDM based large IFFT size is more robust to multipath dispersion owing to an increase in the symbol period; albeit it will be more susceptible to the frequency offset further to be a great computational cost. Therefore, a balance between computational complexity and performance should be considered.

Moreover, the ISI can be mitigated in the OFDM based systems by appending the transmitted symbols with a cyclic prefix (CP). In order to overcome the ISI almost completely, the cyclic prefix interval should be larger or equal to the maximum path delay.

1.3 OFDM-based Wireless Network Overview

The prominent features of the OFDM system, such as the high data rate, relatively simple receiver design and spectral efficiency have led such a system to be a promising candidate in the area of modern networks technologies. Employing OFDM with various deployed applications began to change the landscape of wireless communications as listed below.

1.3.1 Digital broadcasting

Broadcasting was firstly employed in television programs to distribute analog wireless signals. Subsequently, digital video broadcasting (DVB) was established as a common international standard for the move from analog to digital broadcasting. Thereafter, in May 1998, digital video broadcasting-terrestrial (DVB-T) was investigated for mobile applications. The OFDM technique provides the requirements of DVB-T services, such as a high data rate, high spectral efficiency, and simultaneous broadcasting of low rates. Thus, DVB-T services have employed coded OFDM combined with quadrature phase shift keying (QPSK), sixteen-quadrature amplitude modulation (16-QAM) and 64-QAM [6].

1.3.2 WLANs

At the present time, the WLANs are still the most popular global broadband wireless network. By using the protocols of such networks, digital networking can be provided to almost any device at high speeds and inexpensive connection hardware. Moreover, the wireless communications among several devices with mobility and flexibility is introduced by the IEEE standard for WLANs (IEEE 802.11). Due to the power limitation, WLANs are mostly limited to homes and office buildings. In order to provide networks that deliver high data rates, the OFDM technique is utilised in two WLAN standards including IEEE 802.11a and IEEE 802.11g [13].

1.3.3 WiMAX

WiMAX is a promising candidate to bring wireless and internet revolutions to portable devices across the globe. There are two versions of WiMAX that employ the OFDM

physical layer including fixed and mobile, which are based on IEEE 802.16 and IEEE 802.16e standards, respectively. The size of the FFT-based OFDM is different in each version, where 256-points FFT is utilised with the fixed WiMAX; whereas with mobile WiMAX the FFT size can vary from 128 to 2048 [10].

1.4 Aims and Objectives

Recently, great efforts have accomplished by researchers to reduce the negative ramifications of the impairments associated with the OFDM system. Most of the proposed systems have been able to achieve considerable improvements, albeit with the expense of one or more of either an extra cost requirement, data rate losses, power waste or bit error rate (BER) degradation.

The aim of this thesis is to compensate for these transmission impairments by introducing a T-OFDM based system using a low computational complexity T-transform which was developed by Boussakta [2], [3] to combine the Walsh-Hadamard transform (WHT) and the discrete Fourier transform (DFT) into a single fast orthonormal unitary transform. Regarding BER performance improvement, various techniques have been proposed to improve the OFDM system's BER performance over multipath propagation, such as channel coding, adaptive systems, and diversity schemes. Although, these techniques have achieved a considerable BER improvement, albeit with the expense of one or more of high computational complexity, and data rate losses. In this study, the T-OFDM along with three novel receiver designs are proposed, as in Chapter 4, to achieve an outstanding SNR gain with lower complexity requirement compared to the conventional OFDM system. Moreover, the significant BER performance of T-OFDM over that of the conventional OFDM system is supported by deriving new theoretical formulae for the BER of such a system over various communications channels. This derivation is achieved over three channel models, including the additive white Gaussian noise (AWGN), flat fading channel and quasi-static frequency selective fading channel, using zero forcing (ZF) and minimum mean square error (MMSE) equalisers.

Furthermore, the reduction of the high PAPR inherited with the transmitted signal of OFDM systems has received a great deal of attention in recent research. Basically, two categories of PAPR reduction techniques; distortionless techniques and techniques with distortion; have been devised to eliminate the deleterious effect of

high PAPR in OFDM signals, albeit with the expense of high computational complexity, data rate losses and BER performance degradation. As in Chapter 5, this study investigates the ability of the proposed T-OFDM system to produce signals with lower peak power owing to the lower superposition of T-transform. This power reduction is obtained with the preservation of average power and data rate (no data rate losses). Furthermore, based on employing the prominent features of T-transform with the conventional selective mapping (SLM) and partial transmitted sequences (PTS) schemes, three low cost novel techniques; T-SLM, T-PTS-I and T-PTS-II are proposed in this work.

Additionally, owing to the use of FFT on the receiver side further to a long duration, OFDM system providing robustness against weak impulsive noise by spreading impulsive noise energy among transmitted OFDM subcarriers. Nevertheless, this advantage becomes a disadvantage if the impulsive noise energy exceeds a certain threshold. Therefore, recent studies have employed considerable efforts to analyse and mitigate the impact of this phenomenon on OFDM performance. As will be introduced in Chapter 6, the vulnerability of the T-OFDM system performance to impulsive channels is assessed in this work. This can be acquired by deriving a new theoretical BER formula for the T-OFDM system over the disturbance of such a channel model. Furthermore, the beneficial features of WHT and a MI are utilised with the OFDM system to introduce two novel schemes; WHT-MI-OFDM and WHT-MI-OFDM incorporating nonlinear blanking to suppress the negative ramifications of the impulsive channel.

1.5 Publications Arising From This Research

1. **M. Sh. Ahmed** and S. Boussakta and B. Sharif and C. C. Tsimenidis, "OFDM based on low complexity transform to increase multipath resilience and reduce PAPR," IEEE Trans. on Signal Processing, vol. 59, no. 12, pp. 5994-6007, Dec., 2011.

2. **M. Sh. Ahmed** and S. Boussakta and B. Sharif and C. C. Tsimenidis, "OFDM based new transform with BER performance improvement across multipath Transmission," in Proc. IEEE Inter. Conf. on Comm. (ICC), June, 2010, pp. 1-5.

1.6 Outline of the Thesis

The thesis is organised as follows:

Chapter 2 outlines the uncoded OFDM system block diagram further to clarify its three main parts: the transmitter, channel and receiver. In addition, the main merits and drawbacks of the OFDM system are also addressed in this chapter.

Chapter 3 presents the structure of DFT and WHT further to their complexity calculations. Furthermore, the T-transform which combines the WHT and the DFT into a single fast orthonormal unitary transform is studied. Based on the sparsity feature of the T-transform, the fast implementation of such transform is presented in this chapter along with its complexity calculation, which is compared with other related transforms.

Chapter 4 introduces fast implementation of the T-transform with the T-OFDM system along with three novel receiver designs. Additionally, new theoretical BER formulae for the T-OFDM system are derived over communication channels using ZF and MMSE criteria of equalisation. Extensive simulation results confirmed the theoretical analysis are also demonstrated in this chapter.

Chapter 5 quantifies the ability of T-OFDM to reduce the PAPR. Moreover, T-transform is utilised with three novel schemes; T-SLM, T-PTS-I and T-PTS-II to achieve a considerable PAPR reduction with lower computational complexity requirements further to a significant BER improvement, even in the presence of a high power amplifier (HPA).

Chapter 6 assesses the performance of T-OFDM system over the impulsive channel by deriving a new theoretical BER formula of such a system. Furthermore, two novel efficient schemes WHT-MI-OFDM and WHT-MI-OFDM incorporating nonlinear blanking are proposed in this chapter.

Finally, conclusions are drawn in Chapter 7 and the thesis concludes with by describing potential future work.

CHAPTER 2

Background and Methodology

The primary purpose of this chapter is to describe the OFDM system. The overall block diagram of such a system is explained by clarifying transmitter, channel and receiver of this system. In addition, the main strengths and weaknesses of OFDM systems are summarised.

2.1 OFDM Technology

In single carrier transmission systems, a single carrier is utilised to transmit symbols sequentially. Thereby, the entire available bandwidth will be occupied and adaptive equalisation techniques are required to compensate for the distortion arising from the multipath propagation [14]. In high data rate applications, the symbol period becomes shorter which leads to an increase in the number of adjacent faded symbols and therefore the processes of adaptive equalisation become more difficult. Therefore, the transmission of a single data stream over a number of lower rate subcarriers can mitigate the effect of multipath transmission.

Thus, utilising the DFT as a multicarrier modulator or multiplexer in OFDM systems leads to breaking the wideband signal into many narrowband signals (subcarriers). Hence, the overlapping between adjacent subcarriers increases the spectral efficiency of OFDM systems. Moreover, in order to reconstruct the transmitted signals perfectly at the receiver, the ISI caused by the time dispersion of the multipath fading channel should be eliminated. For the purpose of eliminating the ISI, the cyclic prefix (CP) is added by copying the last part of the OFDM symbol and appending it as a guard interval at the beginning of the OFDM symbol. In order to virtually eliminate ISI, the guard interval should be larger or equal to the maximum path delay of the channel. Moreover, due to the cyclic prefix, the OFDM symbol is cyclically extended into the guard interval. The transmitted signal appears periodic and the effect of the time dispersion becomes equivalent to a cyclic convolution. Moreover, CP carries a copy of some OFDM symbol information which wastes power and data rate. However, for an OFDM system which employs a high number of subcarriers, this loss will not be significant. Furthermore, the redundancy contained in the cyclic prefix can be exploited in channel estimation and synchronisation [4].

Additionally, the robustness of OFDM systems as measured against the frequency selectivity of the channel is due to the fact that the spectrum of the subchannels is much smaller than the coherence bandwidth of the channel, and therefore, each

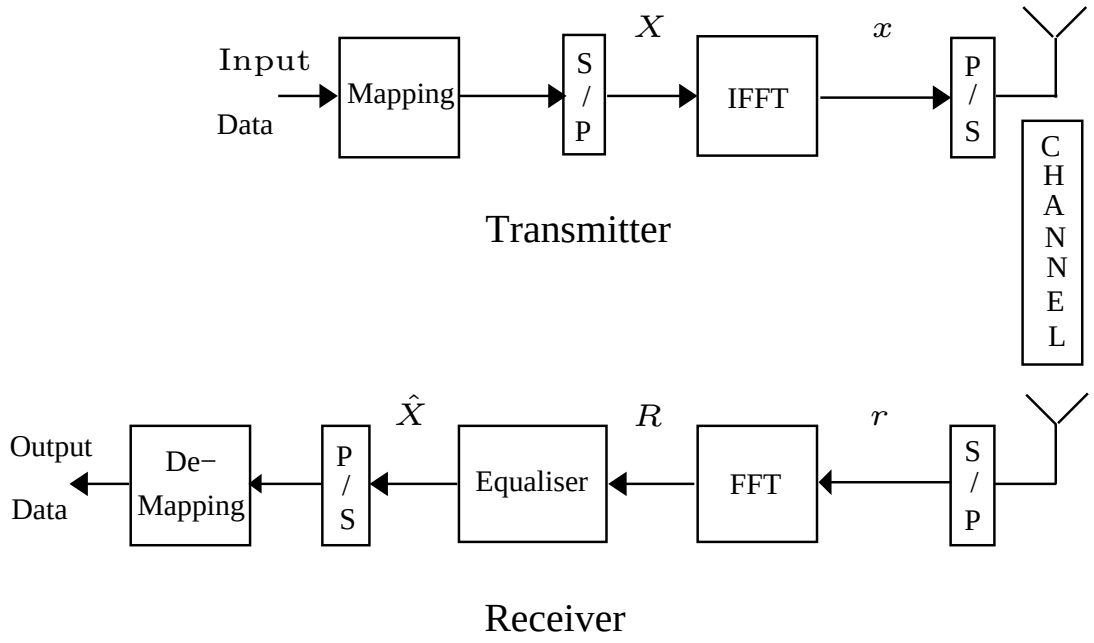

Figure 2.1: Uncoded OFDM system block diagram.

of the subchannels suffers from a flat fading. Since the frequency responses of the subcarriers are relatively flat, a simple one tap equalisation is sufficient at the receiver side for detecting the data constellations [6].

2.2 Overall OFDM System Design

The overall block diagram of the typical uncoded OFDM system is shown in Fig. 2.1. The key concepts in such a system can be briefly reviewed by providing the functions of the main three subblocks, i.e. the transmitter, channel and receiver.

2.2.1 Transmitter

The transmitter of the typical uncoded OFDM system exhibits many sub-blocks. The first block represents the source of the information required to be transmitted, and this source can be speech, images and videos. Before performing baseband modulation, the information or data bits are mapped to a suitable modulation scheme. There is an array of techniques such as M-array phase shift keying (M-PSK) and M-array quadrature amplitude modulation (M-QAM). In order to provide appropriate balance

among data rate, SNR value, and channel capacity, IEEE standards have supported quadrature PSK (QPSK) and sixteen QAM (16-QAM) modulation types widely to be used in many applications that utilised OFDM in their physical layer. Thus, in this thesis, these modulation types are adopted. Subsequently, guards are equally allocated to the left and right sides of the resultant frame, as shown in Fig. 2.2. Finally, the multi-carrier modulation is essentially equivalent to applying the inverse discrete Fourier transform (IDFT) to the original data stream. Similarly, the multi-carrier demodulation at the OFDM receiver can be achieved by utilising a discrete Fourier transform (DFT). The DFT functionality can be implemented via computationally efficient fast Fourier transform (FFT) algorithms. Recent advances in the semiconductor industry have enabled cost effective implementations of large size FFT chips, paving the way for the deployment of commercial OFDM systems. In the sequel, the discrete time-domain signal, $\mathbf{x}$, can be formulated as [4],

$$\mathbf{x} = \mathbf{F}^{H}\mathbf{X}, \tag{2.1}$$

where $\mathbf{X}$ denotes the OFDM symbols assigned to each data sub-carrier, $\{.\}^{H}$ denotes the Hermitian operator and $\mathbf{F}$ stands for the DFT matrix. Consequently, the nth element of x can be expressed as,

$$x_n = \frac{1}{\sqrt{N}} \sum_{k=0}^{N-1} X_k e^{\frac{j2\pi kn}{N}}, \forall\ n, k \in \{0, ..., N-1\}, \tag{2.2}$$

where $\frac{1}{\sqrt{N}}$ is a normalised scale factor, and N is the FFT size.
CP with length of N_g, with constraint $N_g \geq max\{\tau_l\}$, where τ_l is the delay of lth path, is added by copying the front-end of the data frame, $\mathbf{x}$, to the back-end of such a frame.

2.2.2 Channel

The OFDM signal is transmitted to the receiver through multipath fading channels, as shown in Fig. 2.1 and Fig. 2.3. The characteristics of these channels, such as the number of taps and the corresponding delays depend on the parameters of the transmission environment. Basically, the transmitted OFDM signal is linearly convolved with the impulse response of the related channel, $\mathbf{h}$, and is subsequently corrupted by

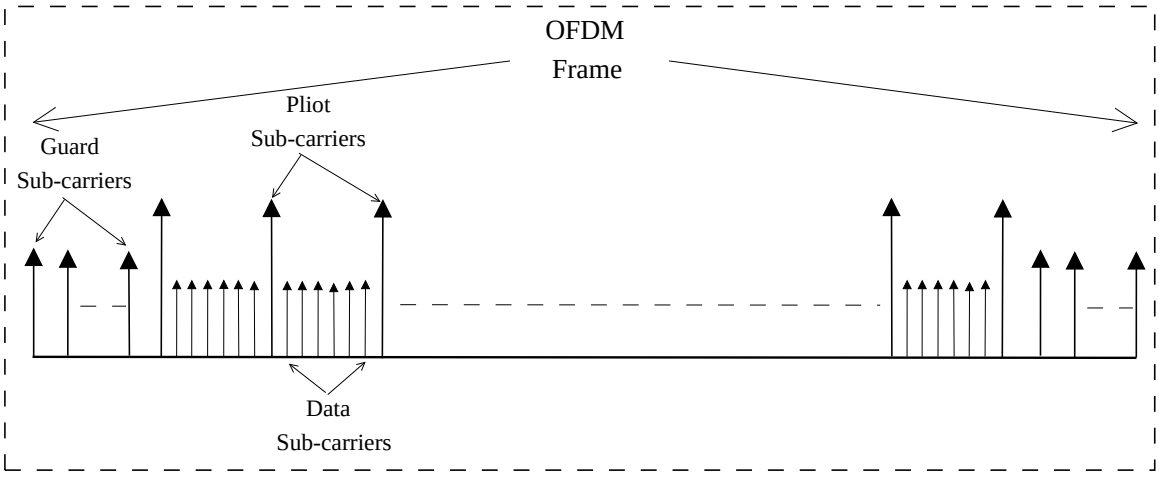

Figure 2.2: OFDM frame structure.

the additive white Gaussian noise (AWGN). As will be shown in Chapter 6, impulsive noise is another type of noise that can be added to the transmitted signal. For the sake of clarity, the disturbance of impulsive noise will not be considered in this chapter. Thus, these operations can be mathematically expressed as,

$$\mathbf{r} = \mathbf{D}\mathbf{x} + \mathbf{z}, \tag{2.3}$$

where $\mathbf{r}$ is the received data vector with elements that can be defined as $r_n = [r_0, r_1, \ldots, r_{N-1}]^T$, $\mathbf{z}$ denotes the additive white Gaussian noise, which has elements defined as $z_n = [z_0, z_1, \ldots, z_{N-1}]^T$ with zero mean and variance σ_z^2, and $\mathbf{D}$ is the $N \times N$ circulant channel matrix, which can be expressed as [15],

$$\mathbf{D} = \begin{bmatrix} h_0 & 0 & \cdots & 0 & h_{\hat{L}} & \cdots & \vdots \\ \vdots & h_0 & \ddots & 0 & 0 & \ddots & h_{\hat{L}} \\ h_{\hat{L}} & \vdots & \ddots & \vdots & 0 & \ddots & 0 \\ 0 & h_{\hat{L}} & \ddots & h_0 & \ddots & \ddots & 0 \\ \vdots & \vdots & \ddots & \vdots & h_0 & \ddots & \vdots \\ 0 & 0 & \cdots & h_{\hat{L}} & \vdots & \cdots & h_0 \end{bmatrix}. \tag{2.4}$$

The baseband equivalent noise signal $z(n) = \Re\{z_n\} + \Im\{z_n\}$, where $\Re\{.\}$ and $\Im\{.\}$ stand for the real and imaginary parts, respectively, will be the circularly symmetric complex Gaussian noise with variance,

$$\sigma_z^2 = \mathbb{E}\left\{z_n z_n^*\right\}, \tag{2.5}$$

where $\mathbb{E}\{\cdot\}$ denotes the expectation operator.

The real and imaginary parts are statistically independent and identically distributed (iid) with zero mean and equal variance σ_z^2. Hence,

$$\mathbb{E}\left\{\Re\{z_n^2\}\right\} = \mathbb{E}\left\{\Im\{z_n^2\}\right\} = \frac{\sigma_z^2}{2}, \tag{2.6}$$

and

$$\mathbb{E}\left\{\Re\{z_n\}\Im\{z_n^*\}\right\} = 0. \tag{2.7}$$

2.2.3 Receiver

As illustrated in Fig. 2.1, the receiver is more complicated than the transmitter, due to the need for solving the transmission problems by utilising the channel estimation and equalisation processes. After the CP removal, the received OFDM signal demodulates and converts into the frequency domain through the use of FFT. Thus, with the assumption of perfect knowledge of channel coefficients and synchronisation, the received signal in the frequency-domain is expressed mathematically as [6],

$$\mathbf{R} = \mathbf{Fr}, \tag{2.8a}$$
$$= \mathbf{FDF}^H\mathbf{X} + \mathbf{Fz}, \tag{2.8b}$$
$$= \mathbf{HX} + \mathbf{Z}, \tag{2.8c}$$

where $\mathbf{Z}$ is the AWGN signal in the frequency-domain and $\mathbf{H}$ denotes the diagonal matrix of the channel coefficients in the frequency-domain.
This means, the kth element of $\mathbf{R}$ can be calculated as,

$$R_k = \frac{1}{\sqrt{N}}\sum_{n=0}^{N-1} r_n e^{\frac{-j2\pi nk}{N}}, \tag{2.9}$$
$$= H_k X_k + W_k, \ \forall\ k \in \{0, ..., N\}. \tag{2.10}$$

In order to combat the phase and amplitude distortions caused by the mobile radio channel on the sub-channels, a one-tap equaliser is employed on the received OFDM sequence $\mathbf{R}$. The one tap equaliser is simply realised by multiplying each individual subcarrier with the complex value of the equaliser, which is computed based on its own channel coefficient. In the sequel, the received sequence at the output of the equaliser can be written as

$$\hat{\mathbf{X}} = \mathbf{QR}, \tag{2.11}$$

where

$$\mathbf{Q} = \begin{bmatrix} Q_{0,0} & 0 & \cdots & 0 \\ 0 & Q_{1,1} & \cdots & 0 \\ \vdots & \vdots & \ddots & \vdots \\ 0 & 0 & \cdots & Q_{N,N} \end{bmatrix}, \tag{2.12}$$

is the diagonal equaliser matrix.
The elements of $\mathbf{Q}$ are evaluated based on the equalisation criterion that is used. Eventually, the the desired transmitted information is obtained by using the demapper.

2.3 Multipath Channel Characteristics

The signal transmitted over wireless links can propagate through different channel paths with distinct spreading delays and attenuation, particularly in urban environments. These paths result from the reflection of the transmitted signal from hills, buildings, cars and other obstructions. This phenomenon is referred as multipath channels which may be either line-of-sight (LOS) (Racian) or non LOS (Rayleigh), as shown in Fig. 2.3. The multipath transmission causes a significant degradation in the system performance, due to the ISI, phase change and attenuation of the received signals [4] [6] [10]. In order to study the characteristics of multipath channels, this section is divided into two parts as follows.

2.3.1 Channel Impulse Response (CIR)

Basically, there are two major types of multipath wireless channels. Time invariant multipath channels are based on fixed attenuation values and associated delays for

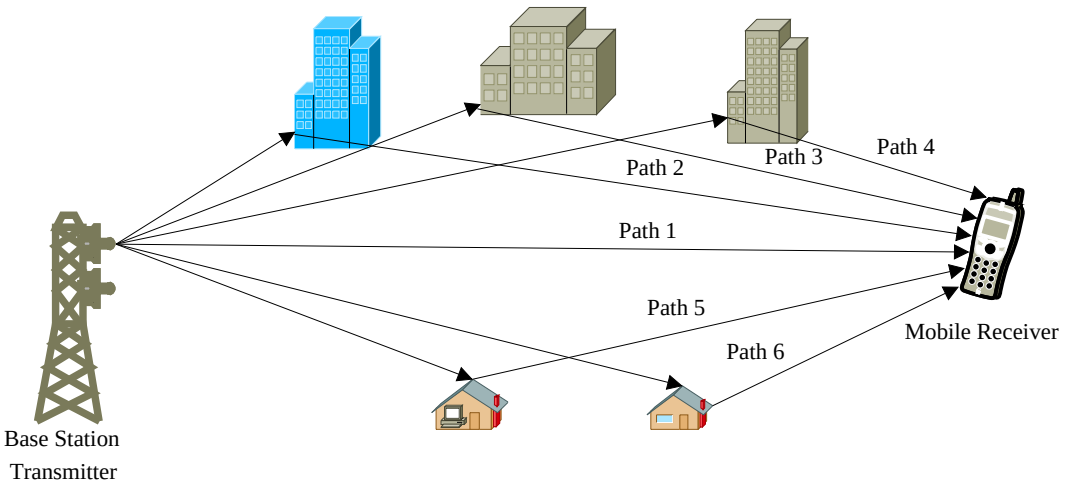

Figure 2.3: Multipath channel diagram.

the paths included over long transmission times. Whereas, the attenuation values and associated delays of the second type of multipath channels, called time variant, can be varied through the transmission time, due to the motion of the transceivers. Thus, the channel impulse response of the first type is fixed during the whole period of transmission; while it can be changed with the time for the second type [4].

In this work, the performance of the considered systems are investigated over LOS channel. Thus, two international telecommunication union (ITU) channel models are adopted. These are the pedestrian ITU-B and vehicular ITU-A. The parameters of the considered channel profiles are listed in Table 2.1 [16]. In this table, the average power and paths delay are mainly considered to realise quasi-static multipath fading channel models. This means, the employed channel models in this work are fixed within the entire OFDM symbol transmission duration. In other words, the effect of Doppler shift is omitted. It is also important to mention that the realisation of these channel models are achieved with the normalised path power (i.e. $\sum_l E[|h_l^t|^2] = 1$, where $E[.]$ denotes the expectation (statistical averaging) operator, and h_l^t is the CIR of tap l at instance t). Fig. 2.4 and Fig. 2.5 show the impulse response of these two considered channels. It is notable that the vehicular ITU-A appears to fluctuate with transmission time faster than the pedestrian ITU-B channel, which is changed slowly.

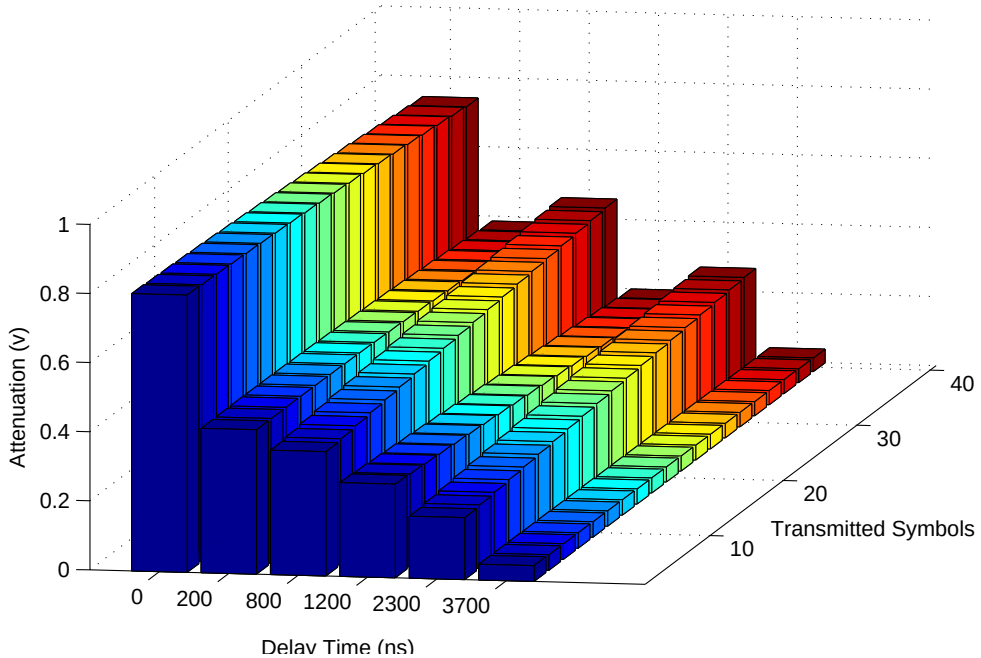

Figure 2.4: Impulse response of the pedestrian ITU-B channel.

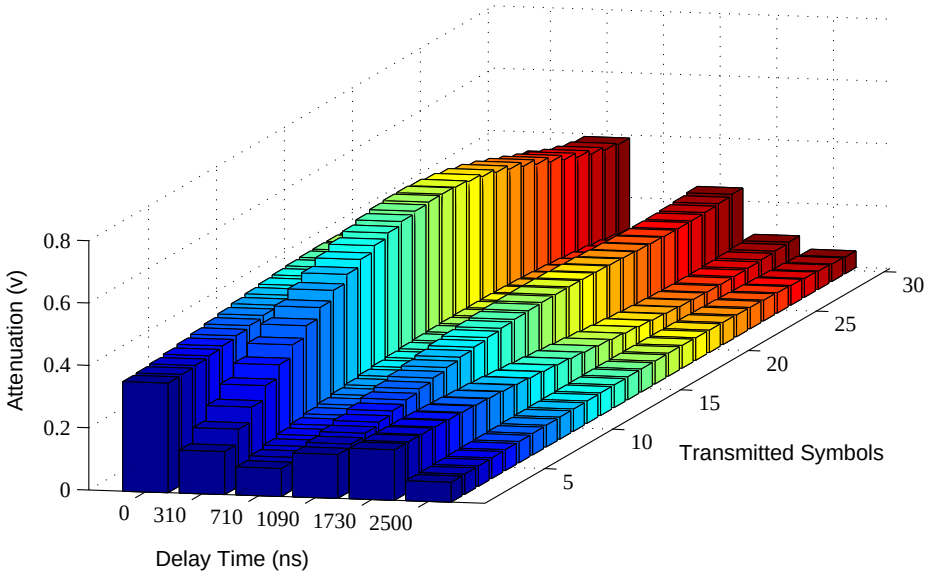

Figure 2.5: Impulse response of the vehicular ITU-A channel.

Table 2.1: ITU channel parameters

Path	Pedestrian ITU-B		Vehicular ITU-A	
	Delay (ns)	Average Power (dB)	Delay (ns)	Average Power (dB)
1	0	0	0	0
2	200	-0.9	310	-1
3	800	-4.9	710	-9.0
4	1200	-8.0	1090	-10.0
5	2300	-7.8	1730	-15.0
6	3700	-23.9	2510	-20.0

2.3.2 Frequency Response of The Channel

The frequency response of multipath channels can be defined as the frequency-domain of the CIR. In this domain, the channel categories are divided into frequency selective and frequency non-selective (flat), depending on the measured frequency coherence bandwidth. Additionally, the channel can be considered to be frequency selective if the signal bandwidth is greater than the coherence bandwidth. In the sequel, each data subcarrier will fade by its own channel coefficient. Conversely, the channel is called frequency non-selective, if the signal bandwidth is smaller than the coherence bandwidth. In this case, the same fading values affect all of the frequency components of the transmitted signal simultaneously. Fig. 2.6 and Fig. 2.7 demonstrate the frequency response of the adopted ITU channel models. In these figures, for every transmitted symbol, the frequency axis represents the center frequency for each subcarrier that will be faded by its own channel coefficient.

2.4 Linear Equaliser Techniques

One of the major advantages of the OFDM technique over single carrier based systems is its simple data detection process, whereby a linear single-tap equaliser is utilised in the frequency-domain for the signal recovery. In contrast, systems based on single carriers require a relatively complicated non-linear detector for the channel compensation process, such as successive interference cancellation (SIC), parallel interference cancellation (PIC) and maximum likelihood (ML) detectors [4]. The channel equalisation with the OFDM system is simply performed by multiplying each individual subcarrier with its associated value of the equaliser sequence, as was shown in (2.11).

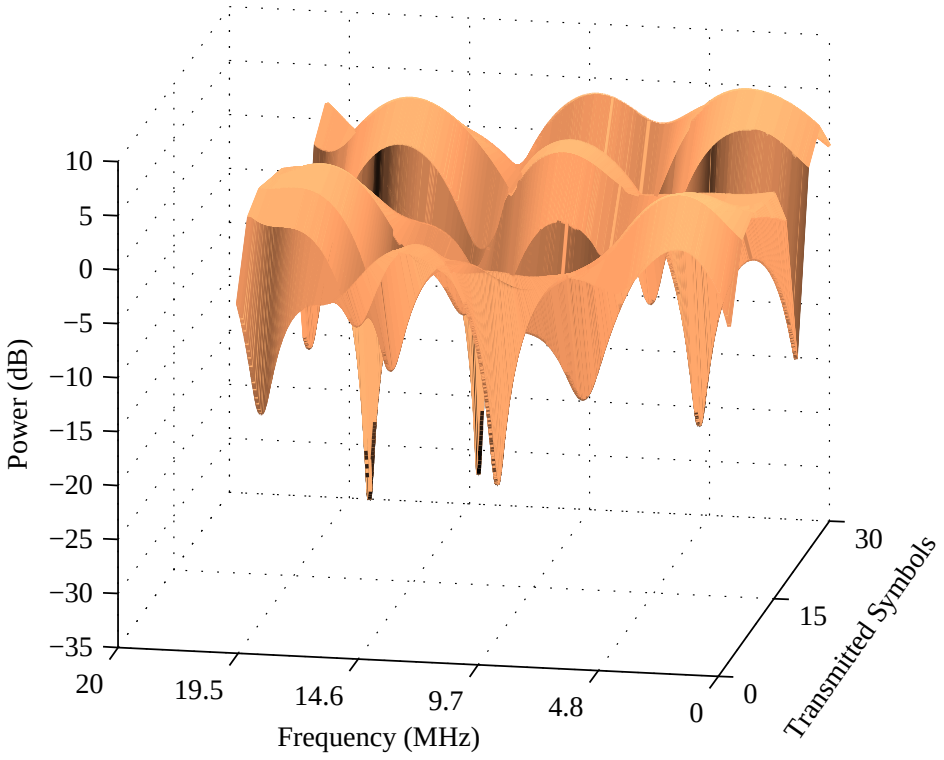

Figure 2.6: Frequency response of the vehicular ITU-A channel.

Two linear single-tap equaliser are considered in this thesis, as follows.

2.4.1 Zero Forcing (ZF) Equaliser

The easiest criteria of linear equaliser which has been used efficiently with OFDM system is the zero forcing (ZF) equaliser. The ZF equaliser applies the inverse of the channel to the received signal, to restore the signal before the channel. Hence, based on this criteria each individual value of $\mathbf{Q}$, which was defined in (2.12) can be expressed as [4],

$$Q_k^{\mathrm{ZF}} = \frac{1}{H_k}, \tag{2.13}$$

where H_k is the frequency response of the channel for the kth subcarrier.
Upon substituting (2.13) into (2.11), the equalised signal using ZF criteria can be written as,

$$\hat{X}_k = X_k + \frac{Z_k}{H_k}, \tag{2.14}$$

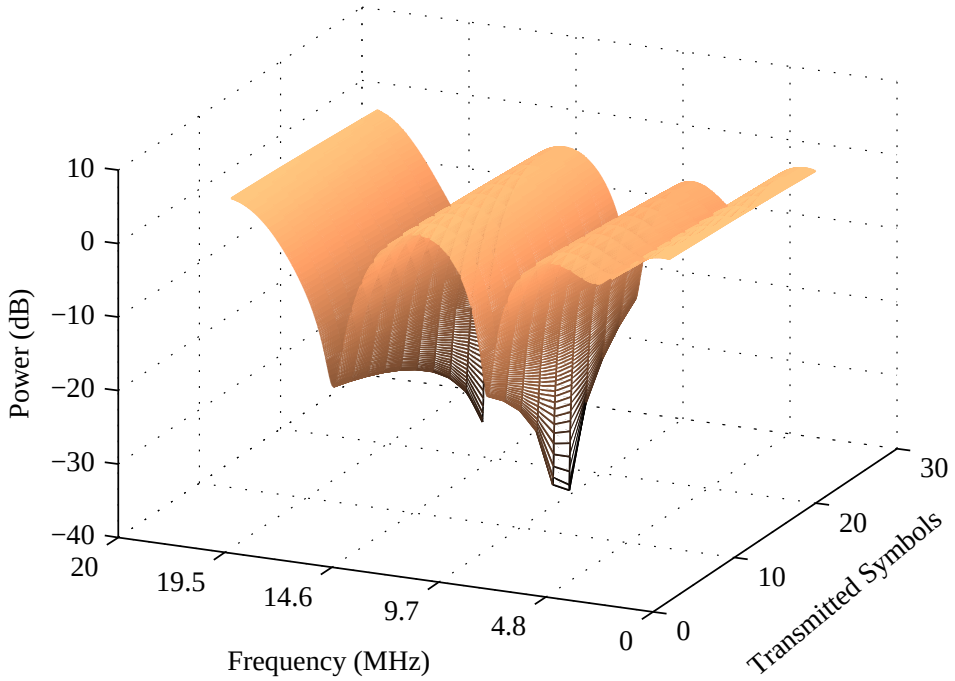

Figure 2.7: Frequency response of the pedestrian ITU-B channel.

The main advantage of using ZF equaliser over other criterion is its low computational complexity, as it does not need any initial knowledge of the channel state. However, in severe channels, i.e. $H_k \simeq 0$, the noise enhancement will be very high which leads to the inferior performance of the system using ZF equaliser.

2.4.2 Minimum Mean Square Error (MMSE) Equaliser

In order to overcome the noise enhancement drawback of the ZF, the MMSE criteria is introduced. This criterion is capable of reducing noise enhancement further to channel equalising. The formula of the MMSE based equaliser can be derived from obtaining the mean square error (MSE) between desired transmitted and recovered received signals. The aim of this equaliser is to minimise the MSE by evaluating the optimal $\mathbf{Q}^{\mathrm{MMSE}}$. Thus, (2.14) can be re-written with MMSE as,

$$\hat{\mathbf{X}} = \mathbf{Q}^{\mathrm{MMSE}}\mathbf{R}. \tag{2.15}$$

Furthermore, the MSE, e, between $\hat{\mathbf{X}}$ and $\mathbf{X}$ can be computed as [4], [17],

$$e = [1 - \mathbf{Q}^{\mathrm{MMSE}}\mathbf{H}][1 - \mathbf{Q}^{\mathrm{MMSE}}\mathbf{H}]^* E\{|\mathbf{X}|^2\} + \mathbf{Q}^{\mathrm{MMSE}}\mathbf{Q}^{*\mathrm{MMSE}} E\{|\mathbf{Z}|^2\}. \tag{2.16}$$

It is important to note that $\sigma_X^2 = E\{|\mathbf{X}|^2\}$ is the variance of the transmitted signal and $\sigma_Z^2 = E\{|\mathbf{Z}|^2\}$ denotes the variance of the AWGN samples. In order to find the $\mathbf{Q}^{\mathrm{MMSE}}$ values that minimise the MSE, e is differentiated with respect to $\mathbf{Q}^{\mathrm{MMSE}}$ (where $\mathbf{Q}^{*\mathrm{MMSE}}$ is constant) and set equal to zero as,

$$\frac{\partial e}{\partial \mathbf{Q}^{\mathrm{MMSE}}} = \mathbf{Q}^{*\mathrm{MMSE}}\sigma_Z^2 - \mathbf{H}[1 - \mathbf{Q}^{\mathrm{MMSE}}\mathbf{H}]^*\sigma_X^2 = 0. \tag{2.17}$$

After some mathematical operations on (2.17), the MMSE equaliser sequence, $\mathbf{Q}^{\mathrm{MMSE}}$, can be computed as,

$$\mathbf{Q}^{\mathrm{MMSE}} = \frac{\mathbf{H}^*\sigma_X^2}{|\mathbf{H}|^2\sigma_X^2 + \sigma_Z^2}. \tag{2.18}$$

This means, the kth elements of $\mathbf{Q}$ based on MMSE criteria can be computed as,

$$Q_k^{\mathrm{MMSE}} = \frac{H_k^*\sigma_X^2}{|H_k|^2\sigma_X^2 + \sigma_Z^2} \tag{2.19a}$$

$$= \frac{\lambda_0 H_k^*}{\lambda_0|H_k|^2+1}, \tag{2.19b}$$

where λ_0 represents the signal-to-noise ratio (SNR) value of the received signal.
It is observed from (2.19b) that the noise variance, σ_Z^2, should be calculated.

2.5 OFDM Merits and Challenges

This section summarises the main strengths and weaknesses of multicarrier modulation based on OFDM.

2.5.1 Merits

The main advantages of the OFDM technique are listed as follows:

1. Robust to Frequency Selective Fading Channel with Simple Channel Equalisation

In single carrier based systems, adaptive equalization techniques with relatively extra cost are required to compensate for the channel effect. Such techniques of channel equalization become very difficult and achieve inferior performance when the symbol period becomes shorter with increasing data rates due to an increase in the number of adjacent symbols affected by a single fade. In contrast, in a multicarrier system, the entire available bandwidth is divided into many narrow band subcarriers. This means, the frequency selective channel is technically regarded as a flat fading in each subband. In such a case, each subcarrier experiences its own flat fading channel which can be simply equalised using the linear single tap equaliser [18].

2. Efficient Use of The Available Frequency Spectrum

   The orthogonality among the subcarriers of OFDM based systems eliminates the inter-carrier interference (ICI) between adjacent subcarriers. Moreover, the OFDM system produces high spectral efficiency by allowing the overlap between adjacent orthogonal subcarriers. The orthogonality between subcarriers is maintained by carefully selecting the spacing between the subcarriers. In the sequel, with perfect synchronisation at the receiver, the information on each subcarrier could be recovered successfully without the interference from other subcarriers [6].

3. Robust to Weak Impulsive Noise

   As mentioned earlier in this chapter, OFDM has been adopted as the physical layer standard in the many digital communications systems, such as ADSL, DAB and WLANs. The performance of these systems has drastically deteriorated as a result of the man-made noises, namely, impulsive in nature further to AWGN. Due to utilising DFT at the receiver of the OFDM system, the impulsive noise energy will spread over large number of subcarriers. In addition, due to the long duration of OFDM symbols transmitted over the impulsive channel, they can still be largely recovered since only a small fraction of each symbol is interfered by noise. Thus, this could support that OFDM is robust to impulsive noises [18].

2.5.2 Challenges

Conversely, there are certain drawbacks that have a deleterious ramification on the performance of OFDM systems. These impairments have received a great deal of attention in recent studies. This section addresses the main impairments which exist in OFDM systems as follows:

1. Sensitivity Against Deep Fading Channel

   Although, there is robustness of the OFDM against frequency selective fading channel. However, the overall OFDM signal spectrum fades selectively; and as a consequence certain subcarriers will be severely attenuated by deep fades [4]. In such cases, OFDM does not offer any improvement in performance since no diversity can be exploited to recover the attenuated subcarriers. Therefore, the deleterious effects arising from the multipath propagation on the OFDM system performance have attained considerable attention in the course of recent studies. Many techniques have been investigated to increase its resilience to the negative ramifications of multipath channel dispersion, such as channel coding, adaptive systems and increased diversity; albeit with the added cost of computational complexity and data rate losses. Additionally, as will be introduced in Chapter 4, T-OFDM is proposed as an attractive technique which can be utilised to significantly reduce the negative effect of such a phenomenon.

2. High Peak-to-Average Power Ratio (PAPR)

   One of the major drawbacks of OFDM is its high PAPR [10]. Because the transmitted signal is the sum of a set of modulated signals owing to the use of IFFT, the peak power of the transmitted signal can be very high compared to its average power. Although occurring only with low probability, such large peaks have negative ramifications for the overall system. For instance, to work with high peak signal, the high power amplifier (HPA) requires large linear range, which, however, is inefficiently used. In addition, HPA working in non-linear range causes in-band distortion and out-band radiation, which may lead to BER degradation and severe interference between the signal transmitted in adjacent frequency bands, respectively. Therefore, various techniques have been proposed to reduce the high PAPR of OFDM systems. Compared to conventional techniques, the attractive features of the T-transform, which will be

introduced in Chapter 3, are utilised in the proposed T-OFDM to obtain noticeable PAPR reduction with lower complexity and lower in-band distortion, even in the presence of HPA, as will be shown in Chapter 5.

3. Disturbance of Heavy-Tailed Distributed Impulsive Noise

   As mentioned early in the merits section, the long duration and large subcarriers number of the OFDM system may help to suppress the disturbance arising from the impulsive channel. However, after exceeding a certain level of impulsive noise energy, the advantage of spreading impulsive noise energy over the transmitted OFDM subcarriers becomes a disadvantage [19], [20]. In the sequel, various techniques have been proposed to mitigate the disturbance of such model of channels. In this work, three new schemes are introduced to suppress the effect of impulsive channels, as will be shown in Chapter 6.

4. Frequency Offset

   In the OFDM system, the carrier frequency mismatch between the transmitter and receiver local oscillators, and/or the Doppler shift, due to mobility, may destroy the orthogonality among the subcarriers leading to ICI, which degrades the performance of such a system [6]. The sensitivity to the frequency offset is out of the scope of this thesis. However, conventional techniques, such as maximum-likelihood (ML) can be used efficiently with the proposed T-OFDM system.

2.6 Chapter Summary

This chapter has provided a brief overview of the OFDM system. Multipath fading channels characteristics have also been briefly highlighted. In addition, the main merits of OFDM that have been exploited in many applications have been presented. Furthermore, the main drawbacks which have received a considerable attention in recent studies are addressed in this chapter in order to evaluate the ability of proposed systems in this study to overcome these challenges, as will be shown in the forthcoming chapters.

CHAPTER 3

T-transform

The T- transform was introduced in 1989 by Boussakta [2], [3] to combine the Walsh-Hadamard transform (WHT) and the discrete Fourier transform (DFT) into a single fast orthonormal unitary transform or as a transition transform between the Walsh-Hadamard and Fourier domains. The aim of this chapter is to discuss this transform in details and analyse its structure and computational complexity.

3.1 Fast Transforms

Processes describing the conversion of a sequence of information from one domain to another with or without acceptable levels of losses can be defined as a transform. Meanwhile, in the case of a fast transform, similar processes can be implemented with lower arithmetic operation by omitting the redundancy of same arithmetic. There are various transforms that are used widely for different engineering applications, such as *DFT, WHT, Hartley Transform, Hilbert Transform, Number Theoretic Transform, Fermat Number Transform*, and so on. Owing to the beneficial features of these applications to our area of research, this chapter focuses on DFT and WHT.

3.1.1 Discrete Fourier Transforms (DFT)

Analogue signals are constructed from an infinite number of contiguous points that make their representation a practical impossibility. Therefore, digital computation is the only practical method that can be used to obtain Fourier data components [1]. In 1965, Cooley and Tukey produced the fast Fourier transform (FFT) as a faster algorithm to implement DFT, which can then be used to provide complementary information in frequency and time domains for the same sets of data [21]. DFT has been adopted widely in various fields in particular with signal processing and additional communications techniques, such as those utilising multicarriers systems. The key point behind employing DFT efficiently in these applications relates to the number of mathematical properties inherited with these transforms, which can be used to simplify any problems which may be faced. Some of them are listed below [1].

1. Completeness

   DFT and IDFT are used for the linear transformation of data from one domain to another. In other words, these transforms are invertible meaning, the discrete

time-domain samples $\mathbf{x}$ of size N discrete frequency-domain subcarriers $\mathbf{X}$ can be computed as,

$$\mathbf{x} = \mathbf{F}^H \mathbf{X}, \tag{3.1}$$

where $(.)^H$ is the Hermitian operator and $\mathbf{F}$ denotes the DFT matrix, i.e. $\mathbf{F}^H$ stands for the IDFT matrix. This means, the n_{th} element of $\mathbf{x}$ is evaluated as

$$x_n = \frac{1}{\sqrt{N}} \sum_{k=0}^{N-1} X_k e^{j2\pi nk/N}, \tag{3.2}$$

where $\frac{1}{\sqrt{N}}$ is the normalisation factor, which will be utilised to construct T-transform.
In contrast,

$$\mathbf{X} = \mathbf{F}\mathbf{x}, \tag{3.3}$$

where the elements of $\mathbf{X}$ can be expressed as

$$X_k = \frac{1}{\sqrt{N}} \sum_{n=0}^{N-1} x_n e^{-j2\pi nk/N}. \tag{3.4}$$

2. Orthogonality

   The orthogonal basis of DFT and IDFT can be shown as

   $$\mathbf{F}^H \mathbf{F} = \mathbf{I}, \tag{3.5}$$

   where $\mathbf{I}$ is the identity matrix. This orthogonality condition can be employed to evaluate the IDFT matrix based on the definition of the DFT matrix, or vice-versa. Moreover, the orthogonality of these transforms is utilised in OFDM systems to provide carriers with zero intercarrier interference (ICI).

3. Parseval's theorem

   Based on Parseval's theorem [22], which originates from a 1799 theorem applied to a series evaluated by Marc-Antoine Parseval, the average power of samples in the time-domain and that of subcarriers in the frequency-domain when using

normalised Fourier transforms are identical. This means,

$$\frac{1}{N}\sum_{n=0}^{N-1}|x(n)|^2=\frac{1}{N}\sum_{k=0}^{N-1}|X(k)|^2. \tag{3.6}$$

This is a key point that should be considered carefully to avoid the negative ramifications of HPA behaviour associated with the PAPR techniques in the OFDM systems, as will be shown in Chapter 5.

4. Symmetry and Antisymmetry

   Symmetry features among the amplitudes of the frequency-domain sequence $\mathbf{X}$ can illustrated as

   $$\Re[X(N-k)] = \Re[X(k)], \tag{3.7}$$

   where $\Re$ denotes the real part. Conversely, the phase spectrum of $\mathbf{X}$ samples are anti-symmetrical as

   $$\Im[X(N-k)] = -\Im[X(k)], \tag{3.8}$$

   where $\Im$ denotes the imaginary part.

5. Periodicity

   The rows and columns of the DFT matrix, $\mathbf{F}$ can be re-calculated based on $w^{nk} = w^{<nk>_N}$, where $<>_N$ represents the modulo-N operation. Similarly but with a reverse sign, the elements of the first half and the second half of the $\mathbf{F}$ matrix enable us to express the relationship between these elements as $w^{nk} = -w^{(nk-\frac{N}{2})}$ for $\frac{N}{2} \leq nk < N$. This feature will be exploited in the next sections to construct a T-transform from WHT and DFT.

6. Circular convolution theorem

   Based on the convolution theorem, the convolution of two sequences **x1** and **x2** in the time-domain can be obtained by evaluating their product in the frequency-domain **X1** and **X2**. This means that

   $$\mathbf{F}^H[\mathbf{X1X2}] \equiv [\mathbf{x1} \circledast \mathbf{x2}], \tag{3.9}$$

or

$$[\mathbf{X1X2}] \equiv \mathbf{F}[\mathbf{x1} \circledast \mathbf{x2}], \tag{3.10}$$

where $\circledast$ denotes the circular convolution operation. This theorem is utilised with the OFDM system to perform a simple channel equalization process.

3.1.1.1 DFT Structure in Matrix Form

Simply described, the normalised DFT matrix can be written as [3],

$$F_N^{nk} = \frac{1}{\sqrt{N}} \begin{bmatrix} w^0 & w^0 & w^0 & w^0 & \dots & w^0 \\ w^0 & w^{-1} & w^{-2} & w^{-3} & \dots & w^{-(N-1)} \\ w^0 & w^{-2} & w^{-4} & w^{-6} & \dots & w^{-2(N-1)} \\ w^0 & w^{-3} & w^{-6} & w^{-9} & \dots & w^{-3(N-1)} \\ \vdots & \vdots & \vdots & \vdots & \ddots & \vdots \\ w^0 & w^{-(N-1)} & w^{-2(N-1)} & w^{-3(N-1)} & \dots & w^{-(N-1)(N-1)} \end{bmatrix}, \tag{3.11}$$

where $w = e^{\frac{j2\pi}{N}}$.

To achieve a clear and simple analysis for the reader, consider, for instance, the case $N = 16$ (*note*: this analysis can be performed for any size). Thus,

$$F_{16}^{nk} = \frac{1}{4} \begin{bmatrix} w^0 & w^0 & w^0 & w^0 & w^0 & w^0 & w^0 & w^0 & w^0 & w^0 & w^0 & w^0 & w^0 & w^0 & w^0 & w^0 \\ w^0 & w^{-1} & w^{-2} & w^{-3} & w^{-4} & w^{-5} & w^{-6} & w^{-7} & w^{-8} & w^{-9} & w^{-10} & w^{-11} & w^{-12} & w^{-13} & w^{-14} & w^{-15} \\ w^0 & w^{-2} & w^{-4} & w^{-6} & w^{-8} & w^{-10} & w^{-12} & w^{-14} & w^{-16} & w^{-18} & w^{-20} & w^{-22} & w^{-24} & w^{-26} & w^{-28} & w^{-30} \\ w^0 & w^{-3} & w^{-6} & w^{-9} & w^{-12} & w^{-15} & w^{-18} & w^{-21} & w^{-24} & w^{-27} & w^{-30} & w^{-33} & w^{-36} & w^{-39} & w^{-42} & w^{-45} \\ w^0 & w^{-4} & w^{-8} & w^{-12} & w^{-16} & w^{-20} & w^{-24} & w^{-28} & w^{-32} & w^{-36} & w^{-40} & w^{-44} & w^{-48} & w^{-52} & w^{-56} & w^{-60} \\ w^0 & w^{-5} & w^{-10} & w^{-15} & w^{-20} & w^{-25} & w^{-30} & w^{-35} & w^{-40} & w^{-45} & w^{-50} & w^{-55} & w^{-60} & w^{-65} & w^{-70} & w^{-75} \\ w^0 & w^{-6} & w^{-12} & w^{-18} & w^{-24} & w^{-30} & w^{-36} & w^{-42} & w^{-48} & w^{-54} & w^{-60} & w^{-66} & w^{-72} & w^{-78} & w^{-84} & w^{-90} \\ w^0 & w^{-7} & w^{-14} & w^{-21} & w^{-28} & w^{-35} & w^{-42} & w^{-49} & w^{-56} & w^{-63} & w^{-70} & w^{-77} & w^{-84} & w^{-91} & w^{-98} & w^{-105} \\ w^0 & w^{-8} & w^{-16} & w^{-24} & w^{-32} & w^{-40} & w^{-48} & w^{-56} & w^{-64} & w^{-72} & w^{-80} & w^{-88} & w^{-96} & w^{-104} & w^{-112} & w^{-120} \\ w^0 & w^{-9} & w^{-18} & w^{-27} & w^{-36} & w^{-45} & w^{-54} & w^{-63} & w^{-72} & w^{-81} & w^{-90} & w^{-99} & w^{-108} & w^{-117} & w^{-126} & w^{-135} \\ w^0 & w^{-10} & w^{-20} & w^{-30} & w^{-40} & w^{-50} & w^{-60} & w^{-70} & w^{-80} & w^{-90} & w^{-100} & w^{-110} & w^{-120} & w^{-130} & w^{-140} & w^{-150} \\ w^0 & w^{-11} & w^{-22} & w^{-33} & w^{-44} & w^{-55} & w^{-66} & w^{-77} & w^{-88} & w^{-99} & w^{-110} & w^{-121} & w^{-132} & w^{-143} & w^{-154} & w^{-165} \\ w^0 & w^{-12} & w^{-24} & w^{-36} & w^{-48} & w^{-60} & w^{-72} & w^{-84} & w^{-96} & w^{-108} & w^{-120} & w^{-132} & w^{-144} & w^{-156} & w^{-168} & w^{-180} \\ w^0 & w^{-13} & w^{-26} & w^{-39} & w^{-52} & w^{-65} & w^{-78} & w^{-91} & w^{-104} & w^{-117} & w^{-130} & w^{-143} & w^{-156} & w^{-169} & w^{-182} & w^{-195} \\ w^0 & w^{-14} & w^{-28} & w^{-42} & w^{-56} & w^{-70} & w^{-84} & w^{-98} & w^{-112} & w^{-126} & w^{-140} & w^{-154} & w^{-168} & w^{-182} & w^{-196} & w^{-210} \\ w^0 & w^{-15} & w^{-30} & w^{-45} & w^{-60} & w^{-75} & w^{-90} & w^{-105} & w^{-120} & w^{-135} & w^{-150} & w^{-165} & w^{-180} & w^{-195} & w^{-210} & w^{-225} \end{bmatrix}. \tag{3.12}$$

However, periodicity, which is one of the basic functions for the DFT previously explained in this chapter, can be used to re-formulate the elements of (3.12). The

rows and columns of the DFT matrix, $\mathbf{F}$, can thus be re-calculated based on

$$w^{-nk} = w^{<-nk>_N}, \tag{3.13}$$

where $<>_N$ stands for the modulo-N operation. For example,

$$w^{-98} = w^{<-98>_{16}} = w^{-2}, \tag{3.14}$$

$$w^{-168} = w^{<-168>_{16}} = w^{-8}, \tag{3.15}$$

$$w^{-80} = w^{<-80>_{16}} = w^{0} = 1, \tag{3.16}$$

$$w^{-117} = w^{<-117>_{16}} = w^{-5}. \tag{3.17}$$

Moreover, the elements of the first half and the second half of the matrix $\mathbf{F}$ are similar but utilise a reverse sign. Thus, this relationship enables us to express these elements as

$$w^{-nk} = -w^{-(nk-\frac{N}{2})} \text{ for } \frac{N}{2} \leq nk < N. \tag{3.18}$$

For example,

$$w^{-11} = -w^{-(11-8)} = -w^{-3}, \tag{3.19}$$

$$w^{-8} = -w^{-(8-8)} = -w^{0} = -1, \tag{3.20}$$

$$w^{-15} = -w^{-(15-8)} = -w^{-7}, \tag{3.21}$$

$$w^{-9} = -w^{-(9-8)} = -w^{-1}. \tag{3.22}$$

In the sequel, when applying (3.13) and (3.18), elements of the DFT matrix in (3.12)

can be calculated as

$$F_{16}^{nk} = \frac{1}{4}\begin{bmatrix}
1 & 1 & 1 & 1 & 1 & 1 & 1 & 1 & 1 & 1 & 1 & 1 & 1 & 1 & 1 & 1 \\
1 & w^{-1} & w^{-2} & w^{-3} & w^{-4} & w^{-5} & w^{-6} & w^{-7} & -1 & -w^{-1} & -w^{-2} & -w^{-3} & -w^{-4} & -w^{-5} & -w^{-6} & -w^{-7} \\
1 & w^{-2} & w^{-4} & w^{-6} & -1 & -w^{-2} & -w^{-4} & -w^{-6} & 1 & w^{-2} & w^{-4} & w^{-6} & -1 & -w^{-2} & -w^{-4} & -w^{-6} \\
1 & w^{-3} & w^{-6} & -w^{-1} & -w^{-4} & -w^{-7} & w^{-2} & w^{-5} & -1 & -w^{-3} & -w^{-6} & w^{-1} & w^{-4} & w^{-7} & -w^{-2} & -w^{-5} \\
1 & w^{-4} & -1 & -w^{-4} & 1 & w^{-4} & -1 & -w^{-4} & 1 & w^{-4} & -1 & -w^{-4} & 1 & w^{-4} & -1 & -w^{-4} \\
1 & w^{-5} & -w^{-2} & -w^{-7} & w^{-4} & -w^{-1} & -w^{-6} & w^{-3} & -1 & -w^{-5} & w^{-2} & w^{-7} & -w^{-4} & w^{-1} & w^{-6} & -w^{-3} \\
1 & w^{-6} & -w^{-4} & w^{-2} & -1 & -w^{-6} & w^{-4} & -w^{-2} & 1 & w^{-6} & -w^{-4} & w^{-2} & -1 & -w^{-6} & w^{-4} & -w^{-2} \\
1 & w^{-7} & -w^{-6} & w^{-5} & -w^{-4} & w^{-3} & -w^{-2} & w^{-1} & -1 & -w^{-7} & w^{-6} & -w^{-5} & w^{-4} & -w^{-3} & w^{-2} & -w^{-1} \\
1 & -1 & 1 & -1 & 1 & -1 & 1 & -1 & 1 & -1 & 1 & -1 & 1 & -1 & 1 & -1 \\
1 & -w^{-1} & w^{-2} & -w^{-3} & w^{-4} & -w^{-5} & w^{-6} & -w^{-7} & -1 & w^{-1} & -w^{-2} & w^{-3} & -w^{-4} & w^{-5} & -w^{-6} & w^{-7} \\
1 & -w^{-2} & w^{-4} & -w^{-6} & -1 & w^{-2} & -w^{-4} & w^{-6} & 1 & -w^{-2} & w^{-4} & -w^{-6} & -1 & w^{-2} & -w^{-4} & w^{-6} \\
1 & -w^{-3} & w^{-6} & w^{-1} & -w^{-4} & w^{-7} & w^{-2} & -w^{-5} & -1 & w^{-3} & -w^{-6} & -w^{-1} & w^{-4} & -w^{-7} & -w^{-2} & w^{-5} \\
1 & -w^{-4} & -1 & w^{-4} & 1 & -w^{-4} & -1 & w^{-4} & 1 & -w^{-4} & -1 & w^{-4} & 1 & -w^{-4} & -1 & w^{-4} \\
1 & -w^{-5} & -w^{-2} & w^{-7} & w^{-4} & w^{-1} & -w^{-6} & -w^{-3} & -1 & w^{-5} & w^{-2} & -w^{-7} & -w^{-4} & -w^{-1} & w^{-6} & w^{-3} \\
1 & -w^{-6} & -w^{-4} & -w^{-2} & -1 & w^{-6} & w^{-4} & w^{-2} & 1 & -w^{-6} & -w^{-4} & -w^{-2} & -1 & w^{-6} & w^{-4} & w^{-2} \\
1 & -w^{-7} & -w^{-6} & -w^{-5} & -w^{-4} & -w^{-3} & -w^{-2} & -w^{-1} & -1 & w^{-7} & w^{-6} & w^{-5} & w^{-4} & w^{-3} & w^{-2} & w^{-1}
\end{bmatrix}. \tag{3.23}$$

When rearranging the DFT matrix in (3.23) by row reversed order, its radix-2 matrix can be obtained as

$$F_{16}^{nk} = \frac{1}{4}\begin{bmatrix}
1 & 1 & 1 & 1 & 1 & 1 & 1 & 1 & 1 & 1 & 1 & 1 & 1 & 1 & 1 & 1 \\
1 & -1 & 1 & -1 & 1 & -1 & 1 & -1 & 1 & -1 & 1 & -1 & 1 & -1 & 1 & -1 \\
1 & w^{-4} & -1 & -w^{-4} & 1 & w^{-4} & -1 & -w^{-4} & 1 & w^{-4} & -1 & -w^{-4} & 1 & w^{-4} & -1 & -w^{-4} \\
1 & -w^{-4} & -1 & w^{-4} & 1 & -w^{-4} & -1 & w^{-4} & 1 & -w^{-4} & -1 & w^{-4} & 1 & -w^{-4} & -1 & w^{-4} \\
1 & w^{-2} & w^{-4} & w^{-6} & -1 & -w^{-2} & -w^{-4} & -w^{-6} & 1 & w^{-2} & w^{-4} & w^{-6} & -1 & -w^{-2} & -w^{-4} & -w^{-6} \\
1 & -w^{-2} & w^{-4} & -w^{-6} & -1 & w^{-2} & -w^{-4} & w^{-6} & 1 & -w^{-2} & w^{-4} & -w^{-6} & -1 & w^{-2} & -w^{-4} & w^{-6} \\
1 & w^{-6} & -w^{-4} & w^{-2} & -1 & -w^{-6} & w^{-4} & -w^{-2} & 1 & w^{-6} & -w^{-4} & w^{-2} & -1 & -w^{-6} & w^{-4} & -w^{-2} \\
1 & -w^{-6} & -w^{-4} & -w^{-2} & -1 & w^{-6} & w^{-4} & w^{-2} & 1 & -w^{-6} & -w^{-4} & -w^{-2} & -1 & w^{-6} & w^{-4} & w^{-2} \\
1 & w^{-1} & w^{-2} & w^{-3} & w^{-4} & w^{-5} & w^{-6} & w^{-7} & -1 & -w^{-1} & -w^{-2} & -w^{-3} & -w^{-4} & -w^{-5} & -w^{-6} & -w^{-7} \\
1 & -w^{-1} & w^{-2} & -w^{-3} & w^{-4} & -w^{-5} & w^{-6} & -w^{-7} & -1 & w^{-1} & -w^{-2} & w^{-3} & -w^{-4} & w^{-5} & -w^{-6} & w^{-7} \\
1 & w^{-5} & -w^{-2} & -w^{-7} & w^{-4} & -w^{-1} & -w^{-6} & w^{-3} & -1 & -w^{-5} & w^{-2} & w^{-7} & -w^{-4} & w^{-1} & w^{-6} & -w^{-3} \\
1 & -w^{-5} & -w^{-2} & w^{-7} & w^{-4} & w^{-1} & -w^{-6} & -w^{-3} & -1 & w^{-5} & w^{-2} & -w^{-7} & -w^{-4} & -w^{-1} & w^{-6} & w^{-3} \\
1 & w^{-3} & w^{-6} & -w^{-1} & -w^{-4} & -w^{-7} & w^{-2} & w^{-5} & -1 & -w^{-3} & -w^{-6} & w^{-1} & w^{-4} & w^{-7} & -w^{-2} & -w^{-5} \\
1 & -w^{-3} & w^{-6} & w^{-1} & -w^{-4} & w^{-7} & w^{-2} & -w^{-5} & -1 & w^{-3} & -w^{-6} & -w^{-1} & w^{-4} & -w^{-7} & -w^{-2} & w^{-5} \\
1 & w^{-7} & -w^{-6} & w^{-5} & -w^{-4} & w^{-3} & -w^{-2} & w^{-1} & -1 & -w^{-7} & w^{-6} & -w^{-5} & w^{-4} & -w^{-3} & w^{-2} & -w^{-1} \\
1 & -w^{-7} & -w^{-6} & -w^{-5} & -w^{-4} & -w^{-3} & -w^{-2} & -w^{-1} & -1 & w^{-7} & w^{-6} & w^{-5} & w^{-4} & w^{-3} & w^{-2} & w^{-1}
\end{bmatrix}. \tag{3.24}$$

Consequently, equation (3.24) can be written in terms of sub-matrices as

$$\mathbf{F}_{16} = \frac{1}{4}\begin{bmatrix} \mathbf{A}_8 & \mathbf{A}_8 \\ \mathbf{B}_8 & -\mathbf{B}_8 \end{bmatrix}, \tag{3.25}$$

where

$$\mathbf{A}_8 = \begin{bmatrix} 1 & 1 & 1 & 1 & 1 & 1 & 1 & 1 \\ 1 & -1 & 1 & -1 & 1 & -1 & 1 & -1 \\ 1 & w^{-4} & -1 & -w^{-4} & 1 & w^{-4} & -1 & -w^{-4} \\ 1 & -w^{-4} & -1 & w^{-4} & 1 & -w^{-4} & -1 & w^{-4} \\ 1 & w^{-2} & w^{-4} & w^{-6} & -1 & -w^{-2} & -w^{-4} & -w^{-6} \\ 1 & -w^{-2} & w^{-4} & -w^{-6} & -1 & w^{-2} & -w^{-4} & w^{-6} \\ 1 & w^{-6} & -w^{-4} & w^{-2} & -1 & -w^{-6} & w^{-4} & -w^{-2} \\ 1 & -w^{-6} & -w^{-4} & -w^{-2} & -1 & w^{-6} & w^{-4} & w^{-2} \end{bmatrix}, \tag{3.26}$$

and

$$\mathbf{B}_8 = \begin{bmatrix} 1 & w^{-1} & w^{-2} & w^{-3} & w^{-4} & w^{-5} & w^{-6} & w^{-7} \\ 1 & -w^{-1} & w^{-2} & -w^{-3} & w^{-4} & -w^{-5} & w^{-6} & -w^{-7} \\ 1 & w^{-5} & -w^{-2} & -w^{-7} & w^{-4} & -w^{-1} & -w^{-6} & w^{-3} \\ 1 & -w^{-5} & -w^{-2} & w^{-7} & w^{-4} & w^{-1} & -w^{-6} & -w^{-3} \\ 1 & w^{-3} & w^{-6} & -w^{-1} & -w^{-4} & -w^{-7} & w^{-2} & w^{-5} \\ 1 & -w^{-3} & w^{-6} & w^{-1} & -w^{-4} & w^{-7} & w^{-2} & -w^{-5} \\ 1 & w^{-7} & -w^{-6} & w^{-5} & -w^{-4} & w^{-3} & -w^{-2} & w^{-1} \\ 1 & -w^{-7} & -w^{-6} & -w^{-5} & -w^{-4} & -w^{-3} & -w^{-2} & -w^{-1} \end{bmatrix}. \tag{3.27}$$

Furthermore, the sub-matrices in (3.26) and (3.27) can be subdivided further into their internal sub-matrices as

$$\mathbf{A}_8 = \begin{bmatrix} \mathbf{A}_4^{'} & \mathbf{A}_4^{'} \\ \mathbf{A}_4^{''} & -\mathbf{A}_4^{''} \end{bmatrix}, \tag{3.28}$$

$$\mathbf{B}_8 = \begin{bmatrix} \mathbf{B}_4^{'} & w^{-4}\mathbf{B}_4^{'} \\ \mathbf{B}_4^{''} & -w^{-4}\mathbf{B}_4^{''} \end{bmatrix}, \tag{3.29}$$

where

$$\mathbf{A}_4^{'} = \begin{bmatrix} 1 & 1 & 1 & 1 \\ 1 & -1 & 1 & -1 \\ 1 & w^{-4} & -1 & -w^{-4} \\ 1 & -w^{-4} & -1 & w^{-4} \end{bmatrix}, \quad \mathbf{A}_4^{''} = \begin{bmatrix} 1 & w^{-2} & w^{-4} & w^{-6} \\ 1 & -w^{-2} & w^{-4} & -w^{-6} \\ 1 & w^{-6} & -w^{-4} & w^{-2} \\ 1 & -w^{-6} & -w^{-4} & -w^{-2} \end{bmatrix},$$

$$\mathbf{B}_4^{'} = \begin{bmatrix} 1 & w^{-1} & w^{-2} & w^{-3} \\ 1 & -w^{-1} & w^{-2} & -w^{-3} \\ 1 & w^{-5} & -w^{-2} & -w^{-7} \\ 1 & -w^{-5} & -w^{-2} & w^{-7} \end{bmatrix}, \text{ and } \mathbf{B}_4^{''} = \begin{bmatrix} 1 & w^{-3} & w^{-6} & -w^{-1} \\ 1 & -w^{-3} & w^{-6} & w^{-1} \\ 1 & w^{-7} & -w^{-6} & w^{-5} \\ 1 & -w^{-7} & -w^{-6} & -w^{-5} \end{bmatrix}.$$

Moreover, matrices $A^{'}$, $A^{''}$, $B^{'}$ and $B^{''}$ can be sub-divided into other sub-matrices, such as

$$\mathbf{A}_4^{'} = \begin{bmatrix} C_2 & C_2 \\ C_2^{'} & -C_2^{'} \end{bmatrix}, \tag{3.30}$$

$$\mathbf{A}_4^{''} = \begin{bmatrix} E_2 & w^{-4}E_2 \\ E_2^{'} & -w^{-4}E_2^{'} \end{bmatrix}, \tag{3.31}$$

$$\mathbf{B}_4^{'} = \begin{bmatrix} A_2^{'''} & w^{-2}A_2^{'''} \\ B_2^{'''} & -w^{-2}B_2^{'''} \end{bmatrix}, \tag{3.32}$$

and

$$\mathbf{B}_4^{''} = \begin{bmatrix} C_2^{'''} & w^{-6}C_2^{'''} \\ E_2^{'''} & -w^{-6}E_2^{'''} \end{bmatrix}, \tag{3.33}$$

where

$$\mathbf{C}_2 = \begin{bmatrix} 1 & 1 \\ 1 & -1 \end{bmatrix}, \quad \mathbf{C}_2^{'} = \begin{bmatrix} 1 & w^{-4} \\ 1 & -w^{-4} \end{bmatrix}, \quad \mathbf{E}_2 = \begin{bmatrix} 1 & w^{-2} \\ 1 & -w^{-2} \end{bmatrix}, \quad \mathbf{E}_2^{'} = \begin{bmatrix} 1 & w^{-6} \\ 1 & -w^{-6} \end{bmatrix},$$

$$\mathbf{A}_2^{'''} = \begin{bmatrix} 1 & w^{-1} \\ 1 & -w^{-1} \end{bmatrix}, \quad \mathbf{B}_2^{'''} = \begin{bmatrix} 1 & w^{-5} \\ 1 & -w^{-5} \end{bmatrix}, \quad \mathbf{C}_2^{'''} = \begin{bmatrix} 1 & w^{-3} \\ 1 & -w^{-3} \end{bmatrix}, \text{ and } \mathbf{E}_2^{'''} = \begin{bmatrix} 1 & w^{-7} \\ 1 & -w^{-7} \end{bmatrix}.$$

In the sequel, the resultant DFT matrix will be combined with the WHT matrix to construct the forward T-transform, as in section 3.2.1.

3.1.1.2 IDFT Structure in Matrix Form

This section presents the normalised IDFT matrix formulation. To ensure clarity, the normalised IDFT matrix will be written as $\hat{\mathbf{F}}$, where $\hat{\mathbf{F}} = \mathbf{F}^H$. Thus, the normalised IDFT matrix can be written as

$$\hat{F}_N^{nk} = \frac{1}{\sqrt{N}} \begin{bmatrix} w^0 & w^0 & w^0 & w^0 & \dots & w^0 \\ w^0 & w^1 & w^2 & w^3 & \dots & w^{(N-1)} \\ w^0 & w^2 & w^4 & w^6 & \dots & w^{2(N-1)} \\ w^0 & w^3 & w^6 & w^9 & \dots & w^{3(N-1)} \\ \vdots & \vdots & \vdots & \vdots & \ddots & \vdots \\ w^0 & w^{(N-1)} & w^{2(N-1)} & w^{3(N-1)} & \dots & w^{(N-1)(N-1)} \end{bmatrix}, \tag{3.34}$$

where $w = e^{\frac{j2\pi}{N}}$.

As detailed in the analysis of the DFT matrix in section 3.1.1.1, consider, for instance, the case $N = 16$ (*note*: once again this analysis can be performed for any size). Thus,

$$\hat{F}_{16}^{nk} = \frac{1}{4} \begin{bmatrix} w^0 & w^0 & w^0 & w^0 & w^0 & w^0 & w^0 & w^0 & w^0 & w^0 & w^0 & w^0 & w^0 & w^0 & w^0 & w^0 \\ w^0 & w^1 & w^2 & w^3 & w^4 & w^5 & w^6 & w^7 & w^8 & w^9 & w^{10} & w^{11} & w^{12} & w^{13} & w^{14} & w^{15} \\ w^0 & w^2 & w^4 & w^6 & w^8 & w^{10} & w^{12} & w^{14} & w^{16} & w^{18} & w^{20} & w^{22} & w^{24} & w^{26} & w^{28} & w^{30} \\ w^0 & w^3 & w^6 & w^9 & w^{12} & w^{15} & w^{18} & w^{21} & w^{24} & w^{27} & w^{30} & w^{33} & w^{36} & w^{39} & w^{42} & w^{45} \\ w^0 & w^4 & w^8 & w^{12} & w^{16} & w^{20} & w^{24} & w^{28} & w^{32} & w^{36} & w^{40} & w^{44} & w^{48} & w^{52} & w^{56} & w^{60} \\ w^0 & w^5 & w^{10} & w^{15} & w^{20} & w^{25} & w^{30} & w^{35} & w^{40} & w^{45} & w^{50} & w^{55} & w^{60} & w^{65} & w^{70} & w^{75} \\ w^0 & w^6 & w^{12} & w^{18} & w^{24} & w^{30} & w^{36} & w^{42} & w^{48} & w^{54} & w^{60} & w^{66} & w^{72} & w^{78} & w^{84} & w^{90} \\ w^0 & w^7 & w^{14} & w^{21} & w^{28} & w^{35} & w^{42} & w^{49} & w^{56} & w^{63} & w^{70} & w^{77} & w^{84} & w^{91} & w^{98} & w^{105} \\ w^0 & w^8 & w^{16} & w^{24} & w^{32} & w^{40} & w^{48} & w^{56} & w^{64} & w^{72} & w^{80} & w^{88} & w^{96} & w^{104} & w^{112} & w^{120} \\ w^0 & w^9 & w^{18} & w^{27} & w^{36} & w^{45} & w^{54} & w^{63} & w^{72} & w^{81} & w^{90} & w^{99} & w^{108} & w^{117} & w^{126} & w^{135} \\ w^0 & w^{10} & w^{20} & w^{30} & w^{40} & w^{50} & w^{60} & w^{70} & w^{80} & w^{90} & w^{100} & w^{110} & w^{-120} & w^{130} & w^{140} & w^{150} \\ w^0 & w^{11} & w^{22} & w^{33} & w^{44} & w^{55} & w^{66} & w^{77} & w^{88} & w^{99} & w^{110} & w^{121} & w^{132} & w^{143} & w^{154} & w^{165} \\ w^0 & w^{12} & w^{24} & w^{36} & w^{48} & w^{60} & w^{72} & w^{84} & w^{96} & w^{108} & w^{120} & w^{132} & w^{144} & w^{156} & w^{168} & w^{180} \\ w^0 & w^{13} & w^{26} & w^{39} & w^{52} & w^{65} & w^{78} & w^{91} & w^{104} & w^{117} & w^{130} & w^{143} & w^{156} & w^{169} & w^{182} & w^{195} \\ w^0 & w^{14} & w^{28} & w^{42} & w^{56} & w^{70} & w^{84} & w^{98} & w^{112} & w^{126} & w^{140} & w^{154} & w^{168} & w^{182} & w^{196} & w^{210} \\ w^0 & w^{15} & w^{30} & w^{45} & w^{60} & w^{75} & w^{90} & w^{105} & w^{120} & w^{135} & w^{150} & w^{165} & w^{180} & w^{195} & w^{210} & w^{225} \end{bmatrix}. \tag{3.35}$$

By using (3.13), (3.18), the elements of (3.35) can be computed as the conjugate of (3.23) elements. When rearranging the resultant normalised IDFT matrix by column

reverse order, its basic functions can be given by

$$\hat{F}_{16}^{nk} = \frac{1}{4}\begin{bmatrix}
1 & 1 & 1 & 1 & 1 & 1 & 1 & 1 & 1 & 1 & 1 & 1 & 1 & 1 & 1 & 1 \\
1 & -1 & w^4 & -w^4 & w^2 & -w^2 & w^6 & -w^6 & w^1 & -w^1 & w^5 & -w^5 & w^3 & -w^3 & w^7 & -w^7 \\
1 & 1 & -1 & -1 & w^4 & w^4 & -w^4 & -w^4 & w^2 & w^2 & -w^2 & -w^2 & w^6 & w^6 & -w^6 & -w^6 \\
1 & -1 & -w^4 & w^4 & w^6 & -w^6 & w^2 & -w^2 & w^3 & -w^3 & -w^7 & w^7 & -w^1 & w^1 & w^5 & -w^5 \\
1 & 1 & 1 & 1 & -1 & -1 & -1 & -1 & w^4 & w^4 & w^4 & w^4 & -w^4 & -w^4 & -w^4 & -w^4 \\
1 & -1 & w^4 & -w^4 & -w^2 & w^2 & -w^6 & w^6 & w^5 & -w^5 & -w^1 & w^1 & -w^7 & w^7 & w^3 & -w^3 \\
1 & 1 & -1 & -1 & -w^4 & -w^4 & w^4 & w^4 & w^6 & w^6 & -w^6 & -w^6 & w^2 & w^2 & -w^2 & -w^2 \\
1 & -1 & -w^4 & w^4 & -w^6 & w^6 & -w^2 & w^2 & w^7 & -w^7 & w^3 & -w^3 & w^5 & -w^5 & w^1 & -w^1 \\
1 & 1 & 1 & 1 & 1 & 1 & 1 & 1 & -1 & -1 & -1 & -1 & -1 & -1 & -1 & -1 \\
1 & -1 & w^4 & -w^4 & w^2 & -w^2 & w^6 & -w^6 & -w^1 & w^1 & -w^5 & w^5 & -w^3 & w^3 & -w^7 & w^7 \\
1 & 1 & -1 & -1 & w^4 & w^4 & -w^4 & -w^4 & -w^2 & -w^2 & w^2 & w^{-2} & -w^6 & -w^6 & w^6 & w^6 \\
1 & -1 & -w^{-4} & w^{-4} & w^6 & -w^6 & w^2 & -w^2 & -w^3 & w^3 & w^7 & -w^7 & w^1 & -w^1 & -w^5 & w^5 \\
1 & 1 & 1 & 1 & -1 & -1 & -1 & -1 & -w^4 & -w^4 & -w^4 & -w^4 & w^4 & w^4 & w^4 & w^4 \\
1 & -1 & w^4 & -w^4 & -w^2 & w^2 & -w^6 & w^6 & -w^5 & w^5 & w^1 & -w^1 & w^7 & -w^7 & -w^3 & w^3 \\
1 & 1 & -1 & -1 & -w^4 & -w^4 & w^4 & w^4 & -w^6 & -w^6 & w^6 & w^6 & -w^2 & -w^2 & w^2 & w^2 \\
1 & -1 & -w^4 & w^4 & -w^6 & w^6 & -w^2 & w^2 & -w^7 & w^7 & -w^3 & w^3 & -w^5 & w^5 & -w^1 & w^1
\end{bmatrix}. \quad (3.36)$$

Consequently, as in (3.24), elements of matrix $\hat{\mathbf{F}}$, as defined in (3.36) can be written in terms of sub-matrices as follows,

$$\hat{\mathbf{F}}_{16} = \frac{1}{4}\begin{bmatrix} \hat{\mathbf{A}}_8 & \hat{\mathbf{B}}_8 \\ \hat{\mathbf{A}}_8 & -\hat{\mathbf{B}}_8 \end{bmatrix}, \quad (3.37)$$

where

$$\hat{\mathbf{A}}_8 = \begin{bmatrix}
1 & 1 & 1 & 1 & 1 & 1 & 1 & 1 \\
1 & -1 & w^4 & -w^4 & w^2 & -w^2 & w^6 & -w^6 \\
1 & 1 & -1 & -1 & w^4 & w^4 & -w^4 & -w^4 \\
1 & -1 & -w^4 & w^4 & w^6 & -w^6 & w^2 & -w^2 \\
1 & 1 & 1 & 1 & -1 & -1 & -1 & -1 \\
1 & -1 & w^4 & -w^4 & -w^2 & w^2 & -w^6 & w^6 \\
1 & 1 & -1 & -1 & -w^4 & -w^4 & w^4 & w^4 \\
1 & -1 & -w^4 & w^4 & -w^6 & w^6 & -w^2 & w^2
\end{bmatrix}, \quad (3.38)$$

and

$$\hat{\mathbf{B}}_8 = \begin{bmatrix} 1 & 1 & 1 & 1 & 1 & 1 & 1 & 1 \\ w^1 & -w^1 & w^5 & -w^5 & w^3 & -w^3 & w^7 & -w^7 \\ w^2 & w^2 & -w^2 & -w^2 & w^6 & w^6 & -w^6 & -w^6 \\ w^3 & -w^3 & -w^7 & w^7 & -w^1 & w^1 & w^5 & -w^5 \\ w^4 & w^4 & w^4 & w^4 & -w^4 & -w^4 & -w^4 & -w^4 \\ w^5 & -w^5 & -w^1 & w^1 & -w^7 & w^7 & w^3 & -w^3 \\ w^6 & w^6 & -w^6 & -w^6 & w^2 & w^2 & -w^2 & -w^2 \\ w^7 & -w^7 & w^3 & -w^3 & w^5 & -w^5 & w^1 & -w^1 \end{bmatrix}. \tag{3.39}$$

Once again, matrices $\hat{\mathbf{A}}$ and $\hat{\mathbf{B}}$ can be subdivided further into sub-matrices as,

$$\hat{\mathbf{A}}_8 = \begin{bmatrix} \hat{\mathbf{A}}_4^{'} & \hat{\mathbf{A}}_4^{''} \\ \hat{\mathbf{A}}_4^{'} & -\hat{\mathbf{A}}_4^{''} \end{bmatrix}, \tag{3.40}$$

$$\hat{\mathbf{B}}_8 = \begin{bmatrix} \hat{\mathbf{B}}_4^{'} & \hat{\mathbf{B}}_4^{''} \\ w^4\hat{\mathbf{B}}_4^{'} & -w^4\hat{\mathbf{B}}_4^{''} \end{bmatrix}, \tag{3.41}$$

where

$$\hat{\mathbf{A}}_4^{'} = \begin{bmatrix} 1 & 1 & 1 & 1 \\ 1 & -1 & w^4 & -w^4 \\ 1 & 1 & -1 & -1 \\ 1 & -1 & -w^4 & w^4 \end{bmatrix}, \ \hat{\mathbf{A}}_4^{''} = \begin{bmatrix} 1 & 1 & 1 & 1 \\ w^2 & -w^2 & w^6 & -w^6 \\ w^4 & w^4 & -w^4 & -w^4 \\ w^6 & -w^6 & w^2 & -w^2 \end{bmatrix}, \tag{3.42}$$

$$\hat{\mathbf{B}}_4^{'} = \begin{bmatrix} 1 & 1 & 1 & 1 \\ w^1 & -w^1 & w^5 & -w^5 \\ w^2 & w^2 & -w^2 & -w^2 \\ w^3 & -w^3 & -w^7 & w^7 \end{bmatrix}, \ \hat{\mathbf{B}}_4^{''} = \begin{bmatrix} 1 & 1 & 1 & 1 \\ w^3 & -w^3 & w^7 & -w^7 \\ w^6 & w^6 & -w^6 & -w^6 \\ -w^1 & w^1 & w^5 & -w^5 \end{bmatrix}. \tag{3.43}$$

Eventually, matrices $\hat{A}^{'}$, $\hat{A}^{''}$, $\hat{B}^{'}$ and $\hat{B}^{''}$ can be sub-divided into alternative sub-

matrices as

$$\hat{\mathbf{A}}_4^{'} = \begin{bmatrix} \hat{C}_2 & \hat{C}_2^{'} \\ \hat{C}_2 & -\hat{C}_2^{'} \end{bmatrix}, \ \hat{\mathbf{A}}_4^{''} = \begin{bmatrix} \hat{E}_2 & \hat{E}_2^{'} \\ w^4\hat{E}_2 & -w^4\hat{E}_2^{'} \end{bmatrix}, \tag{3.44}$$

$$\hat{\mathbf{B}}_4^{'} = \begin{bmatrix} \hat{A}_2^{'''} & \hat{B}_2^{'''} \\ w^2\hat{A}_2^{'''} & -w^2\hat{B}_2^{'''} \end{bmatrix}, \ \hat{\mathbf{B}}_4^{''} = \begin{bmatrix} \hat{C}_2^{'''} & \hat{E}_2^{'''} \\ w^6\hat{C}_2^{'''} & -w^6\hat{E}_2^{'''} \end{bmatrix}, \tag{3.45}$$

where

$$\hat{\mathbf{C}}_2 = \begin{bmatrix} 1 & 1 \\ 1 & -1 \end{bmatrix}, \ \hat{\mathbf{C}}_2^{'} = \begin{bmatrix} 1 & 1 \\ w^4 & -w^4 \end{bmatrix}, \ \hat{\mathbf{E}}_2 = \begin{bmatrix} 1 & 1 \\ w^2 & -w^2 \end{bmatrix}, \ \hat{\mathbf{E}}_2^{'} = \begin{bmatrix} 1 & 1 \\ w^6 & -w^6 \end{bmatrix},$$

$$\hat{\mathbf{A}}_2^{'''} = \begin{bmatrix} 1 & 1 \\ w^1 & -w^1 \end{bmatrix}, \ \hat{\mathbf{B}}_2^{'''} = \begin{bmatrix} 1 & 1 \\ w^5 & -w^5 \end{bmatrix}, \ \hat{\mathbf{C}}_2^{'''} = \begin{bmatrix} 1 & 1 \\ w^3 & -w^3 \end{bmatrix}, \text{ and } \hat{\mathbf{E}}_2^{'''} = \begin{bmatrix} 1 & 1 \\ w^7 & -w^7 \end{bmatrix}.$$

As will be shown in section 3.2.2, the resultant IDFT matrix will be combined with the WHT matrix to construct the inverse T-transform. DFT ad IDFT operations can be simplified into a butterfly structure as shown in Fig. 3.1.

3.1.1.3 DFT Computational Complexity

Direct implementation of the DFT matrix illustrated in (3.11) requires N^2 and $N(N-1)$ complex multiplications and complex additions, respectively. Whereas, in the case of the butterfly structure for the fast Fourier transform (FFT), as shown in Fig. 3.1, there are $\log_2 N$ stages, and $N/2$ butterfly per stage. This means, the total number of butterflies required to implement size $N \times N$ FFT matrix is $\frac{N}{2}\log_2 N$. The implementation of each butterfly requires one complex multiplication and two complex additions. Consequently, the total complex multiplications C_M and complex additions C_A required to implement $N \times N$ FFT matrix are [3],

$$C_M^{\text{FFT}} = \frac{N}{2}\log_2 N. \tag{3.46}$$

$$C_A^{\text{FFT}} = N\log_2 N. \tag{3.47}$$

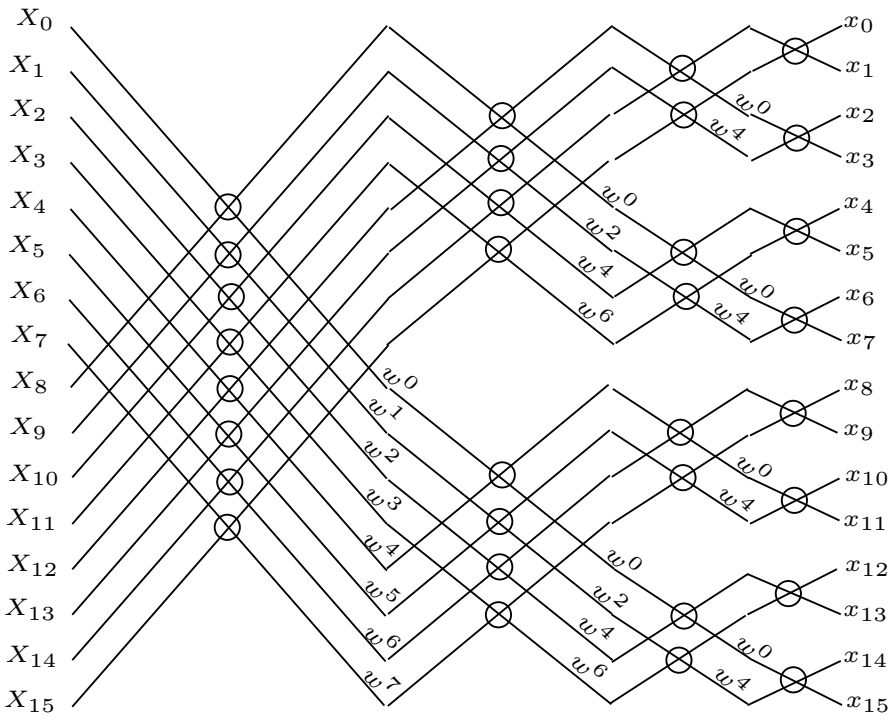

Figure 3.1: The IFFT flowchart with N=16 [1].

3.1.2 Walsh-Hadamard Transforms (WHT)

The notion of employing WHT functions to well-formulated applications, such as nonlinear problems, did not appear until the early 1960's, with the appearance of the works by Corrington [23] and Weiser [24]. Since then, WHT has been successfully applied to engineering, physics and other physical science problems. Moreover, this transform has achieved a noticeable usefulness when combined with the signal processing fields [25], [26]. Furthermore, it has been applied in a medical area and in the geological and biological sciences.

There are many important factors that have led to an increase in the use of WHT. WHT is a set of orthogonal basis functions that is entirely based on elements ± 1. Also, if we compare WHT to DFT, we find it is much simpler and faster to compute. Therefore, WHT implementation requires simple software and hardware. Moreover, entries ± 1, which are the nature of WHT elements, require fewer operations compared to FFT; hence this in turn implies saving in processing time and storage allocation.

Meanwhile, WHT can operate in conjunction with DFT in the case of certain properties that have been previously mentioned, such as orthogonality, Parseval's

theorem, and symmetry. However, circular convolution theorem cannot be accomplished with WHT. Alternatively, dyadic convolution theorem can be applied with WHT. As established by this theorem [27], the WHT of the product of two sequences is equivalent to the dyadic convolution of their WHT. This means,

$$\mathbf{W}[\mathbf{X1}.\mathbf{X2}] = \mathbf{WX1}\overline{\otimes}\mathbf{WX2}, \tag{3.48}$$

where **X1** and **X2** are any two vectors of discrete data in the frequency-domain, and $\overline{\otimes}$ stands for the dyadic convolution. This theorem will be utilised to design a schematic of T-OFDM receivers in the next chapter. All the other properties of WHT are described in details in [28].

Furthermore, WHT elements can be calculated by

$$W_N^{k\hat{m}} = \frac{1}{\sqrt{N}}(-1)^{\sum_{\hat{r}=0}^{\log_2 N-1} k_{\hat{r}}\hat{m}_{\hat{r}}}, \tag{3.49}$$

where $\frac{1}{\sqrt{N}}$ is the normalised factor, $k_{\hat{r}}$ and $\hat{m}_{\hat{r}}$ are the bits representation of the integer values k and $\hat{m}$. Normalization is utilised with WHT to construct identical matrices in both inverse and forward WHT. Therefore,the matrix form of this transform will be considered in greater depth in the next subsequent section.

3.1.2.1 WHT in Matrix Form

The normalised $N \times N$ inverse WHT (IWHT) matrix can be constructed using lower order matrices as

$$\mathbf{W}_N = \overbrace{\mathbf{W}_2 \otimes \mathbf{W}_2 \otimes \cdots \otimes \mathbf{W}_2}^{J}, \tag{3.50}$$

where $N = 2^J$, J is an integer value, $\otimes$ denotes the tensor or Kronecker product, and matrix $\mathbf{W}_2$ defines the 2-points of the Walsh-Hadamard matrix, which can be written as

$$\mathbf{W}_2 = \begin{bmatrix} 1 & 1 \\ 1 & -1 \end{bmatrix}. \tag{3.51}$$

For the sake of clarity, as an example we can give the tensor product of two two-dimensional square matrices as:

$$\begin{bmatrix} a_{1,1} & a_{1,2} \\ a_{2,1} & a_{2,2} \end{bmatrix} \otimes \begin{bmatrix} b_{1,1} & b_{1,2} \\ b_{2,1} & b_{2,2} \end{bmatrix} = \begin{bmatrix} a_{1,1} \begin{bmatrix} b_{1,1} & b_{1,2} \\ b_{2,1} & b_{2,2} \end{bmatrix} & a_{1,2} \begin{bmatrix} b_{1,1} & b_{1,2} \\ b_{2,1} & b_{2,2} \end{bmatrix} \\ a_{2,1} \begin{bmatrix} b_{1,1} & b_{1,2} \\ b_{2,1} & b_{2,2} \end{bmatrix} & a_{2,2} \begin{bmatrix} b_{1,1} & b_{1,2} \\ b_{2,1} & b_{2,2} \end{bmatrix} \end{bmatrix} \tag{3.52a}$$

$$= \begin{bmatrix} a_{1,1}b_{1,1} & a_{1,1}b_{1,2} & a_{1,2}b_{1,1} & a_{1,2}b_{1,2} \\ a_{1,1}b_{2,1} & a_{1,1}b_{2,2} & a_{1,2}b_{2,1} & a_{1,2}b_{2,2} \\ a_{2,1}b_{1,1} & a_{2,1}b_{1,2} & a_{2,2}b_{1,1} & a_{2,2}b_{1,2} \\ a_{2,1}b_{2,1} & a_{2,1}b_{2,2} & a_{2,2}b_{2,1} & a_{2,2}b_{2,2} \end{bmatrix}. \tag{3.52b}$$

Consequently, with an assumption of $N = 16$, i.e. $J = 4$; by substituting (3.51) into (3.50), a normalised $\mathbf{W}_{16}$ matrix can be written as

$$\mathbf{W}_{16} = \frac{1}{4} \begin{bmatrix} 1 & 1 & 1 & 1 & 1 & 1 & 1 & 1 & 1 & 1 & 1 & 1 & 1 & 1 & 1 & 1 \\ 1 & -1 & 1 & -1 & 1 & -1 & 1 & -1 & 1 & -1 & 1 & -1 & 1 & -1 & 1 & -1 \\ 1 & 1 & -1 & -1 & 1 & 1 & -1 & -1 & 1 & 1 & -1 & -1 & 1 & 1 & -1 & -1 \\ 1 & -1 & -1 & 1 & 1 & -1 & -1 & 1 & 1 & -1 & -1 & 1 & 1 & -1 & -1 & 1 \\ 1 & 1 & 1 & 1 & -1 & -1 & -1 & -1 & 1 & 1 & 1 & 1 & -1 & -1 & -1 & -1 \\ 1 & -1 & 1 & -1 & -1 & 1 & -1 & 1 & 1 & -1 & 1 & -1 & -1 & 1 & -1 & 1 \\ 1 & 1 & -1 & -1 & -1 & -1 & 1 & 1 & 1 & 1 & -1 & -1 & -1 & -1 & 1 & 1 \\ 1 & -1 & -1 & 1 & -1 & 1 & 1 & -1 & 1 & -1 & -1 & 1 & -1 & 1 & 1 & -1 \\ 1 & 1 & 1 & 1 & 1 & 1 & 1 & 1 & -1 & -1 & -1 & -1 & -1 & -1 & -1 & -1 \\ 1 & -1 & 1 & -1 & 1 & -1 & 1 & -1 & 1 & -1 & 1 & -1 & 1 & -1 & 1 & -1 \\ 1 & 1 & -1 & -1 & 1 & 1 & -1 & -1 & -1 & -1 & 1 & 1 & -1 & -1 & 1 & 1 \\ 1 & -1 & -1 & 1 & 1 & -1 & -1 & 1 & -1 & 1 & 1 & -1 & -1 & 1 & 1 & -1 \\ 1 & 1 & 1 & 1 & -1 & -1 & -1 & -1 & -1 & -1 & -1 & -1 & 1 & 1 & 1 & 1 \\ 1 & -1 & 1 & -1 & -1 & 1 & -1 & 1 & -1 & 1 & -1 & 1 & 1 & -1 & 1 & -1 \\ 1 & 1 & -1 & -1 & -1 & -1 & 1 & 1 & -1 & -1 & 1 & 1 & 1 & 1 & -1 & -1 \\ 1 & -1 & -1 & 1 & -1 & 1 & 1 & -1 & -1 & 1 & 1 & -1 & 1 & -1 & -1 & 1 \end{bmatrix}. \tag{3.53}$$

In the sequel, as in the case of any orthogonal transform, such as DFT, a WHT matrix in (3.53) can be written as a function of lower order matrices as

$$\mathbf{W}_N = \frac{1}{\sqrt{N}} \begin{bmatrix} \mathbf{W}_{\frac{N}{2}} & \mathbf{W}_{\frac{N}{2}} \\ \mathbf{W}_{\frac{N}{2}} & -\mathbf{W}_{\frac{N}{2}} \end{bmatrix}. \tag{3.54}$$

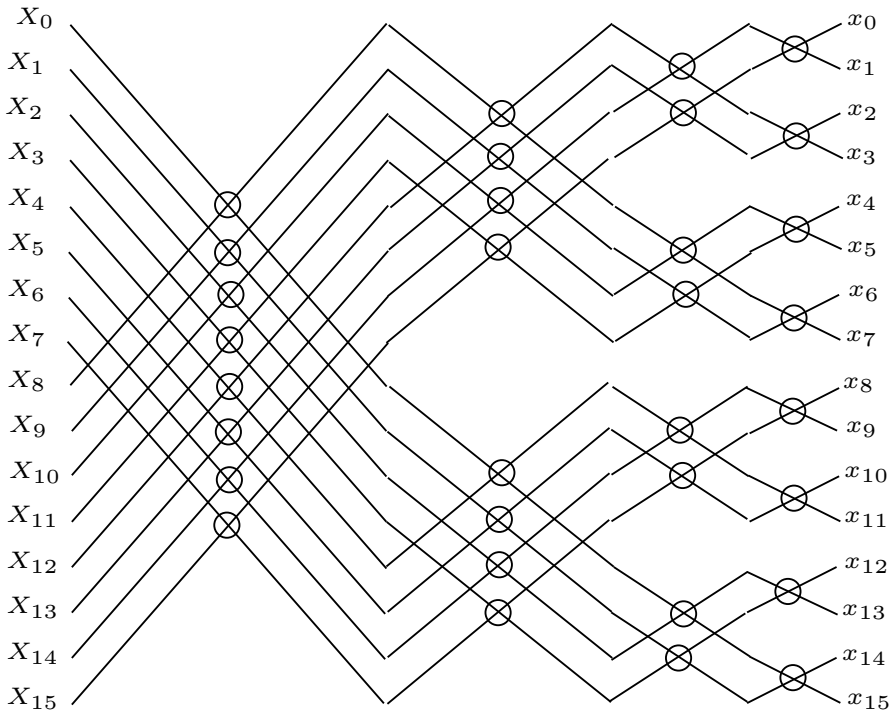

Figure 3.2: The WHT flowchart with N=16.

3.1.2.2 WHT Computational Complexity

Direct implementation of a WHT matrix, as illustrated in (3.53), requires $N(N-1)$ complex additions. Whereas, fast implementation is depicted in the butterfly structure of WHT, as shown in Fig. 3.2; there are $\log_2 N$ stages, and an $N/2$ butterfly per stage. This means, the total butterflies required to implementation a size $N \times N$ WHT matrix is $\frac{N}{2}\log_2 N$. The implementation of each butterfly requires two complex additions. Consequently, the total number of complex additions, C_A, required to implement $N \times N$ WHT matrix is

$$C_A^{\text{WHT}} = N \log_2 N. \tag{3.55}$$

3.2 T-transform

It would be very efficient, if the DFT and WHT were to be performed together using a single fast transform. In fact, this transform was introduced in [2], [3]. In the rest of the thesis, will be referred to as the T-transform. This transform can be applied in many communications techniques, such as multi-carrier code division multiple access (MC-CDMA) and precoded OFDM, as will be shown in the forthcoming chapters.

3.2.1 Forward T-transform (FTT)

The size N forward T-transform (FTT), $\mathbf{T}$ is evaluated as [2], [3]

$$\mathbf{T} = \mathbf{FW}, \tag{3.56}$$

where $\mathbf{F}$ and $\mathbf{W}$ are the normalised $N \times N$ DFT and WHT matrices, as described in equations (3.24) and (3.53), respectively.

3.2.1.1 Normal FTT

Upon substituting (3.25) and (3.54) into (3.56) we obtain the following

$$\begin{aligned} \mathbf{T}_N &= \frac{1}{N} \begin{bmatrix} \mathbf{A}_{\frac{N}{2}} & \mathbf{A}_{\frac{N}{2}} \\ \mathbf{B}_{\frac{N}{2}} & -\mathbf{B}_{\frac{N}{2}} \end{bmatrix} \begin{bmatrix} \mathbf{W}_{\frac{N}{2}} & \mathbf{W}_{\frac{N}{2}} \\ \mathbf{W}_{\frac{N}{2}} & -\mathbf{W}_{\frac{N}{2}} \end{bmatrix} \\ &= \frac{1}{N} \begin{bmatrix} 2\mathbf{A}_{\frac{N}{2}}\mathbf{W}_{\frac{N}{2}} & 0 \\ 0 & 2\mathbf{B}_{\frac{N}{2}}\mathbf{W}_{\frac{N}{2}} \end{bmatrix}, \end{aligned} \tag{3.57}$$

where the lower part of (3.57) permits an extension to a high order transform matrix and the upper part is then the forward transform matrix of order $\frac{N}{2}$ and can be factorised further. Repeating the process $\log_2 N$ times yields the general form, given

by

$$\mathbf{T}_N = \frac{1}{N}\begin{bmatrix} \frac{N}{2}\mathbf{C}_2\mathbf{W}_2 & 0 & 0 & \cdots & 0 & 0 \\ 0 & \frac{N}{2}\mathbf{C'}_2\mathbf{W}_2 & 0 & \cdots & 0 & 0 \\ 0 & 0 & \frac{N}{4}\mathbf{A''}_4\mathbf{W}_4 & \cdots & 0 & 0 \\ \ddots & \ddots & \ddots & \cdots & \ddots & \ddots \\ 0 & 0 & 0 & \cdots & 4\mathbf{B}_{\frac{N}{4}}\mathbf{W}_{\frac{N}{4}} & 0 \\ 0 & 0 & 0 & \cdots & 0 & 2\mathbf{B}_{\frac{N}{2}}\mathbf{W}_{\frac{N}{2}} \end{bmatrix}. \tag{3.58}$$

To show the block diagonal structure of $\mathbf{T}$ in equation (3.58), once again we should consider, for instance, the case $N = 16$ (*note*: as in the case of DFT and WHT, this analysis can be performed for any size). Thus,

$$\mathbf{T}_{16} = \begin{bmatrix} \frac{1}{2}\mathbf{C}_2\mathbf{W}_2 & 0 & 0 & 0 & \\ 0 & \frac{1}{2}\mathbf{C'}_2\mathbf{W}_2 & 0 & 0 & \\ 0 & 0 & \frac{1}{4}\mathbf{A''}_4\mathbf{W}_4 & 0 & 0 \\ 0 & 0 & 0 & \frac{1}{8}(1+w^{-4})\mathbf{B'}_4\mathbf{W}_4 & \frac{1}{8}(1-w^{-4})\mathbf{B''}_4\mathbf{W}_4 \\ 0 & 0 & 0 & \frac{1}{8}(1-w^{-4})\mathbf{B''}_4\mathbf{W}_4 & \frac{1}{8}(1+w^{-4})\mathbf{B'}_4\mathbf{W}_4 \end{bmatrix}, \tag{3.59}$$

where $\mathbf{C}$, $\mathbf{C'}$, $\mathbf{A''}$, $\mathbf{B'}$, and $\mathbf{B''}$ are the sub-matrices which were expressed in section 3.1.1.1. Hence, substituting these matrices with their values in (3.59) yields the

forward T-transform matrix for $N = 16$, which is

$$\mathbf{T}_{16} = \begin{bmatrix}
1 & 0 & 0 & 0 & 0 & 0 & 0 & 0 & 0 & 0 & 0 & 0 & 0 & 0 & 0 & 0 \\
0 & 1 & 0 & 0 & 0 & 0 & 0 & 0 & 0 & 0 & 0 & 0 & 0 & 0 & 0 & 0 \\
0 & 0 & a' & b' & 0 & 0 & 0 & 0 & 0 & 0 & 0 & 0 & 0 & 0 & 0 & 0 \\
0 & 0 & b' & a' & 0 & 0 & 0 & 0 & 0 & 0 & 0 & 0 & 0 & 0 & 0 & 0 \\
0 & 0 & 0 & 0 & c'a' & d'a' & c'b' & d'b' & 0 & 0 & 0 & 0 & 0 & 0 & 0 & 0 \\
0 & 0 & 0 & 0 & d'a' & c'a' & d'b' & c'b' & 0 & 0 & 0 & 0 & 0 & 0 & 0 & 0 \\
0 & 0 & 0 & 0 & e'b' & f'b' & e'a' & f'a' & 0 & 0 & 0 & 0 & 0 & 0 & 0 & 0 \\
0 & 0 & 0 & 0 & f'b' & e'b' & f'a' & e'a' & 0 & 0 & 0 & 0 & 0 & 0 & 0 & 0 \\
0 & 0 & 0 & 0 & 0 & 0 & 0 & 0 & g'c'a' & h'c'a' & g'd'a' & h'd'a' & l'e'b' & m'e'b' & l'f'b' & m'f'b' \\
0 & 0 & 0 & 0 & 0 & 0 & 0 & 0 & h'c'a' & g'c'a' & h'd'a' & g'd'a' & m'e'b' & l'e'b' & m'f'b' & l'f'b' \\
0 & 0 & 0 & 0 & 0 & 0 & 0 & 0 & n'd'a' & o'd'a' & n'c'a' & o'c'a' & p'f'b' & q'f'b' & p'e'b' & q'e'b' \\
0 & 0 & 0 & 0 & 0 & 0 & 0 & 0 & o'd'a' & n'd'a' & o'c'a' & n'c'a' & q'f'b' & p'f'b' & q'e'b' & p'e'b' \\
0 & 0 & 0 & 0 & 0 & 0 & 0 & 0 & g'c'b' & h'c'b' & g'd'b' & h'd'b' & l'e'a' & m'e'a' & l'f'a' & m'f'a' \\
0 & 0 & 0 & 0 & 0 & 0 & 0 & 0 & h'c'b' & g'c'b' & h'd'b' & g'd'b' & m'e'a' & l'e'a' & m'f'a' & l'f'a' \\
0 & 0 & 0 & 0 & 0 & 0 & 0 & 0 & n'd'b' & o'd'b' & n'c'b' & o'c'b' & p'f'a' & q'f'a' & p'e'a' & q'e'a' \\
0 & 0 & 0 & 0 & 0 & 0 & 0 & 0 & o'd'b' & n'd'b' & o'c'b' & n'c'b' & q'f'a' & p'f'a' & q'e'a' & p'e'a'
\end{bmatrix}, \tag{3.60}$$

where $a' = \frac{1+w^{-4}}{2}$, $b' = \frac{1-w^{-4}}{2}$, $c' = \frac{1+w^{-2}}{2}$, $d' = \frac{1-w^{-2}}{2}$, $e' = \frac{1+w^{-6}}{2}$, $f' = \frac{1-w^{-6}}{2}$, $g' = \frac{1+w^{-1}}{2}$, $h' = \frac{1-w^{-1}}{2}$, $l' = \frac{1+w^{-3}}{2}$, $m' = \frac{1-w^{-3}}{2}$, $n' = \frac{1+w^{-5}}{2}$, $o' = \frac{1-w^{-5}}{2}$, $p' = \frac{1+w^{-7}}{2}$ and $q' = \frac{1-w^{-7}}{2}$. Equation (3.60) has a block diagonal structure and more than two thirds of the elements are given as zero. The number of arithmetic operations necessary to multiply by the T-transform matrix is around 1/3 of those involved in multiplying the DFT or IDFT matrices.

3.2.1.2 Fast FTT

The FTT matrix $\mathbf{T}$ described in (3.59) can be transformed into a product of sparse matrices leading to a much faster algorithm for calculating this transform as follows [2], [3].

The resultant matrices of $\frac{1}{2}[\mathbf{C}_2\mathbf{W}_2]$ and $\frac{1}{2}[\mathbf{C'}_2\mathbf{W}_2]$ can be evaluated, respectively, as

$$\frac{1}{2}[\mathbf{C}_2\mathbf{W}_2] = \frac{1}{2}\begin{bmatrix} 1 & 1 \\ 1 & -1 \end{bmatrix} \times \begin{bmatrix} 1 & 1 \\ 1 & -1 \end{bmatrix} \tag{3.61a}$$

$$= \begin{bmatrix} 1 & 0 \\ 0 & 1 \end{bmatrix}. \tag{3.61b}$$

and

$$\frac{1}{2}[\mathbf{C'}_2\mathbf{W}_2] = \frac{1}{2}\begin{bmatrix}1 & w^{-4}\\ 1 & -w^{-4}\end{bmatrix} \times \begin{bmatrix}1 & 1\\ 1 & -1\end{bmatrix} \tag{3.62a}$$

$$= \begin{bmatrix}\frac{(1+w^{-4})}{2} & \frac{(1-w^{-4})}{2}\\ \frac{(1-w^{-4})}{2} & \frac{(1+w^{-4})}{2}\end{bmatrix}. \tag{3.62b}$$

In the same way, the values of $\frac{1}{4}[\mathbf{A''}_4\mathbf{W}_4]$ matrices are computed as

$$\frac{1}{4}[\mathbf{A''}_4\mathbf{W}_4] = \frac{1}{4}\begin{bmatrix}1 & w^{-2} & w^{-4} & w^{-6}\\ 1 & -w^{-2} & w^{-4} & -w^{-6}\\ 1 & w^{-6} & -w^{-4} & w^{-2}\\ 1 & -w^{-6} & -w^{-4} & -w^{-2}\end{bmatrix} \times \begin{bmatrix}1 & 1 & 1 & 1\\ 1 & -1 & 1 & -1\\ 1 & 1 & -1 & -1\\ 1 & -1 & -1 & 1\end{bmatrix} \tag{3.63a}$$

$$= \begin{bmatrix}\frac{(1+w^{-2})}{2}\frac{(1+w^{-4})}{2} & \frac{(1-w^{-2})}{2}\frac{(1+w^{-4})}{2} & \frac{(1+w^{-2})}{2}\frac{(1-w^{-4})}{2} & \frac{(1-w^{-2})}{2}\frac{(1-w^{-4})}{2}\\ \frac{(1-w^{-2})}{2}\frac{(1+w^{-4})}{2} & \frac{(1+w^{-2})}{2}\frac{(1+w^{-4})}{2} & \frac{(1-w^{-2})}{2}\frac{(1-w^{-4})}{2} & \frac{(1+w^{-2})}{2}\frac{(1-w^{-4})}{2}\\ \frac{(1+w^{-6})}{2}\frac{(1-w^{-4})}{2} & \frac{(1-w^{-6})}{2}\frac{(1-w^{-4})}{2} & \frac{(1+w^{-6})}{2}\frac{(1+w^{-4})}{2} & \frac{(1-w^{-6})}{2}\frac{(1+w^{-4})}{2}\\ \frac{(1-w^{-6})}{2}\frac{(1-w^{-4})}{2} & \frac{(1+w^{-6})}{2}\frac{(1-w^{-4})}{2} & \frac{(1-w^{-6})}{2}\frac{(1+w^{-4})}{2} & \frac{(1+w^{-6})}{2}\frac{(1+w^{-4})}{2}\end{bmatrix} \tag{3.63b}$$

$$= \begin{bmatrix}\frac{(1+w^{-2})}{2} & \frac{(1-w^{-2})}{2} & 0 & 0\\ \frac{(1-w^{-2})}{2} & \frac{(1+w^{-2})}{2} & 0 & 0\\ 0 & 0 & \frac{(1+w^{-6})}{2} & \frac{(1-w^{-6})}{2}\\ 0 & 0 & \frac{(1-w^{-6})}{2} & \frac{(1+w^{-6})}{2}\end{bmatrix} \times \begin{bmatrix}\frac{(1+w^{-4})}{2} & 0 & \frac{(1-w^{-4})}{2} & 0\\ 0 & \frac{(1+w^{-4})}{2} & 0 & \frac{(1-w^{-4})}{2}\\ \frac{(1-w^{-4})}{2} & 0 & \frac{(1+w^{-4})}{2} & 0\\ 0 & \frac{(1-w^{-4})}{2} & 0 & \frac{(1+w^{-4})}{2}\end{bmatrix} \tag{3.63c}$$

Also, the matrix of $\frac{1}{8}(1+w^{-4})[\mathbf{B'}_4\mathbf{W}_4]$ can be written as

$$\frac{1}{8}(1+w^{-4})[\mathbf{B'}_4\mathbf{W}_4] = \frac{1}{8}(1+w^{-4})\begin{bmatrix}1 & w^{-1} & w^{-2} & w^{-3}\\ 1 & -w^{-1} & w^{-2} & -w^{-3}\\ 1 & w^{-5} & -w^{-2} & -w^{-7}\\ 1 & -w^{-5} & -w^{-2} & w^{-7}\end{bmatrix} \times \begin{bmatrix}1 & 1 & 1 & 1\\ 1 & -1 & 1 & -1\\ 1 & 1 & -1 & -1\\ 1 & -1 & -1 & 1\end{bmatrix} \tag{3.64a}$$

$$= \begin{bmatrix} \frac{(1+w^{-1})}{2}\frac{(1+w^{-2})}{2}\frac{(1+w^{-4})}{2} & \frac{(1-w^{-1})}{2}\frac{(1+w^{-2})}{2}\frac{(1+w^{-4})}{2} & \frac{(1+w^{-1})}{2}\frac{(1-w^{-2})}{2}\frac{(1+w^{-4})}{2} & \frac{(1-w^{-1})}{2}\frac{(1-w^{-2})}{2}\frac{(1+w^{-4})}{2} \\ \frac{(1-w^{-1})}{2}\frac{(1+w^{-2})}{2}\frac{(1+w^{-4})}{2} & \frac{(1+w^{-1})}{2}\frac{(1+w^{-2})}{2}\frac{(1+w^{-4})}{2} & \frac{(1-w^{-1})}{2}\frac{(1-w^{-2})}{2}\frac{(1+w^{-4})}{2} & \frac{(1+w^{-1})}{2}\frac{(1-w^{-2})}{2}\frac{(1+w^{-4})}{2} \\ \frac{(1+w^{-5})}{2}\frac{(1-w^{-2})}{2}\frac{(1+w^{-4})}{2} & \frac{(1-w^{-5})}{2}\frac{(1-w^{-2})}{2}\frac{(1+w^{-4})}{2} & \frac{(1+w^{-5})}{2}\frac{(1+w^{-2})}{2}\frac{(1+w^{-4})}{2} & \frac{(1-w^{-5})}{2}\frac{(1+w^{-2})}{2}\frac{(1+w^{-4})}{2} \\ \frac{(1-w^{-5})}{2}\frac{(1-w^{-2})}{2}\frac{(1+w^{-4})}{2} & \frac{(1+w^{-5})}{2}\frac{(1-w^{-2})}{2}\frac{(1+w^{-4})}{2} & \frac{(1-w^{-5})}{2}\frac{(1+w^{-2})}{2}\frac{(1+w^{-4})}{2} & \frac{(1+w^{-5})}{2}\frac{(1+w^{-2})}{2}\frac{(1+w^{-4})}{2} \end{bmatrix}. \tag{3.64b}$$

Consequently, the decomposition of (3.64b) in terms of sparse matrices is given by

$$\frac{1}{8}(1+w^{-4})[\mathbf{B'}_4\mathbf{W}_4] = \begin{bmatrix} \frac{(1+w^{-1})}{2} & \frac{(1-w^{-1})}{2} & 0 & 0 \\ \frac{(1-w^{-1})}{2} & \frac{(1+w^{-1})}{2} & 0 & 0 \\ 0 & 0 & \frac{(1+w^{-5})}{2} & \frac{(1-w^{-5})}{2} \\ 0 & 0 & \frac{(1-w^{-5})}{2} & \frac{(1+w^{-5})}{2} \end{bmatrix}$$

$$\times \begin{bmatrix} \frac{(1+w^{-2})}{2} & 0 & \frac{(1-w^{-2})}{2} & 0 \\ 0 & \frac{(1+w^{-2})}{2} & 0 & \frac{(1-w^{-2})}{2} \\ \frac{(1-w^{-2})}{2} & 0 & \frac{(1+w^{-2})}{2} & 0 \\ 0 & \frac{(1-w^{-2})}{2} & 0 & \frac{(1+w^{-2})}{2} \end{bmatrix} \times \begin{bmatrix} \frac{(1+w^{-4})}{2} & 0 & 0 & 0 \\ 0 & \frac{(1+w^{-4})}{2} & 0 & 0 \\ 0 & 0 & \frac{(1+w^{-4})}{2} & 0 \\ 0 & 0 & 0 & \frac{(1+w^{-4})}{2} \end{bmatrix}. \tag{3.65}$$

Similarly, the final three sub-matrices of $\frac{1}{8}(1-w^{-4})[\mathbf{B'}_4\mathbf{W}_4]$ are evaluated as

$$\frac{1}{8}(1-w^{-4})[\mathbf{B'}_4\mathbf{W}_4] = \begin{bmatrix} \frac{(1+w^{-1})}{2} & \frac{(1-w^{-1})}{2} & 0 & 0 \\ \frac{(1-w^{-1})}{2} & \frac{(1+w^{-1})}{2} & 0 & 0 \\ 0 & 0 & \frac{(1+w^{-5})}{2} & \frac{(1-w^{-5})}{2} \\ 0 & 0 & \frac{(1-w^{-5})}{2} & \frac{(1+w^{-5})}{2} \end{bmatrix}$$

$$\times \begin{bmatrix} \frac{(1+w^{-2})}{2} & 0 & \frac{(1-w^{-2})}{2} & 0 \\ 0 & \frac{(1+w^{-2})}{2} & 0 & \frac{(1-w^{-2})}{2} \\ \frac{(1-w^{-2})}{2} & 0 & \frac{(1+w^{-2})}{2} & 0 \\ 0 & \frac{(1-w^{-2})}{2} & 0 & \frac{(1+w^{-2})}{2} \end{bmatrix} \times \begin{bmatrix} \frac{(1-w^{-4})}{2} & 0 & 0 & 0 \\ 0 & \frac{(1-w^{-4})}{2} & 0 & 0 \\ 0 & 0 & \frac{(1-w^{-4})}{2} & 0 \\ 0 & 0 & 0 & \frac{(1-w^{-4})}{2} \end{bmatrix}. \tag{3.66}$$

Furthermore, the $\frac{1}{8}(1-w^{-4})[\mathbf{B''}_4\mathbf{W}_4]$ matrix can be expressed as

$$\frac{1}{8}(1-w^{-4})[\mathbf{B''}_4\mathbf{W}_4] = \begin{bmatrix} \frac{(1+w^{-3})}{2} & \frac{(1-w^{-3})}{2} & 0 & 0 \\ \frac{(1-w^{-3})}{2} & \frac{(1+w^{-3})}{2} & 0 & 0 \\ 0 & 0 & \frac{(1+w^{-7})}{2} & \frac{(1-w^{-7})}{2} \\ 0 & 0 & \frac{(1-w^{-7})}{2} & \frac{(1+w^{-7})}{2} \end{bmatrix}$$

$$\times \begin{bmatrix} \frac{(1+w^{-6})}{2} & 0 & \frac{(1-w^{-6})}{2} & 0 \\ 0 & \frac{(1+w^{-6})}{2} & 0 & \frac{(1-w^{-6})}{2} \\ \frac{(1-w^{-6})}{2} & 0 & \frac{(1+w^{-6})}{2} & 0 \\ 0 & \frac{(1-w^{-6})}{2} & 0 & \frac{(1+w^{-6})}{2} \end{bmatrix} \times \begin{bmatrix} \frac{(1-w^{-4})}{2} & 0 & 0 & 0 \\ 0 & \frac{(1-w^{-4})}{2} & 0 & 0 \\ 0 & 0 & \frac{(1-w^{-4})}{2} & 0 \\ 0 & 0 & 0 & \frac{(1-w^{-4})}{2} \end{bmatrix}. \tag{3.67}$$

By the same method, the matrix $\frac{1}{8}(1+w^{-4})[\mathbf{B''}_4\mathbf{W}_4]$ can be factorized as

$$\frac{1}{8}(1+w^{-4})[\mathbf{B''}_4\mathbf{W}_4] = \begin{bmatrix} \frac{(1+w^{-3})}{2} & \frac{(1-w^{-3})}{2} & 0 & 0 \\ \frac{(1-w^{-3})}{2} & \frac{(1+w^{-3})}{2} & 0 & 0 \\ 0 & 0 & \frac{(1+w^{-7})}{2} & \frac{(1-w^{-7})}{2} \\ 0 & 0 & \frac{(1-w^{-7})}{2} & \frac{(1+w^{-7})}{2} \end{bmatrix}$$

$$\times \begin{bmatrix} \frac{(1+w^{-6})}{2} & 0 & \frac{(1-w^{-6})}{2} & 0 \\ 0 & \frac{(1+w^{-6})}{2} & 0 & \frac{(1-w^{-6})}{2} \\ \frac{(1-w^{-6})}{2} & 0 & \frac{(1+w^{-6})}{2} & 0 \\ 0 & \frac{(1-w^{-6})}{2} & 0 & \frac{(1+w^{-6})}{2} \end{bmatrix} \times \begin{bmatrix} \frac{(1+w^{-4})}{2} & 0 & 0 & 0 \\ 0 & \frac{(1+w^{-4})}{2} & 0 & 0 \\ 0 & 0 & \frac{(1+w^{-4})}{2} & 0 \\ 0 & 0 & 0 & \frac{(1+w^{-4})}{2} \end{bmatrix}. \tag{3.68}$$

3.2.2 Inverse T-transform (ITT)

By following the same steps in section 3.2.1, but by applying suitable parameters, the inverse T-transform (ITT) can be computed. Thus, the $N \times N$ ITT matrix, $\hat{\mathbf{T}}$, can be expressed as [2], [3],

$$\hat{\mathbf{T}} = \hat{\mathbf{W}}\ \hat{\mathbf{F}}, \tag{3.69}$$

where $\hat{\mathbf{W}}$ (=$\mathbf{W}$) and $\hat{\mathbf{F}}$ are the normalised $N \times N$ IWHT and the IFFT matrices, respectively. Using equations (3.13) and (3.18), $\hat{\mathbf{F}}$ will be re-calculated, and rearranged according to column reversed order, as described in (3.36).

3.2.2.1 Normal ITT

Upon substituting (3.37) and (3.54) into (3.69), we obtain the results as

$$\hat{\mathbf{T}} = \frac{1}{N}\begin{bmatrix} 2\hat{\mathbf{W}}_{\frac{N}{2}}\hat{\mathbf{A}}_{\frac{N}{2}} & 0 \\ 0 & 2\hat{\mathbf{W}}_{\frac{N}{2}}\hat{\mathbf{B}}_{\frac{N}{2}} \end{bmatrix}. \tag{3.70}$$

Thus, by the same way used in (3.59), the block diagonal structure of 16×16 $\hat{\mathbf{T}}$ matrix, can be expressed as

$$\hat{\mathbf{T}}_{16} = \begin{bmatrix} \frac{1}{2}\hat{\mathbf{W}}_2\hat{\mathbf{C}}_2 & 0 & 0 & 0 & \\ 0 & \frac{1}{2}\hat{\mathbf{W}}_2\hat{\mathbf{C}}'_2 & 0 & 0 & \\ 0 & 0 & \frac{1}{4}\hat{\mathbf{W}}_4\hat{\mathbf{A}}''_4 & 0 & 0 \\ 0 & 0 & 0 & \frac{1}{8}(1+w^4)\hat{\mathbf{W}}_4\hat{\mathbf{B}}'_4 & \frac{1}{8}(1-w^4)\hat{\mathbf{W}}_4\hat{\mathbf{B}}''_4 \\ 0 & 0 & 0 & \frac{1}{8}(1-w^4)\hat{\mathbf{W}}_4\hat{\mathbf{B}}''_4 & \frac{1}{8}(1+w^4)\hat{\mathbf{W}}_4\hat{\mathbf{B}}'_4 \end{bmatrix}, \tag{3.71}$$

where $\hat{\mathbf{C}}$,$\hat{\mathbf{C}}'$, $\hat{\mathbf{A}}''$, $\hat{\mathbf{B}}'$, and $\hat{\mathbf{B}}''$ are the sub-matrices expressed in section 3.1.1.2. Consequently, size 16×16 ITT matrix can be written as

$$\hat{\mathbf{T}}_{16} = \begin{bmatrix}
1 & 0 & 0 & 0 & 0 & 0 & 0 & 0 & 0 & 0 & 0 & 0 & 0 & 0 & 0 & 0 \\
0 & 1 & 0 & 0 & 0 & 0 & 0 & 0 & 0 & 0 & 0 & 0 & 0 & 0 & 0 & 0 \\
0 & 0 & \hat{a}' & \hat{b}' & 0 & 0 & 0 & 0 & 0 & 0 & 0 & 0 & 0 & 0 & 0 & 0 \\
0 & 0 & \hat{b}' & \hat{a}' & 0 & 0 & 0 & 0 & 0 & 0 & 0 & 0 & 0 & 0 & 0 & 0 \\
0 & 0 & 0 & 0 & \hat{a}'\hat{c}' & \hat{a}'\hat{d}' & \hat{b}'\hat{c}' & \hat{b}'\hat{d}' & 0 & 0 & 0 & 0 & 0 & 0 & 0 & 0 \\
0 & 0 & 0 & 0 & \hat{a}'\hat{d}' & \hat{a}'\hat{c}' & \hat{b}'\hat{d}' & \hat{b}'\hat{c}' & 0 & 0 & 0 & 0 & 0 & 0 & 0 & 0 \\
0 & 0 & 0 & 0 & \hat{b}'\hat{e}' & \hat{b}'\hat{f}' & \hat{a}'\hat{e}' & \hat{a}'\hat{f}' & 0 & 0 & 0 & 0 & 0 & 0 & 0 & 0 \\
0 & 0 & 0 & 0 & \hat{b}'\hat{f}' & \hat{b}'\hat{e}' & \hat{a}'\hat{f}' & \hat{a}'\hat{e}' & 0 & 0 & 0 & 0 & 0 & 0 & 0 & 0 \\
0 & 0 & 0 & 0 & 0 & 0 & 0 & 0 & \hat{a}'\hat{c}'\hat{g}' & \hat{a}'\hat{c}'\hat{h}' & \hat{a}'\hat{d}'\hat{g}' & \hat{a}'\hat{d}'\hat{h}' & \hat{b}'\hat{e}'\hat{l}' & \hat{b}'\hat{e}'\hat{m}' & \hat{b}'\hat{f}'\hat{l}' & \hat{b}'\hat{f}'\hat{m}' \\
0 & 0 & 0 & 0 & 0 & 0 & 0 & 0 & \hat{a}'\hat{c}'\hat{h}' & \hat{a}'\hat{c}'\hat{g} & \hat{a}'\hat{d}'\hat{h}' & \hat{a}'\hat{d}'\hat{g}' & \hat{b}'\hat{e}'\hat{m}' & \hat{b}'\hat{e}'\hat{l}' & \hat{b}'\hat{f}'\hat{m}' & \hat{b}'\hat{f}'\hat{l}' \\
0 & 0 & 0 & 0 & 0 & 0 & 0 & 0 & \hat{a}'\hat{d}'\hat{n}' & \hat{a}'\hat{d}'\hat{o}' & \hat{a}'\hat{c}'\hat{n}' & \hat{a}'\hat{c}'\hat{o}' & \hat{b}'\hat{f}'\hat{p}' & \hat{b}'\hat{f}'\hat{q}' & \hat{b}'\hat{e}'\hat{p}' & \hat{b}'\hat{e}'\hat{q}' \\
0 & 0 & 0 & 0 & 0 & 0 & 0 & 0 & \hat{a}'\hat{c}'\hat{g}' & \hat{a}'\hat{d}'\hat{n}' & \hat{a}'\hat{c}'\hat{o}' & \hat{a}'\hat{c}'\hat{n}' & \hat{b}'\hat{f}'\hat{q}' & \hat{b}'\hat{f}'\hat{p}' & \hat{b}'\hat{e}'\hat{q}' & \hat{b}'\hat{e}'\hat{p}' \\
0 & 0 & 0 & 0 & 0 & 0 & 0 & 0 & \hat{b}'\hat{c}'\hat{g}' & \hat{b}'\hat{c}'\hat{h}' & \hat{b}'\hat{d}'\hat{g}' & \hat{b}'\hat{d}'\hat{h}' & \hat{a}'\hat{e}'\hat{l}' & \hat{a}'\hat{e}'\hat{m}' & \hat{a}'\hat{f}'\hat{l}' & \hat{a}'\hat{f}'\hat{m}' \\
0 & 0 & 0 & 0 & 0 & 0 & 0 & 0 & \hat{b}'\hat{c}'\hat{h}' & \hat{b}'\hat{c}'\hat{g}' & \hat{b}'\hat{d}'\hat{h}' & \hat{b}'\hat{d}'\hat{g}' & \hat{a}'\hat{e}'\hat{m}' & \hat{a}'\hat{e}'\hat{l}' & \hat{a}'\hat{f}'\hat{m}' & \hat{a}'\hat{f}'\hat{l}' \\
0 & 0 & 0 & 0 & 0 & 0 & 0 & 0 & \hat{b}'\hat{d}'\hat{n}' & \hat{b}'\hat{d}'\hat{o}' & \hat{b}'\hat{c}'\hat{n}' & \hat{b}'\hat{c}'\hat{o}' & \hat{a}'\hat{f}'\hat{p}' & \hat{a}'\hat{f}'\hat{q}' & \hat{a}'\hat{e}'\hat{p}' & \hat{a}'\hat{e}'\hat{q}' \\
0 & 0 & 0 & 0 & 0 & 0 & 0 & 0 & \hat{b}'\hat{c}'\hat{g}' & \hat{b}'\hat{d}'\hat{n}' & \hat{b}'\hat{c}'\hat{o}' & \hat{b}'\hat{c}'\hat{n}' & \hat{a}'\hat{f}'\hat{q}' & \hat{a}'\hat{f}'\hat{p}' & \hat{a}'\hat{e}'\hat{q}' & \hat{a}'\hat{e}'\hat{p}'
\end{bmatrix}, \tag{3.72}$$

where $\hat{a}' = \frac{1+w^4}{2}$, $\hat{b}' = \frac{1-w^4}{2}$, $\hat{c}' = \frac{1+w^2}{2}$, $\hat{d}' = \frac{1-w^2}{2}$, $\hat{e}' = \frac{1+w^6}{2}$,$\hat{f}' = \frac{1-w^6}{2}$, $\hat{g}' = \frac{1+w^1}{2}$, $\hat{h}' = \frac{1-w^1}{2}$, $\hat{l}' = \frac{1+w^3}{2}$, $\hat{m}' = \frac{1-w^3}{2}$, $\hat{n}' = \frac{1+w^5}{2}$, $\hat{o}' = \frac{1-w^5}{2}$, $\hat{p}' = \frac{1+w^7}{2}$ and $\hat{q}' = \frac{1-w^7}{2}$. Obviously, the arithmetic operations required to implement the ITT matrix, $\hat{\mathbf{T}}$, defined in equation (3.72) and the FTT matrix, $\mathbf{T}$, are identical.

3.2.2.2 Fast ITT

Similar to the FTT matrix described in (3.59), the ITT matrix described in (3.72) can be transformed into a product of sparse matrices as follows.

The resultant matrices of $\frac{1}{2}[\hat{\mathbf{W}}_2\hat{\mathbf{C}}_2]$ and $\frac{1}{2}[\hat{\mathbf{W}}_2]\hat{\mathbf{C}}_2'$ can be evaluated, respectively, as

$$\frac{1}{2}[\hat{\mathbf{W}}_2\hat{\mathbf{C}}_2] = \frac{1}{2}\begin{bmatrix} 1 & 1 \\ 1 & -1 \end{bmatrix} \times \begin{bmatrix} 1 & 1 \\ 1 & -1 \end{bmatrix} \tag{3.73a}$$

$$= \begin{bmatrix} 1 & 0 \\ 0 & 1 \end{bmatrix}. \tag{3.73b}$$

and

$$\frac{1}{2}[\mathbf{W}_2\hat{\mathbf{C}}_2^{'}] = \frac{1}{2}\begin{bmatrix}1 & 1\\ 1 & -1\end{bmatrix} \times \begin{bmatrix}1 & 1\\ w^4 & -w^4\end{bmatrix} \tag{3.74a}$$

$$= \begin{bmatrix}\frac{(1+w^4)}{2} & \frac{(1-w^4)}{2}\\ \frac{(1-w^4)}{2} & \frac{(1+w^4)}{2}\end{bmatrix}. \tag{3.74b}$$

Similarly, the values of the $\frac{1}{4}[\hat{\mathbf{W}}_4\hat{\mathbf{A}}_4^{''}]$ matrices are computed as

$$\frac{1}{4}[\hat{\mathbf{W}}_4\hat{\mathbf{A}}_4^{''}] = \frac{1}{4}\begin{bmatrix}1 & 1 & 1 & 1\\ 1 & -1 & 1 & -1\\ 1 & 1 & -1 & -1\\ 1 & -1 & -1 & 1\end{bmatrix} \times \begin{bmatrix}1 & 1 & 1 & 1\\ w^2 & -w^2 & w^6 & -w^6\\ w^4 & w^4 & -w^4 & -w^4\\ w^6 & -w^6 & w^2 & -w^2\end{bmatrix} \tag{3.75a}$$

$$= \begin{bmatrix}\frac{(1+w^4)}{2}\frac{(1+w^2)}{2} & \frac{(1+w^4)}{2}\frac{(1-w^2)}{2} & \frac{(1-w^4)}{2}\frac{(1+w^6)}{2} & \frac{(1-w^4)}{2}\frac{(1-w^6)}{2}\\ \frac{(1+w^4)}{2}\frac{(1-w^2)}{2} & \frac{(1+w^4)}{2}\frac{(1+w^2)}{2} & \frac{(1-w^4)}{2}\frac{(1-w^6)}{2} & \frac{(1-w^4)}{2}\frac{(1+w^6)}{2}\\ \frac{(1-w^4)}{2}\frac{(1+w^2)}{2} & \frac{(1-w^4)}{2}\frac{(1-w^2)}{2} & \frac{(1+w^4)}{2}\frac{(1+w^6)}{2} & \frac{(1+w^4)}{2}\frac{(1-w^6)}{2}\\ \frac{(1-w^4)}{2}\frac{(1-w^2)}{2} & \frac{(1-w^4)}{2}\frac{(1+w^2)}{2} & \frac{(1+w^4)}{2}\frac{(1-w^6)}{2} & \frac{(1+w^4)}{2}\frac{(1+w^6)}{2}\end{bmatrix} \tag{3.75b}$$

$$= \begin{bmatrix}\frac{(1+w^4)}{2} & 0 & \frac{(1-w^4)}{2} & 0\\ 0 & \frac{(1+w^4)}{2} & 0 & \frac{(1-w^4)}{2}\\ \frac{(1-w^4)}{2} & 0 & \frac{(1+w^4)}{2} & 0\\ 0 & \frac{(1-w^4)}{2} & 0 & \frac{(1+w^4)}{2}\end{bmatrix} \times \begin{bmatrix}\frac{(1+w^2)}{2} & \frac{(1-w^2)}{2} & 0 & 0\\ \frac{(1-w^2)}{2} & \frac{(1+w^2)}{2} & 0 & 0\\ 0 & 0 & \frac{(1+w^6)}{2} & \frac{(1-w^6)}{2}\\ 0 & 0 & \frac{(1-w^{-6})}{2} & \frac{(1+w^6)}{2}\end{bmatrix}. \tag{3.75c}$$

Also, the matrix of $\frac{1}{8}(1+w^4)[\hat{\mathbf{W}}_4\hat{\mathbf{B}}_4^{'}]$ can be written as

$$\frac{1}{8}(1+w^4)[\hat{\mathbf{W}}_4\hat{\mathbf{B}}_4^{'}] = \frac{1}{8}(1+w^4)\begin{bmatrix}1 & 1 & 1 & 1\\ 1 & -1 & 1 & -1\\ 1 & 1 & -1 & -1\\ 1 & -1 & -1 & 1\end{bmatrix} \times \begin{bmatrix}1 & 1 & 1 & 1\\ w^1 & -w^1 & w^5 & -w^5\\ w^2 & w^2 & -w^2 & -w^2\\ w^3 & -w^3 & -w^7 & w^7\end{bmatrix} \tag{3.76a}$$

$$= \begin{bmatrix} \frac{(1+w^4)}{2}\frac{(1+w^2)}{2}\frac{(1+w^1)}{2} & \frac{(1+w^4)}{2}\frac{(1+w^2)}{2}\frac{(1-w^1)}{2} & \frac{(1+w^4)}{2}\frac{(1-w^2)}{2}\frac{(1+w^5)}{2} & \frac{(1+w^4)}{2}\frac{(1-w^2)}{2}\frac{(1-w^5)}{2} \\ \frac{(1+w^4)}{2}\frac{(1+w^2)}{2}\frac{(1-w^1)}{2} & \frac{(1+w^4)}{2}\frac{(1+w^2)}{2}\frac{(1+w^1)}{2} & \frac{(1+w^4)}{2}\frac{(1-w^2)}{2}\frac{(1-w^5)}{2} & \frac{(1+w^4)}{2}\frac{(1-w^2)}{2}\frac{(1+w^5)}{2} \\ \frac{(1+w^4)}{2}\frac{(1-w^2)}{2}\frac{(1+w^1)}{2} & \frac{(1+w^4)}{2}\frac{(1-w^2)}{2}\frac{(1-w^1)}{2} & \frac{(1+w^4)}{2}\frac{(1+w^2)}{2}\frac{(1+w^5)}{2} & \frac{(1+w^4)}{2}\frac{(1+w^2)}{2}\frac{(1-w^5)}{2} \\ \frac{(1+w^4)}{2}\frac{(1-w^2)}{2}\frac{(1-w^1)}{2} & \frac{(1+w^4)}{2}\frac{(1-w^2)}{2}\frac{(1+w^1)}{2} & \frac{(1+w^4)}{2}\frac{(1+w^2)}{2}\frac{(1-w^5)}{2} & \frac{(1+w^4)}{2}\frac{(1+w^2)}{2}\frac{(1+w^5)}{2} \end{bmatrix}. \tag{3.76b}$$

The decomposition of (3.76b) in terms of sparse matrices is given by

$$\frac{1}{8}(1+w^4)[\hat{\mathbf{W}}_4\hat{\mathbf{B}}_4'] = \begin{bmatrix} \frac{(1+w^4)}{2} & 0 & 0 & 0 \\ 0 & \frac{(1+w^4)}{2} & 0 & 0 \\ 0 & 0 & \frac{(1+w^4)}{2} & 0 \\ 0 & 0 & 0 & \frac{(1+w^4)}{2} \end{bmatrix}$$

$$\times \begin{bmatrix} \frac{(1+w^2)}{2} & 0 & \frac{(1-w^2)}{2} & 0 \\ 0 & \frac{(1+w^2)}{2} & 0 & \frac{(1-w^2)}{2} \\ \frac{(1-w^2)}{2} & 0 & \frac{(1+w^2)}{2} & 0 \\ 0 & \frac{(1-w^2)}{2} & 0 & \frac{(1+w^2)}{2} \end{bmatrix} \times \begin{bmatrix} \frac{(1+w^1)}{2} & \frac{(1-w^1)}{2} & 0 & 0 \\ \frac{(1-w^1)}{2} & \frac{(1+w^1)}{2} & 0 & 0 \\ 0 & 0 & \frac{(1+w^5)}{2} & \frac{(1-w^5)}{2} \\ 0 & 0 & \frac{(1-w^5)}{2} & \frac{(1+w^5)}{2} \end{bmatrix}. \tag{3.77}$$

Then, the final three sub-matrices of $\frac{1}{8}(1-w^4)[\hat{\mathbf{W}}_4\hat{\mathbf{B}}_4']$ are evaluated as

$$\frac{1}{8}(1-w^4)[\hat{\mathbf{W}}_4\hat{\mathbf{B}}_4'] = \begin{bmatrix} \frac{(1-w^4)}{2} & 0 & 0 & 0 \\ 0 & \frac{(1-w^4)}{2} & 0 & 0 \\ 0 & 0 & \frac{(1-w^4)}{2} & 0 \\ 0 & 0 & 0 & \frac{(1-w^4)}{2} \end{bmatrix}$$

$$\times \begin{bmatrix} \frac{(1+w^2)}{2} & 0 & \frac{(1-w^2)}{2} & 0 \\ 0 & \frac{(1+w^2)}{2} & 0 & \frac{(1-w^2)}{2} \\ \frac{(1-w^2)}{2} & 0 & \frac{(1+w^2)}{2} & 0 \\ 0 & \frac{(1-w^2)}{2} & 0 & \frac{(1+w^2)}{2} \end{bmatrix} \times \begin{bmatrix} \frac{(1+w^1)}{2} & \frac{(1-w^1)}{2} & 0 & 0 \\ \frac{(1-w^1)}{2} & \frac{(1+w^1)}{2} & 0 & 0 \\ 0 & 0 & \frac{(1+w^5)}{2} & \frac{(1-w^5)}{2} \\ 0 & 0 & \frac{(1-w^5)}{2} & \frac{(1+w^5)}{2} \end{bmatrix}. \tag{3.78}$$

Furthermore, the $\frac{1}{8}(1-w^4)[\hat{\mathbf{W}}_4\hat{\mathbf{B}}_4''']$ matrix can be expressed as

$$\frac{1}{8}(1-w^4)[\hat{\mathbf{W}}_4\hat{\mathbf{B}}_4'''] = \begin{bmatrix} \frac{(1-w^4)}{2} & 0 & 0 & 0 \\ 0 & \frac{(1-w^4)}{2} & 0 & 0 \\ 0 & 0 & \frac{(1-w^4)}{2} & 0 \\ 0 & 0 & 0 & \frac{(1-w^4)}{2} \end{bmatrix}$$

$$\times \begin{bmatrix} \frac{(1+w^6)}{2} & 0 & \frac{(1-w^6)}{2} & 0 \\ 0 & \frac{(1+w^6)}{2} & 0 & \frac{(1-w^6)}{2} \\ \frac{(1-w^6)}{2} & 0 & \frac{(1+w^6)}{2} & 0 \\ 0 & \frac{(1-w^6)}{2} & 0 & \frac{(1+w^6)}{2} \end{bmatrix} \times \begin{bmatrix} \frac{(1+w^3)}{2} & \frac{(1-w^3)}{2} & 0 & 0 \\ \frac{(1-w^3)}{2} & \frac{(1+w^3)}{2} & 0 & 0 \\ 0 & 0 & \frac{(1+w^7)}{2} & \frac{(1-w^7)}{2} \\ 0 & 0 & \frac{(1-w^7)}{2} & \frac{(1+w^7)}{2} \end{bmatrix}, \quad (3.79)$$

and similarly, the matrix $\frac{1}{8}(1+w^4)[\hat{\mathbf{W}}_4\hat{\mathbf{B}}_4''']$ can be factorized as

$$\frac{1}{8}(1+w^4)[\hat{\mathbf{W}}_4\hat{\mathbf{B}}_4'''] = \begin{bmatrix} \frac{(1+w^4)}{2} & 0 & 0 & 0 \\ 0 & \frac{(1+w^4)}{2} & 0 & 0 \\ 0 & 0 & \frac{(1+w^4)}{2} & 0 \\ 0 & 0 & 0 & \frac{(1+w^4)}{2} \end{bmatrix}$$

$$\times \begin{bmatrix} \frac{(1+w^6)}{2} & 0 & \frac{(1-w^6)}{2} & 0 \\ 0 & \frac{(1+w^6)}{2} & 0 & \frac{(1-w^6)}{2} \\ \frac{(1-w^6)}{2} & 0 & \frac{(1+w^6)}{2} & 0 \\ 0 & \frac{(1-w^6)}{2} & 0 & \frac{(1+w^6)}{2} \end{bmatrix} \times \begin{bmatrix} \frac{(1+w^3)}{2} & \frac{(1-w^3)}{2} & 0 & 0 \\ \frac{(1-w^3)}{2} & \frac{(1+w^3)}{2} & 0 & 0 \\ 0 & 0 & \frac{(1+w^7)}{2} & \frac{(1-w^7)}{2} \\ 0 & 0 & \frac{(1-w^7)}{2} & \frac{(1+w^7)}{2} \end{bmatrix}. \quad (3.80)$$

The above sparse matrices for both FTT and ITT can be extended to any transform length. In the sequel, a flowchart of the T-transform for $N = 16$ is given in Fig. 3.3, where S_0, S_1 and S_2 represent the sections of this transform. The structure of each butterfly is as shown by Fig. 3.4. The output data, o_1 and o_2 for each butterfly are calculated as $o_1 = i_1 - (i_1 - i_2)\hat{w}^n$ and $o_2 = i_2 + (i_1 - i_2)\hat{w}^n$, respectively, where i_1 and i_2 are the input data, and $\hat{w}^n$ is the twiddle factor, which has a value of $\hat{w}^n = (1 - e^{j2\pi n/N})/2$ in the ITT and $\hat{w}^n = (1 - e^{-j2\pi n/N})/2$ in the FTT, within the

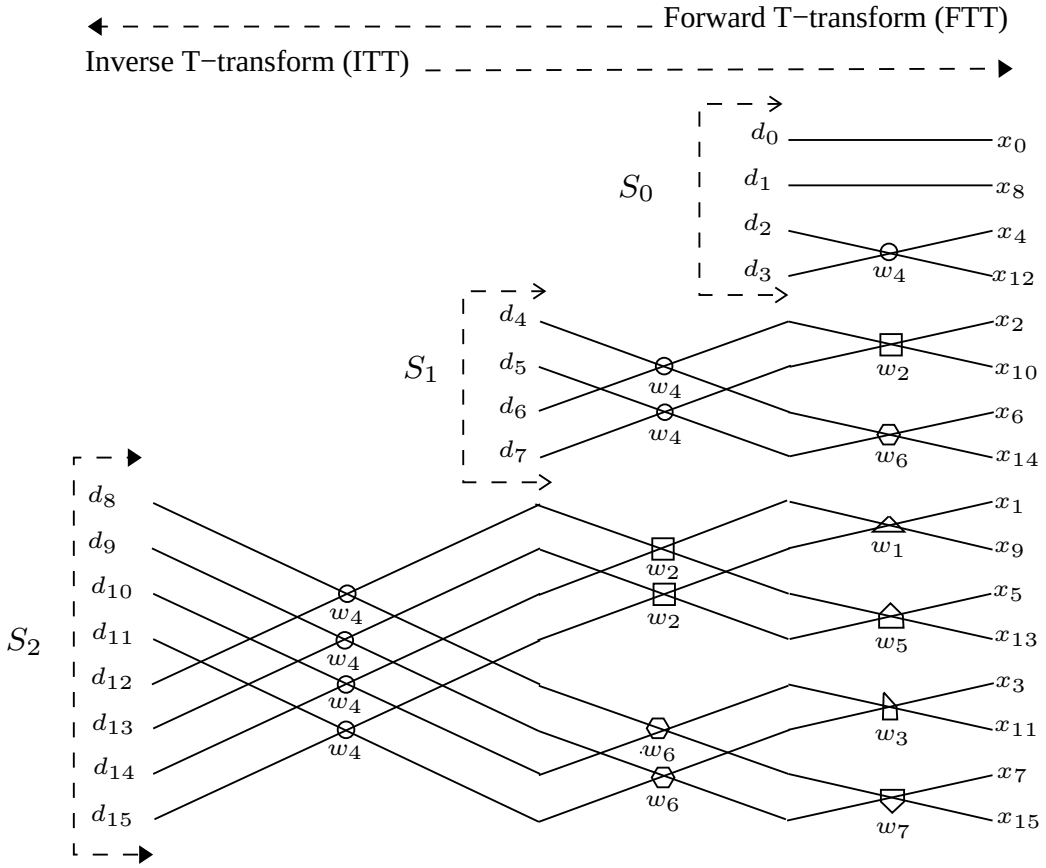

Figure 3.3: T-transform flowchart [2], [3].

index range $n = (0, 1, \ldots, \frac{N}{2} - 1)$.

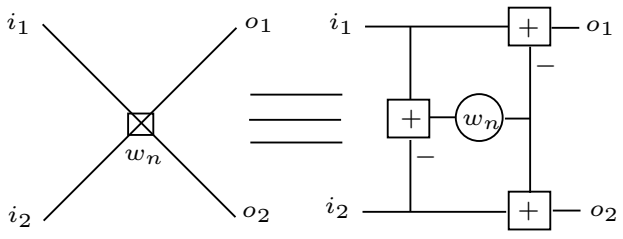

Figure 3.4: One butterfly structure of the T-transform [2], [3].

3.3 Computational Complexity

For any transform to be judged a good candidate for use in practical communication systems, it must be efficient in terms of the computational time and speed involved. This section evaluates the computational costs of the T-transform and compares these with similar transforms.

3.3.1 Evaluation of the T-transform

One advantage of the T-transform is that it has a simple structure and low computational complexity. Usually for radix-2 and $N = 16$ there are four stages required. However, as can be seen from Fig. 3.3, the T-transform relies upon three stages only and in each stage many of the butterflies are zero, therefore do not need to be calculated, reducing the computational complexity. Also, scalability is much easier in the case of the T-transform than it is with other well known transforms, as increasing the transform length involves adding the lower part only, as shown in Fig. 3.3.

3.3.1.1 Direct Implementation of T-transform

Equations (3.60) and (3.72) show that FTT and ITT matrices are sparse matrices, with two thirds of their elements being zero; hence, the direct implementation of each individual matrix will involve $N^2/3$ multiplications and $N(N-1)/3$ additions, while the direct calculation of WHT-IDFT as separated cascaded transforms will involve N^2 complex multiplications and $2N(N-1)$ complex additions. The real operations can be computed based on the fact that the complexity of a single complex multiplication is equivalent to either the complexity of four real multiplications and two real additions (4/2) or to the complexity of three real multiplications and three real additions (3/3) [29]. In this thesis, the (4/2) criterion is adopted. Moreover, one complex addition is deemed equivalent to two real additions. This means that the direct implementation of T-transform requires

$$R_{\mathrm{M}}^{\text{T-transform}} = \frac{4}{3}N^2, \tag{3.81}$$

$$R_{\mathrm{A}}^{\text{T-transform}} = \frac{4}{3}N^2 - \frac{2}{3}N, \tag{3.82}$$

where R_{M} and R_{A} denote real multiplications and real additions, respectively. On the other hand, the direct implementations of IDFT and WHT-IDFT, when they are used as separated cascaded transforms, require

$$R_{\mathrm{M}}^{\mathrm{IDFT}} = 4N^2, \tag{3.83}$$

$$R_{\mathrm{A}}^{\mathrm{IDFT}} = 4N^2 - 2N. \tag{3.84}$$

$$R_{\mathrm{M}}^{\text{WHT-IDFT}} = 4N^2, \tag{3.85}$$

$$R_{\mathrm{A}}^{\text{WHT-IDFT}} = 6N^2 - 4N. \tag{3.86}$$

Further, the total computational complexity in terms of real additions can be expressed as

$$R_{\mathrm{Total}} = R_{\mathrm{A}} + fR_{\mathrm{M}}, \tag{3.87}$$

where f represents the real additions required for each operation involving multiplication. Based on the assumptions in [30] and [31], f will be equal to four in the complexity calculations. In the sequel, the total number of real additions required in the considered transforms can be evaluated as

$$R_{\mathrm{Total}}^{\mathrm{IDFT}} = N(20N - 2). \tag{3.88}$$

$$R_{\mathrm{Total}}^{\text{WHT-IDFT}} = N(22N - 4). \tag{3.89}$$

$$R_{\mathrm{Total}}^{\text{T-transform}} = \frac{N}{3}(20N - 2). \tag{3.90}$$

Direct implementation of transforms is usually advantageous when the transform length is short or when a systolic array implementation is used.

The overall computational complexity reduction ratio (CCRR), η, can be computed as [32],

$$\eta = \left(1 - \frac{C_1}{C_2}\right) \times 100\%, \tag{3.91}$$

where C_1 and C_2 denote the total number of real additions of the T-transform and either IDFT or WHT-IDFT, respectively. With the assumption of $N = 64$, the T-transform achieves 66.66% and 69.70% CCRR compared to IDFT and WHT-IDFT, respectively.

3.3.1.2 Fast Implementation of T-transform

The length of the T-transform is powers of two, so it is amenable to fast algorithms, and it can be deduced from Fig. 3.3 that the N-points T-transform requires $\frac{1}{2}\left[N\log_2(N)-(2N-2)\right]$ butterflies only [2], [3]. Furthermore, each individual butterfly can be expressed as shown in Fig. 3.4. The calculation for each butterfly involves one complex multiplication and three complex additions. Therefore, the total number of complex multiplications and additions, including trivial operations for the calculation of the T-transform, can be calculated as

$$C_{\mathrm{M}}^{\text{T-transform}} = \frac{1}{2}\left[N\log_2(N)-(2N-2)\right], \tag{3.92}$$

$$C_{\mathrm{A}}^{\text{T-transform}} = \frac{3}{2}\left[N\log_2(N)-(2N-2)\right]. \tag{3.93}$$

This means that the real multiplications, R_{M}, and real additions, R_{A}, can be computed as

$$R_{\mathrm{M}}^{\text{T-transform}} = 2\left[N\log_2(N)-(2N-2)\right], \tag{3.94}$$

$$R_{\mathrm{A}}^{\text{T-transform}} = 4\left[N\log_2(N)-(2N-2)\right]. \tag{3.95}$$

while the use of IFFT and WHT-IFFT will involve

$$R_{\mathrm{M}}^{\mathrm{IFFT}} = 2\left[N\log_2(N)\right], \tag{3.96}$$

$$R_{\mathrm{A}}^{\mathrm{IFFT}} = 3N\log_2(N), \tag{3.97}$$

$$R_{\mathrm{M}}^{\text{WHT-IFFT}} = 2\left[N\log_2(N)\right], \tag{3.98}$$

$$R_{\mathrm{A}}^{\text{WHT-IFFT}} = 5N\log_2(N), \tag{3.99}$$

Consequently, the total real additions required in the transforms considered are

$$R_{\mathrm{Total}}^{\mathrm{IFFT}} = 11\left[N\log_2(N)\right]. \tag{3.100}$$

$$R_{\mathrm{Total}}^{\text{WHT-IFFT}} = 13\left[N\log_2(N)\right]. \tag{3.101}$$

$$R_{\mathrm{Total}}^{\text{T-transform}} = 12\left[N\log_2(N)-(2N-2)\right]. \tag{3.102}$$

Table 3.1: Real additions using the fast implementation of the T-transform, IFFT and WHT-IFFT based on single butterfly implementation.

N	Real Additions				
	T-transform	IFFT	η_1 (%)	WHT-IFFT	η_2 (%)
64	3096	4224	26.70	4992	37.98
256	18456	22528	18.07	26624	30.68
1024	98328	112640	12.70	133120	26.16

Eventually, the CCRR of the fast T-transform over IFFT and WHT-IFFT is given in Table 3.1, where η_1 denotes the CCRR of the T-transform over the IFFT, whereas η_2 denotes the CCRR of the T-transform over the WHT-IFFT.

3.4 Chapter Summary

This chapter has discussed the key concept, T-transform, which will be used extensively in this thesis. This chapter has also outlined the fast transforms and concentrated on the discrete Fourier transform (DFT) and Walsh-Hadamard transform (WHT) as two well-known transforms that can be used efficiently for communication purposes. Moreover, the T-transform that combines the WHT and DFT into a single fast orthonormal unitary transform is also discussed in this chapter. In addition, the computational complexity reduction of the T-transform, as compared to WHT/DFT, when used together as separately cascaded transforms is highlighted in this chapter. This chapter serves as a building block for the proposed systems in the next chapters as the T-transform will be used to solve more severe problems such as the multipath dispersion mitigation in the T-OFDM system, peak-to-average-power ratio (PAPR) and complexity reductions, and impulsive noise suppression; as will be explained in chapters 4, 5 and 6, respectively.

CHAPTER 4

Proposed T-OFDM System

This chapter introduces a new multicarrier system using the low computational complexity T-transform that was presented in [2] and discussed in Chapter 3 as a single fast orthonormal unitary transform. The T-transform is used with a new orthogonal frequency division multiplexing (T-OFDM) system instead of WHT and IFFT, leading to a significant improvement in BER. Use of the proposed T-OFDM system, along with three new receivers design, has been found to attain high frequency diversity gain, by combining all the data samples present, resulting in transmission over many subcarriers. Consequently, the detrimental effect arising from channel fading on the subcarrier power is minimized. In addition, a new theoretical BER formulae for the T-OFDM system are derived over AWGN, flat fading, quasi-static (fixed within the entire period of OFDM symbol transmission) frequency selective fading channel models using ZF and MMSE equalisers. Analytical results confirmed by simulations have demonstrated that the proposed T-OFDM system achieves the same BER when measured over AWGN and flat fading channels. Compared to OFDM, T-OFDM has better BER when a MMSE equaliser is used, but it is slightly worse when a ZF equaliser is used.

4.1 Introduction

Despite the attractive features of OFDM system, it is noteworthy that the overall OFDM signal spectrum fades selectively; consequently, certain subcarriers will be severely attenuated by deep fades. In such cases, OFDM does not offer any improvement in performance since no diversity can be exploited to recover the attenuated subcarriers. Therefore, the deleterious effects arising from the multipath propagation on the OFDM system performance have attained considerable attention in the course of recent studies. Many techniques have been investigated to increase its resilience to the negative ramifications of multipath channel dispersion, such as channel coding, adaptive systems and increased diversity; albeit with the added cost of computational complexity and data rate losses.

4.1.1 Channel Coding

In order to increase the resistance of OFDM systems to multipath channel impairments, channel coding (also called forward error correction (FEC)) is invariably used

in conjunction with OFDM systems. There are many types of error correction code that can be used with OFDM-based systems, such as block codes [33], convolutional codes [6] [34], Trellis code [35], turbo codes [4], [36] and low-density parity-check (LDPC) coding [37], [38], [39].

More recent systems have been designed that employ iterative turbo decoding, including turbo codes and LDPC codes, in order to obtain the desired solution. Depending on the system used to employ these codes, they can be concatenated with other codes; for example Reed-Solomon codes, that can be used with systems that implement media *Forward Link Only* (MediaFLO) technology [40], and BCH (BoseChaudhuri-Hocquenghem) codes when used with the second generation digital video broadcasting and satellite (DVB-S2) system [41].

Nevertheless, some severe transmission environments can impact on the coded system's performance by fading a concentrated bit-stream group. Therefore, a bit interleaver is used in conjunction with coding in order to distribute the faded bits throughout the bit-stream rather than in a concentrated manner. In a sequel, the overhead for high computational complexity which increases exponentially in coded systems is the main drawback of such a system. Furthermore, based on the coding rate, some data bandwidth is unnecessarily absorbed; thus, data rate losses increase.

4.1.2 Adaptive System

Many techniques including ADSL and VDSL utilise adaptive transmission to increase their resilience to severe channel conditions. Adaptive transmission can be implemented by applying adaptive modulation, channel coding and power allocation across all sub-carriers, or by passing it individually to each sub-carrier. Based on the feedback information returned from the receiver to the transmitter carrying the channel state information (CSI), various modulation, channel coding and power allocation types are adopted with each OFDM symbol [4]. The main drawbacks of adaptive transmission are [42]:

1. An overhead requiring extra hardware complexity is needed to implement adaptive transmission.

2. There is also a requirement to offer an accurate channel coefficients estimator at the transmitter.

3. Buffering/delay of the input data since the transmission rate varies with the channel conditions.

4. Adaptive systems work efficiently with the slow fading channel, i.e. they are fixed until the CSI cycle is complete, whereas its performance may be impaired by the fast fading channel.

4.1.3 Diversity

The reliability of a signal when measured against multipath dispersion can be improved by increasing the diversity of the signal. Diversity refers to transmitting multiple versions of the same signal using various categories of diversity schemes including:

1. Frequency diversity: The deleterious effect of frequency-selective fading channels can be reduced by transmitting a signal via several subcarriers. A precoder can be used in the frequency-domain in order to increase diversity by spreading itself across each individual subcarrier [43], [44]. Thus, a specific subcarrier that may be destroyed by deep fade can be replaced by other subcarriers. Therefore, a precoded OFDM system achieves a significant BER performance over multipath transmission. However, owing to the use of cascaded transforms, the cost of computational complexity is the main drawback impacting on the use of such a system with different applications.

2. Time diversity: Multiple versions of the same signal are transmitted at different time interval [45], [46].

3. Spatial diversity: The same sequence of data is transmitted via multiple transmission paths. Multiple wires and antennas are used with wired and wireless transmission to provide these types of diversity. Examples of this transmission scheme are multiple input multiple output (MIMO) [47], and space time coding (STC) [48].

4. Polarization diversity: This scheme is similar to the space diversity scheme but antennas are used with different polarization [49].

5. Multiuser diversity: The best user is selected according to its channel to provide a multiuser diversity, i.e. there is an opportunistic user scheduling scheme [50].

6. Cooperative diversity: Antennas are distributed in a manner that allows cooperation among them in order to provide a signal with suitable diversity [51], [52], [53].

Relating to our proposed T-OFDM system, increasing frequency diversity is an attractive proposal describing a potential way to improve OFDM performance over multipath propagation. The precoded or spread OFDM (known as the WHT-OFDM) system has received a considerable amount of attention with the aim of improving the performance of such systems in these environments [54]. Moreover, the spreading of subcarriers using a WHT-OFDM system is a more convenient approach to exploiting wideband channel diversity potential than is using an adaptive system. Furthermore, WHT-OFDM has lower complexity, better bandwidth efficiency, and a better data rate as compared to an adaptive system [4]. In addition, the benefits of adding WHT to an OFDM system to reduce the influence of the selective fading channel on system performance have been demonstrated by [55], [56], [57], and [58]. However, this improvement is only achievable at the expense of the consequent increase in computational complexity resulting from using WHT and the DFT separately in a cascaded form. Therefore, as described in [59] and [60], OFDM can be exploited very efficiently to provide full diversity without spectral losses by using ITT and FTT, which were described in Chapter 3, instead of IFFT and FFT, respectively.

4.2 Proposed T-OFDM System Model

It is important to note that in the remainder of this thesis, T-OFDM is referred to as the uncoded OFDM-based T-transform. Also, this system is analysed with the assumption made that perfect channel response knowledge and perfect time and frequency synchronizations apply.

4.2.1 Transmitter

Fig. 4.1 shows a block diagram of a typical uncoded T-OFDM system transmitter. The transmitted bits are mapped to $1 \times N$ complex modulated signal vector, $\mathbf{X} = [X_0, X_1, ..., X_{N-1}]^T$, which are fed into the ITT to obtain the $1 \times N$ vector of

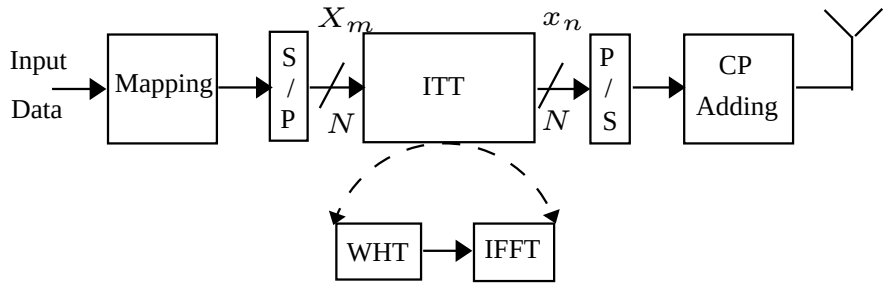

Figure 4.1: T-OFDM transmitter.

the discrete-time complex baseband signal as

$$\mathbf{x} = \hat{\mathbf{T}}\mathbf{X}, \tag{4.1}$$

where $\hat{\mathbf{T}}$ is an ITT matrix. The transmitted vector, $\mathbf{x} = [x_0, x_1, ..., x_{N-1}]^T$, is padded with N_g samples as a CP and convolved with $\hat{L}$-taps CIR, $\mathbf{h} = [h_0, h_1, ..., h_{\hat{L}-1}]$, and then corrupted by the AWGN. The value of N_g is chosen based on a constraint greater than or equal to the maximum path delay of the multipath channel.

At the receiver side, with the assumption of perfect time and frequency synchronization, the received time-domain data vector $\mathbf{r}$, can be expressed as

$$\mathbf{r} = \mathbf{D}\mathbf{x} + \mathbf{z}, \tag{4.2}$$

where $r_n = [r_0, r_1, \ldots, r_{N-1}]^T$, $z_n = [z_0, z_1, \ldots, z_{N-1}]^T$ denotes the AWGN with zero mean and variance σ_z^2, and $\mathbf{D}$ is the circulant channel matrix, which was defined in (2.4).

4.2.2 Receiver

Subsequently, the distorted signal, $\mathbf{r}$, needs to be equalised. In a conventional OFDM system the channel equalization is performed in the frequency-domain by multiplying the received signal with the equaliser sequence [4]. Whereas; in the proposed T-OFDM system, three receivers, designed based on the channel equalization process, can be utilised, as will be clarified in the forthcoming sections.

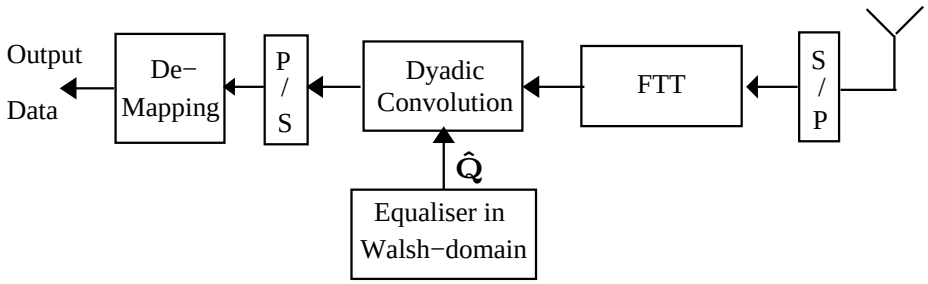

Figure 4.2: Block diagram of ReceiverI.

4.2.2.1 ReceiverI

As has been established in the dyadic convolution theorem [61], the WHT of the product of two sequences is equivalent to the dyadic convolution of their WHT. Thus, as shown in Fig. 4.2, the first approach of channel equalization in the T-OFDM system is accomplished by dyadic convolution between the output signals of the FTT block, $\mathbf{Y}$, and the WHT of equaliser sequence, as proposed in [59]. Consequently, the output of the dyadic convolution process will be

$$\hat{X_k} = \sum_{m=0}^{N-1} Y_{m \oplus k} \, \hat{Q}_m, \tag{4.3}$$

where $m \oplus k$ denotes the bit-by-bit modulo 2 sum of the integers m and k (Exclusive-OR operation between the bits of the binary representation of m and k) and $\hat{\mathbf{Q}}$ is the equaliser sequence in the Walsh-domain, which can be computed as

$$\hat{\mathbf{Q}} = \mathbf{W} \, \mathbf{Q}, \tag{4.4}$$

where $\mathbf{Q}$ is the frequency-domain of the equaliser sequence, as was defined in (2.12).

Due to the relatively high computational cost of Dyadic convolution, alternative two new receivers schemes were proposed in [60] with a significant complexity reduction, as will be described in the following sections.

4.2.2.2 ReceiverII

In ReceiverII, the channel equalization process is similar to the frequency equalization in the conventional OFDM system followed by the WHT of the equalised signal, as

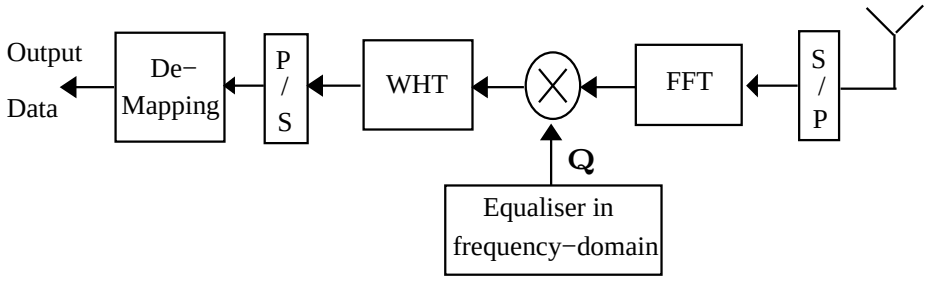

Figure 4.3: Block diagram of ReceiverII.

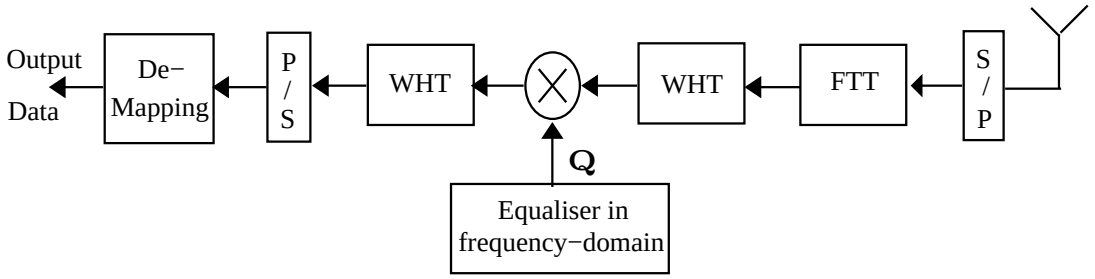

Figure 4.4: Block diagram of ReceiverIII.

shown in Fig. 4.3. Thus, the equalised signal can be expressed as

$$\mathbf{R} = \hat{\mathbf{R}} \cdot \mathbf{Q}, \tag{4.5}$$

where $\{\cdot\}$ denotes point-by-point multiplication of the two vectors, $\hat{\mathbf{R}} = [\hat{R}_0, \hat{R}_1, ..., \hat{R}_{N-1}]^T$ vector is equal to $[\mathbf{F}\ \mathbf{r}]$, and $\mathbf{F}$ denotes the $N \times N$ normalized FFT matrix. As will be verified in the performance analysis section, the T-OFDM system achieves an outstanding BER performance when the MMSE criterion is utilised in the channel equalization process. The key motivation for using the MMSE criterion is its ability to suppress noise enhancement combined with equalizing the channel [4]. Eventually, the resultant signal is given as

$$\hat{\mathbf{X}} = \mathbf{W}\ \mathbf{R}. \tag{4.6}$$

4.2.2.3 ReceiverIII

As shown in Fig. 4.4, the third receiver scheme, which can be utilised with the T-OFDM system is based on using FTT and traditional channel equalization in the

frequency-domain. The channel equalization in this receiver scheme is accomplished by leading the vector $\mathbf{r} = [r_0, r_1, ..., r_{N-1}]^T$ to the FTT block to acquire the signal as

$$\mathbf{Y} = \mathbf{T}\,\mathbf{r}, \tag{4.7}$$

The WHT of the FTT block output is computed as

$$\hat{\mathbf{R}} = \mathbf{W}\mathbf{Y}^T. \tag{4.8}$$

Then, the resultant symbols are multiplied element-by-element, together with the frequency-domain equaliser elements. Therefore, the equalised signal can be expressed as

$$\mathbf{R} = \hat{\mathbf{R}} \cdot \mathbf{Q}, \tag{4.9}$$

Once again, WHT is used to calculate the equalised signal in the Walsh-domain by using equation (4.6).

Eventually, the considered methods of channel equalization with the T-OFDM allow us to perform an equalization in the frequency-domain that is similar to that in the OFDM system. This allows the T-OFDM and OFDM systems to co-exist. In fact, we can use the T-OFDM at the transmitter and the OFDM at the receiver, and vice versa.

4.3 Computational Complexity Calculations

This section evaluates the computational costs of the proposed T-OFDM, comparing it with that of WHT-OFDM system.

4.3.1 Evaluation of WHT-OFDM Complexity

Firstly, we consider the total complex operations required to implement the WHT-OFDM system with the frequency-domain equaliser; including the computation of the WHT and IFFT at the transmitter, FFT and WHT at the receiver, and the N multiplications for the channel equalization process should also be computed. Thus, the total number of complex multiplications C_{M} and complex additions C_{A} in such a

system can be calculated as

$$C_{\mathrm{M}}^{\text{WHT-OFDM}} = N \log_2 N + N, \tag{4.10}$$

$$C_{\mathrm{A}}^{\text{WHT-OFDM}} = 4N \log_2 N. \tag{4.11}$$

Thus, the total number of real multiplications R_{M} and real additions R_{A} can be evaluated as

$$R_{\mathrm{M}}^{\text{WHT-OFDM}} = 4\left[N \log_2 N + N\right], \tag{4.12}$$

$$R_{\mathrm{A}}^{\text{WHT-OFDM}} = 10N \log_2 N + 2N. \tag{4.13}$$

Consequently, the total computational complexity of the WHT-OFDM system in terms of real additions can be expressed as

$$R_{\text{Total}}^{\text{WHT-OFDM}} = R_{\mathrm{A}}^{\text{WHT-OFDM}} + f R_{\mathrm{M}}^{\text{WHT-OFDM}}, \tag{4.14}$$

Based on the same assumption that used in Chapter 3, f will be equal to four in the complexity calculations. In the sequel, the total number of real additions required in the WHT-OFDM system can be evaluated as

$$R_{\text{Total}}^{\text{WHT-OFDM}} = 26N \log N + 18N. \tag{4.15}$$

To ensure a fair comparison, the complexity of the T-OFDM system using the above three receiver schemes should be considered and compared to that of the WHT-OFDM system. Hence, the computational complexity of the T-OFDM system with the three receiver schemes will be evaluated in the following sections.

4.3.2 Evaluation of the T-OFDM System With ReceiverI

As shown in Fig. 4.2, T-OFDM with ReceiverI utilises equalization in the Walsh-domain. Thus, the computational complexity of dyadic convolution should be added to the complexity of ITT and FTT in order to calculate the overall complexity of such a scheme. Basically, as presented in (4.3), the Dyadic convolution operation requires N^2 and $(N-1)N$ complex multiplications and complex additions, respectively. Thus, the total number of complex operations (multiplications and additions) required with

the implementation of T-OFDM/ReceiverI can be expressed as

$$C_{\mathrm{M}}^{\text{T-OFDM/ReceiverI}} = N\log_2 N - (2N-2) + N^2, \tag{4.16}$$

$$C_{\mathrm{A}}^{\text{T-OFDM/ReceiverI}} = 3[N\log_2 N - (2N-2)] + (N-1)N. \tag{4.17}$$

Obviously, this scheme is much more related to computational cost than WHT-OFDM, due to the dyadic convolution operations. Therefore, ReceiverII and ReceiverIII, proposed in [60], have much lower computational complexity and will be explained in the subsequent sections.

4.3.3 Evaluation of the T-OFDM System With ReceiverII

ReceiverII, as shown in Fig. 4.3, requires $\frac{1}{2}N\log_2 N + N$ (the extra N complex multiplications considered are for the channel equalization process) and $2N\log_2 N$ complex multiplications and complex additions, respectively. Consequently, the total computational complexity of the T-OFDM with ReceiverII can be calculated as

$$C_{\mathrm{M}}^{\text{T-OFDM/ReceiverII}} = N\log_2 N + 1, \tag{4.18}$$

$$C_{\mathrm{A}}^{\text{T-OFDM/ReceiverII}} = \frac{7}{2}N\log_2 N - (3N-3). \tag{4.19}$$

This means that the real multiplications, R_{M}, and real additions, R_{A}, associated with this scheme are

$$R_{\mathrm{M}}^{\text{T-OFDM/ReceiverII}} = 4\left[N\log_2 N + 1\right], \tag{4.20}$$

$$R_{\mathrm{A}}^{\text{T-OFDM/ReceiverII}} = 9N\log_2 N - (6N-8). \tag{4.21}$$

Based on the same criterion used before, the total real additions R_{Total} required to implement the T-OFDM system with ReceiverII are

$$R_{\mathrm{Total}}^{\text{T-OFDM/ReceiverII}} = 25N\log N - 6N + 24. \tag{4.22}$$

Consequently, the T-OFDM system with ReceiverII achieves a noticeable CCRR, η, over the WHT-OFDM system as shown in Table 4.1.

Table 4.1: Comparison of the total real arithmetic operations (including equalization) in the proposed T-OFDM/ReceiverII and WHT-OFDM systems.

	Real Operations		
N	T-OFDM/ReceiverII	WHT-OFDM	CCRR, $\eta(\%)$
64	9240	11136	17.03
256	49688	57856	14.12
1024	249880	284672	12.22

4.3.4 Evaluation of the T-OFDM System With ReceiverIII

The third receiver design requires $\frac{1}{2}[N\log_2 N+2]$ and $\frac{7}{2}N\log_2 N-(3N-3)$ complex multiplications and complex additions, respectively. Thus, the overall complexity of the T-OFDM system with ReceiverIII, including the complexity of ITT at the transmitter, and ReceiverIII can be evaluated as

$$C_{\mathrm{M}}^{\text{T-OFDM/ReceiverIII}} = N\log_2 N-(N-2), \tag{4.23}$$

$$C_{\mathrm{A}}^{\text{T-OFDM/ReceiverIII}} = 5N\log_2 N-(6N-6). \tag{4.24}$$

This means that the total real multiplications, R_{M}, and real additions, R_{A}, of the T-OFDM/ReceiverIII system can be calculated as

$$R_{\mathrm{M}}^{\text{T-OFDM/ReceiverIII}} = 4\left[N\log_2 N-(N-2)\right], \tag{4.25}$$

$$R_{\mathrm{A}}^{\text{T-OFDM/ReceiverIII}} = 12N\log_2 N-(14N-16). \tag{4.26}$$

The total real additions required in this scheme are

$$R_{\mathrm{Total}}^{\text{T-OFDM/ReceiverIII}} = 28N\log_2 N-(30N-48). \tag{4.27}$$

Consequently, the considerable CCRR of the T-OFDM with ReceiverIII over the WHT-OFDM is illustrated in Table 4.2.

Table 4.2: Comparison of the total real arithmetic operations (including equalization) in the proposed T-OFDM/ReceiverIII and WHT-OFDM systems.

	Real Operations		
N	T-OFDM/ReceiverIII	WHT-OFDM	CCRR, $\eta(\%)$
64	8880	11136	20.26
256	49712	57856	14.08
1024	256048	284672	10.06

4.4 Performance Analysis

To study the BER performance of the proposed T-OFDM, this section will illustrate the performance analysis of the conventional OFDM and T-OFDM systems across three different channel models, including AWGN, flat-fading, and quasi-static frequency selective fading channel. Furthermore, this analysis will be performed to assist in both QPSK and 16-QAM modulation. As will be verified mathematically and supported by simulation results, the BER performance of the T-OFDM system is a function of the equaliser sequence. In other words, there is a huge difference between the performance of the T-OFDM system with the ZF criterion and its performance when the MMSE criterion is utilised for channel equalization.

The performance of M-PSK and M-QAM systems over the AWGN channel in terms of probability of error (P_e) can be expressed as [14]

$$P_{e\text{M-PSK}} = \frac{\varepsilon}{m} Q\left(\sqrt{2\lambda}\sin(\pi/M)\right), \tag{4.28}$$

$$P_{e\text{M-QAM}} = \frac{(4 - 2^{(2-m/2)})}{m} Q\left(\sqrt{3\lambda/(M-1)}\right), \tag{4.29}$$

where ε stands for the average number of nearest neighbour signal points, and $m = \log_2 M$ is the number of bits in each constellation sample. λ is the SNR, which is computed as σ_X^2/σ_Z^2, where σ_X^2 is the desired signal average power, σ_Z^2 stands for the Gaussian noise average power, and $Q(x)$ is the Q-function of variable x, which can be computed as $Q(x) = \frac{1}{\sqrt{2\pi}} \int_x^\infty e^{-t^2/2}\, dt$.
As presented in [60], the BER performances of the conventional OFDM and the proposed T-OFDM systems over various channel models can be analysed based on the

use of equations (4.28) and (4.29), with the newly computed values of λ. Thus, the general formula to compute the average SNR value of the received signal can be computed as,

$$\lambda = \frac{\text{Desired Signal Average Power}}{\text{Noise Average Power}} = \frac{\sigma_X^2}{\sigma_Z^2}. \tag{4.30}$$

4.4.1 Conventional OFDM Performance Analysis

Basically, a performance analysis of an OFDM system is studied in different impairments in terms of devices distortion or transmission media obstacles [62], [63], [64], [65], [66], [67], [5] and [68]. In this chapter, the performance analysis is presented based on the calculation of the ratio σ_X^2/σ_Z^2 over the various channel models (AWGN channel, flat fading channel, and quasi-static frequency selective fading channel) and the two criteria for linear equalization (ZF and MMSE).

4.4.1.1 AWGN Channel

The performance of M-PSK-OFDM and M-QAM-OFDM systems over the AWGN channel is similar to the performance of M-PSK and M-QAM systems. For a conventional OFDM system across an AWGN channel, let $\mathbf{X}$ be the subcarriers data vector (the desired signal) with the assumption that each independent subcarrier has a variance σ_X^2, so that $E\{\mathbf{X}\mathbf{X}^*\} = \sigma_X^2\mathbf{I}$, where $\mathbf{I}$ is the identity matrix, $\mathbf{Z}$ is the frequency domain of the uncorrelated Gaussian random variables $\mathbf{z}$ with average power σ_Z^2, and $\hat{\mathbf{X}}$ is the received data sequence. This means,

$$\hat{\mathbf{X}} = \mathbf{X} + \mathbf{Z}. \tag{4.31}$$

Based on (4.30), SNR values λ of equation (4.31) can be calculated as

$$\lambda = \frac{E\{|\mathbf{X}|^2\}}{E\{|\mathbf{Z}|^2\}} = \frac{\sigma_X^2}{\sigma_Z^2}, \tag{4.32}$$

where $E\{.\}$ denotes the expectation (statistical averaging) operation. Eventually, the BER performance of OFDM system across AWGN channel can be calculated by substituting equation (4.32) into equations (4.28) and (4.29) for QPSK and 16-QAM, respectively.

4.4.1.2 Flat Fading Channel

With a flat fading channel, i.e. all subcarriers are faded by the same channel coefficient H_k, and a ZF equaliser sequence, the received equalised signal can be calculated as

$$\hat{\mathbf{X}} = \mathbf{X} + \mathbf{Q}^{\mathrm{ZF}}\mathbf{Z}, \tag{4.33}$$

where $Q_k^{\mathrm{ZF}} = 1/H_k$, and H_k is the k-th frequency domain channel coefficient. The SNR of k-th subcarrier will be

$$\lambda_k^{\mathrm{Flat}} = \frac{|X_k|^2}{|Z_k|^2|Q_k^{\mathrm{ZF}}|^2}. \tag{4.34}$$

Thus, the average SNR for the OFDM system over the single path transmission media, i.e. flat fading H_k for all values of k, can be expressed as

$$\lambda^{\mathrm{Flat}} = \frac{\sigma_X^2}{\sigma_Z^2|Q_k^{\mathrm{ZF}}|^2}. \tag{4.35}$$

By substituting equation (4.35) into equations (4.28) and (4.29), the theoretical BER of OFDM with a flat fading channel can be computed as

$$P_{e\mathrm{OFDM_{QPSK}}}^{\mathrm{Flat}} = \frac{\varepsilon}{m} Q\left(\sqrt{2\lambda^{\mathrm{flat}}}\sin(\pi/M)\right), \tag{4.36}$$

$$P_{e\mathrm{OFDM_{16\text{-}QAM}}}^{\mathrm{Flat}} = \frac{(4 - 2^{(2-m/2)})}{m} Q\left(\sqrt{3\lambda^{\mathrm{flat}}/(M-1)}\right). \tag{4.37}$$

Moreover, the same performance is achieved by using the MMSE equaliser. To verify this with an example, the k-th subcarrier, after equalization based on the MMSE criterion can be expressed as

$$\hat{X}_k = \Omega_k^{\mathrm{MMSE}} X_k + Q_k^{\mathrm{MMSE}} Z_k, \tag{4.38}$$

where $Q_k^{\mathrm{MMSE}} = \frac{\lambda_0 H_k^*}{\lambda_0|H_k|^2+1}$ is the optimal approximation of the MMSE criterion and $\Omega_k^{\mathrm{MMSE}} = Q_k^{\mathrm{MMSE}} H_k = \frac{\lambda_0|H_k|^2}{\lambda_0|H_k|^2+1}$. Therefore, the SNR of the k-th subcarrier in equation (4.38) can be computed as

$$\lambda_k = \frac{\left(\Omega_k^{\mathrm{MMSE}}\right)^2 |X_k|^2}{|Q_k^{\mathrm{MMSE}}|^2|Z_k|^2} \tag{4.39a}$$

$$= \frac{|X_k|^2|H_k|^2}{|Z_k|^2}. \tag{4.39b}$$

This verifies that the performance of a conventional OFDM system over a flat fading channel is identical when using ZF or MMSE.

4.4.1.3 Frequency Selective Fading Channel

Over a quasi-static frequency selective (FS) fading channel, each individual subcarrier is faded according to its own channel coefficient H_k. Thus, the SNR for each subcarrier that is faded individually can be written as

$$\lambda_k^{\mathrm{FS}} = \frac{|X_k|^2|H_k|^2}{|Z_k|^2}. \tag{4.40}$$

Substituting equation (4.40) into equations (4.28) and (4.29), the average BER of OFDM with frequency selective fading channel can be expressed as

$$P_{e_{\mathrm{OFDM_{QPSK}}}}^{\mathrm{FS}} = \frac{\varepsilon}{mN} \sum_{k=0}^{N-1} Q\left(\sqrt{2\lambda_k^{\mathrm{FS}}} \sin(\pi/M)\right), \tag{4.41}$$

$$P_{e_{\mathrm{OFDM_{16\text{-}QAM}}}}^{\mathrm{FS}} = \frac{(4 - 2^{(2-m/2)})}{mN} \sum_{k=0}^{N-1} Q\left(\sqrt{3\lambda_k^{\mathrm{FS}}/(M-1)}\right). \tag{4.42}$$

Similar to equation (4.39b), we can verify that the performance of the OFDM system over multipath transmission using MMSE criterion is similar to that when using the ZF criterion.

4.4.2 Proposed T-OFDM System Performance Analysis

In this subsection, the effect of the T-transform based OFDM system on the SNR value will be investigated. For simplicity, the effect of the receiver shown in Fig. 4.3 on the SNR values will be analysed.

4.4.2.1 AWGN Channel

With the Gaussian noise channel, the received signal at the receiver of the T-OFDM system shown in Fig. 4.3 can be expressed as

$$\hat{\mathbf{X}} = \mathbf{X} + \mathbf{W}\ \mathbf{Z}. \tag{4.43}$$

Let each element of noise be expressed as $\rho_n = \frac{1}{\sqrt{N}} \sum_{k=0}^{N-1} Z_k W_{k,n}$. Thus, the variance of ρ can be written as

$$E\{|\rho_n|^2\} = \frac{1}{N^2} \sum_{n=0}^{N-1} \left(\sum_{k=0}^{N-1} Z_k\ W_{n,k} \sum_{k=0}^{N-1} Z_k^*\ W_{k,n}^* \right) \tag{4.44a}$$

$$= \frac{1}{N^2} \sum_{n=0}^{N-1} \left(\sum_{k=0}^{N-1} |Z_k|^2 |W_{n,k}|^2 \right) + \frac{1}{N^2} \sum_{n=0}^{N-1} \left(\sum_{k=0}^{N-1} \sum_{g=0, g\neq k}^{N-1} Z_k Z_g^* W_{k,n} W_{g,n}^* \right). \tag{4.44b}$$

Due to the orthogonality of the basis functions of WHT, the second term of the right hand side of (4.44b) is equal to zero. Consequently,

$$E\{|\rho_n|^2\} = \frac{1}{N^2} \sum_{k=0}^{N-1} |Z_k|^2 \sum_{n=0}^{N-1} |W_{n,k}|^2 \tag{4.45a}$$

$$= \frac{1}{N} \sum_{k=0}^{N-1} |Z_k|^2 \tag{4.45b}$$

$$= \sigma_Z^2. \tag{4.45c}$$

Therefore, the performances of T-OFDM and conventional OFDM systems over an AWGN channel are identical.

4.4.2.2 Flat Fading Channel

With a fading channel, the received equalised signal $\hat{\mathbf{X}}$ can be computed as

$$\hat{\mathbf{X}} = \mathbf{WQF} \left(\mathbf{D}\hat{\mathbf{T}}\mathbf{X} \right) + \mathbf{WQFz}, \tag{4.46a}$$

$$= \mathbf{W}\boldsymbol{\Omega}\hat{\mathbf{R}} + \mathbf{WQZ}, \tag{4.46b}$$

where $E[|\hat{\mathbf{R}}|^2]$=$E[|\mathbf{X}|^2] = \sigma_X^2$.

In the case of a flat fading channel, the values of Ω_k for all k are identical. Therefore, average power of the desired signal can be computed as

$$E|\mathbf{W}\boldsymbol{\Omega}\hat{\mathbf{R}}|^2 = a^2\sigma_X^2 \tag{4.47a}$$

$$= \sigma_X^2 \left(\Omega_k^{\text{MMSE}}\right)^2, \tag{4.47b}$$

where $a = \frac{1}{N}\sum_{k=0}^{N-1} \Omega_k^{\text{MMSE}}$. Then, the noise variance can be computed as

$$E\{\hat{\mathbf{X}}\hat{\mathbf{X}}^*\} - E|\mathbf{W}\boldsymbol{\Omega}\hat{\mathbf{R}}|^2 = \sigma_X^2\frac{1}{N}\sum_{k=0}^{N-1}\left(\Omega_k^{\text{MMSE}}\right)^2 + \sigma_Z^2\frac{1}{N}\sum_{k=0}^{N-1}|Q_k^{\text{MMSE}}|^2 - \sigma_X^2\left(\Omega_k^{\text{MMSE}}\right)^2 \tag{4.48a}$$

$$= \sigma_X^2|\Omega_k^{\text{MMSE}}|^2 + \sigma_Z^2|Q_k^{\text{MMSE}}|^2 - \sigma_X^2\left(\Omega_k^{\text{MMSE}}\right)^2 \tag{4.48b}$$

$$= \sigma_Z^2|Q_k^{\text{MMSE}}|^2, \tag{4.48c}$$

where $k \in \{0 \dots N-1\}$. Substituting (4.47*b*) and (4.48*c*) into (4.30), we obtain

$$\lambda_{k_{\text{T-OFDM}}}^{\text{flat}} = \frac{\sigma_X^2(\Omega_k^{\text{MMSE}})^2}{\sigma_Z^2|Q_k^{\text{MMSE}}|^2} \tag{4.49a}$$

$$= \frac{\sigma_X^2 H_k^2}{\sigma_Z^2}. \tag{4.49b}$$

It is clear from equation (4.49b) that the SNR value of the T-OFDM system over the flat fading channel with MMSE criterion is similar to that with ZF. Also, that it is similar to the SNR value for the conventional OFDM system. Consequently, the performances of both systems over the flat fading channel are identical with MMSE and ZF equalization criteria.

4.4.2.3 Frequency Selective Fading Channel

On the other hand, as will be verified, with a frequency selective fading channel the performance of a T-OFDM system is altered dramatically when using the ZF instead of an MMSE equaliser, or vice-versa. Based on the ZF criterion, the received equalised

signal $\hat{\mathbf{X}}$ can be expressed as

$$\hat{\mathbf{X}} = \mathbf{W}\mathbf{Q}^{\mathrm{ZF}}\mathbf{F}\left(\mathbf{D}\hat{\mathbf{T}}\mathbf{X}\right) + \mathbf{W}\mathbf{Q}^{\mathrm{ZF}}\mathbf{F}\mathbf{z}, \tag{4.50a}$$

$$= \mathbf{X} + \mathbf{W}\mathbf{Q}^{\mathrm{ZF}}\mathbf{Z}. \tag{4.50b}$$

By applying equation (4.30), the SNR values in equation (4.50b) can be evaluated as

$$\lambda_{\text{T-OFDM}}^{\mathrm{ZF}} = \frac{\sigma_X^2}{\underbrace{\sigma_Z^2 \frac{1}{N}\sum_{k=0}^{N-1}|Q_k^{\mathrm{ZF}}|^2}_{\mathbf{\Delta}}}. \tag{4.51}$$

Equation (4.51) verifies that the T-transform will average the value $\mathbf{\Delta}$ on all sub-carriers, which in the initial stages may be helpful, but with a null spectral channel, i.e. $H_k = 0$, the value of $\mathbf{\Delta}$ will be infinity, leading to destruction of the received samples. As a result, the BER performance of the T-OFDM system will degrade seriously owing to the use of the ZF equaliser, and this should be taken into account.

Alternatively, the MMSE criterion can be employed in order to resolve the null channels challenge. Thus, the received signal of the T-OFDM system with MMSE equaliser can be expressed as

$$\hat{\mathbf{X}} = \mathbf{W}\mathbf{\Omega}^{\mathrm{MMSE}}\hat{\mathbf{R}} + \mathbf{W}\mathbf{Q}^{\mathrm{MMSE}}\mathbf{Z}. \tag{4.52}$$

Parts of (4.30) can be recalculated for (4.52) as

$$E|\mathbf{W}\mathbf{\Omega}^{\mathrm{MMSE}}\hat{\mathbf{R}}|^2 = a^2\sigma_X^2. \tag{4.53}$$

Also, the noise variance can be computed as

$$E\{|\hat{\mathbf{X}}|^2\} - E|\mathbf{W}\mathbf{\Omega}^{\mathrm{MMSE}}\hat{\mathbf{R}}|^2 = \sigma_X^2\frac{1}{N}\sum_{k=0}^{N-1}\left(\Omega_k^{\mathrm{MMSE}}\right)^2 + \sigma_Z^2\frac{1}{N}\sum_{k=0}^{N-1}|Q_k^{\mathrm{MMSE}}|^2 - a^2\sigma_X^2 \tag{4.54a}$$

$$= \sigma_X^2\frac{1}{N}\sum_{k=0}^{N-1}\frac{(\lambda|H_k|^2)^2}{(\lambda|H_k|^2+1)^2} + \sigma_X^2\frac{1}{N}\frac{1}{\lambda}\sum_{k=0}^{N-1}\frac{\lambda^2|H_k|^2}{(\lambda|H_k|^2+1)^2} - a^2\sigma_X^2 \tag{4.54b}$$

$$= \sigma_X^2 \frac{1}{N} \sum_{k=0}^{N-1} \frac{\lambda|H_k|^2(1+\lambda|H_k|^2)}{(\lambda|H_k|^2+1)^2} - a^2\sigma_X^2 \tag{4.54c}$$

$$= \sigma_X^2 \frac{1}{N} \sum_{k=0}^{N-1} \frac{\lambda|H_k|^2}{(\lambda|H_k|^2+1)} - a^2\sigma_X^2 \tag{4.54d}$$

$$= \sigma_X^2(a - a^2). \tag{4.54e}$$

Upon substituting (4.54e) and (4.53) into (4.30), we obtain

$$\lambda_{\text{T-OFDM}}^{\text{MMSE}} = \frac{a^2}{a - a^2} \tag{4.55a}$$

$$= \frac{a}{1-a} \tag{4.55b}$$

$$= \frac{\sum_{k=0}^{N-1} \frac{\lambda|H_k|^2}{\lambda|H_k|^2+1}}{N\left(1 - \frac{1}{N}\sum_{k=0}^{N-1} \frac{\lambda|H_k|^2}{\lambda|H_k|^2+1}\right)}. \tag{4.55c}$$

For the sake of simplicity, let $\Lambda_k = \lambda|H_k|^2$. Thus, (4.55c) can be rewritten as

$$\lambda_{\text{T-OFDM}}^{\text{MMSE}} = \frac{\sum_{k=0}^{N-1} \frac{\Lambda_k}{\Lambda_k+1}}{N\left(1 - \frac{1}{N}\sum_{k=0}^{N-1} \frac{\Lambda_k}{\Lambda_k+1}\right)}. \tag{4.56}$$

Basically,

$$\sum_{k=0}^{N-1} \frac{\Lambda_k}{\Lambda_k+1} + \sum_{k=0}^{N-1} \frac{1}{\Lambda_k+1} = N. \tag{4.57}$$

Thus, the denominator of (4.56) can rewritten as

$$N\left(1 - \frac{1}{N}\sum_{k=0}^{N-1} \frac{\Lambda_k}{\Lambda_k+1}\right) = \sum_{k=0}^{N-1} \frac{1}{\Lambda_k+1}. \tag{4.58}$$

By substituting (4.58) into (4.56), the average SNR of T-OFDM with MMSE criterion and across the frequency selective channel can be expressed as

$$\lambda_{\text{T-OFDM}}^{\text{MMSE}} = \frac{\sum_{k=0}^{N-1} \frac{\Lambda_k}{\Lambda_k+1}}{\sum_{k=0}^{N-1} \frac{1}{\Lambda_k+1}}. \tag{4.59}$$

Table 4.3: Simulation results parameters.

Parameter	Value
T-transform size	1024
CP Length	256
Sample Time	88 ns
Band width	10 MHz
Number of transmitted Frames	10^4

Finally, the BER performance of the T-OFDM over frequency selective fading channel with QPSK and 16-QAM, using the MMSE criterion, can be evaluated as

$$Pe^{\mathrm{FS}}_{\text{T-OFDM}_{\mathrm{QPSK}}} = \frac{\varepsilon}{m} Q\left(\sqrt{2\lambda^{\mathrm{MMSE}}_{\text{T-OFDM}}}\sin(\pi/M)\right), \tag{4.60}$$

$$Pe^{\mathrm{FS}}_{\text{T-OFDM}_{\text{16-QAM}}} = \frac{(4-2^{(2-m/2)})}{m} Q\left(\sqrt{3\lambda^{\mathrm{MMSE}}_{\text{T-OFDM}}/(M-1)}\right). \tag{4.61}$$

4.5 Numerical Results

It should be noted that BER performance comparisons are accomplished with assumptions of perfect knowledge in regards to channel response and perfect frequency and time synchronization. Further, the parameters required to investigate the performances of the conventional OFDM and proposed T-OFDM systems are as illustrated in Table 4.3.

In our simulations, the performances of the systems considered were investigated over AWGN, flat fading, and quasi-static frequency selective fading channel models. Also, the semi-analytical curves in Fig. 4.16-4.25 represented the numerical evaluation of the BER formulae that appeared in section 4.4 for both OFDM and T-OFFDM systems.

4.5.1 AWGN Channel

As was proven in section 4.4.2.1 and shown in Fig. 4.5-4.15, due to the orthogonality of the unitary T-transform, the T-OFDM and OFDM systems have an identical performance across the AWGN channel model with QPSK and 16-QAM mapper.

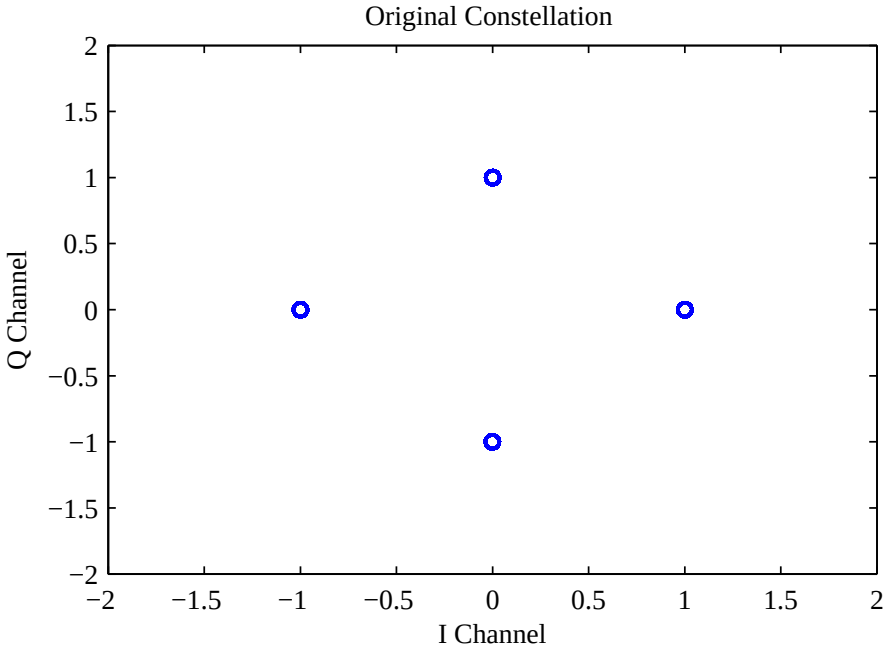

Figure 4.5: Original QPSK constellation.

These results are measured with different values of SNR. The original signal constellation shown in Figs. 4.5 and 4.10 is the output of the mapper on the transmitter side. Whereas, Figs. 4.6 and 4.11 represent the received distorted time-domain samples. Then, the constellation of the symbols in the frequency-domain are depicted in Figs. 4.7, 4.8, 4.9, 4.12 , 4.13 and 4.14. Finally, the BER performances of the conventional OFDM and proposed T-OFDM systems are demonstrated in Fig. 4.15.

4.5.2 Flat Fading Channel

Due to orthogonal transforms, the single transmission path in time-domain is equivalent to flat (non-selective) fading in the frequency-domain, i.e. all subcarriers will fade based on the same channel coefficient, and single path in the Walsh-domain. Therefore, a T-OFDM system using an orthonormal unitary T-transform achieves similar performance to a conventional OFDM system across this type of channel, as shown in Fig. 4.16.

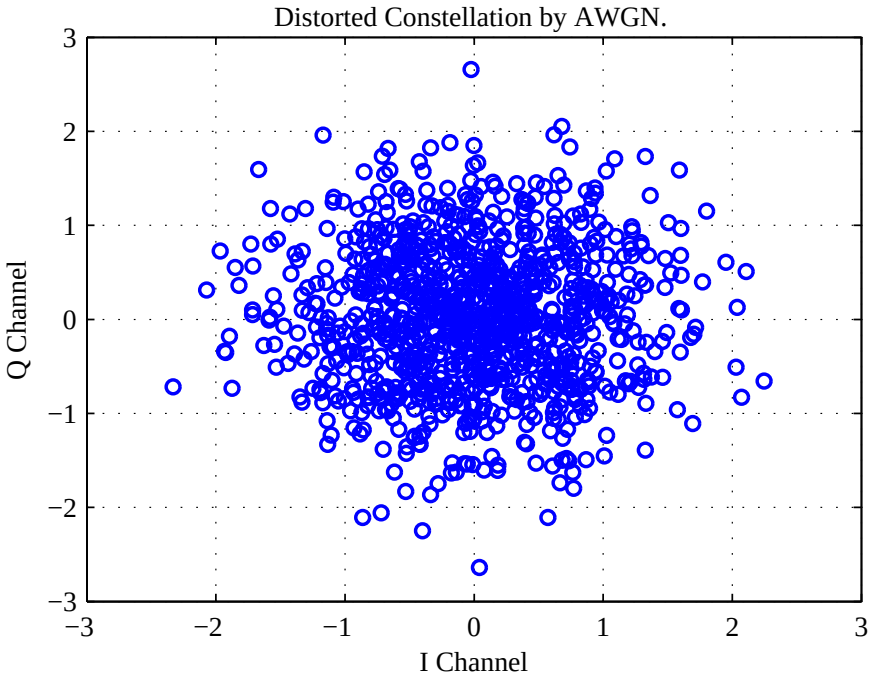

Figure 4.6: Distorted signal by Gaussian noise.

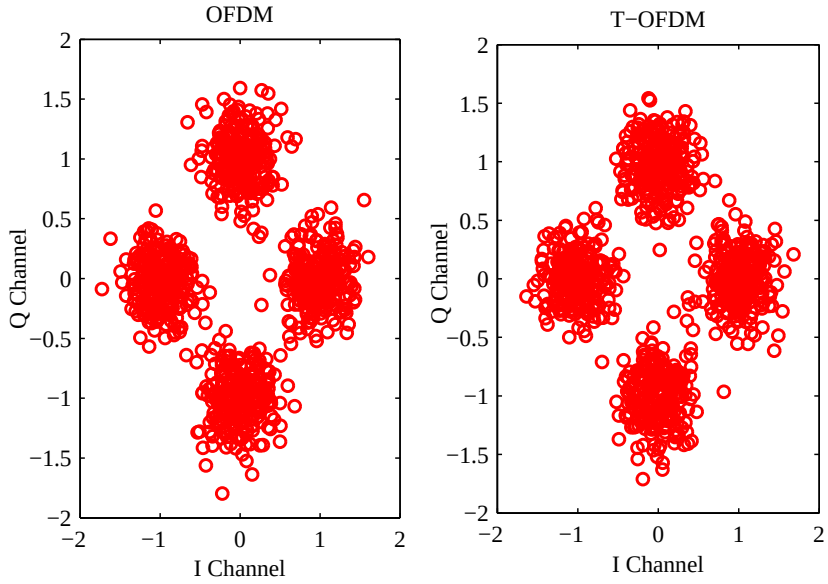

Figure 4.7: Constellation of the T-OFDM and OFDM systems across AWGN with QPSK and SNR=10 dB.

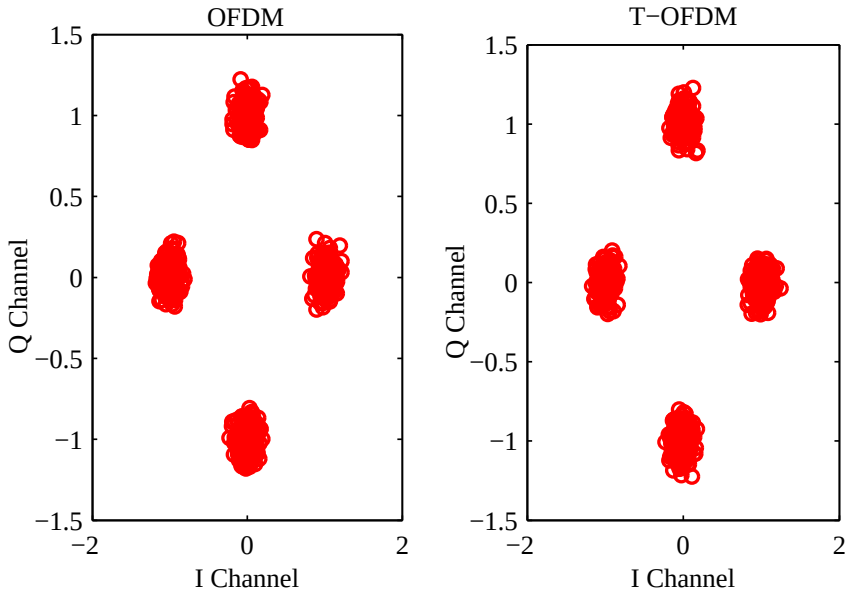

Figure 4.8: Constellation of the T-OFDM and OFDM systems across AWGN with QPSK and SNR=20 dB.

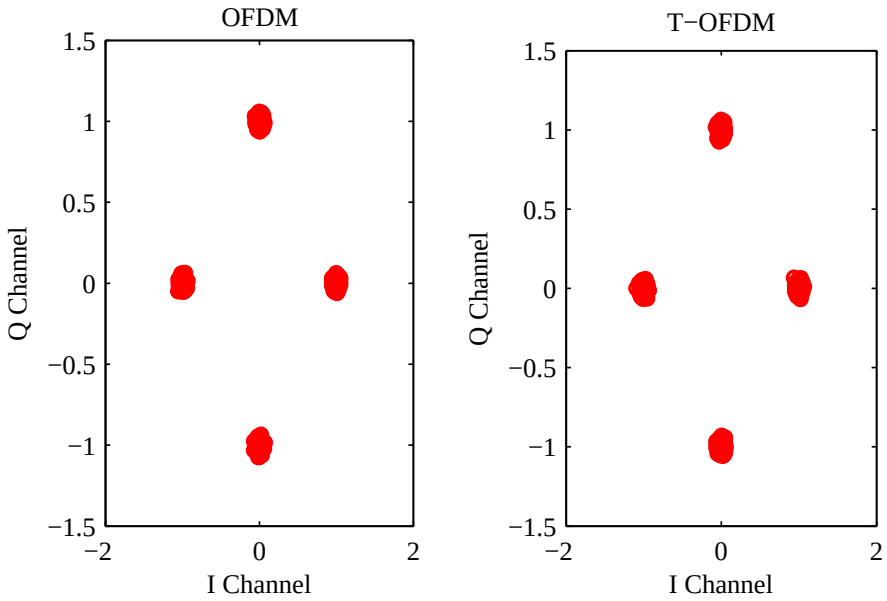

Figure 4.9: Constellation of the T-OFDM and OFDM systems across AWGN with QPSK and SNR=30 dB.

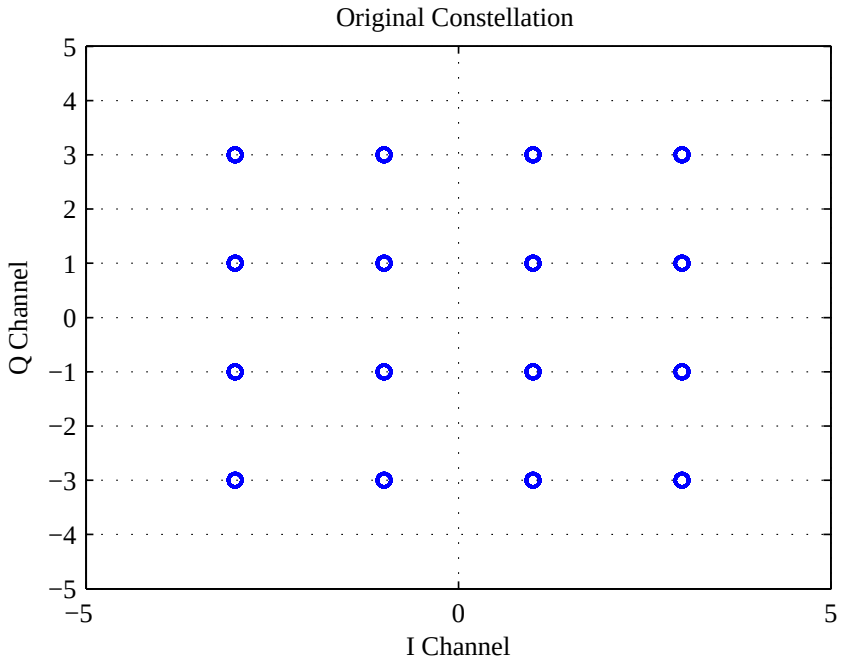

Figure 4.10: Original 16-QAM constellation.

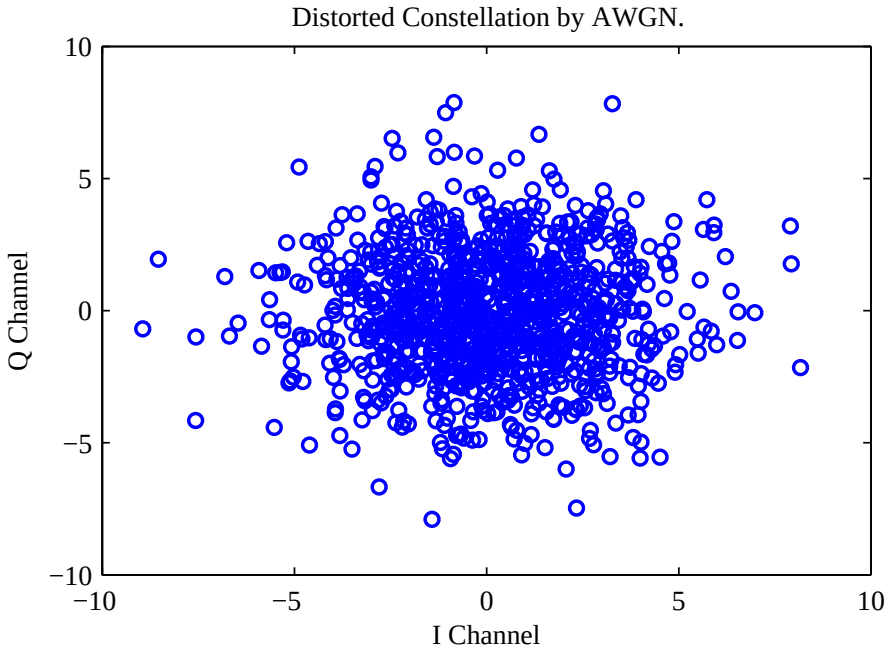

Figure 4.11: Signal distorted by Gaussian noise.

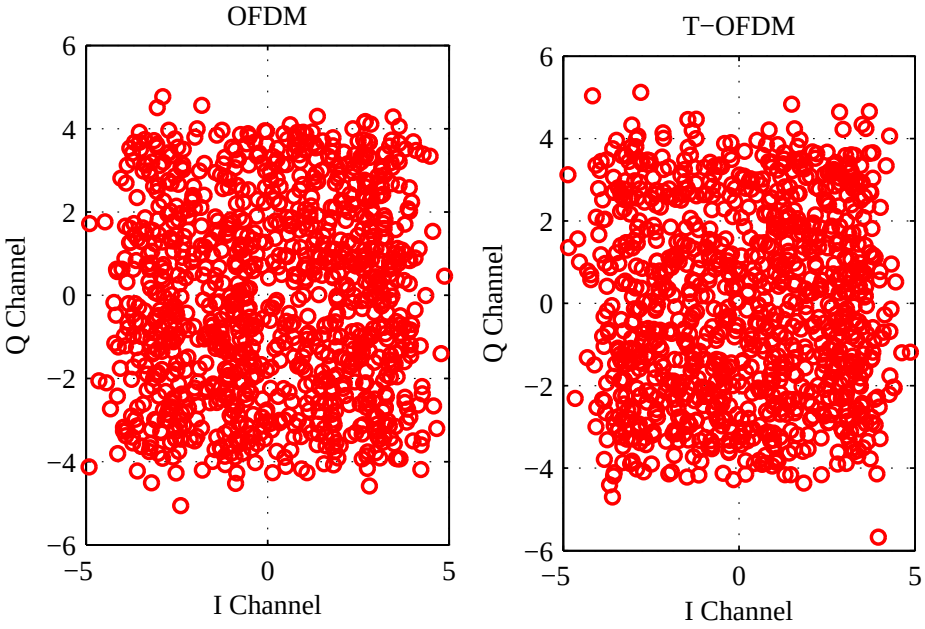

Figure 4.12: Constellation of the T-OFDM and OFDM systems across AWGN with 16-QAM and SNR=10 dB.

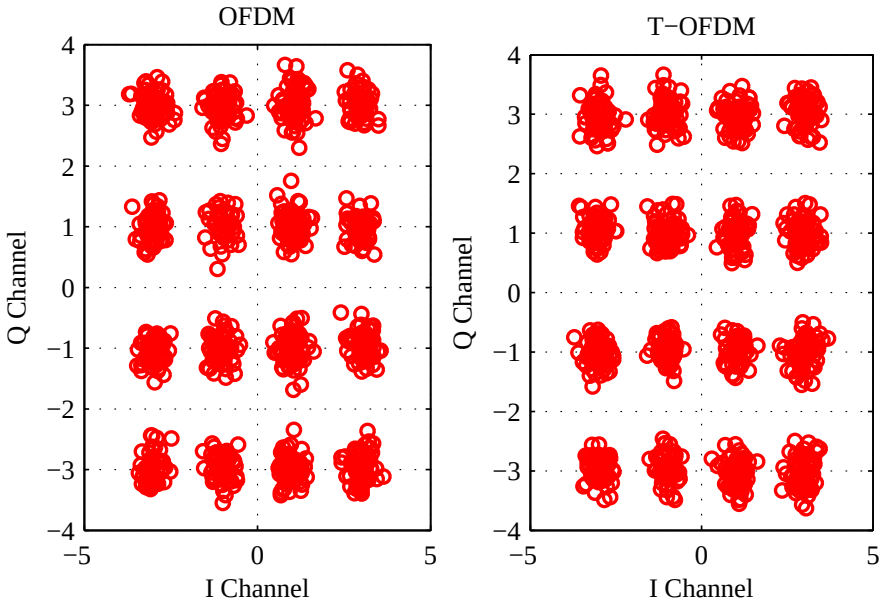

Figure 4.13: Constellation of the T-OFDM and OFDM systems across AWGN with 16-QAM and SNR=20 dB.

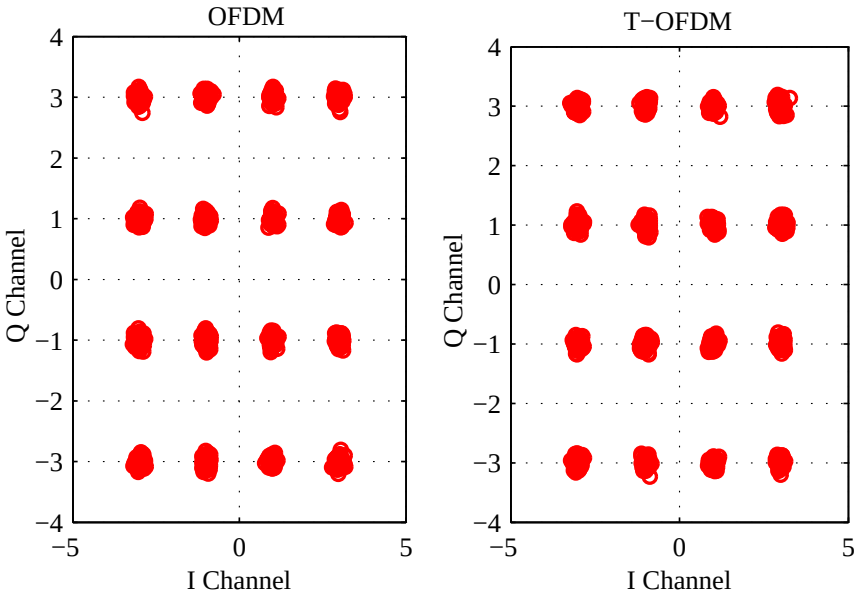

Figure 4.14: Constellation of the T-OFDM and OFDM systems across AWGN with 16-QAM and SNR=30 dB.

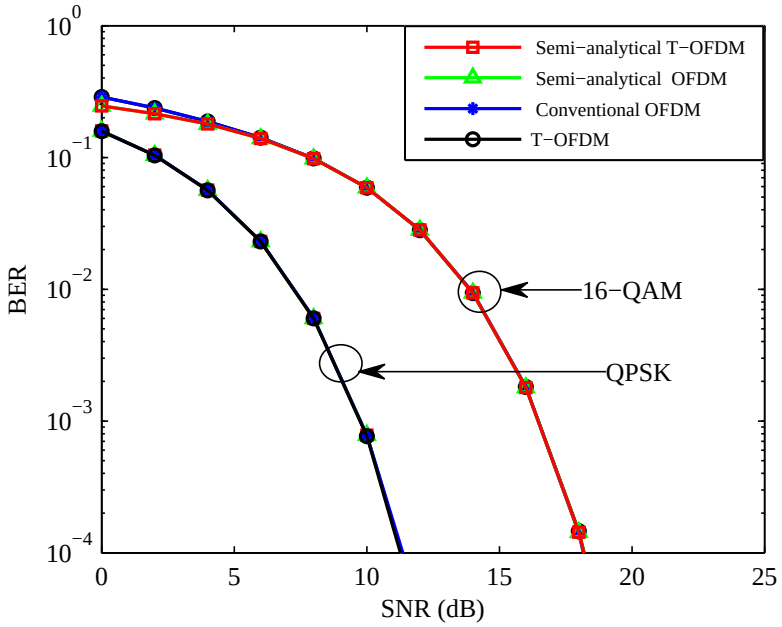

Figure 4.15: BER performance of the T-OFDM and OFDM systems across AWGN channel model, with QPSK and 16-QAM mapping.

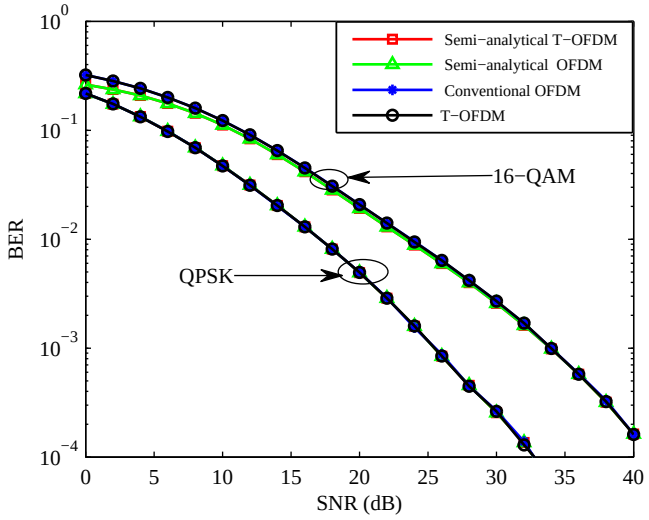

Figure 4.16: BER performance of the T-OFDM and OFDM systems across flat fading channel model, with QPSK and 16-QAM mapping using the MMSE equaliser.

4.5.3 Frequency Selective Fading Channel

In order to investigate the BER performance of the T-OFDM and OFDM systems across the multipath fading channel, the quasi-static pedestrian ITU-B and vehicular ITU-A channel models [16], as were described in Chapter 2, are adopted here as the base of each paths average power. In addition, the performance is evaluated in this research using the ZF and MMSE criteria of equalization.

4.5.3.1 ZF Criterion

As was shown in (4.51), the T-transform will average the value of noise enhancement, $\mathbf{\Delta}$, on all subcarriers, which with a deep fading subchannel, i.e. $H_k \simeq 0$, will be infinity. As a result, serious degradation in the BER performance owing to use ZF equaliser with the T-OFDM system will be apparent, as shown in Fig. 4.17.

4.5.3.2 MMSE Criterion

The MMSE criterion is employed in order to resolve the null subchannels challenge that impacts on the T-OFDM performance when a ZF equaliser is used. Thus, as shown in Fig. 4.18-4.20, even though at low SNR, the T-OFDM system outperforms the conventional OFDM system with QPSK modulation by achieving a SNR gain

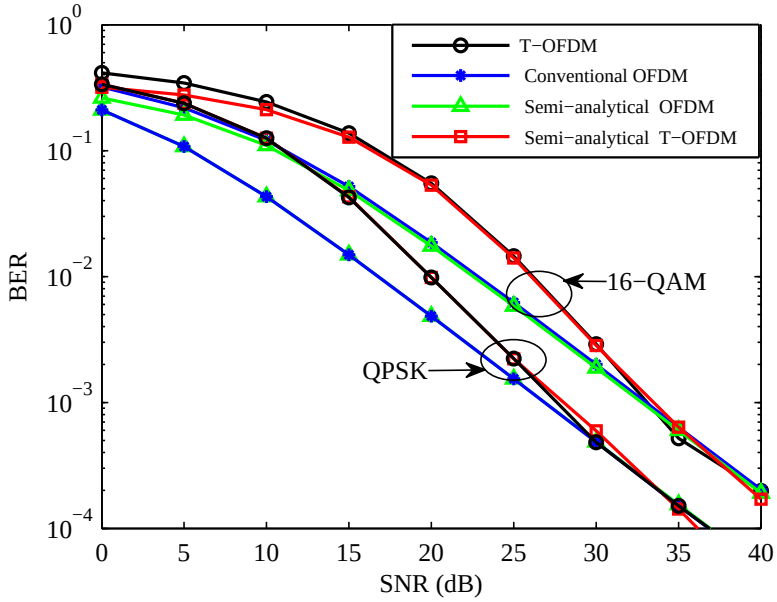

Figure 4.17: BER performance of the T-OFDM and OFDM systems across pedestrian ITU-B channel model, with QPSK and 16-QAM mapping using the ZF equaliser.

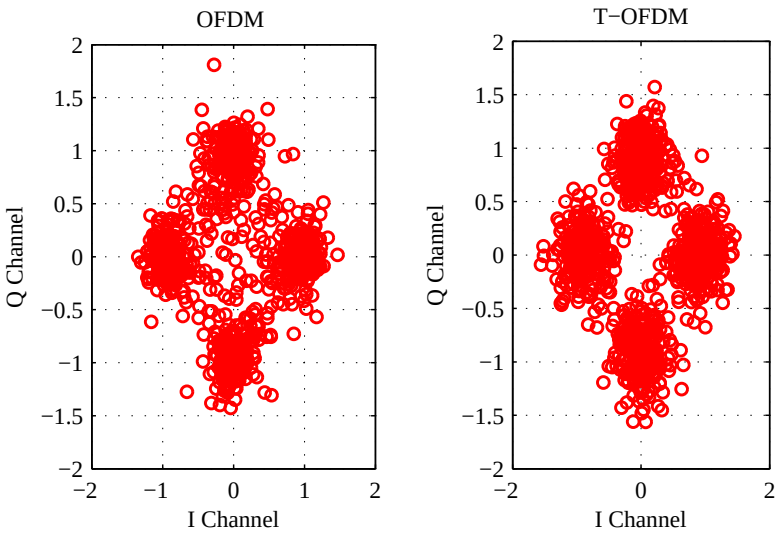

Figure 4.18: Constellation of the T-OFDM and OFDM systems across frequency selective fading channel with QPSK using the MMSE equaliser and SNR=10 dB.

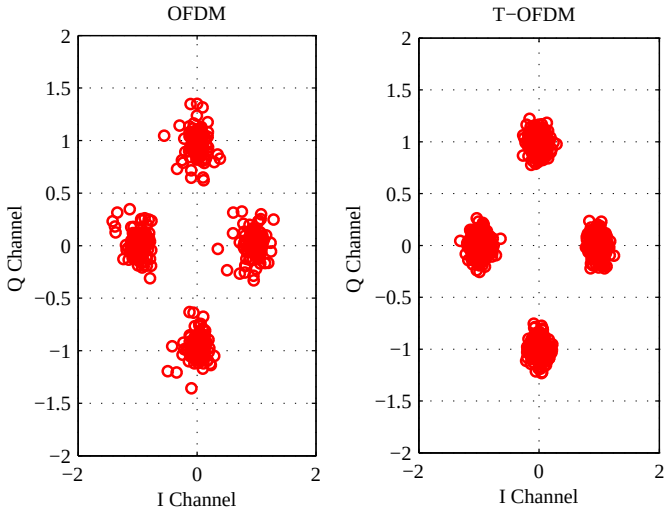

Figure 4.19: Constellation of the T-OFDM and OFDM systems across frequency selective fading channel with QPSK using the MMSE equaliser and SNR=20 dB.

about 16dB measured at 10^{-4} BER over pedestrian ITU-B and vehicular ITU-A channel models. The outstanding BER improvement is a consequence of the frequency diversity attained by the T-transform, which combines the effect of WHT and IDFT. This diversity helps to mitigate the deep fade effect on individual subcarriers. Also, as stated in [69], the conventional OFDM has a drawback, in that the symbol transmitted on the k-th subcarrier cannot be recovered when it is hit by channel zero (i.e. $H_k = 0$). This is not the case in the T-OFDM system, as each symbol is transmitted over many subcarriers.

Nevertheless, with 16-QAM, the OFDM system outperforms the T-OFDM at low SNR as a consequence of the fact that the total received SNR across Rayleigh fading channels is distributed amongst the diverse signals of the proposed transform. Whereas, at high SNR, the T-OFDM system outperforms the conventional OFDM system by achieving a SNR gain about 9dB measured at 10^{-4} BER, as shown in Fig. 4.21-4.25 The precoded-OFDM system [70] performance plots shown in Fig. 4.24 and 4.25 are added for comparative purposes only. The Walsh-Hadamard matrix is utilised as a linear precoder with various column sizes, i.e. various precoder depths, such as 16, 64 and 1024. Evidently, the precoded-OFDM that utilises the $N \times N$ Walsh-Hadamard matrix as a linear precoder and the T-OFDM achieve identical performances.

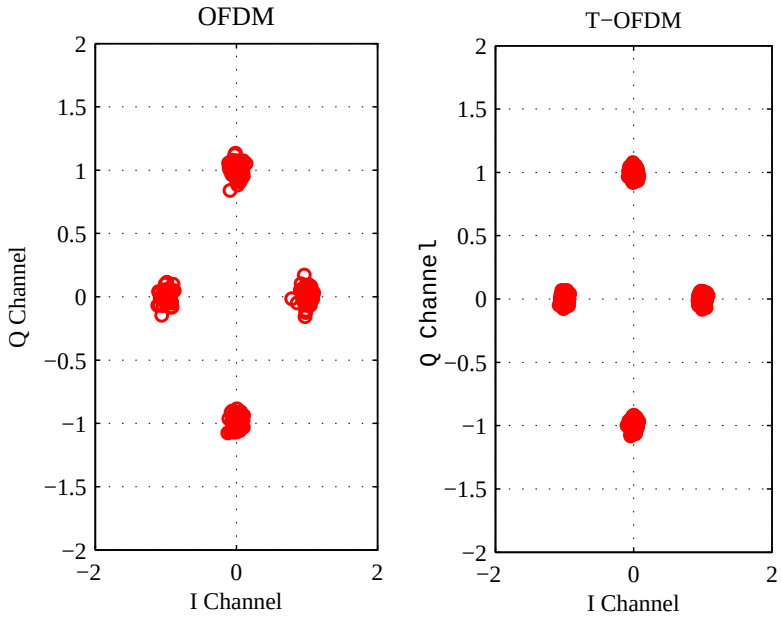

Figure 4.20: Constellation of the T-OFDM and OFDM systems across frequency selective fading channel with QPSK using the MMSE equaliser and SNR=30 dB.

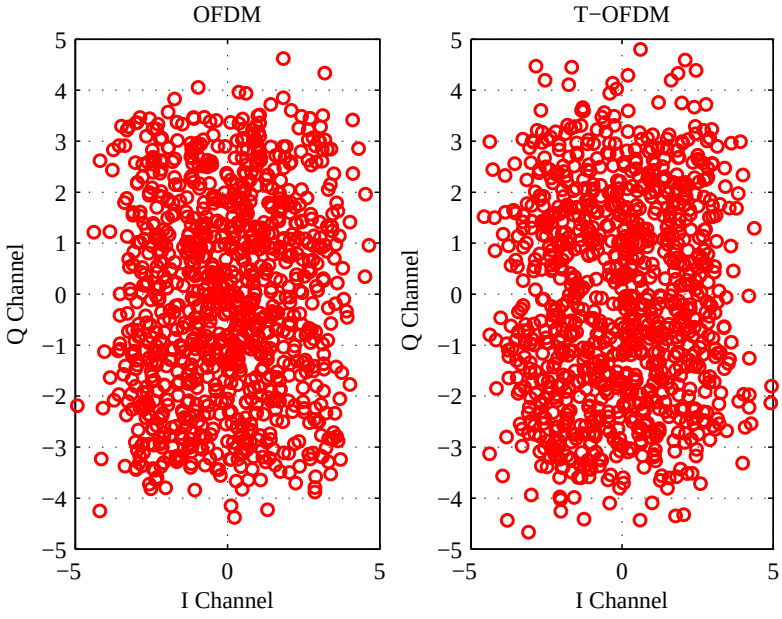

Figure 4.21: Constellation of the T-OFDM and OFDM systems across frequency selective fading channel with 16-QAM using the MMSE equaliser and SNR=10 dB.

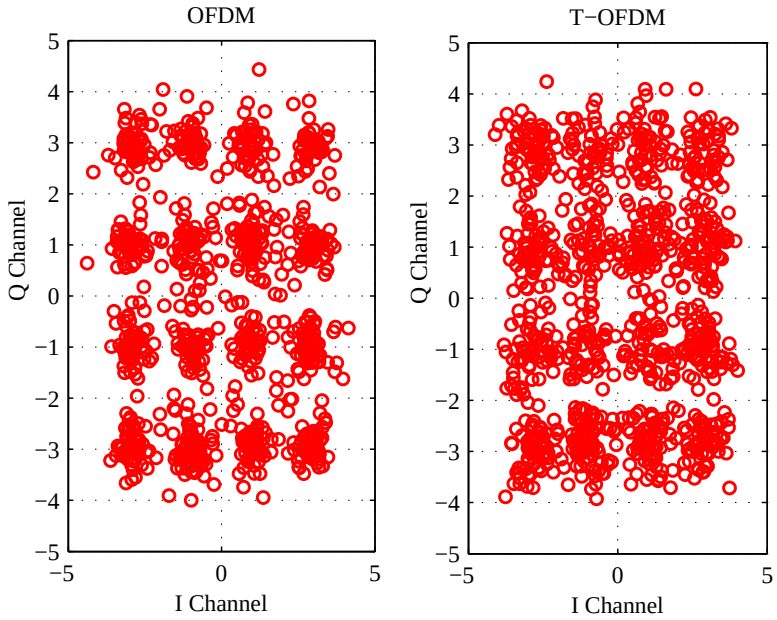

Figure 4.22: Constellation of the T-OFDM and OFDM systems across frequency selective fading channel with 16-QAM using the MMSE equaliser and SNR=20 dB.

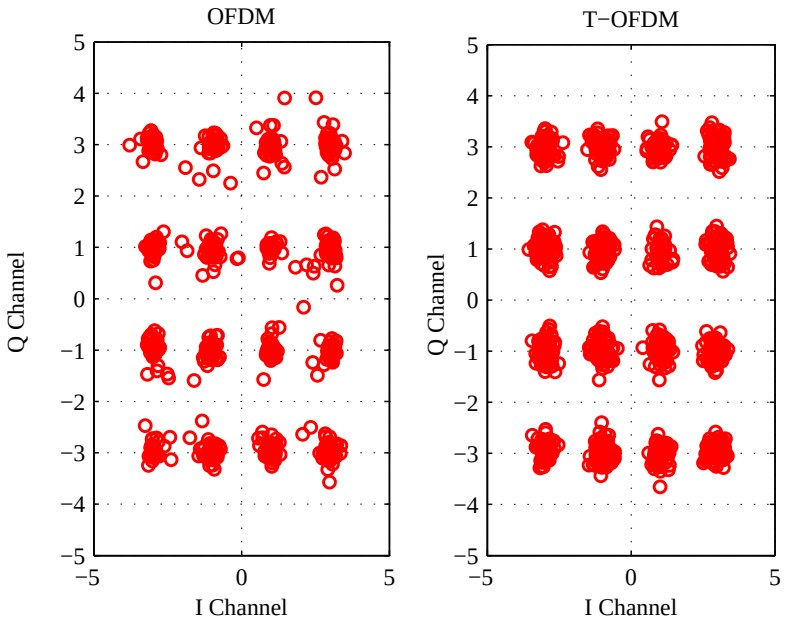

Figure 4.23: Constellation of the T-OFDM and OFDM systems across frequency selective fading channel with 16-QAM using the MMSE equaliser and SNR=30 dB.

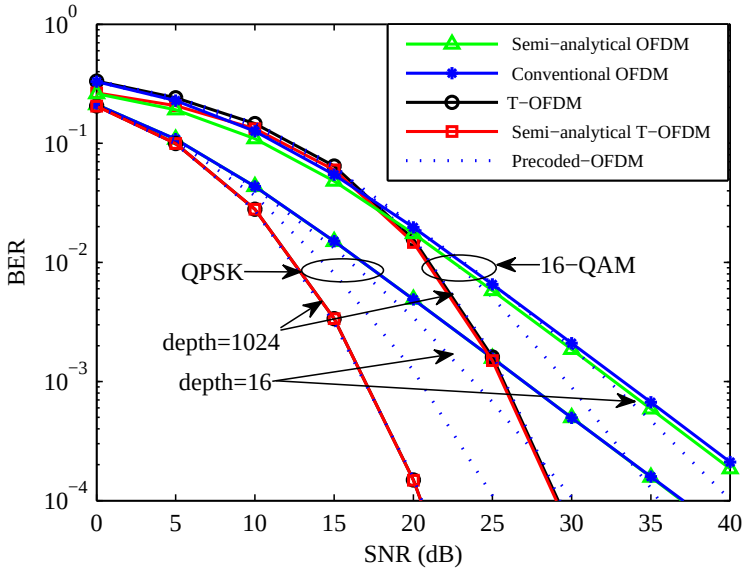

Figure 4.24: BER performance of the T-OFDM, precoded-OFDM with the precoder depth $\in \{16, 64, 1024\}$, and the conventional OFDM systems across the pedestrian ITU-B channel model, with QPSK and 16-QAM mapping using the MMSE equaliser.

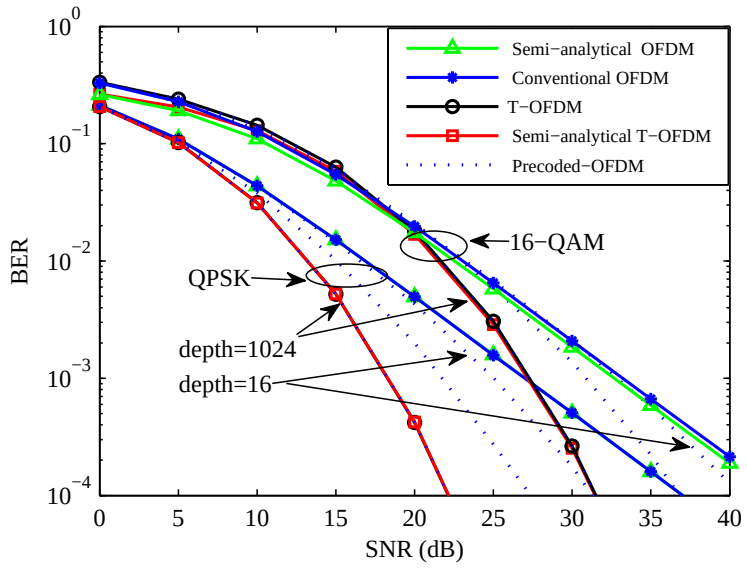

Figure 4.25: BER performance of the T-OFDM, precoded-OFDM with the precoder depth $\in \{16, 64, 1024\}$, and the conventional OFDM systems across vehicular ITU-A channel model, with QPSK and 16-QAM mapping using MMSE equaliser.

4.6 Chapter Summary

This chapter began by briefly presenting the techniques that have been used to date to increase the resilience of OFDM systems to multipath fading channel dispersion. The focus of the chapter has been on the proposed T-OFDM system. This system was implemented using ITT instead of WHT and IFFT at the transmitter side, and FTT instead of FFT and WHT at the receiver side. Three receiver structures that can be used with T-OFDM were presented. Furthermore, the complexity calculations relating to the proposed system and the three receiver schemes were provided and compared with those for the WHT-OFDM system, in order to show the considerable complexity reduction attained with the T-OFDM system. Moreover, the theoretical analysis of the proposed system given over three channel models (AWGN, flat fading, frequency selective fading) was introduced in this chapter. Analytical results confirmed by simulations demonstrated that the proposed T-OFDM system achieves the same BER as a conventional OFDM over AWGN and flat fading channels. Whereas, T-OFDM is found to have better BER when the MMSE equaliser is used, but slightly worse when a ZF equaliser is used. The next chapter presents the use of a T-OFDM system to reduce PAPR. In addition, three schemes T-SLM, T-PTS-I, T-PTS-II are proposed to achieve lower PAPR, lower computational complexity, and better BER, when compared with conventional SLM and PTS schemes.

CHAPTER 5

PAPR of T-OFDM System

In this chapter, the performances of T-OFDM system in terms of PAPR reduction, and BER performance in the presence of high-power amplifier (HPA) are investigated. Thereafter, selective mapping (SLM) and partial transmit sequence (PTS) are described as attractive solutions mitigating the negative ramifications of high peak power in cases of a transmitted signal in OFDM systems. To date, high computational complexity requirements and redundant side information (SI) bits have been identified as the main limitations of such techniques. The high computational complexity inherent to these techniques is mainly results from the need to perform several IFFT operations and phase optimisations on the transmitter side. Consequently, many studies have been conducted to reduce the computational complexity requirements of the SLM and PTS. Moreover, the attractive features of T-transform are exploited to introduce three new schemes; T-SLM, T-PTS-I, T-PTS-II. T-SLM scheme has achieved considerable reduction in computational complexity and in the PAPR as well. To explore other possibilities, two schemes for utilising the T-transform with the OFDM-PTS system are proposed. One scheme, T-PTS-I, has achieved considerable PAPR and complexity reduction with the same SI. Whereas, the second scheme, T-PTS-II, has achieved a significant complexity reduction and has reduced the SI bits by two bits, with negligible PAPR degradation. None of the proposed schemes have any negative effects on the original power spectrum of the OFDM signals. Indeed, the simulations results demonstrated that the proposed schemes are resilient to dispersion arising from multipath transmission, owing to the frequency diversity of transmitted subcarriers introduced by WHT, even in the presence of a HPA.

5.1 Introduction

In OFDM systems, the coherent superposition of a large number of subcarriers through IFFT may produces samples with very high peak values in respect to their average power. The PAPR is the common metric for this phenomenon. Therefore, various schemes have been devised to eliminate the deleterious effect of high PAPR in OFDM signals, albeit with the expense of high computational complexity, data rate losses and BER performance degradation. This includes techniques with distortion and techniques without distortion.

In the category of techniques with distortion, the peak of the transmitted signal is reduced by clipping the large peak depending on a specific threshold. These

techniques have achieved considerable PAPR reduction, despite a noticeable BER degradation. Examples of these schemes are iterative clipping [71], filtering [72], and nonlinear companding [73].

On the other hand, a considerable PAPR reduction without BER degradation is obtained when distortionless schemes are used. However, the main drawbacks of this category are computational complexity and data rate losses, due to the redundant bits sent as SI. There are many schemes that may be included in this category, such as tone reservation (TR), active constellation extension (ACE) [74], coding techniques [75], selective mapping (SLM) [76], [77], [78], [79], [80], [81], and partial transmitting sequences (PTS) [82], [83], [84], [85], [86], [30].

SLM and PTS schemes have received substantial interest because they can reduce the PAPR without BER degradation. However, high computational complexity requirements and SI are the main limitations of such techniques.

Regarding SI, [87], [88] and [89] attempted to solve the SI challenge inherent in these two schemes by utilizing a variety of techniques at the expense of additional complexity.

The high complexity of these techniques is then mainly due to the necessity of performing several IFFT operations and phase optimisations at the transmitter side. Consequently, reducing the complexity and SI of the OFDM-SLM and OFDM-PTS systems is crucial. In the sequel, many studies were conducted to reduce computational complexity requirements of the SLM and PTS. Thus, the potential for reducing complexity in OFDM-based SLM received considerable attention in recent studies [76], [77], [78], [79], [80], [81]. However, the burden of SLM complexity is reduced in cases of similar or inferior PAPR and BER performance.

Conversely, additional recent studies have made similar efforts to reduce the complexity of OFDM-PTS systems [82], [83], [84], [85], [86], [30]. The complexity of such systems is reduced either by downwardly adjusting the number of IFFTs, or by reducing the complexity of the phase optimisation process, albeit with PAPR or BER degradation.

To specify our approach, [90] proposed a method for PAPR reduction in multicarrier systems by combining SLM and dummy sequence iteration (DSI) with WHT. PAPR reduction was achieved, albeit with the trade-off of high complexity, as a result of using several IFFTs and WHTs. Moreover, [91] suggested a new PAPR reduction technique including a WHT in the OFDM system. Although this technique provided

better PAPR, there relatively high complexity requirements arose owing to adding WHT in a cascaded format.

5.2 High-Power Amplifier (HPA)

Transmission of a high peak power signal through a nonlinear device, such as a HPA or a digital-to-analog converter (DAC) generates out-of-band energy (spectral regrowth) and in-band distortion (constellation scattering). In the sequel, the system performance may be subject to severe degradation. Therefore, in order to avoid such an undesirable nonlinear effect, the high peak power of the transmitted signal must be reduced.

Based on the type of HPA, the nonlinearity of such devices has a deleterious effect on the amplitude or the phase of the pass through the complex signal. Thus, this effect can be characterized as [92]

$$p[x(t)] = g(|x(t)|)e^{j(\theta(|x(t)|)+\phi(t))}, \tag{5.1}$$

where $|x(t)|e^{j\phi(t)}$ is the input signal to the HPA, $p[x(t)]$ stand for the output of the HPA, $g(|x(t)|)$ and $\theta(|x(t)|)$ are the AM/AM and the AM/PM distortion functions, respectively, of HPA; where AM and PM denote the amplitude modulation, and phase modulation, respectively. Generally, there are three categories of HPAs:

1. Soft Limiter Amplifier (SLA);
2. Solid State Power Amplifier (SSPA);
3. Travelling-Wave Tube Amplifier (TWTA);

More details about these types of HPA are available in [92], [93], and [94].

5.2.1 Soft Limiter Amplifier (SLA)

The Soft limiter amplifier (SLA) is the simplest model of the HPA, and clips the magnitude of the pass through signal when exceeding a specific threshold without any phase distortion. Consequently, the output signal from such a type can be expressed

as [93]

$$p[x(t)] = \left\{ \begin{array}{ll} S_{\text{HPA}} e^{j\phi(t)} & \text{if } |x(t)| > S_{\text{HPA}} \\ x(t) & \text{elsewhere} \end{array} \right\}, \tag{5.2}$$

where S_{HPA} denotes the threshold of clipping of the HPA.

5.2.2 Solid State Power Amplifier (SSPA)

In applications with wireless communications, SSPA is used. Similar to SLA, this amplifier does not cause any deleterious phase distortion. Whereas, the AM/AM distortion can be computed as, [94]

$$g(|x(t)|) = \frac{|x(t)|}{\left[1 + \left(\frac{|x(t)|}{S_{\text{HPA}}}\right)^{2p}\right]^{\frac{1}{2p}}}, \tag{5.3}$$

where p is a parameter which controls the smoothness of the transition from the linear region to the saturation region, which for practical SSPA takes the value of $p = 2$ or $p = 3$. Thus, the output of SSPA can be characterized as,

$$p[x(t)] = g(|x(t)|)e^{j\phi(t)}. \tag{5.4}$$

5.2.3 Travelling-Wave Tube Amplifier (TWTA)

For satellite applications, TWTA is the most commonly used option. In this category both AM/AM and AM/PM distortions are introduced. Hence, the function of TWTA can be written as, [94]

$$p[x(t)] = \frac{|x(t)|}{1 + \left(\frac{|x(t)|}{2S_{\text{HPA}}}\right)^2} e^{j\left(\frac{\pi|x(t)|^2}{3|x(t)|^2 + 4S_{\text{HPA}}^2} + \phi(t)\right)}. \tag{5.5}$$

5.3 PAR Distribution of T-OFDM System

Once again, in OFDM, adding a large number of subcarriers coherently may produce samples with very high peak values with respect to the OFDM average power. The PAPR is the common metric for this phenomenon, which is defined for discrete-time

signals according to [95] as,

$$\text{PAPR}[x_n] = \frac{\zeta_{\max}}{\zeta_{\text{ave}}}, \tag{5.6}$$

where $\zeta_{\max} = \underset{0 \le n \le NL-1}{max}[|x_n|^2]$ is the peak power of the discrete-time signal, x_n, $\zeta_{\text{ave}} = E[|x_n|^2]$ is the average transmitted power, N is the number of the subcarrier, and L is the oversampling factor. Oversampling is pivotal in order to provide an accurate approximation for the PAPR of the continuous-time signal based on the oversampled discrete-frequency signal. A sufficiently accurate approximation can be achieved using $L = 4$ [96]. In the case of OFDM, oversampling can be achieved by padding the frequency-domain signal with $\mathbf{0}^{1\times(L-1)N}$.

Similarly, the same approach can be used with a WHT-OFDM system, padding the WHT output signal with zeros. However, an alternative method that has a similar effect can be used to up-sample the signal in such a system. This can be achieved by duplicating a signal $\mathbf{X}$, which describes the entries to WHT, L times as,

$$\mathbf{X}_{\text{Sampling}} = [\mathbf{X}_0, \mathbf{X}_1, \ldots, \mathbf{X}_L], \tag{5.7}$$

where $\mathbf{X}_0, \mathbf{X}_1, \ldots, \mathbf{X}_L$ are L copies of the signals $\mathbf{X}$. This oversampling approach will be used with the T-OFDM system as well.

The T-transform allows for the preservation of the average transmitted power, thus, the average power for (4.1) can be calculated as,

$$E\{|\mathbf{x}|^2\} = E\{\mathbf{x}\mathbf{x}^*\} \tag{5.8a}$$

$$= E\{(\hat{\mathbf{T}}\mathbf{X})(\mathbf{T}\mathbf{X}^*)\}, \tag{5.8b}$$

where $\{.\}^*$ stands for the complex conjugate. The n-th element of $|\mathbf{x}|^2$ can be written as,

$$|x_n|^2 = \left(\sum_{m=0}^{N-1} X_m \hat{T}_{m,n}\right)\left(\sum_{m=0}^{N-1} X_m^* T_{m,n}\right), \tag{5.9a}$$

$$= \left(\sum_{m=0}^{N-1} |X_m|^2 |\hat{T}_{m,n}|^2\right) + \left(\sum_{m=0}^{N-1}\sum_{g=0,g\neq m}^{N-1} X_m X_g^* T_{m,n} T_{g,n}^*\right). \tag{5.9b}$$

Upon substituting (5.9b) into (5.8b), we get

$$E\{|\mathbf{x}|^2\} = \frac{1}{N}\sum_{n=0}^{N-1}\left(\sum_{m=0}^{N-1}|X_m|^2|\hat{T}_{m,n}|^2\right) + \frac{1}{N}\sum_{n=0}^{N-1}\left(\sum_{m=0}^{N-1}\sum_{g=0,g\neq m}^{N-1} X_m X_g^* T_{m,n} T_{g,n}^*\right). \tag{5.10}$$

Due to orthogonality of matrix $\mathbf{T}$, the second term on the right hand side of (5.10) is equal to zero. Thus, (5.10) can be simply rewritten as,

$$E\{|\mathbf{x}|^2\} = \frac{1}{N}\sum_{m=0}^{N-1}|X_m|^2. \tag{5.11}$$

The average power is preserved by the T-transform, hence the PAPR reduction will depend on peak power reduction.

Moreover, as shown in Fig 3.3, the T-transform involves $\log_2(N) - 1$ stages only and has a block diagonal structure with $\log_2(N) - 1$ sections and two direct pathways. The maximum number of non-zero elements in each section is $\leq N/2$. As a result, the superposition of the input signals in the case of the T-transform is less than in the case of the IFFT; leading to a lower PAPR, as shown in the results section. However, when the number of sub-carriers increases, the number of sections with Gaussian distributions increases, therefore the overall probability density function (PDF) of the T-transform can also be approximated as Gaussian and the peak of the T-OFDM system is then closer to that of the OFDM system for the larger N.

5.4 Proposed T-OFDM-SLM system

5.4.1 Scheme Structure

As clearly shown in the literature, the conventional SLM scheme is constructed by creating U copies of the frequency-domain symbols $\mathbf{X}$ as,

$$\mathbf{d}^{(u)} = \mathbf{X}, \tag{5.12}$$

where $u \in \{0, 1, ..., U-1\}$.
Each branch is multiplied by an N distinct points phase rotation vector

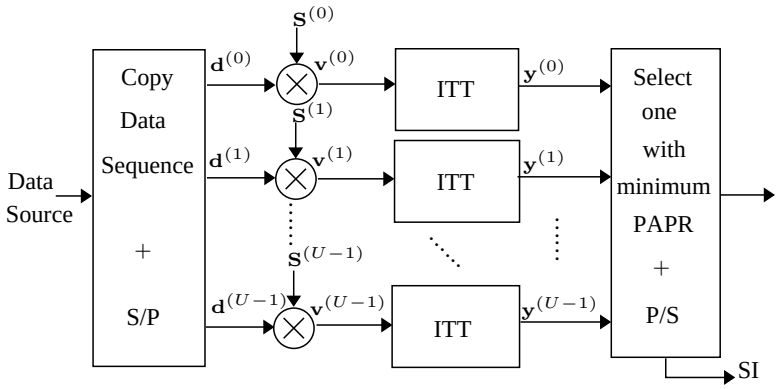

Figure 5.1: Block diagram of OFDM-based T-SLM scheme.

$\mathbf{s}^{(u)} = [s_0^{(u)},\ s_1^{(u)}, ...,\ s_{N-1}^{(u)}]$ and the multiplication process can be expressed as,

$$\mathbf{v}^{(u)} = \mathbf{s}^{(u)} \cdot \mathbf{d}, \tag{5.13}$$

where $\{\cdot\}$ denotes the element-by-element multiplication process. The result of multiplication $\mathbf{v}^{(u)}$ at each branch is up-sampled by a factor $L = 4$, and applied to LN-points IFFT to generate discrete-time samples and then the PAPR is computed. The branch with the lowest PAPR is selected for transmission. This side information is to be transmitted, given that the transmitter and the receiver share a common knowledge of the vectors $\mathbf{s}^{(u)}$.

The SLM described above can be directly applied to the WHT-OFDM system [90], preceeding the IFFT with the WHT, in order to achieve more PAPR reduction at the expense of increasing the complexity owing to the WHTs. This means

$$\mathbf{y}_{\text{WHT}}^{(u)} = \mathbf{W}\mathbf{v}^{(u)}. \tag{5.14}$$

The remaining operations are identical to those of the conventional OFDM-SLM system. Consequently, the T-transform can be applied to the OFDM-SLM system by replacing the WHT-IFFT processes with the inverse T-transforms [97], as shown in Fig. 5.1. This means,

$$\mathbf{y}_{\text{T-transform}}^{(u)} = \hat{\mathbf{T}}\mathbf{v}^{(u)}. \tag{5.15}$$

Once again, in OFDM, oversampling can be achieved by padding the frequency-domain signal with $\mathbf{0}^{1\times(L-1)N}$. Similarly, an identical approach can be used with WHT-OFDM by padding the WHT output signal with zeros. However, an alternative

method with a similar effect can also be used to up-sample the signal in such a system. This method can be achieved by duplicating the signals in (5.13) L times as,

$$\mathbf{q}^{(u)} = [\mathbf{v}_0^{(u)}, \mathbf{v}_1^{(u)}, \ldots, \mathbf{v}_L^{(u)}]. \tag{5.16}$$

5.4.2 Computational Complexity

In SLM, the computational complexity consists of the following three parts:
a) U NL-points IFFTs operations at the transmitter side;
b) phase factor multiplications in (5.13);
c) PAPR computation and comparison among candidate signals.
The SLM for OFDM, WHT-OFDM and T-OFDM requires identical operations for the entire system, except that the complexities of IFFT, WHT, and T-transform are compared. Therefore, the computational complexity in a) compared to the other related transforms is mainly considered. Accordingly, the computational complexity of the conventional SLM scheme is calculated based on the complexity of U NL-points IFFTs. The complexity of the IFFT is calculated based on of two criteria of design including full-butterfly IFFT design, and pruning IFFTs design; i.e. omitting multiplications or additions with zero [98].

5.4.2.1 Complexity Calculation Based on Full-Butterfly IFFT Design

Full-butterfly IFFT design requires an $NL/2 \log_2 NL$ and $NL \log_2 NL$ of complex multiplications and additions, respectively [76], [77], [78], [79], [80], [81]. Thus, based on a full-butterfly IFFT design, the total computational complexity of considered schemes (transmitter only), in terms of real additions, using the same criteria as those described in Chapter 4 can be expressed as,

$$R_{\text{Total}}^{\text{Conv. SLM}} = 11UNL \log_2(NL), \tag{5.17}$$

$$R_{\text{Total}}^{\text{WHT-SLM}} = R_{\text{Total}}^{\text{Conv. SLM}} + 2UN \log_2(N), \tag{5.18}$$

$$R_{\text{Total}}^{\text{T-SLM}} = 12U[NL \log_2(NL) - (2NL - 2)], \tag{5.19}$$

where U is the number of disjoint subblocks.

5.4.2.2 Complexity Calculation Based on Pruning IFFTs Design

Based on the pruning IFFTs design, the computational complexity of a) in a conventional SLM scheme depends on the sparseness of data, i.e. non-zero data at the transmitted side, and full FFT at the receiver side. Thus, the pruning IFFTs of the SLM scheme require $\frac{1}{2}UNL\log_2 N + UN(L-1)$ and $UNL\log_2 N$ complex multiplications and additions, respectively. Hence, the total complexity of such a scheme, in terms of real additions (computed only for pruning-IFFTs at the transmitter side), can be evaluated as,

$$R_{\text{Total}}^{\text{pruning-SLM}} = 11UNL\log_2(N) + 18UN(L-1). \tag{5.20}$$

Similarly, in the case of a Pruning-WHT-SLM system with oversampling, the total computational complexity in terms of real additions can be expressed as

$$R_{\text{Total}}^{\text{WHT-Pruning-SLM}} = R_{\text{Total}}^{\text{pruning-SLM}} + 2UN\log_2 N. \tag{5.21}$$

On the other hand, employment of the up-sampling technique clarified in (5.16) with the proposed T-SLM scheme leads to obtaining the same data samples after the first stage (from left) of the last section (with size N/2) of T-transform shown in Fig. 3.3. Consequently, the complexity of $\frac{N}{4}$ butterflies will be dropped from the total computational complexity of the oversampled T-SLM scheme. This means, the number of total butterflies in the Pruning-T-SLM will be $\frac{1}{2}[NL\log_2 NL-(2NL-2)]-\frac{NL}{4}$. In a sequel, the total computational complexity of T-SLM in terms of real additions can be expressed as,

$$R_{\text{Total}}^{\text{Pruning-T-SLM}} = 12U[NL\log_2(NL) - (2NL-2)] - 6UNL. \tag{5.22}$$

5.5 Proposed T-PTS-I/II Schemes

5.5.1 Conventional PTS Scheme

As reported in the literature, the PTS scheme is based on partitioning the input data block $\mathbf{X}$, which consists of N symbols into U disjoint sets $\hat{\mathbf{q}}^{(u)}$, $u = 0, 1, \ldots, U-1$.

Then each set of $\hat{\mathbf{q}}$ is padded with zeros on the left and right sides to obtain

$$\hat{\mathbf{q}}^{(u)} = [\mathbf{0}^{1\times uN/U}, \{\mathbf{X}\}_{u\,N/U}^{(u+1)N/U-1}, \mathbf{0}^{1\times[N-(u+1)N/U]}]. \tag{5.23}$$

Each sub-block of $\hat{\mathbf{q}}$ is fed to individual NL-points IFFT attempting to reach the time-domain samples $\mathbf{x}^{(u)}$ as,

$$\mathbf{x}^{(u)} = \hat{\mathbf{F}}\,\hat{\mathbf{q}}^{(u)}. \tag{5.24}$$

The n-th sample of $\mathbf{x}^{(u)}$ can be written as,

$$x_n^{(u)} = \frac{1}{\sqrt{NL}} \sum_{k=0}^{NL-1} q_k^{(u)} \mathrm{e}^{j2\pi kn/NL}, \quad n = 0, 1, \ldots, NL-1. \tag{5.25}$$

Subsequently, each partially transmitted sequence $\mathbf{x}^{(u)}$ is multiplied by individual weighting phase factors, $b^{(u)} \in \{\pm 1, \pm j\}$, $u \in \{0, 1, ..., U-1\}$. Based on the weight, P of $b^{(u)}$, there are $B^{'} = P^{U-1}$ alternative representations for the OFDM symbol.

Finally, the transmitted OFDM symbol is composed by adding the optimised U sequences, thus

$$\hat{d}_n = \sum_{u=0}^{U-1} b^{(u)} x_n^{(u)}. \tag{5.26}$$

The PTS described above can be directly applied to WHT-OFDM systems by preceding the IFFT with the WHT. As will be shown in the next two sub-sections, the data partition can be achieved in two ways, pre-/post-WHT.

The computational complexity of PTS scheme will be composed based on the complexity of the three parts a), b) and c) from the operations mentioned formerly in section 5.1. As reported in [31], the complexity of b) and c) operations in terms of real additions can be expressed as,

$$D^{'} = NL(U(20B^{'} - 18) + 7B^{'}). \tag{5.27}$$

The complexity of $D^{'}$ is identical in both full-butterfly and pruning IFFT design. Furthermore, the burden of IFFTs computational complexity in the PTS scheme will be computed in the next sections based on the IFFT architecture design.

5.5.1.1 Complexity Calculation Based on Full-Butterfly IFFT Design

Similar to Section 5.4.2.1, the burden of IFFTs in conventional PTS and WHT-PTS (where data partition performs after WHT, i.e. one WHT is required) schemes require $11UNL\log_2(NL)$ and $11UNL\log_2(NL)+2N\log_2 N$ real additions, respectively. This means, total real operations in conventional PTS and WHT-PTS schemes can be computed as,

$$R_{\text{Total}}^{\text{Conv. PTS}} = 11UNL\log_2(NL) + D^{'}, \tag{5.28}$$

$$R_{\text{Total}}^{\text{WHT-PTS}} = 11UNL\log_2(NL) + 2N\log_2 N + D^{'}, \tag{5.29}$$

where $D^{'}$ was formerly defined in (5.27).

5.5.1.2 Complexity Calculation Based on Pruning IFFT Design

Non-zero data in the oversampled-PTS scheme is lower than in the case of the oversampled-SLM scheme because spare data depends on the oversampling factor L and the number of disjoint partitions , U; whereas it depends on L in the case of a SLM scheme. Consequently, the required complex multiplications, C_M, and additions, C_A, in the pruning IFFTs (at the transmitter side) of the conventional PTS and WHT-PTS schemes can be computed as,

$$C_M^{\text{pruning-IFFT}} = \frac{1}{2}UNL\log_2(\frac{N}{U}) + N(UL-1), \tag{5.30}$$

$$C_A^{\text{pruning-IFFT}} = UNL\log_2(\frac{N}{U}), \tag{5.31}$$

$$C_M^{\text{pruning-WHT-IFFT}} = C_M^{\text{pruning-IFFT}}, \tag{5.32}$$

$$C_A^{\text{pruning-WHT-IFFT}} = C_A^{\text{pruning-IFFT}} + N\log_2(N). \tag{5.33}$$

Consequently, the total real additions in the conventional PTS and WHT-PTS (including pruning IFFT, full-butterfly IWHT/WHT, PAPR calculation and phase optimisation process) can be expressed as,

$$R_{\text{Total}}^{\text{pruning-PTS}} = 11UNL\log_2\frac{N}{U} + 18NUL - 18N + D^{'}, \tag{5.34}$$

$$R_{\text{Total}}^{\text{pruning-WHT-PTS}} = R_{\text{Total}}^{\text{pruning-PTS}} + 2N\log_2(N). \tag{5.35}$$

5.5.2 Proposed T-PTS-I Scheme

5.5.2.1 Scheme Design

As introduced in [97], in the first proposed scheme, T-PTS-I , the WHT of the data symbol $\mathbf{X}$ is computed as,

$$\mathbf{d} = \mathbf{W}\mathbf{X}. \tag{5.36}$$

Then, the U disjoint partitions of the data vector, $\mathbf{d}^{(u)}$, $u = 0, ..., U-1$, and the remainder of the processes are evaluated in a similar way to those in a traditional PTS scheme. Alternatively, the same disjoint partitions $\mathbf{d}^{(u)}$ can be computed by copying U-times the data samples $\mathbf{X}$ as, $\mathbf{X}^{(u)} = \mathbf{X}$, $u = 0, 1, \ldots, U-1$, and each copy is multiplied with a new normalised symmetrical matrix, $\mathbf{G}$. The U-versions of the normalised $\mathbf{G}$ matrix are computed as,

$$\mathbf{G}^{(u)} = \mathbf{P}^{(u)}\mathbf{W}, \tag{5.37}$$

where $\mathbf{P}^{(u)}$ are new matrices that have $\frac{N}{U}$ data samples, which are equivalent to the uth part of WHT matrix, $\mathbf{W}$, and $\frac{(U-1)}{U}N$ of zeros. This means that the elements of these matrices can be computed as,

$$\mathbf{P}^{(u)} = [\mathbf{0}^{(:,1:uN/U}, \{\mathbf{W}\}^{(:,u\,N/U:(u+1)N/U-1)}, \mathbf{0}^{(:,1:[N-(u+1)N/U])}]. \tag{5.38}$$

Consequently, each individual normalised $\mathbf{G}^{(u)}$ matrix has U elements comprising of uniformly distributed ones and $N-U$ zeros in each column and row. Thus, the U versions of $\mathbf{X}$ are multiplied with each individual $\mathbf{G}^{(u)}$ matrix as,

$$\mathbf{q}^{(u)} = \mathbf{G}^{(u)}\mathbf{X}^{(u)}. \tag{5.39}$$

Therefore, the same non-overlapped sub-blocks partitions of (5.36) will be obtained by feeding each individual sequence in (5.39) into the WHT, as followed by the other steps in the PTS scheme. The up-sampling of (5.39) can be performed, as in (5.16) by generating U copies of $\mathbf{q}$, then each divided by $\sqrt{L}$. Thus,

$$\hat{\mathbf{v}}^{(u)} = \mathbf{v}^{(u)}/\sqrt{L}, \tag{5.40}$$

where $\mathbf{v}^{(u)} = [\mathbf{q}_0^{(u)}, \mathbf{q}_1^{(u)}, \ldots, \mathbf{q}_L^{(u)}]$, and $\mathbf{q}_l^{(u)} = \mathbf{q}^{(u)}$, $l = 0, 1, \ldots, L-1$.

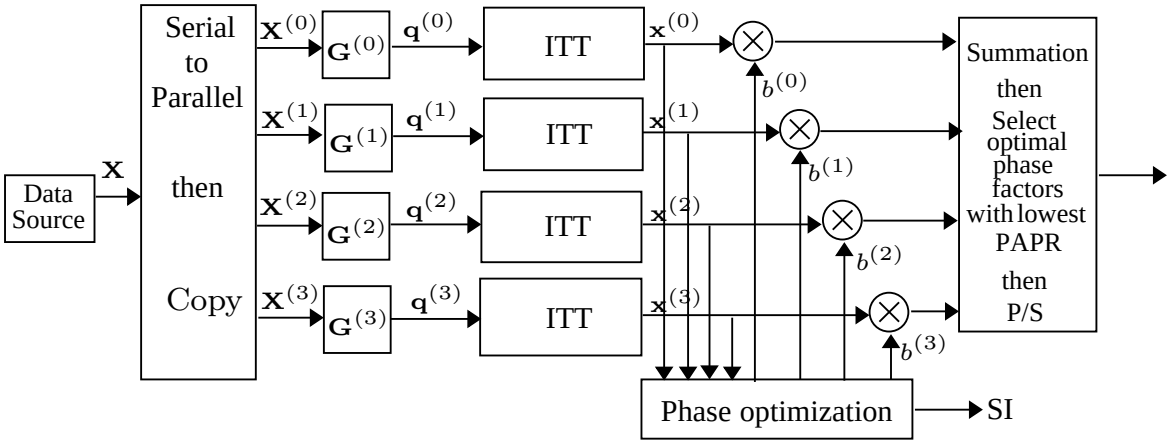

Figure 5.2: Block diagram of T-PTS-I scheme with $U = 4$.

The computational complexity burden of employing WHT with OFDM-PTS should be taken into consideration. Therefore, the WHT-IFFT can be simply replaced by the T-transform, as shown in Fig. 5.2. The U disjoint sub-blocks of the new scheme can be attained by passing each individual sequence of (5.40) to the inverse T-transform as,

$$\mathbf{x}^{(u)} = \hat{\mathbf{T}}\hat{\mathbf{v}}^{(u)}. \tag{5.41}$$

Then, the phase optimisation and PAPR calculation steps are similar to those of a conventional PTS scheme.

5.5.2.2 Computational Complexity Calculation

The computational complexity requirements of the proposed T-PTS-I scheme are evaluated based on the complexities of ITT, phase optimisation process, PAPR calculations and $\mathbf{G}^{(u)}$ matrices. The complexity of phase optimisation and PAPR calculations, which are identical in the T-PTS-I, conventional PTS and WHT-PTS schemes can be reduced significantly as in [99]. Therefore, the computational complexity of ITT and $\mathbf{G}^{(u)}$ matrices are mainly considered in comparison with IFFTs and WHTs-IFFTs. Utilizing U-matrices of $\mathbf{G}$ requires $2U(U-1)N$ real additions. Thus, the total real additions in the T-PTS-I (accounting ITT and $\mathbf{G}^{(u)}$ matrices complexity) as based on the full-butterfly T-transform can be expressed as,

$$R_{\text{Total}}^{\text{Full-T-PTS-I}} = 12U[NL\log_2(NL) - (2NL-2)] + 2U(U-1)N. \tag{5.42}$$

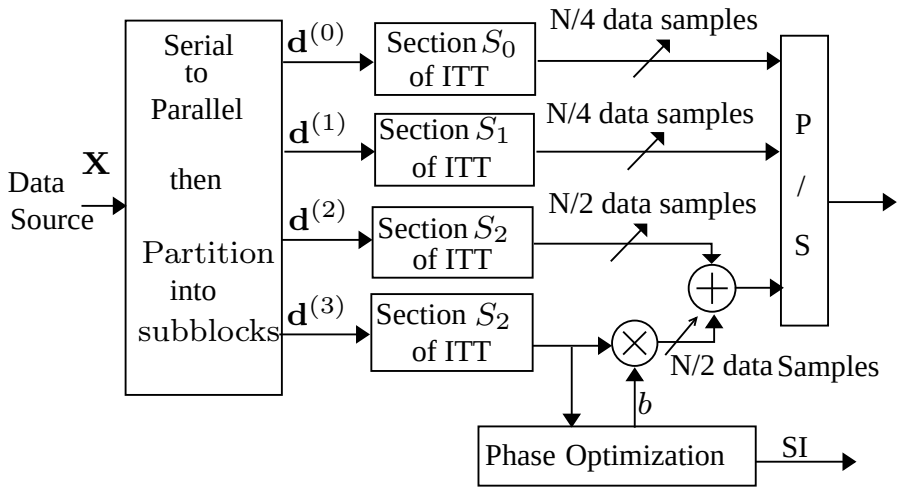

Figure 5.3: Block diagram of T-PTS-II scheme with $U = 4$.

On the other hand, the total real additions in the oversampled T-PTS-I scheme based on pruning-T-transform, i.e. by omitting the butterfly of the same data symbols, can be computed as,

$$R_{\text{Total}}^{\text{Pruning-T-PTS-I}} = R_{\text{Full-T-PTS-I}} - 6UNL. \tag{5.43}$$

5.5.3 Proposed T-PTS-II Scheme

5.5.3.1 Scheme Design

In the second proposed scheme, T-PTS-II [97], the data symbol $\mathbf{X}$ is firstly partitioned to U non-overlap sub-blocks then fed to ITT. The unique butterfly structure of the ITT, which was shown in Chapter 3, can be exploited to significantly reduce the complexity of the PTS, as shown in Fig. 5.3. However, related to this proposed scheme, as shown in Fig. 3.3, the N-points T-transform has $\log_2(N) - 1$ uncorrelated butterfly sections and two direct pathways. Consequently, up-sampling the time-domain samples, by zero padding the frequency-domain symbols is not feasible when applying this scheme. Alternatively, conventional up-sampling in the time-domain can be applied. However, the complexity of up-sampling in the time-domain is identical in all the systems considered in this work. Hence for the purpose of simplicity, up-sampling has not been applied in this scheme.

To simplify the discussion, we can assume that $N = 16$ and $U = 4$, as in the

traditional PTS, the data symbols $\mathbf{X}$ are partitioned into four disjoint subblocks, $\mathbf{d}^{(u)}$, $u = \{0, ..., 3\}$, therefore, each partition has $\frac{N}{U}$ (four in our example) non-zero elements and $\frac{U-1}{U}N$ (twelve in our example) zeros. This means,

$$\mathbf{d}^{(0)} = [X_0,\ X_1,\ X_2,\ X_3,\ \underbrace{0, ..., 0}_{12}], \tag{5.44}$$

$$\mathbf{d}^{(1)} = [\underbrace{0, ..., 0}_{4},\ X_4,\ X_5,\ X_6,\ X_7, \underbrace{0, ..., 0}_{8}], \tag{5.45}$$

$$\mathbf{d}^{(2)} = [\underbrace{0, ..., 0}_{8},\ X_8,\ X_9,\ X_{10},\ X_{11},\ \underbrace{0, ..., 0}_{4}], \tag{5.46}$$

$$\mathbf{d}^{(3)} = [\underbrace{0, ..., 0}_{12},\ X_{12},\ X_{13},\ X_{14},\ X_{15}]. \tag{5.47}$$

The first partition $\mathbf{d}^{(0)}$ which contains the first four data symbols applies to the ITT as,

$$\mathbf{v}^{(0)} = \hat{\mathbf{T}}\mathbf{d}^{(0)} \tag{5.48a}$$

$$= [x_0, 0, 0, 0, x_8, 0, 0, 0, x_4, 0, 0, 0, x_{12}, 0, 0, 0], \tag{5.48b}$$

where x_0, x_8, x_4 and x_{12} are the time-domain samples that result from processing X_0, X_1, X_2 and X_3 through section S_0. Therefore, $\mathbf{v}^{(0)}$ can be simply obtained by applying the non-zero elements of $\mathbf{d}^{(0)}$ to section S_0 of the butterfly; taking into consideration the correct sample order. Arranging the samples in the proper order can be achieved by changing the position of the most significant bits from right to left. Similarly, the sequence $\mathbf{v}^{(1)}$ can be obtained by applying vector $\mathbf{d}^{(1)}$, which has the second partition of data vector $\mathbf{d}$, to the ITT as,

$$\mathbf{v}^{(1)} = \hat{\mathbf{T}}\mathbf{d}^{(1)} \tag{5.49a}$$

$$= [0, 0, x_2, 0, 0, 0, x_6, 0, 0, 0, x_{10}, 0, 0, 0, x_{14}, 0], \tag{5.49b}$$

Hence, the non-zero elements of $\mathbf{v}^{(1)}$ can be obtained by applying the non-zero elements of $\mathbf{d}^{(1)}$ to section S_1 of the ITT; taking into consideration the precise order of the samples. On the other hand, the output of passing the third and fourth subblocks,

i.e. $\mathbf{d}^{(2)}$ and $\mathbf{d}^{(3)}$, respectively through ITT can be expressed as,

$$\mathbf{v}^{(2)} = \hat{\mathbf{T}}\mathbf{d}^{(2)} \tag{5.50a}$$

$$= [0, a_1, 0, a_3, 0, a_5, 0, a_7, 0, a_9, 0, a_{11}, 0, a_{13}, 0, a_{15}], \tag{5.50b}$$

$$\mathbf{v}^{(3)} = \hat{\mathbf{T}}\mathbf{d}^{(3)} \tag{5.51a}$$

$$= [0, b_1, 0, b_3, 0, b_5, 0, b_7, 0, b_9, 0, b_{11}, 0, b_{13}, 0, b_{15}]. \tag{5.51b}$$

Obviously, the data elements of $\mathbf{v}^{(2)}$ and $\mathbf{v}^{(3)}$ can be obtained with a bit reverse order by applying the data elements of $\mathbf{d}^{(2)}$ and $\mathbf{d}^{(3)}$, respectively, through section S_2. Due to the alignment of the non-zero elements in all the partitions, it is evident that $\mathbf{v}^{(0)}$ and $\mathbf{v}^{(1)}$ branches cannot be used to reduce the PAPR, because they do not add up to the other non-zero element in other branches. Moreover, multiplying either $\mathbf{v}^{(2)}$ or $\mathbf{v}^{(3)}$ by phase optimisation vector, but not both, is sufficient to minimize the PAPR. Finally, all vectors are combined together to compose the transmitted data sequence as,

$$\acute{\mathbf{d}} = \mathbf{v}^{(0)} + \mathbf{v}^{(1)} + \mathbf{v}^{(2)} + b\mathbf{v}^{(3)}. \tag{5.52}$$

Obviously, for PAPR reduction, the effective disjoint sub-blocks number in the proposed T-PTS-II scheme is $U^{'} = U - 2$ and the number of phase optimisation factors is $B^{''} = P^{U^{'}-1}$. Consequently, the required SI redundant bits will be one when compared with three bits in the case of conventional PTS scheme with four sub-blocks, and binary weight phase rotation.

5.5.3.2 Computational Complexity Calculation

The computational complexity requirements of the proposed T-PTS-II scheme are evaluated based on the ITT/FTT complexities, and the complexity of the partial sequence phase optimisation process. Based on the assumption of $U = 4$, the implementation of sections, S_0 and S_1 of Fig. 3.3, require $\left[\frac{N}{4}\log_2(\frac{N}{2}) - (\frac{N}{2} - 1)\right]$ butterflies. This means, $\frac{N}{4}\log_2(\frac{N}{2}) - (\frac{N}{2} - 1)$ complex multiplications and $\frac{3}{4}N\log_2(\frac{N}{2}) - (\frac{3N}{2} - 3)$ complex additions are required. Similarly, the computational complexity of section S_2 is computed as $\frac{N}{4}\log_2(N) - \frac{N}{4}$ and $\frac{3}{4}N\log_2(N) - \frac{3}{4}N$ complex multiplications and complex additions, respectively. Moreover, the computational complexity of section S_2 should be considered twice due to feeding the third sub-block $\mathbf{d}^{(2)}$ and fourth

sub-block $\mathbf{d}^{(3)}$ into S_2.

Contrastingly, with the assumption $U = 4$, the phase optimisation and PAPR calculations are required only for the S_2 output signal with a length of $\frac{N}{2}$. This means, the phase optimisation process requires $(U^{'} - 1)(B^{''} - 1)\frac{N}{2}$ complex multiplications and equivalent value complex additions. Furthermore, a PAPR calculation in such a scheme requires $(B^{''} - 1)N$ real multiplications and $\frac{(B^{''}-1)N}{2}$ real additions. Thus, the total real additions, R_{Total}, of T-PTS-II scheme with four disjoint subblocks are

$$R_{\text{Total}}^{T-PTS-II} = 18N\log_2(N) - (30N - 24) + \hat{K^{'}}, \tag{5.53}$$

where $\hat{K^{'}} = 10U^{'}B^{''}N - 10U^{'}N - \frac{11}{2}(N(B^{''} + 1))$.
Eventually, the proposed T-PTS-II scheme achieves a significant complexity reduction compared with the conventional PTS and WHT-PTS schemes, as will be demonstrated in the simulation results section.

5.6 Numerical Results

Without loss of generality, the results presented in this section are achieved based on the assumptions of a perfect knowledge of the channel response, perfect frequency and time synchronization and optimal SI transmission. Also, all the systems considered are uncoded.

5.6.1 Computational complexity

As clearly shown in Table 5.1, the proposed T-SLM scheme requires lower computational complexity than the conventional SLM and WHT-SLM schemes with full-butterfly and pruning-butterfly design criteria. With an assumption of $N = 64$, $L = 1$ and $U = 4$ the T-SLM scheme achieves a CCRR of about 26.70% and 38% over conventional SLM and WHT-SLM schemes, when the full-butterfly design criterion is used in the considered transforms. Furthermore, with oversampling, i.e. $L = 4$ and the above parameters, the attained CCRR are in the region of 18.08% and 20.78%, respectively. The complexity reduction ratio η_1 is obtained by computing C_1 and C_2 that was appeared in (3.91) using (5.19) and (5.17), respectively. η_2 is computed in the same way, except that C_2 is computed using (5.18).

Table 5.1: Computational complexity reduction ratio (CCRR) of the proposed T-SLM scheme over conventional SLM and WHT-SLM schemes (η_1 and η_2, respectively), based on full-butterfly transforms design criterion.

	Computational complexity reduction ratio (CCRR)			
	Without oversampling ($L = 1$)		With oversampling ($L = 4$)	
N	η_1 (%)	η_2 (%)	η_1 (%)	η_2 (%)
64	26.70	37.98	18.08	20.78
256	18.08	30.68	12.70	15.77
1024	12.70	26.14	9.09	12.40

Table 5.2: Computational complexity reduction ratio (CCRR) of the proposed T-SLM scheme over conventional SLM and WHT-SLM schemes (η_1 and η_2, respectively), based on pruning-butterfly transform design criterion.

	Computational complexity reduction ratio (CCRR)	
N	η_1 (%)	η_2 (%)
64	16.86	19.89
256	11.30	14.67
1024	7.69	11.28

On the other hand, in the case of pruning-butterfly design criterion with an oversampling factor $L = 4$, the obtained CCRR of T-SLM scheme and over the pruning-SLM and WHT-pruning-SLM schemes are 16.86% and 19.89% with $N = 64$, and 7.69% and 11.28% with $N = 1024$, respectively, as shown in Table 5.2. η_1 is obtained by computing C_1 and C_2 using (5.22) and (5.20), respectively. η_2 is computed in the same way, except that C_2 is computed using (5.21).

The value of phase optimisation and PAPR calculation $D^{'}$ is identical in the proposed T-PTS-I, conventional PTS and WHT-PTS schemes. Therefore, for a fair comparison, the computational complexity of $D^{'}$ will be omitted in the complexity comparison among the considered schemes. As shown in Table 5.3, the T-PTS-I scheme based on the full-butterfly transform design criterion, attains CCRR of about 19.43% and 24.89% with $N = 64$ and $L = 1$, and about 16.83% and 18.17% with $L = 4$ over the conventional PTS and WHT-PTS schemes, respectively. However, with pruning transforms design criterion, T-PTS-I requires a slightly higher complexity of about 9% when compared to the conventional PTS scheme.

Table 5.3: Computational complexity reduction ratio (CCRR) of the proposed T-PTS-I scheme over conventional PTS and WHT-PTS schemes (η_1 and η_2, respectively), based on full-butterfly transform design criterion.

	Computational complexity reduction ratio (CCRR)			
	Without oversampling ($L = 1$)		With oversampling ($L = 4$)	
N	η_1 (%)	η_2 (%)	η_1 (%)	η_2 (%)
64	17.61	21.20	16.37	17.08
256	11.26	15.12	11.34	12.14
1024	7.25	11.28	7.97	8.81

Table 5.4: Computational complexity reduction ratio (CCRR) of the proposed T-PTS-II scheme over pruning PTS and pruning WHT-PTS schemes (η_1 and η_2, respectively).

	Computational complexity reduction ratio (CCRR)	
N	η_1 (%)	η_2 (%)
64	90.41	90.54
256	87.52	87.73
1024	85.09	85.38

Interestingly, as shown in Table 5.4, proposed T-PTS-II scheme achieved a significant CCRR of about 90% over other considered pruning systems. In addition, the data rate of the T-PTS-II scheme is higher than the conventional PTS scheme, because the required SI bits with the proposed scheme is lower than that required with the conventional PTS scheme by two.

5.6.2 PAPR Reduction

A good estimation of the power density of the considered systems can be acquired from the histogram plot of peak power of such systems, as shown in Fig. 5.4-5.7. In those figures, X-axis represents the peak range measured in dB; whereas Y-axis represents the number of peaks in each range in X-axis. As is clear in Fig. 5.4, the variance change of the T-OFDM peaks is smaller than that of the conventional OFDM; therefore, this figure clearly shows how the T-OFDM system outperforms conventional OFDM by having the fewest signals with high peaks, i.e. lower PAPR. Employment of the T-transform in OFDM systems reduces the superposition of the subcarriers due to

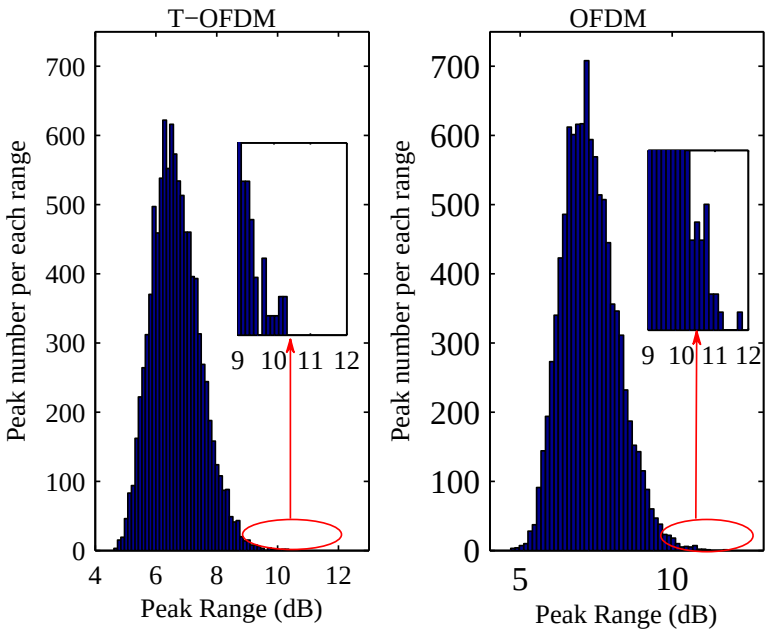

Figure 5.4: Histogram for peak power of conventional OFDM and T-OFDM systems with N=128.

the sparsity and block diagonal structure of the T-transform and its lower summation processes, as can be seen from Fig. 3.3. Thus, the peak of the transmitted signals will be reduced and the transmitted average power preserved. Furthermore, this PAPR reduction is achieved without any redundant side information (i.e. no data rate losses). Fig. 5.5 depicts the complementary cumulative distribution function (CCDF) (a statistical description most commonly used to measure the PAPR of the transmitted signal) of the PAPR for OFDM and T-OFDM signals with various subcarrier numbers and an oversampling factor equal to four ($L = 4$). As clearly shown in this figure, the PAPR values of the transmitted signal in the T-OFDM system are less than those of the OFDM system by a range of $0.75 \sim 1.2$ dB. The proposed T-OFDM system will help to reduce the PAPR as a consequence of reducing the superposition of the subcarriers passed through the T-transform. As shown in Fig.3.3, the number of stages in the T-transform are $\log_2 N - 1$ and the maximum number of subcarriers that will be processed together through the T-transform is $\frac{N}{2}$; whereas in IFFT, we require $\log_2 N$ stages and N subcarriers that will be processed through the IFFT.

Moreover, the lowest high peaks, i.e. lower PAPR, of T-SLM, and T-PTS-I sys-

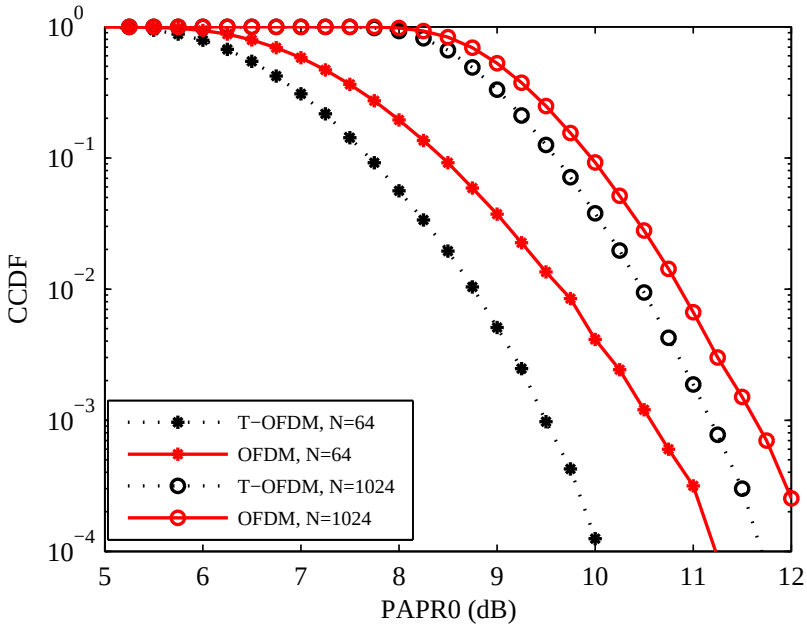

Figure 5.5: CCDF for the OFDM and T-OFDM systems, with various data size.

tems are compared to that of conventional SLM and PTS schemes, respectively, with the same value of SI, as clearly shown in Fig. 5.6-5.7, respectively. Consequently, the T-SLM scheme achieved a low peak signal compared to the conventional SLM when both were used with the OFDM system. Moreover, this peak reduction is achieved with the preservation of the average power of the transmitted signal, owing to the unitary characteristics of the T-transform. Fig. 5.8 depicts the ability of the proposed T-SLM scheme to achieve more PAPR reduction, about 0.8 dB less than the OFDM-based SLM scheme and roughly 3.1 dB less than the conventional OFDM system in the case of $U = 4$. It also achieves 0.8 dB and 3.9 dB less than the OFDM-SLM and conventional OFDM systems, respectively, with the case of $U = 8$. These results were achieved with 128 subcarriers (i.e. N=128). Based on the same former parameters used with the T-SLM system, Fig. 5.9 presents the PAPR of the proposed T-OFDM-PTS-I, OFDM-PTS and conventional OFDM systems. As evident from Fig. 5.9, the T-PTS-I scheme achieves a considerable PAPR reduction with both values of U when using the same values of SI. Conversely, Fig. 5.10 depicts the PAPR of the proposed T-OFDM-PTS-II, OFDM-PTS and conventional OFDM systems with parameters of 128 subcarriers (N=128), two values of phase rotation vectors ($U = [4, 8]$) and $L = 1$. Interestingly, the T-PTS-II scheme achieves significant computational complexity re-

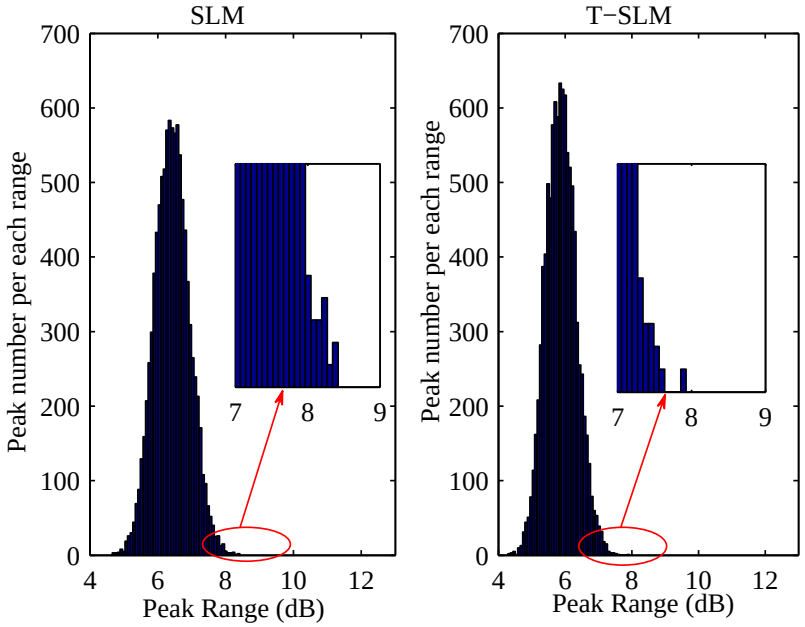

Figure 5.6: Histogram for peak power of conventional SLM, and T-SLM schemes with N=128.

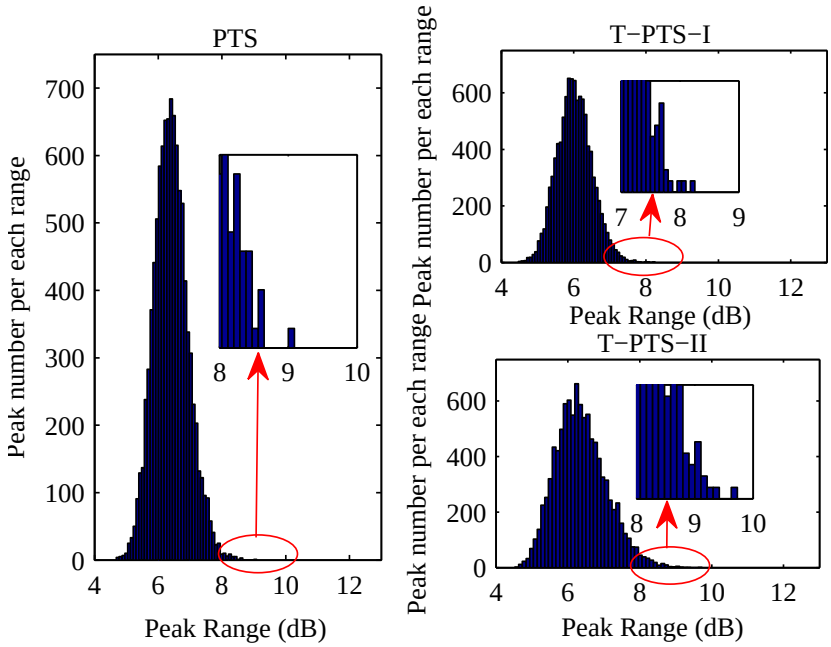

Figure 5.7: Histogram for peak power of conventional PTS, T-PTS-I and T-PTS-II schemes with N=128.

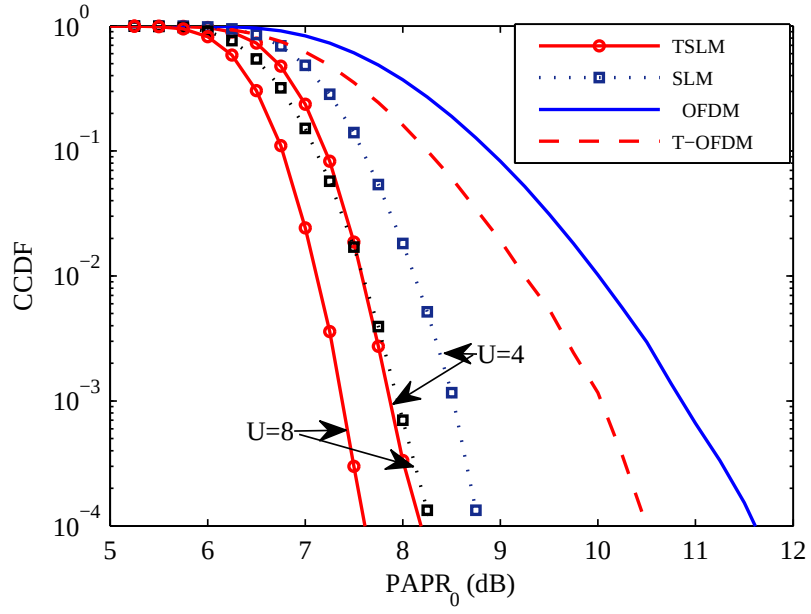

Figure 5.8: CCDF for conventional OFDM, OFDM-SLM, and T-OFDM-SLM systems with N=128, $L = 4$ and U=[4,8].

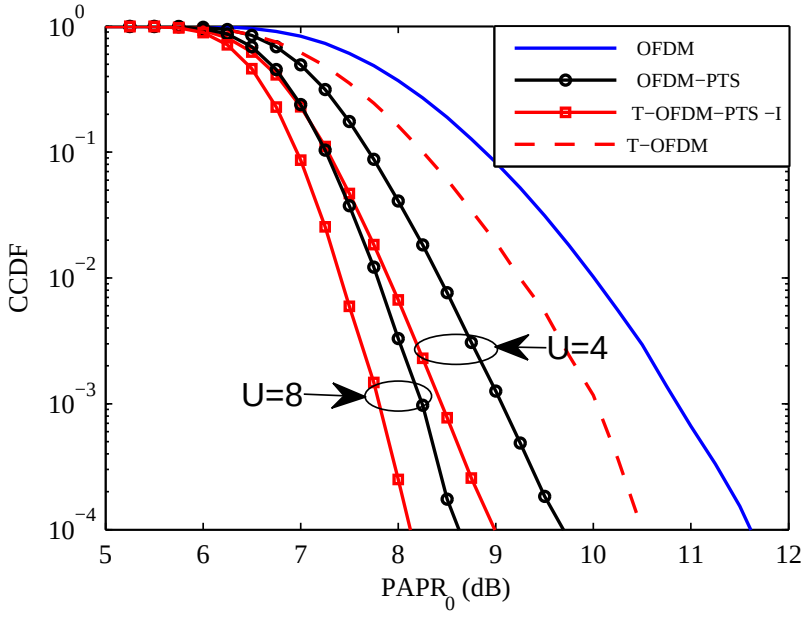

Figure 5.9: CCDF for conventional OFDM, OFDM-PTS and T-OFDM-PTS-I systems with N=128, $L = 4$ and U=[4,8].

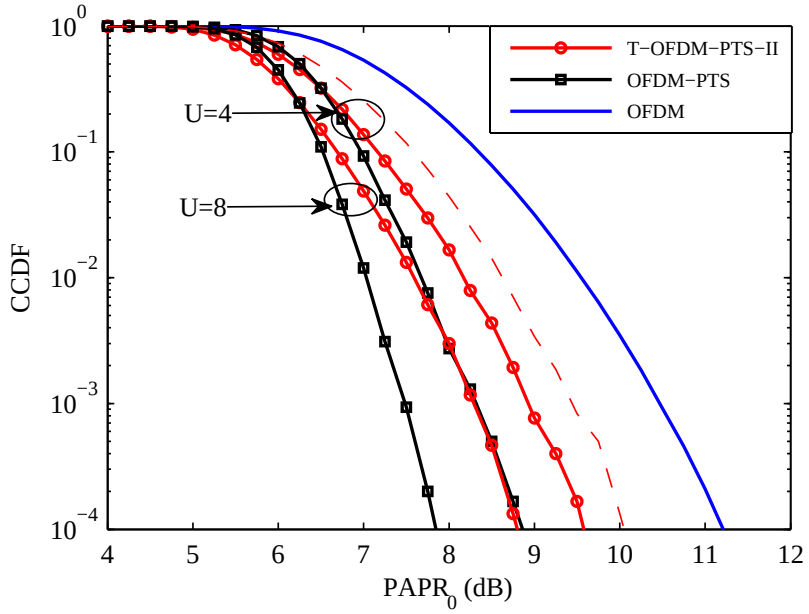

Figure 5.10: CCDF for conventional OFDM, OFDM-PTS, T-OFDM-PTS-II systems with N=128, $L = 1$ and U=[4,8].

duction and reduces the data rate losses of the system by reducing the SI by two; however, with slight degradation in the PAPR performance compared to the conventional PTS scheme, as clearly shown in Fig. 5.10.

Many PAPR reduction techniques cause in-band and out-band distortions for the spectrum of the OFDM signal as a consequence of slower spectrum roll-off, more spectrum side-lobes, and higher adjacent channel interference [100]. As shown in Fig. 5.11, the proposed T-OFDM-SLM, T-OFDM-PTS-I and T-OFDM-PTS-II systems do not have a detrimental effect on the original power spectrum of OFDM signals. (Note: Normalised factor for frequencies in Fig. 5.11 is 1 MHz.)

5.6.3 BER Performance

BER is a typical performance measure for quantifying the benefits of using the proposed T-OFDM, T-SLM, T-PTS-I and T-PTS-II schemes, to reduce the peak power.

In order to investigate the BER performance of such systems over multipath transmission, we have evaluated their performance based on the same system parameters and channel profile as that used with the T-OFDM system in Chapter 4. The BER performance of the investigated systems with such parameters is demonstrated in Fig.

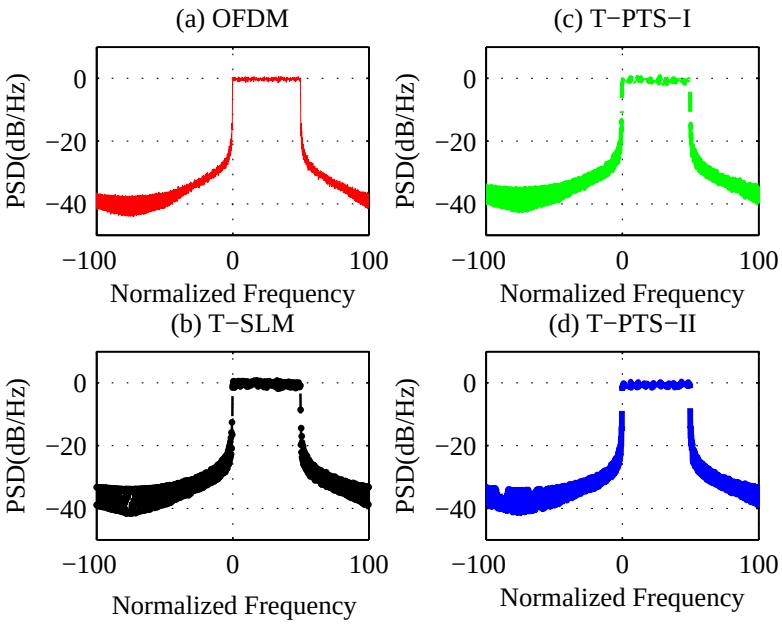

Figure 5.11: PSD for baseband signals of conventional OFDM, T-OFDM-SLM, T-OFDM-PTS-I and T-OFDM-PTS-II systems with N=128, QPSK and U=4.

5.12-5.15, in which the SSPA, with a typical value of random positive integer parameter, i.e. $P = 3$, and input-back off (IBO)$\in$[5,7] is considered. As is clear in these figures, the T-SLM, T-PTS-I and T-PTS-II schemes exhibit a significant improvement in the BER performance with QPSK modulation over the multipath propagation, even in the presence of HPA, when compared with conventional OFDM-SLM and OFDM-PTS systems. Whereas, a noticeable BER improvement is attained with 16-QAM. The improvement in performance is a consequence of exploiting the WHT to achieve frequency diversity by spreading subcarriers over each other. These high diversity systems help to mitigate the deep fade effect arising from the multipath channel on an individual subcarrier, even in the presence of a clipping distortion owing to use SSPA. Consequently, the superiority of the OFDM-based T-SLM, T-PTS-I and T-PTS schemes is obvious. Moreover, in the presence of the HPA clipping distortion, BER performance improvement of the T-OFDM system can be increased by reducing PAPR. In the sequel, an outstanding BER performance can be achieved using a T-OFDM system even with high clipping distortion, i.e. IBO$\simeq$ 0, when an efficient PAPR reduction scheme is used. It should be noted that all the results given above are achieved by utilizing the MMSE equaliser.

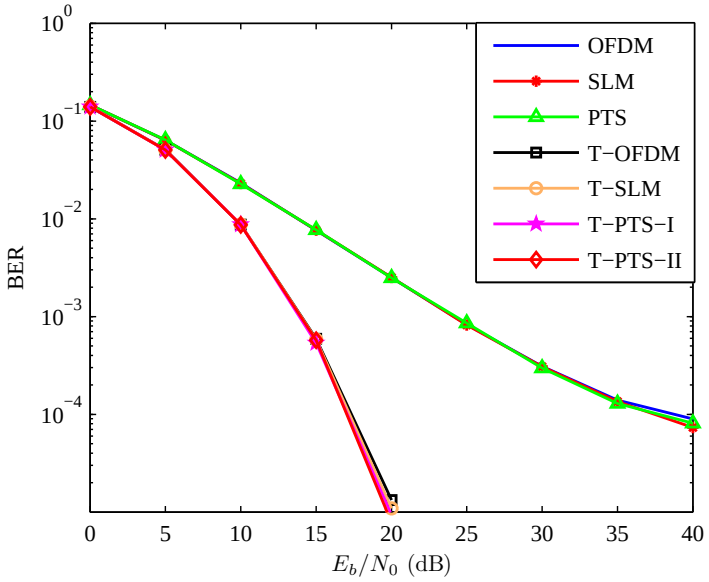

Figure 5.12: BER performance of T-OFDM, T-OFDM-SLM, T-OFDM-PTS-I, T-OFDM-II, conventional OFDM, OFDM-SLM and OFDM-PTS systems with QPSK and SSPA (IBO=7).

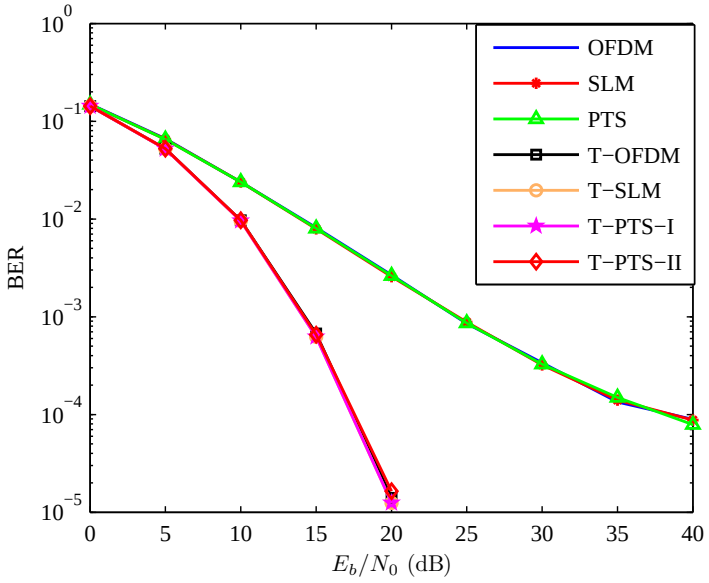

Figure 5.13: BER performance of T-OFDM, T-OFDM-SLM, T-OFDM-PTS-I, T-OFDM-II, conventional OFDM, OFDM-SLM and OFDM-PTS systems with QPSK and SSPA (IBO=5).

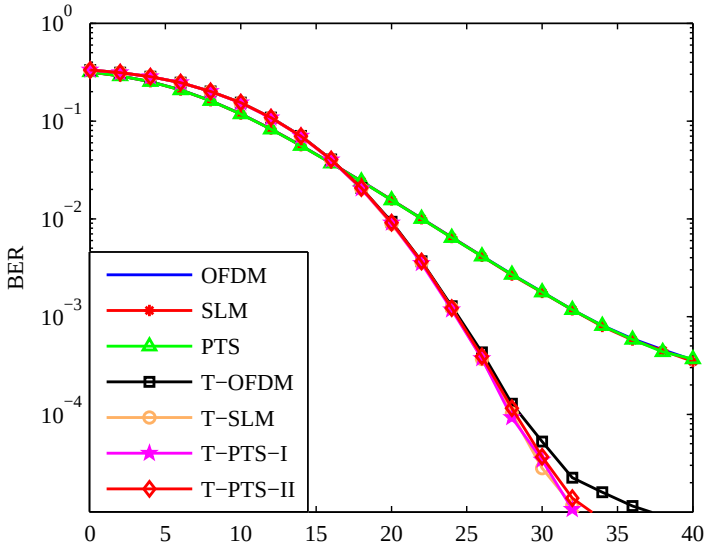

Figure 5.14: BER performance of T-OFDM, T-OFDM-SLM, T-OFDM-PTS-I, T-OFDM-II, conventional OFDM, OFDM-SLM and OFDM-PTS systems with 16-QAM and SSPA (IBO=7).

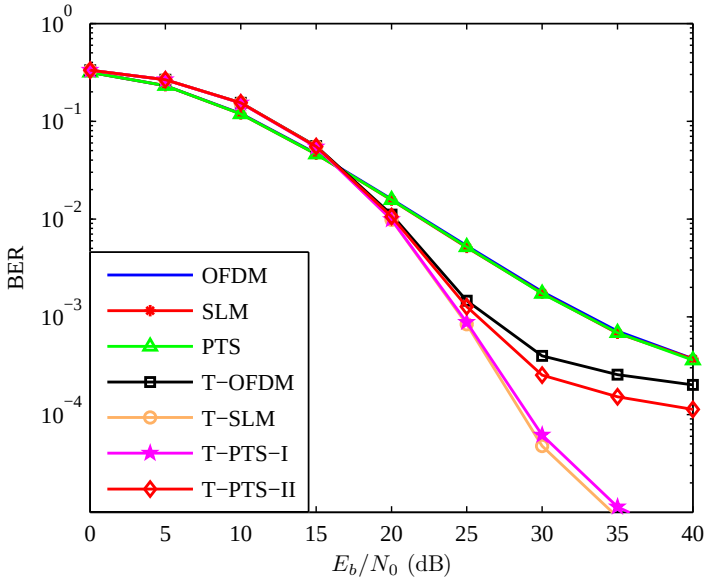

Figure 5.15: BER performance of T-OFDM, T-OFDM-SLM, T-OFDM-PTS-I, T-OFDM-II, conventional OFDM, OFDM-SLM and OFDM-PTS systems with 16-QAM and SSPA (IBO=5).

5.7 Chapter Summary

The focus of this chapter was on the PAPR of the T-OFDM system. In addition, efficient techniques have been proposed to achieve more PAPR reduction, namely, T-SLM, T-PTS-I and T-PTS-II. The proposed schemes offer significant CCRR and PAPR improvement over conventional SLM and PTS schemes. Furthermore, the proposed T-PTS-II scheme achieves a considerable complexity reduction, as well as reducing the SI; i.e. lower data rate losses, albeit with a negligible PAPR degradation. Moreover, the spreading of each subcarrier over others introduces frequency diversity. Consequently, the proposed schemes achieve a significant improvement in BER performance across multipath fading channels, even in the presence of HPA. Simulation results have demonstrated that the proposed systems require less SNR compared to the traditional systems. Consequently, a multicarrier system utilizing the proposed schemes will benefit from low computational complexity requirements, a low PAPR, and reduced SNR requirements over multipath transmission, even in the presence of HPA.

CHAPTER 6

T-OFDM With the Impulsive Noise Channel

One of the major sources of disturbance in OFDM systems that impacts on the performance of such systems is impulsive noise. Therefore, recent studies have been compiled with the stated intention of suppressing the negative ramifications of this phenomenon. In this chapter, the BER performance of the T-OFDM system is investigated under conditions of man-made noise. In addition, a new theoretical BER formula over such a transmission media is derived. Moreover, the independent section of T-transforms is found to have a deleterious effect on the T-OFDM BER performance under heavy-tail impulsive noise. Therefore, in order to suppress the negative ramification of a severe impulsive noise burst on the performance of T-OFDM system, a new scheme WHT-MI-OFDM based on using WHT and a matrix interleaver (MI) with an OFDM system is proposed. A WHT-MI-OFDM system achieves a considerable BER performance improvement over multipath transmission and under the disturbance of medium and heavy impulsive noise. However, a severe impulsive noise burst has a noticeable deleterious effect on the BER performance of such a system. Therefore, a memoryless nonlinear blanking method (which is already used with the traditional OFDM systems to overcome man-made disturbance) is used on the receiver side of the WHT-MI-OFDM system. Proposed WHT-MI-OFDM and WHT-MI-OFDM with blanking systems are used to suppress the effect of impulsive noise channel, by averaging its effect over large OFDM symbols, and further to spread the reduced effect again across all the other subcarriers, owing to the use of WHT. Proposed schemes are also resilient to dispersion arising from multipath transmission, owing to the frequency diversity of the transmitted subcarriers introduced by WHT.

6.1 Introduction

OFDM symbols have a long duration, owing to the use of FFT on the receiver side, providing robustness against weak impulsive noise by spreading impulsive noise energy among transmitted OFDM subcarriers. Nevertheless, this advantage becomes a disadvantage if the impulsive noise energy exceeds a certain threshold [19], [20]. The disturbance caused by impulsive (man-made) noise arises primarily from power lines, heavy current switches and other sources, having a negative ramification on the BER performance of such systems. Therefore, recent studies have employed considerable efforts to analyse and mitigate the impact of this phenomenon on OFDM performance.

Regarding performance analysis, researchers in [19], [101], and [102] conducted an investigation of the limitations of single and multicarriers (SC/ MC) systems' performance over impulsive noise channels. Its was determined that the MC systems' performance was considerably impaired compared to the SC systems, over this media of transmission. Thus, the effect of the severe impulsive noise on the MC systems performance must be accompanied by an efficient impulsive noise suppression technique. Moreover, Amirshahi *et al.* analysed the effects of impulsive noise and the frequency selective fading channel on the performance of an OFDM system [103]. A time domain model based on Markov modelling and a statistical model based on Poisson distribution were deployed in this analysis. Furthermore, Zhodkov investigated the OFDM receiver with blanking nonlinearity in various man-made noise scenarios and undertook a worst case scenario determination [104]. Whereas, the performance assessments and comparison of the OFDM receiver with clipping, blanking and combined clipping-blanking memoryless nonlinearity techniques over various impulsive noise models were introduced in [20].

Conversely, a considerable effort has been devoted to suppress the impact of impulsive noise in recent studies. [105] used pilot tones as syndromes to quantify man-made noise locations in order to mitigate them. Matrix interleaver (MI) was used with the conventional OFDM system in the frequency-domain to eliminate the deleterious effect of the noisy (background Gaussian plus impulsive noise) channel [101]. Moreover, Al-Dweik *et al.* used MI post the IDFT (i.e. in time-domain) to reduce the effect of impulsive noise, by spreading the damaged bits over a large number of symbols [106], further to reduce the channel error rate [107]. A significant BER performance was achieved over the AWGN [106] and multipath fading channel models [107], even in the presence of impulsive noise; although there was relatively high computational complexity at the receiver side owing to the use of an extra two IFFT and FFT with the channel equalization process. Furthermore, channel estimation in such a system requires either a coherent technique, which based on adding pilot to data samples in the time-domain, then channel estimation and compensation perform in the frequency-domain, or time-domain data recovery techniques, that inherently requiring high computational complexity.

Relating to the systems considered in this work, Bogucka in [108] studied the impact of impulsive noise on the WHT-OFDM system's performance over background Gaussian plus the impulsive noise channel model. Impulsive noise bursts with different

durations and the hit position revealed significantly different performances.

6.2 Impulsive Noise Effect

As described in [105], impulsive noise elements β_n can be modelled as

$$\beta_n = \zeta_n \varphi_n, \forall n \in \{0 \dots N_t - 1\}, \tag{6.1}$$

where $N_t = N + N_g$ is the total length of the transmitted data sequence, N and N_g denote the DFT and CP lengths, respectively, ζ_n stands for a Bernoulli process with a sequence of zeros and ones based on probability $\Gamma = P(\zeta_n = 1) = \delta$ and $\hat{\Gamma} = P(\zeta_n = 0) = 1 - \delta$, and $\varphi_n = [\varphi_0, \varphi_1, \dots, \varphi_{N_t-1}]^T$ is the complex Gaussian noise sequence with zero mean and variance σ_φ^2, such as $\sigma_\varphi^2 \gg \sigma_z^2$ and the ratio of the man-made noise variance, σ_φ^2, over the background Gaussian noise variance σ_z^2 is μ, i.e. $\mu = \frac{\sigma_\varphi^2}{\sigma_z^2}$.

The number of impulsive noise bursts within a specific transmission period, the man-made noise variance, σ_φ^2, and the number of samples hit by each individual burst, γ, depend on the considered application. In some applications, each transmitted symbol may be hit by at most one burst, with a duration $\gamma \leq N_t$. Hence, the probability of impulsive noise occurrence was defined formerly and can be reformulated as, $\Gamma = \frac{\gamma}{N_t}$. Furthermore, impulsive noise distribution can be classified into three categories: (1) Weak distribution (WD); (2) Medium distribution (MD); and (3) Heavy distribution (HD) [102]. In this chapter, this classification will be used based on the assumption of one impulsive noise burst appears every 10 T-OFDM symbols during the transmission period. Hence, the values of μ and γ that are defined early in this section are considered in each category, as shown in Table 6.1.

6.3 T-OFDM System With the Impulsive Noise Channel

Consider the T-OFDM system model, which was developed and analysed in Chapter 4, as a resilient system against the dispersion arising from the multipath fading channel, under the impulsive noise disturbance, as shown in Fig. 6.1 . The i-th time-

Table 6.1: Impulsive noise categories

	Impulsive noise categories		
	Weak distribution	Medium distribution	Heavy distribution
$10^1 <= \mu < 10^2$	√	√	
$10^2 <= \mu < 10^3$	√	√	
$10^3 <= \mu < 10^4$	√		√
$\Gamma <= 0.1$	√		
$0.1 < \Gamma <= 0.25$		√	√
$0.25 < \Gamma <= 1$			√

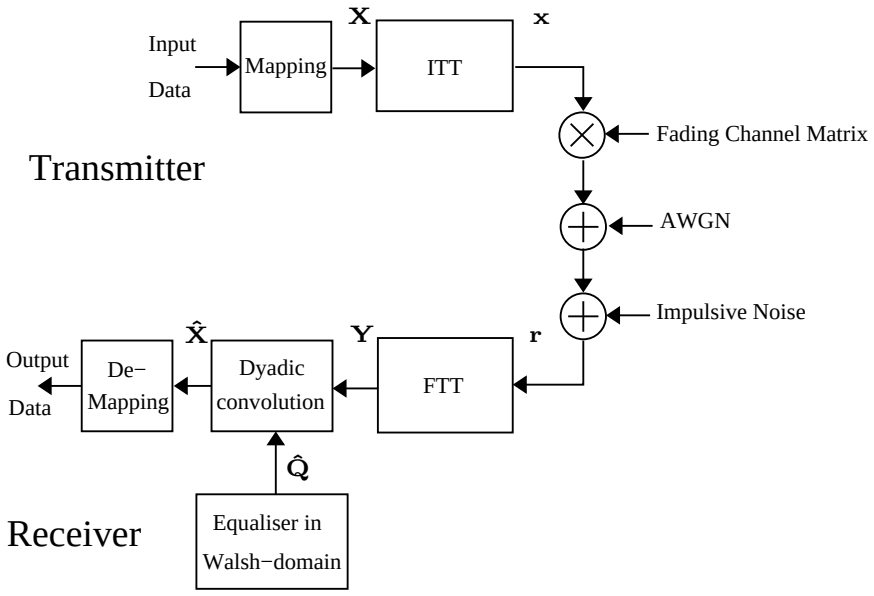

Figure 6.1: T-OFDM system block diagram under impulsive noise.

domain block of N-points incoming modulated data vector, $\mathbf{X}^{(i)} = [X_0^{(i)}, X_1^{(i)}, \ldots, X_{N-1}^{(i)}]^T$, which is selected uniformly from the QAM or PSK constellations, can be computed as,

$$\mathbf{x}^{(i)} = \hat{\mathbf{T}}\mathbf{X}^{(i)}, \tag{6.2}$$

where $\mathbf{x}^{(i)} = [x_0^{(i)}, x_1^{(i)}, \ldots, x_{N-1}^{(i)}]^T$ and $\hat{\mathbf{T}}$ is the ITT.

In a dispersive channel, a guard interval with N_g samples of the back-end of $\mathbf{x}$

should be appended to the front-end in order to mitigate the ISI phenomenon. The constraint of choosing the value of N_g is similar to that described in Chapter 4.

On the receiver side, with the assumption of perfect time and frequency synchronization, the i-th block of the received time domain data vector transmitted through the multipath fading channel and under impulsive noise after the CP removing, can be expressed as,

$$\mathbf{r}^{(i)} = \mathbf{D}^{(i)}\mathbf{x}^{(i)} + \mathbf{\Psi}^{(i)}, \tag{6.3}$$

where $r_n^{(i)} = [r_0^{(i)}, r_1^{(i)}, \ldots, r_{N-1}^{(i)}]^T$, $\mathbf{\Psi}^{(i)} = \mathbf{z}^{(i)} + \beta^{(i)}$, $z_n^{(i)} = [z_0^{(i)}, z_1^{(i)}, \ldots, z_{N-1}^{(i)}]^T$ denotes the additive white Gaussian noise with zero mean and variance σ_z^2, β is the impulsive noise vector expressed in section 6.2, and $\mathbf{D}$ is the circulant channel matrix, which was defined in Chapter 4. Thus, the output of the FTT can be computed as,

$$\mathbf{Y}^{(i)} = \mathbf{T}\ \mathbf{r}^{(i)}. \tag{6.4}$$

Subsequently, in order to mitigate the negative effect of the fading channel dispersion, three schemes of channel equalization that were described in Chapter 4 also can be used in this chapter.

For clear performance analysis, which will be introduced in the next section, the receiver that was shown in Fig. 4.2 is utilised here as shown in Fig. 6.1. For the sake of simplicity, the Dyadic convolution operation will translate to multiplications based on Dyadic convolution theorem [61]. As used in Chapter 4, the MMSE equaliser is utilised for channel equalization purpose. In the sequel, the recovered data vector $\hat{\mathbf{X}}^{(i)} = [\hat{X}_0^{(i)}, \hat{X}_1^{(i)}, \ldots, \hat{X}_{N-1}^{(i)}]^T$ can be expressed as,

$$\hat{\mathbf{X}}^{(i)} = \hat{\mathbf{Q}}^{(i)} \overline{\otimes} \mathbf{Y}^{(i)} \tag{6.5a}$$

$$= (\mathbf{W}\mathbf{Q}^{(i)}) \overline{\otimes} (\mathbf{T}\mathbf{r}) \tag{6.5b}$$

$$= (\mathbf{W}\mathbf{Q}^{(i)}) \overline{\otimes} (\mathbf{W}\mathbf{F}\mathbf{r}^{(i)}), \tag{6.5c}$$

where $\hat{\mathbf{Q}}$ is the equaliser sequence in the Walsh-domain, i.e. $\hat{\mathbf{Q}} = \mathbf{W}\mathbf{Q}$, $\overline{\otimes}$ denotes the Dyadic convolution operation, and $\mathbf{Q}$ stands for the equaliser sequence in the frequency-domain.

Using the logical (dyadic) convolution theorem [61], (6.5c) can be re-written as,

$$\hat{\mathbf{X}}^{(i)} = \mathbf{W}\left(\mathbf{Q}^{(i)}\mathbf{F}\mathbf{r}^{(i)}\right) \tag{6.6a}$$

$$= \mathbf{W}\boldsymbol{\Omega}^{(i)}\mathbf{X}^{(i)} + \mathbf{W}\mathbf{Q}^{(i)}\mathbf{Z}^{(i)} + \mathbf{W}\mathbf{Q}^{(i)}\boldsymbol{\Phi}^{(i)}, \tag{6.6b}$$

where $\boldsymbol{\Omega} = \mathbf{QH}$, and $\mathbf{Z}$ and $\boldsymbol{\Phi}$ are the discrete-frequency samples of the Gaussian and man-made noises, respectively. For simplicity, the index of received frame i will be dropped in subsequent equations.

In the following sections, we will study the performance analysis for conventional OFDM and T-OFDM systems over multipath transmission in the presence of impulsive noise by computing the SNR values of the received signals for both systems. The approach used in Chapter 4 will be used to present this analysis with two equalization criteria (ZF and MMSE).

6.4 Performance Analysis

6.4.1 Conventional OFDM System

Without loss of generality, we assume that the elements of the desired signal $\mathbf{X}$, background Gaussian noise $\mathbf{z}$ and impulsive noise β vectors are independent.

Interestingly, by using $\mathbf{W} = \mathbf{I}$, where $\mathbf{I}$ stands for the identity matrix, (6.6b) can be regarded as the received signal of the conventional OFDM system. Thus, the kth received subcarrier in the OFDM symbol can be expressed as,

$$\hat{X}_k = \Omega_k X_k + Q_k Z_k + Q_k \Phi_k. \tag{6.7}$$

Consequently, based on (4.30), the SNR value of the kth subcarrier in (6.7) can be computed as,

$$\lambda_k^{\mathrm{OFDM}} = \frac{|X_k|^2}{|Z_k|^2 + |\Phi_k|^2}\epsilon_k, \tag{6.8}$$

where $\epsilon_k = \frac{|\Omega_k|^2}{|Q_k|^2}$. The elements of equaliser sequence, $\mathbf{Q}$, based on ZF and MMSE criteria were computed in (2.13) and (2.19b), respectively. Thus, the kth value of $\boldsymbol{\Omega}$ with ZF and MMSE criteria can be expressed as,

$$\Omega_k^{\mathrm{ZF}} = Q_k^{\mathrm{ZF}} H_K = 1, \tag{6.9}$$

$$\Omega_k^{\text{MMSE}} = Q_k^{\text{MMSE}} H_K = \frac{\lambda_0 |\mathbf{H}_k|^2}{\lambda_0 |\mathbf{H}_k|^2 + 1}, \tag{6.10}$$

where the multiplication and division operations in these equations are element-by-element operations. Thus, with both ZF and MMSE criteria, the value of ϵ_k, which appeared previously in (6.8), is equivalent to $|H_k|^2$. Therefore, the BER performances of the OFDM system over multipath fading channels in the presence of impulsive noise when utilizing ZF or MMSE equalisers are identical. Consequently, the average SNR for the symbol of such a system transmitted over such transmission circumstances can be computed as,

$$\lambda^{\text{OFDM}} = \frac{\sigma_X^2}{\sigma_Z^2 + \sigma_\Phi^2} E[|\mathbf{H}|^2], \tag{6.11}$$

where σ_X^2, σ_Z^2 and σ_Φ^2 are the average power of the received desired signal, white Gaussian noise and impulsive noise, respectively. Basically, the average power for the time-domain Gaussian noise and impulsive noise sequences and that for their symbols in frequency-domain are identical. Thus, the impulsive noise average power can be evaluated as,

$$\sigma_\Phi^2 = E[|\Phi|^2]. \tag{6.12}$$

For Gaussian distribution vector, φ_n, the value of $E[|\Phi|^2]$ can be approximately re-calculated as,

$$E[|\Phi|^2] \simeq \Gamma \sigma_\varphi^2 \tag{6.13a}$$

$$\simeq \Gamma \mu \sigma_z^2. \tag{6.13b}$$

In the sequel, (6.11) can be reformulated as,

$$\lambda^{\text{OFDM}} = \frac{\sigma_X^2}{\sigma_z^2 (1 + \Gamma\mu)} E[|\mathbf{H}|^2], \tag{6.14a}$$

$$= \frac{\lambda_0}{(1 + \Gamma\mu)} E[|\mathbf{H}|^2]. \tag{6.14b}$$

Eventually, upon substituting (6.14b) into (4.28) and (4.29), the theoretical BER performance of the conventional OFDM system under the disturbance of the impulsive

noise and with M-PSK and M-QAM data mappers can be expressed as,

$$P_{e\text{M-PSK}}^{\text{OFDM}} = \frac{\varepsilon}{mN} \sum_{k=0}^{N-1} Q\left(\sqrt{2\lambda_k^{\text{OFDM}}} \sin(\pi/M)\right), \tag{6.15}$$

$$P_{e\text{M-QAM}}^{\text{OFDM}} = \frac{\alpha}{N} \sum_{k=0}^{N-1} Q\left(\sqrt{3\lambda_k^{\text{OFDM}}/(M-1)}\right), \tag{6.16}$$

where $\alpha = \frac{(4-2^{(2-m/2)})}{m}$.

6.4.2 T-OFDM System

The impact of impulsive noise on the WHT-OFDM system performance over background Gaussian plus impulsive noise channel model is introduced in [108], where it was shown that the effect of impulsive noise bursts on the performance of WHT-OFDM system was altered significantly with the change in duration (hitted samples number) and position of hitting. In this section, as in [109], a comprehensive study will be introduced to identify the effect of the multipath fading channel dispersion and impulsive noise disturbance in order to propose an efficient approach to suppress these negative ramifications.

Once again, the received signal of the T-OFDM system shown in Fig. 6.1 can be expressed as,

$$\hat{\mathbf{X}} = \mathbf{W}\boldsymbol{\Omega}\mathbf{X} + \mathbf{W}\mathbf{Q}\mathbf{Z} + \mathbf{W}\mathbf{Q}\boldsymbol{\Phi}, \tag{6.17}$$

where $\mathbf{W}$ is the $N \times N$ normalised Walsh-Hadamard matrix. By using (4.30), the average SNR of the T-OFDM system under the dispersion of frequency selective fading and man-made noise channel with ZF equaliser can be written as, [109]

$$\lambda^{\text{ZF}} = \frac{\sigma_X^2}{(1+\Gamma\mu)\frac{\sigma_Z^2}{N} \underbrace{\sum_{k=0}^{N-1} \frac{1}{|H_k|^2}}_{\boldsymbol{\Delta}}}, \tag{6.18}$$

As clearly shown in (6.18) the values of SNR are more susceptible to the channel dispersion than the impulsive noise duration or power change, where in the case of

deep fade, i.e. $H_k \simeq 0$, the value of $\mathbf{\Delta}$ will be very high, i.e. $\mathbf{\Delta} \simeq \infty$ and $\lambda \simeq 0$. In the sequel, by using ZF criterion, the performance of the T-OFDM system will be worse than that of conventional OFDM system. Thus, the theoretical BER performance of the T-OFDM system over the multipath fading channel in the presence of man-made noise with M-PSK and M-QAM modulation using ZF equaliser can be expressed as,

$$P_{e\text{M-PSK}}^{\text{T-OFDM}} = \frac{\varepsilon}{m} Q\left(\sqrt{2\lambda^{\text{ZF}}}\sin(\pi/M)\right), \tag{6.19}$$

$$P_{e\text{M-QAM}}^{\text{T-OFDM}} = \alpha Q\left(\sqrt{3\lambda^{\text{ZF}}/(M-1)}\right), \tag{6.20}$$

Alternatively, an MMSE equaliser can be utilised in order to significantly reduce the deleterious effects of the null channel coefficient, i.e. $H_k \simeq 0$, on the performance of such a system over multipath fading channels. However, the negative ramifications of impulsive noise will clearly appear. Thus, with MMSE criterion, the desired signal power of (6.17) can be computed as,

$$\text{Desired Signal Power} = a^2\sigma_X^2, \tag{6.21}$$

where $a = \frac{1}{N}\sum_{k=0}^{N-1}\Omega_k^{\text{MMSE}}$. Moreover, the received signal power, $\sigma_{\hat{X}}^2$, can be evaluated as,

$$\sigma_{\hat{X}}^2 = \sigma_X^2\frac{1}{N}\sum_{k=0}^{N-1}\frac{(\lambda_0|H_k|^2)^2}{(\lambda_0|H_k|^2+1)^2}$$

$$+\frac{1}{N}\sigma_X^2\sum_{k=0}^{N-1}\frac{\lambda_0|H_k|^2}{(\lambda_0|H_k|^2+1)^2} + \frac{\Gamma\mu\sigma_X^2}{N}\sum_{k=0}^{N-1}\frac{\lambda_0|H_k|^2}{(\lambda_0|H_k|^2+1)^2} \tag{6.22a}$$

$$= \sigma_X^2\frac{1}{N}\sum_{k=0}^{N-1}\frac{\lambda_0|H_k|^2}{\lambda_0|H_k|^2+1} + \frac{\Gamma\mu\sigma_X^2}{N}\sum_{k=0}^{N-1}\frac{\lambda_0|H_k|^2}{(\lambda_0|H_k|^2+1)^2} \tag{6.22b}$$

$$= \sigma_X^2\frac{1}{N}\left(\sum_{k=0}^{N-1}\left(\frac{\lambda_0|H_k|^2(1+\Gamma\mu+\lambda_0|H_k|^2)}{(\lambda_0|H_k|^2+1)^2}\right)\right) \tag{6.22c}$$

Upon substituting (6.21) and (6.22c) into (4.30), the SNR value at the T-OFDM system receiver with the MMSE equaliser can be written as,

$$\lambda^{\text{MMSE}} = \frac{1}{\frac{\sum_{k=0}^{N-1} \frac{\lambda_0 |H_k|^2 (1+\Gamma\mu+\lambda_0 |H_k|^2)}{(\lambda_0 |H_k|^2+1)^2}}{Na^2} - 1}, \tag{6.23}$$

Eventually, the theoretical average BER performance of the conventional T-OFDM system with M-PSK and M-QAM data mapping and MMSE equalization criterion can be expressed as,

$$P_{e\text{M-PSK}}^{\text{T-OFDM}} = \frac{\varepsilon}{m} Q\left(\sqrt{2\lambda^{\text{MMSE}}} \sin(\pi/M)\right), \tag{6.24}$$

$$P_{e\text{M-QAM}}^{\text{T-OFDM}} = \alpha Q\left(\sqrt{3\lambda^{\text{MMSE}}/(M-1)}\right), \tag{6.25}$$

As was proven in [60] and clearly shown in Chapter 4, the T-OFDM system was resilient to the dispersion arising from the multipath transmission. However, the impact of impulsive noise on the performance of such a system requires more identification. The conventional OFDM system outperforms SC based systems under weak and medium distributed impulsive noise bursts, due to its ability to distribute the power of impulsive noise over N subcarriers owing to the use of DFT. This is not the case in the T-OFDM, where the WHT and FFT are replaced by a single fast orthonormal unitary T-transform. Thus, the performance of the T-OFDM system is significantly changed in relation to the location, in which the samples are targeted by the impulsive noise burst. To clarify further, with the assumption of $N = 1024$ subcarriers, if the burst of impulsive noise is discovered in the section with sixteen input-output samples, the performance will be worse, due to the fact that the power of this burst will be distributed across the sixteen samples only; whereas a better performance would be obtained when the distorted samples located in the final section with the $N = 512$ samples. Therefore, this issue will be taken into consideration and new schemes will be proposed in the next sections to improve the performance of such a system within these transmission environments.

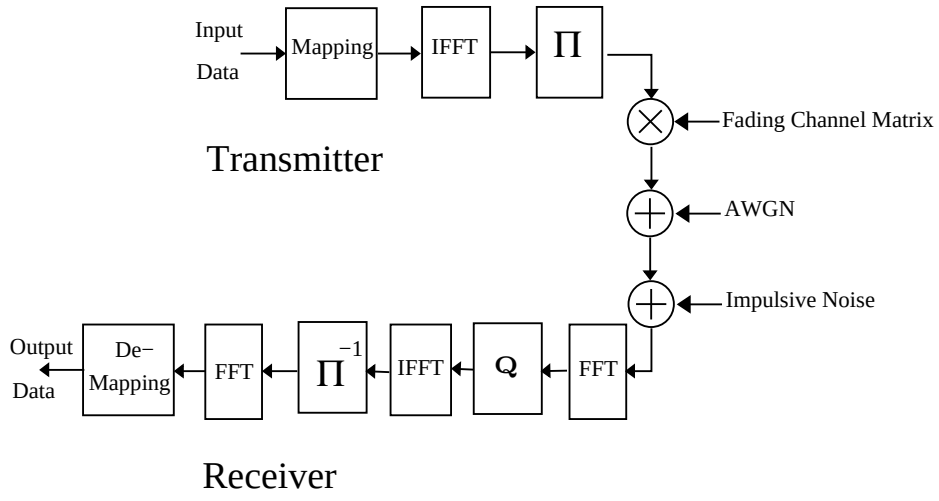

Figure 6.2: OFDM-MI system block diagram.

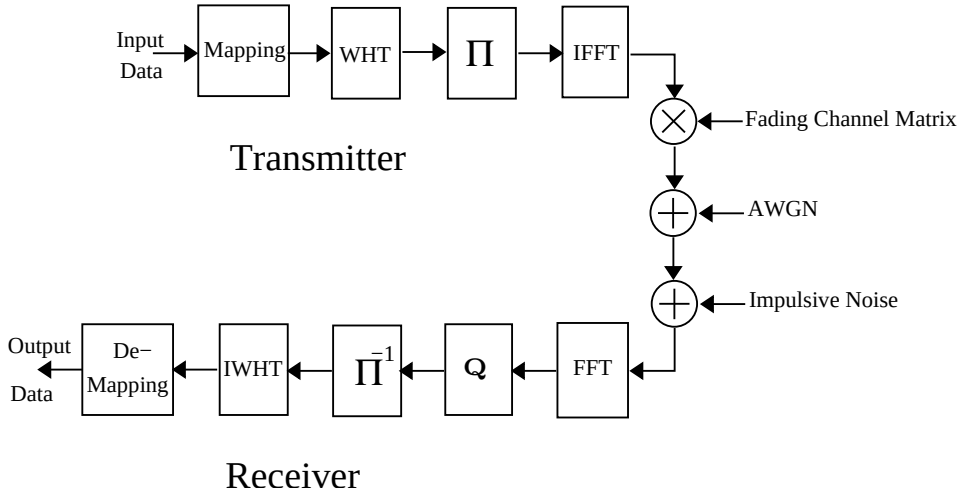

Figure 6.3: WHT-MI-OFDM system block diagram.

6.5 Proposed WHT-MI-OFDM System

6.5.1 WHT-MI-OFDM Structure

A matrix-interleaver (MI) is used with an OFDM system in the frequency-domain [101] to suppress the disturbance of the impulsive noise channel. However, such a system is still susceptible to the heavily distributed impulsive noise channel. Therefore, Al-Dweik *et al.* proposed using MI post-IDFT on the transmitter side and deinter-

leaver pre-DFT on the receiver side of OFDM system, as shown in Fig. 6.2 [106], [107]. As a consequence of reducing the effect of impulsive noise by spreading the damaged bits over a large number of symbols, this further reduces the channel error rate and the OFDM-MI system achieved a significant BER performances over the AWGN channel and multipath fading channel, even in the presence of impulsive noise. However, this requires two additional transforms (IFFT and FFT) to perform the channel equalization process on the receiver side, which will increase the computational complexity of the system. Therefore, MI spreading ability and the diversity acquired from the use of WHT with OFDM system will be employed together with the proposed WHT-MI-OFDM system, which will be investigated in this section, to suppress the negative effects of impulsive channels [109].

The proposed WHT-MI-OFDM and conventional MI-OFDM [101] systems have identical operations across the entire system, except that the WHT will be used before the interleaver at the transmitter side and after the deinterleaver at the receiver side, as shown in Fig. 6.3. Also, for the sake of brevity, all the mathematical models mentioned in section 6.4.2 will not be repeated in this section. Hence, the WHT of N-points incoming modulated data vector $\mathbf{X} = [X_0, X_1, \ldots, X_{N-1}]^T$, is computed as,

$$\mathbf{X}^{'} = \mathbf{W}\mathbf{X}, \tag{6.26}$$

Then, $\mathbf{X}^{'}$ interleaves using MI. The interleaved sequences $\hat{\mathbf{X}}^{'}$ are fed simultaneously into IFFT. This means, the n-th time-domain sample can be computed as,

$$x_n = \frac{1}{\sqrt{N}} \sum_{k=0}^{N-1} \hat{X}_k^{'} e^{j2\pi nk/N}, n = 0, 1, \ldots, N-1. \tag{6.27}$$

Thereafter, the signal x is faded by the multiplicative channel and distorted by background Gaussian and impulsive noises.

On the receiver side of the WHT-MI-OFDM system, with an assumption of perfect time and frequency synchronization, the received time-domain samples r_n, which were defined formerly in (6.3), are processed by FFT and the conventional frequency-domain channel equalization is performed by using MMSE criterion. Eventually, after the deinterleaving operation, the normalised WHT is applied to the equalised sequence to recover the data symbols. For the sake of clarity, the stages of WHT-MI-OFDM system suppressing the man-made noise are simply presented in Fig. 6.4 {*Note*: Font

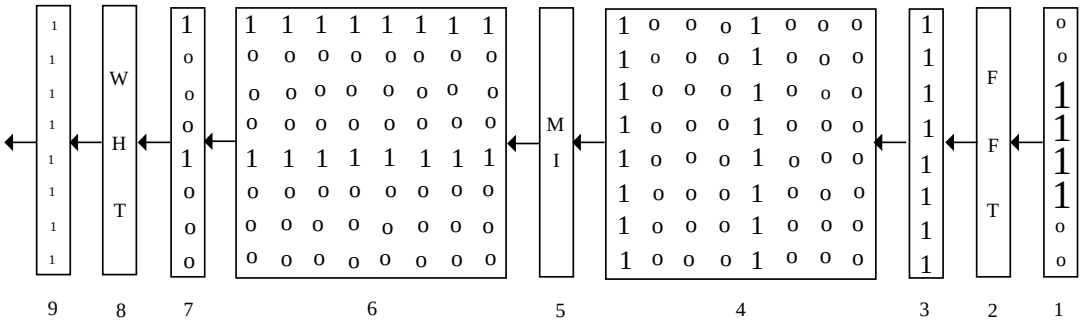

Figure 6.4: Impulsive noise burst power through the WHT-MI-OFDM system, where 1 and 0 stand for value and valueless impulsive noise samples, respectively.

size of 1s is changed as a sign of the impulsive noise power change}. As clearly shown in this figure, with an assumption of $N = 8$ and four impulsive noise samples, the high power impulsive noise samples (sub-block 1) are spread over N subcarriers through FFT (sub-block 2), which is the case with the conventional OFDM system. The impulsive noise samples with relatively low power (sub-block 3) are buffered as a matrix (sub-block 4) and then fed to MI (sub-block 5) to obtain a new interleaved matrix of data (sub-block 6). Every frame (sub-block 7) is processed and distributed again using a WHT (sub-block 8) to obtain a new frame of noise samples with a lower power (sub-block 9). In the sequel, a considerable power suppression for impulsive noise samples is achieved using a WHT-MI-OFDM system. However, with severe man-made noise in sub-block 1, the power of the resultant noise vector (sub-block 9) will be relatively high. Thus, the disturbance of this noise will obviously impair the performance of WHT-MI-OFDM system. This means that the proposed WHT-MI-OFDM system will work efficiently across weak and medium categories of impulsive noise distribution. Therefore, with heavily impulsive noise distribution, a simple nonlinearity blanking scheme will be incorporated with the WHT-MI-OFDM system in order to suppress the deleterious effect of such heavily impulsive noise distribution. The blanking nonlinearity scheme is applied for the time-domain samples as [20]

$$\hat{y}_n = \begin{cases} r_n & \text{if } |r_n| \leq \hat{\mathbf{S}} \\ 0 & \text{if } |r_n| > \hat{\mathbf{S}} \end{cases}, \tag{6.28}$$

where r_n is the received time-domain samples, as defined formerly in (6.3), and $\hat{\mathbf{S}}$ is the blanking threshold. Depending on the appropriate choice of $\hat{\mathbf{S}}$, the deleterious

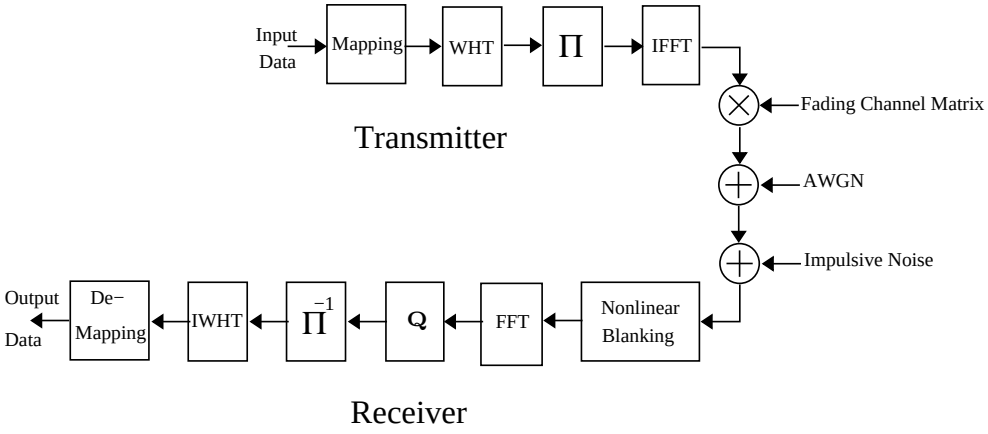

Figure 6.5: WHT-MI-OFDM system block diagram with nonlinearity blanking scheme.

effect of heavily impulsive noise can be reduced. In this proposed scheme, the position of the impulsive noise burst is assumed to be known, and many techniques found in the literature can be used to identify this position. Then, the suppressed samples are fed to the other parts of the system receiver shown in Fig. 6.5.

6.5.2 BER and Computational Complexity Comparison of Proposed WHT-MI-OFDM and Conventional OFDM-MI Systems

In order to highlight the features by which the proposed WHT-MI-OFDM system outperforms the OFDM-MI system a fair comparison will be made between two such systems in terms of BER and computational complexity.

The ability of the OFDM-MI system to reduce the effect of impulsive noise by spreading the damaged bits over a large number of symbols, to further reduce the channel error rate will be provided in the proposed WHT-MI-OFDM system by performing the WHT and MI operations. Hence, as previously clarified in Section 6.5.1, utilizing WHT on the deinterleaved samples will help to spread the impulsive noise effect over a large number of symbols, further to provide high fading channel diversity. Therefore, the BER performances of the proposed WHT-MI-OFDM and OFDM-MI systems are slightly closed, as shown in Figs 6.6 and 6.7. These results are obtained by the systems considered under the effect of the impulsive noise burst, which appears every 2560 samples during the transmission period.

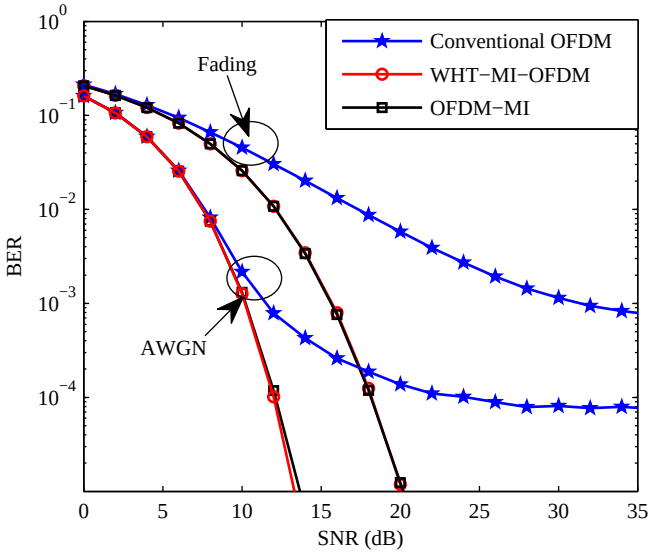

Figure 6.6: BER performance of WHT-MI-OFDM and OFDM-MI systems with QPSK,$\Gamma = 0.1$, and $\mu = 1000$ over AWGN and fading channels, with the presence of impulsive noise.

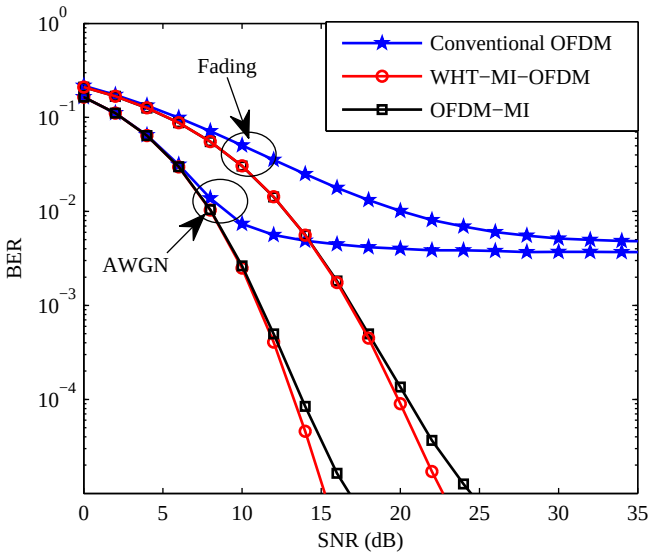

Figure 6.7: BER performance of WHT-MI-OFDM and OFDM-MI systems with QPSK, $\Gamma = 0.25$, and $\mu = 1000$ over AWGN and fading channels, with the presence of impulsive noise.

On the other hand, as shown in Fig. 6.2-6.3, the required complexities of modulation and interleaving processes in both systems are identical. Therefore, these will be omitted in the computational complexity calculation for both systems. Thus, the total complexity of operations required to implement the WHT-MI-OFDM system involves the computation of the WHT and IFFT at the transmitter, WHT and FFT at the receiver, plus N multiplications of the channel equalization processes. Whereas, the total complexity of operations required to implement the OFDM-MI system, where the channel equalization process is performed in the frequency-domain, involved the computation of the IFFT at the transmitter side, an equalization process, which includes DFT and IDFT operations plus N multiplications, and FFT at the receiver side. Thus, the required complex multiplications C_M and complex additions C_A in both WHT-MI-OFDM and OFDM-MI systems can be computed as,

$$C_M^{\text{WHT-MI-OFDM}} = \underbrace{N \log_2 N}_{\text{IFFT+FFT}} + \underbrace{N}_{\text{Equalization}} \tag{6.29}$$

$$C_A^{\text{WHT-MI-OFDM}} = \underbrace{2N \log_2 N}_{\text{IWHT+WHT}} + \underbrace{2N \log_2 N}_{\text{IFFT+FFT}} \tag{6.30}$$

$$C_M^{\text{OFDM-MI}} = \underbrace{N \log_2 N}_{\text{IFFT+FFT}} + \underbrace{\underbrace{N \log_2 N}_{\text{IFFT+FFT}} + N}_{\text{Equalization}} \tag{6.31}$$

$$C_A^{\text{OFDM-MI}} = \underbrace{2N \log_2 N}_{\text{IFFT+FFT}} + \underbrace{\underbrace{2N \log_2 N}_{\text{IFFT+FFT}}}_{\text{Equalization}} \tag{6.32}$$

Consequently, the total real additions, R_A, required in both systems can be computed as,

$$R_A^{\text{WHT-MI-OFDM}} = 26N \log_2 N + 18N \tag{6.33}$$

$$R_A^{\text{OFDM-MI}} = 44N \log_2 N + 18N \tag{6.34}$$

In the sequel, the OFDM-MI system requires $18N \log_2 N$ real operations more than WHT-MI-OFDM system. This means, the CCRR of the WHT-MI-OFDM system, as compared with the OFDM-MI system will be 39.3%, with $N = 1024$.

In addition, any traditional channel estimation technique that is already used with conventional OFDM system can be used with the proposed WHT-MI-OFDM.

Whereas, in the case of OFDM-MI system, the pilots should be added to the time-domain samples then channel estimation and equalization processes should be conducted in the frequency-domain. Thus, a new scheme of channel estimation should be investigated. Alternately, nonlinear equalisers, which inherently require high computational complexity, can be used with the OFDM-MI system for data recovery purpose.

6.6 Numerical Results

It is important to state that the results demonstrated in this chapter are achieved with the assumption of perfect knowledge in respect of the channel response, and perfect frequency/time synchronizations. The negative ramifications of impulsive noise on the systems considered are investigated over two channel models, including the AWGN and quasi-static frequency selective fading channel.

6.6.1 BER Performances of T-OFDM and Conventional OFDM Systems

Interestingly, with the probability of $P(\zeta_n = 1) = 1$, i.e. $\Gamma = 1$, the theoretical performance in (6.24) or (6.25) is close to the simulation results performance, as shown in Fig. 6.8-6.9. As clearly shown in these figures, the T-OFDM system can be used efficiently with applications that suffer from weak power impulsive noise, i.e. $\mu <= 10$; whereas the employment of this system with applications working under relatively high power impulsive noise is ineffective in terms of BER performance, albeit with complexity and PAPR reduction achievements reported in Chapters 4 and 5.

On the other hand, with $0 < P(\zeta_n = 1) < 1$, there is some deviation in simulation performances beyond the theoretical performances of the T-OFDM system; owing to the fact that the distribution of impulsive noise burst when it hits lower order sections in T-transform, is much lower than that when it hits the higher order sections, as shown in Fig. 6.10-6.13. Consequently, with applications that impact unregulated locations of noise burst, the T-OFDM system achieves different BER performances. However, the T-OFDM system can be used efficiently with applications that work under the impulsive noise power ranges $10 < \mu <= 100$ and $10 < \mu <= 1000$, when

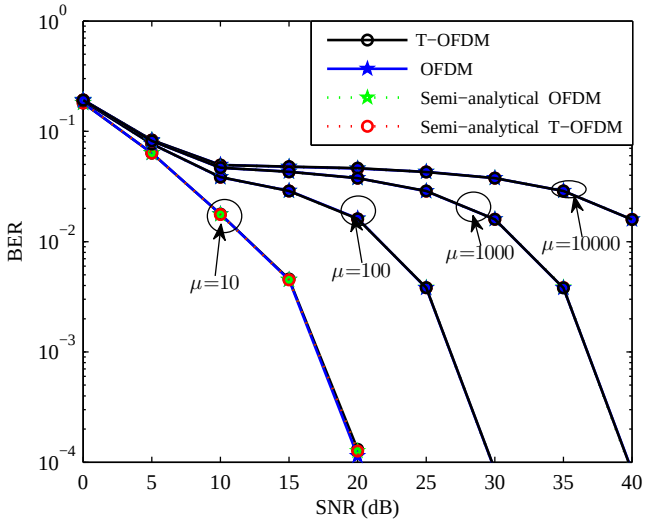

Figure 6.8: BER performance of T-OFDM and conventional OFDM systems with QPSK and $\Gamma = 1$ over AWGN and impulsive noise channel models.

$0.1 < \Gamma <= 0.25$ and $\Gamma <= 0.1$, respectively. In a sequel, the deleterious effect of severe impulsive noise burst on the BER performance of a T-OFDM system is reduced using the proposed WHT-MI-OFDM system [109].

6.6.2 BER Performances of Proposed WHT-MI-OFDM and Conventional MI-OFDM Systems

The ability of the proposed WHT-MI-OFDM system to suppress the deleterious effect of impulsive noise is clearly explained in Fig. 6.4. This means that considerable improvement in the BER performance of the proposed WHT-MI-OFDM system as shown in Fig. 6.14-6.19 is a consequence of two stages of impulsive noise power spreading. Firstly, the noise power is spread over a large number of subcarriers in each symbol using FFT and WHT. Secondly, it is spread once again over the entire OFDM block owing to the utilization of the matrix interleaver. *Note* : Lines with markers circle $\circ$ and star $\star$ in these figures depict the performances of WHT-MI-OFDM and MI-OFDM systems, respectively. However, over multipath transmission and under high power and long duration impulsive noise burst, the distribution of high power samples has negative ramifications on the BER performance of the WHT-MI-OFDM system, as shown in the sub-figures (c) and (d) of Fig. 6.14-6.19.

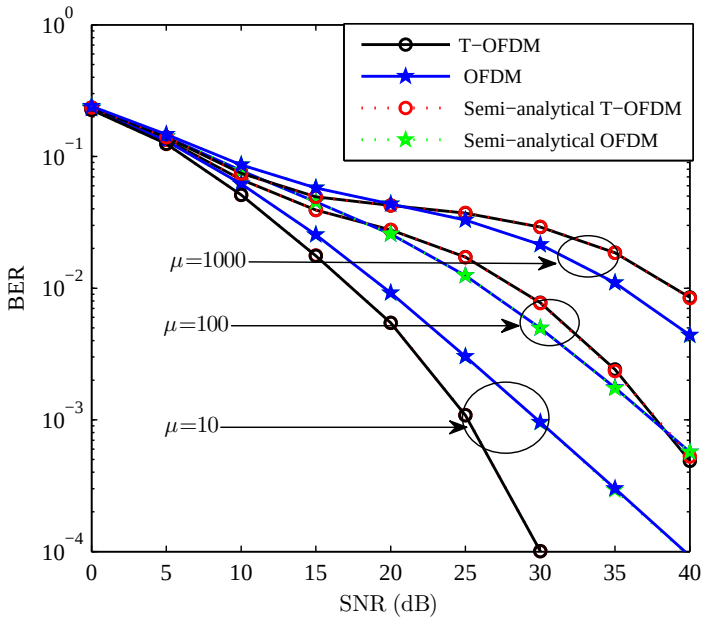

Figure 6.9: BER performance of T-OFDM and conventional OFDM systems with QPSK and $\Gamma = 1$ over frequency selective fading and impulsive noise channel models.

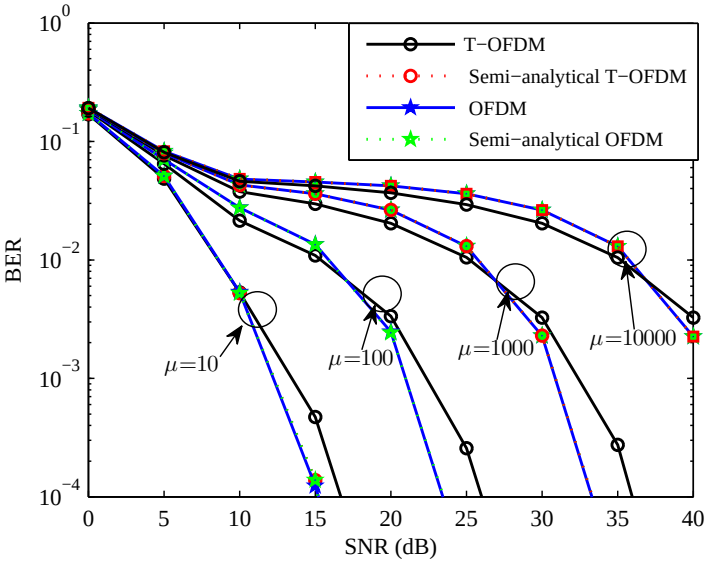

Figure 6.10: BER performance of T-OFDM and conventional OFDM systems with QPSK and $\Gamma = 0.25$ over AWGN and impulsive noise channel models.

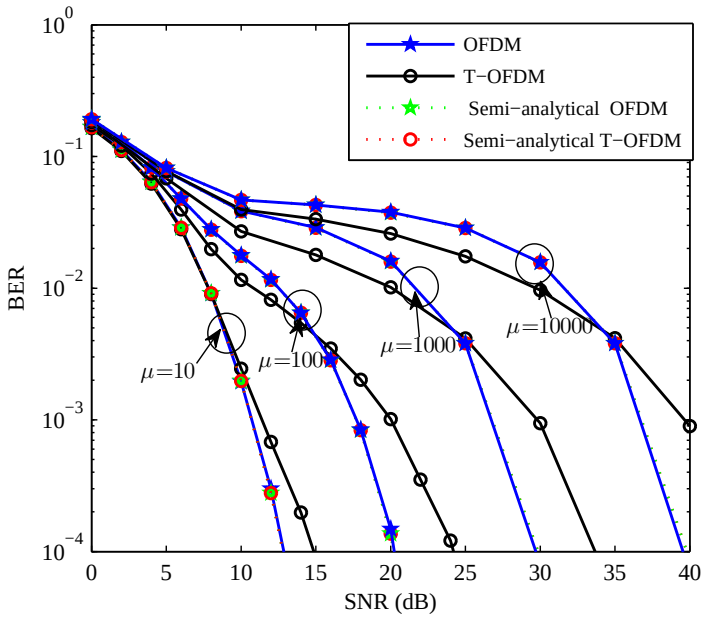

Figure 6.11: BER performance of T-OFDM and conventional OFDM systems with QPSK and $\Gamma = 0.1$ over AWGN and impulsive noise channel models.

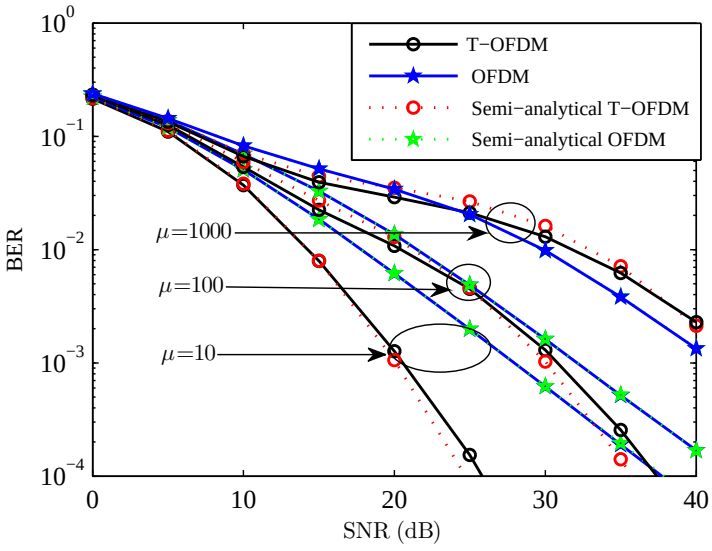

Figure 6.12: BER performance of T-OFDM and conventional OFDM systems with QPSK and $\Gamma = 0.25$ over frequency selective fading and impulsive noise channel models.

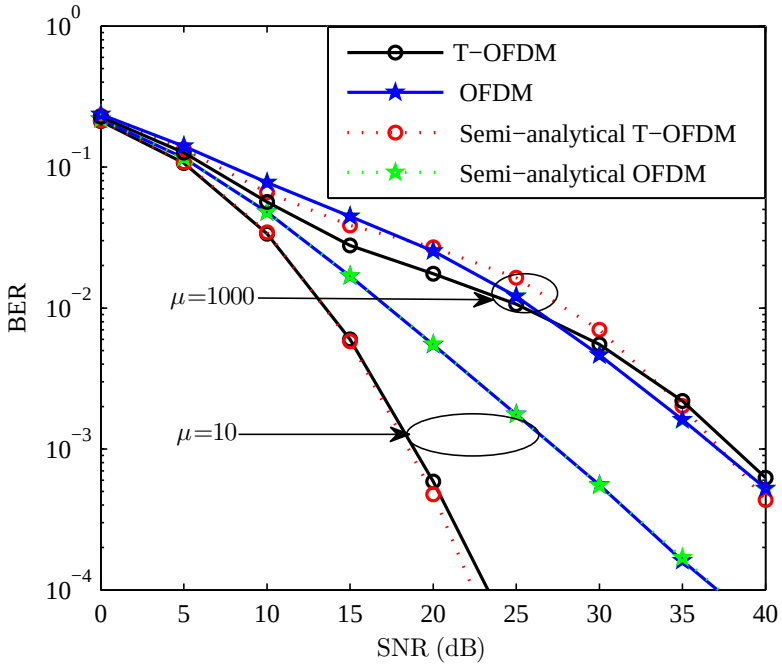

Figure 6.13: BER performance of T-OFDM and conventional OFDM systems with QPSK and $\Gamma = 0.1$ over frequency selective fading and impulsive noise channel models.

Therefore, the nonlinear blanking scheme is incorporated with WHT-MI-OFDM to suppress such deleterious effects. With an assumption of perfect knowledge of impulsive noise sample locations, the samples in these locations are blanked, i.e. equal zeros. Thus, the negative ramification of the high power man-made noise will reduce significantly, as shown in Fig. 6.20-6.22. As clearly shown in these figures, the BER performance of the WHT-MI-OFDM system with nonlinear blanking is not susceptible to the change of μ. Hence, the effect of μ is omitted in these figures. Consequently, the WHT-MI-OFDM system with blanking can be used efficiently with applications that are impaired with unstable impulsive noise burst power. Finally, it is worthwhile mentioning that all the systems considered use an MMSE equaliser.

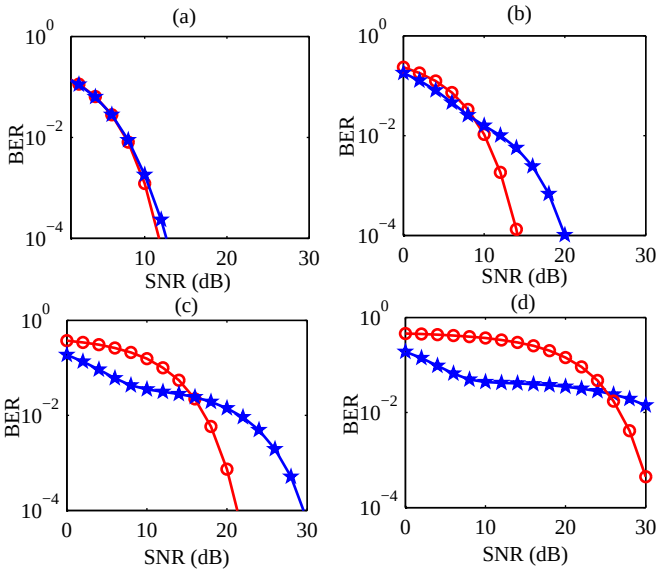

Figure 6.14: BER performance of WHT-MI-OFDM (marker ∘) and conventional MI-OFDM (marker ⋆) systems with QPSK over AWGN and impulsive noise channel models $\Gamma = 0.1$ (a. μ=10, b. μ=100, c. μ=1000, d. μ=10000).

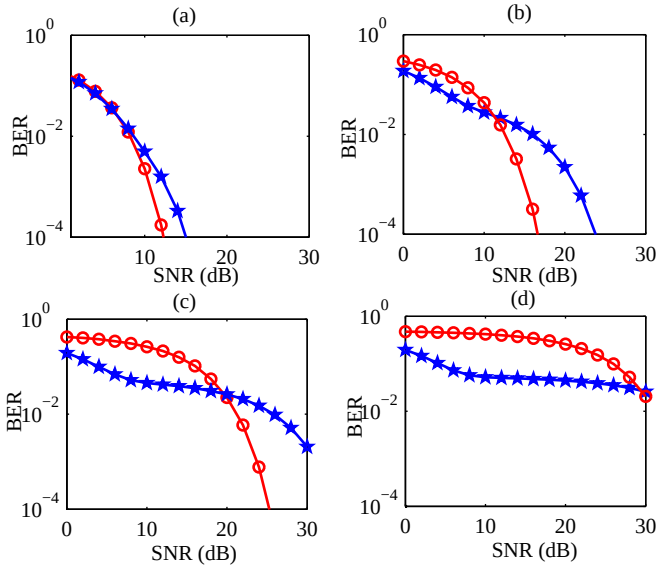

Figure 6.15: BER performance of WHT-MI-OFDM (marker ∘) and conventional MI-OFDM (marker ⋆) systems with QPSK over AWGN and impulsive noise channel models $\Gamma = 0.25$ (a. μ=10, b. μ=100, c. μ=1000, d. μ=10000).

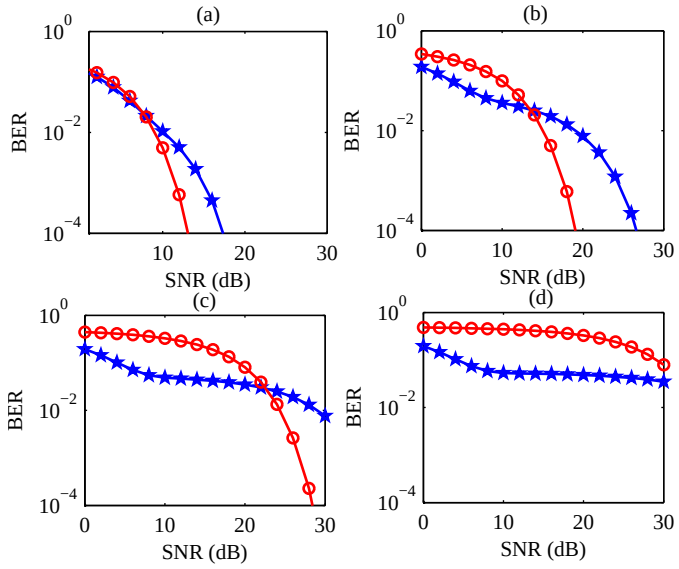

Figure 6.16: BER performance of WHT-MI-OFDM (marker $\circ$) and conventional MI-OFDM (marker $\star$) systems with QPSK over AWGN and impulsive noise channel models $\Gamma = 0.5$ (a. μ=10, b. μ=100, c. μ=1000, d. μ=10000).

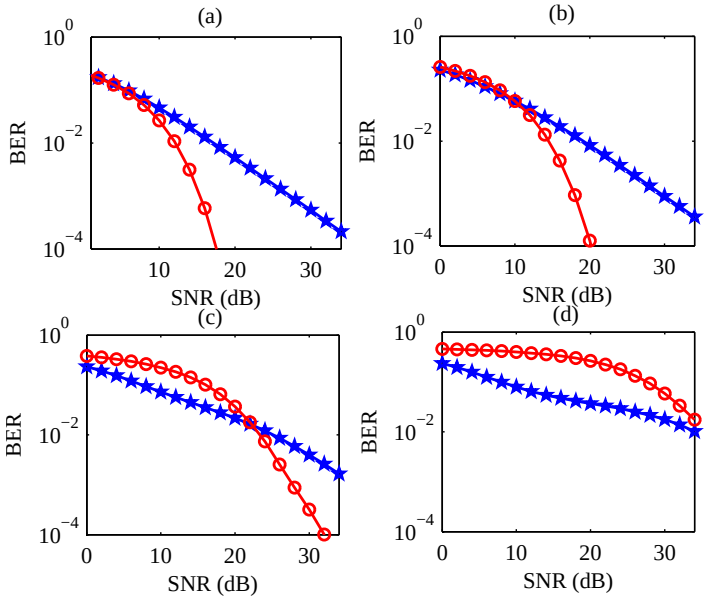

Figure 6.17: BER performance of WHT-MI-OFDM (marker $\circ$) and conventional MI-OFDM (marker $\star$) systems with QPSK over frequency selective fading and impulsive noise channel models $\Gamma = 0.1$ (a. μ=10, b. μ=100, c. μ=1000, d. μ=10000).

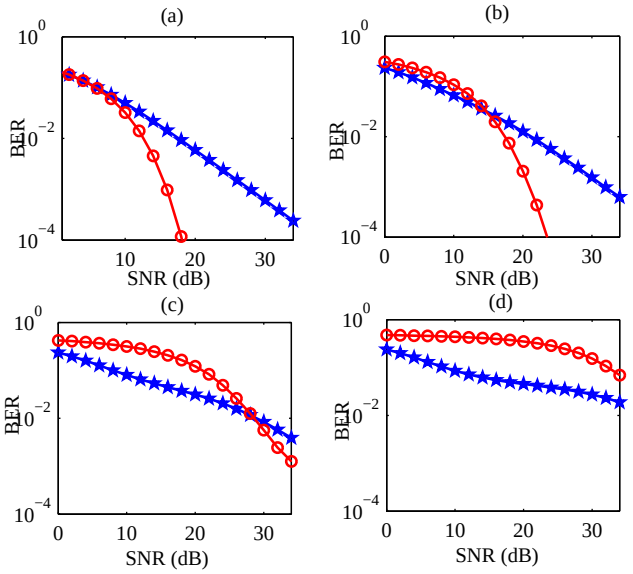

Figure 6.18: BER performance of WHT-MI-OFDM (marker $\circ$) and conventional MI-OFDM (marker $\star$) systems with QPSK over frequency selective fading and impulsive noise channel models $\Gamma = 0.25$ (a. μ=10, b. μ=100, c. μ=1000, d. μ=10000).

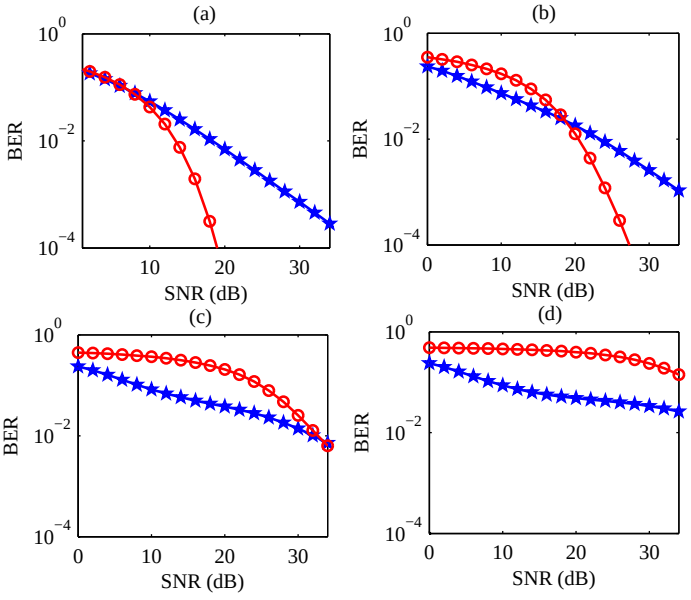

Figure 6.19: BER performance of WHT-MI-OFDM (marker $\circ$) and conventional MI-OFDM (marker $\star$) systems with QPSK over frequency selective fading and impulsive noise channel models $\Gamma = 0.5$ (a. μ=10, b. μ=100, c. μ=1000, d. μ=10000).

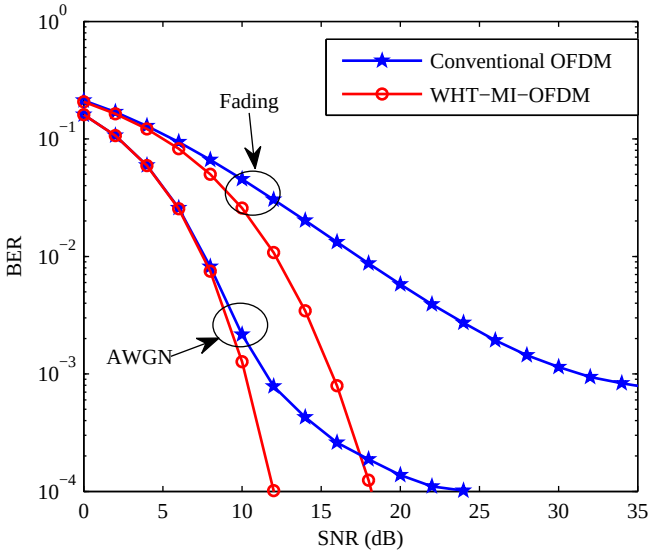

Figure 6.20: BER performance of WHT-MI-OFDM and conventional MI-OFDM systems with nonlinear blanking, QPSK and over multipath fading channel and impulsive noise ($\Gamma = 0.1$).

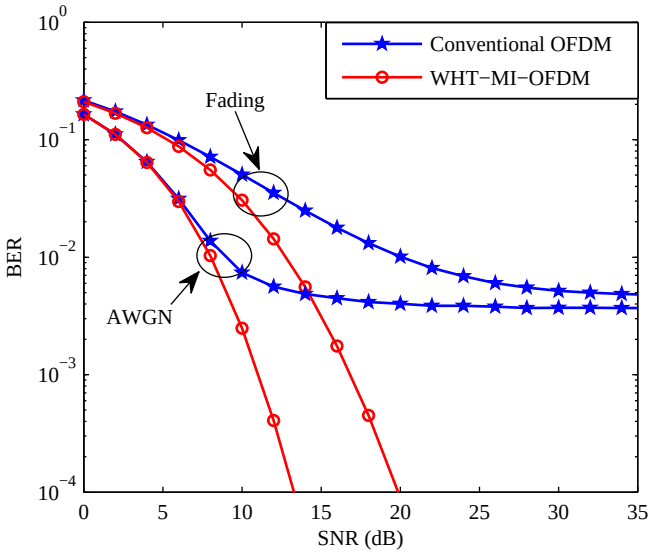

Figure 6.21: BER performance of WHT-MI-OFDM and conventional MI-OFDM systems with nonlinear blanking, QPSK and over multipath fading channel and impulsive noise ($\Gamma = 0.25$).

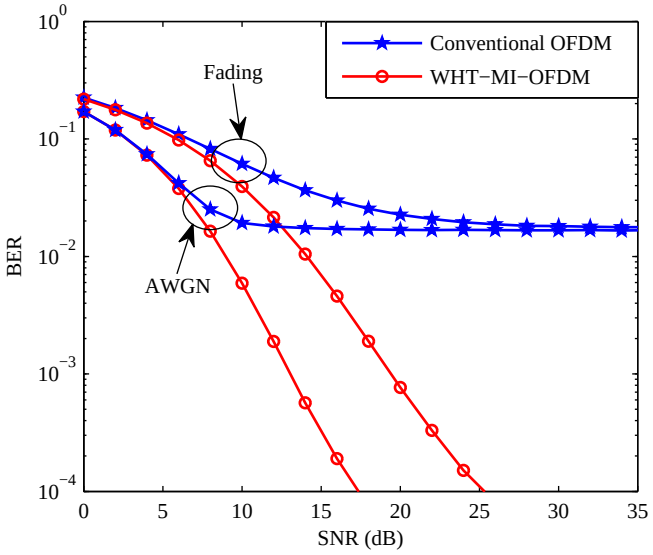

Figure 6.22: BER performance of WHT-MI-OFDM and conventional MI-OFDM systems with nonlinear blanking, QPSK and over multipath fading channel and impulsive noise ($\Gamma = 0.5$).

6.7 Chapter Summary

In this chapter, the BER performance of T-OFDM over a multipath fading channel in the presence of impulsive noise disturbance was investigated. Moreover, a new BER formula for the T-OFDM system over the impulsive channel was derived. In addition, under medium and quiet severe distributions of man-made noise, an attractive system WHT-MI-OFDM has been proposed to suppress the deleterious effect of such noise. The proposed system is capable of suppressing the impulsive noise effect by averaging the impaired sample over large OFDM symbols owing to the use of DFT and WHT, further to the MI. These high diversity systems help to mitigate the deep fade effect arising from the multipath channel on an individual subcarrier. Therefore, the proposed system achieves considerable BER performance improvement compared to a conventional MI-OFDM system over a multipath fading channel in the presence of impulsive noise. Furthermore, the resilience of the WHT-MI-OFDM system to severe impulsive noise is enhanced by utilizing a memoryless nonlinear blanking approach. In the sequel, compared to the conventional OFDM system, and based on the transmission applications, each individual system that is considered in this chapter can be used efficiently in line with requirements for reduced SNR.

CHAPTER 7

Conclusions and Future Work

7.1 Concluding Remarks

To overcome the drawbacks associated with OFDM systems, great efforts have been done in recent studies, however at the expense of high computational complexity, data rate losses, wasted power, and BER degradation.

The motivation behind this research was to utilise the prominent features of T-transform which was introduced by Boussakta [2] to combine the Walsh-Hadamard transform (WHT) and the discrete Fourier transform (DFT) into a single fast orthonormal unitary transform, including low complexity, diversity, sparsity, and unity diagonal structure, with the OFDM system instead of IFFT/FFT to construct the proposed T-OFDM system.

The lower complexity requirement of the T-OFDM has been addressed by comparing its complexity along with three proposed receivers design with conventional systems. Moreover, the length of the T-transform was shown to be the same as the number of subcarriers, thus there has been no bandwidth expansion (i.e. no data rate losses) when utilising the T-transform with the transmission techniques. Regarding the BER performance, the new T-OFDM system has the same performance as the WHT-OFDM but involves much less computational complexity. The computational analysis demonstrated the low computational complexity requirements of the proposed T-OFDM system compared with the conventional WHT-OFDM system. Furthermore, a new theoretical BER formulae for the T-OFDM system have been derived over AWGN, flat fading and quasi-static frequency selective fading channel models with ZF and MMSE equalisers. Analytical results confirmed by simulations demonstrated that the proposed T-OFDM system achieves the same BER over AWGN and flat fading channels. Compared to OFDM, the proposed T-OFDM system has achieved a SNR gain range of between 9dB and 16dB measured at 10^{-4} BER over the quasi-static frequency selective fading channels when MMSE equaliser is used, but slightly worse when ZF equaliser is used.

Additionally, due to the reduction of the superposition among the samples passing through the T-transform, T-OFDM has the ability to mitigate the serious challenge of high peak power in the OFDM-based system with a range of 0.75dB $\sim$ 1.2dB whilst ensuring multipath resilience, even in the presence of HPA without any data rate losses or an increase in the average transmitted power. Moreover, the sparsity and diagonal structure of T-transform have been utilised with conventional SLM and

PTS schemes to introduce three novel schemes; T-SLM, T-PTS-I and T-PTS-II. The proposed T-SLM scheme requires lower computational complexity than the conventional SLM and WHT-SLM schemes with full-butterfly and pruning-butterfly design criteria. As example, with non oversampling, i.e. $L = 1$, $N = 64$ and $U = 4$, the T-SLM scheme has achieved CCRR about 26.70% and 38% over the conventional SLM and WHT-SLM schemes, when full-butterfly design criterion is used in the considered transforms. Furthermore, with oversampling by sampling factor $L = 4$ and the above parameters, the attained CCRR were about 18.08% and 20.78%, respectively. Moreover, in the case of pruning-butterfly design criterion with $L = 4$, the obtained CCRR of T-SLM scheme over the pruning-SLM and WHT-pruning-SLM schemes were 16.86% and 33.90% with $N = 64$, and 7.69% and 25.00% with $N = 1024$, respectively. Conversely, with full-butterfly transform design criterion, proposed T-PTS-I scheme has attained CCRR with $N = 64$ and $L = 1$ about 19.43% and 24.89%, and about 16.83% and 18.17% with $L = 4$ over the conventional PTS and WHT-PTS schemes, respectively. However, with pruning transforms design criterion, T-PTS-I required slightly higher complexity about 9% compared to the conventional PTS scheme. Interestingly, proposed T-PTS-II has achieved a significant CCRR more than 90% over the considered systems. In addition, the data rate of T-PTS-II scheme was higher than the conventional PTS scheme because the proposed scheme required two bits lower than the conventional PTS scheme, transmitted as SI. Furthermore, the proposed T-SLM scheme has achieved a low peak signal compared to the conventional SLM when both are used with the OFDM system. Moreover, this peak reduction was achieved with the preservation of the transmission average power owing to the unitary characteristics of the T-transform. The PAPR of T-SLM scheme was measured to be about 0.8 dB less than the OFDM-based SLM scheme and about 3.1 dB less than the conventional OFDM system in the case of four phase factors, i.e. $U = 4$ are utilised. It also achieved 0.8 dB and 4.1 dB less than the OFDM-SLM and conventional OFDM systems, respectively, with the case of $U = 8$. In addition, the proposed T-PTS-I scheme has achieved a noticeable PAPR reduction about 0.7 dB less than the OFDM-based PTS scheme and about 2.6 dB less than the conventional OFDM system in the case of four disjoint subblocks, i.e. $U = 4$ are utilised. It also has achieved 0.5 dB and 3.6 dB less than the OFDM-PTS and conventional OFDM systems, respectively, in the case of $U = 8$. Both proposed T-SLM and T-PTS-I schemes were utilised the same values of SI that used with the conventional SLM and

PTS schemes. Conversely, compared to the conventional PTS scheme, a significant CCRR about 90% and lower required SI by two has been achieved with the proposed T-PTS-II scheme; however, with slight degradation in the PAPR performance. Interestingly, although the attractive gains, the proposed T-OFDM-SLM, T-OFDM-PTS-I and T-OFDM-PTS-II systems have had no detrimental effect on the original power spectrum of the OFDM signals.

Moreover, the BER performance of T-OFDM over the impulsive channel has been investigated by addressing the effect of independent sections of T-transform on the performance of such system under the effect of such transmission circumstances. Simulation results have been confirmed by deriving a new theoretical BER formula for the T-OFDM system under these deleterious transmission circumstances has been derived. It has been found that the T-OFDM system can be used efficiently with applications that suffer from weak power impulsive noise, i.e. $\mu <= 10$; whereas the employment of this system with applications working under relatively high power impulsive noise is ineffective in terms of BER performance, albeit with complexity and PAPR reduction achievements. Moreover, with $0 < P(\zeta_n = 1) < 1$, there is some deviation in simulation performances beyond the theoretical performances of the T-OFDM system; owing to the fact that the distribution of impulsive noise burst when it hits lower order sections in T-transform, is much lower than that when it hits the higher order sections. Consequently, with applications that impact unregulated locations of noise burst, the T-OFDM system achieves different BER performances. However, the T-OFDM system can be used efficiently with applications that work under the impulsive noise power ranges $10 < \mu <= 100$ and $10 < \mu <= 1000$, when $0.1 < \Gamma <= 0.25$ and $\Gamma <= 0.1$, respectively. In addition, under a medium and quiet severe distribution of man-made noise; an attractive system WHT-MI-OFDM, which effectively suppress the deleterious effect of such noise has been proposed. The proposed system is capable of suppressing the impulsive noise effect by averaging the impaired sample over the large OFDM symbols owing to the use of DFT and WHT, further to the matrix interleaver (MI). These high diversity systems help to mitigate the deep fade effect arising from the multipath channel on an individual subcarrier. Therefore, the proposed system achieves considerable BER performance improvement as compared to the conventional MI-OFDM system over a multipath fading channel in the presence of impulsive noise. Furthermore, the resilience of the WHT-MI-OFDM system to severe impulsive noise is enhanced by utilising a memoryless nonlinear

blanking approach.

In the sequel, a multicarrier system utilising the T-transform will benefit from the reduced PAPR, SNR and computational complexity requirements. The T-transform is easy to scale up or down for different transform lengths or subcarriers. In addition, the T-OFDM system can co-exist with the existing OFDM systems.

7.2 Future Work

1. The utilised approach to generalise the T-transform which combines the WHT and the DFT into one orthonormal unitary transform can be utilised to generate other new transforms from the other existing transforms, such as Hartley transform, Hilbert transform, number theoretic transform, Fermat number transform and Haar transform . This means, the advantages of any two cascaded transforms can be combined together and utilised with different communication systems.

2. This research project has concentrated primarily on point-to-point (single user) communication. However, the future work should consider both the downlink and uplink multi-users communications. The orthogonality of T-transform can be utilised with the multi-users system to obtain zero multi-access interference (MAI). Moreover, the diversity of each individual user can be increased by spreading its symbols over the symbols of other users. Additionally, the T-OFDM system can be used with alternative diversity techniques such as multiple input multiple output (MIMO) in order to increase diversity over different media of transmission.

3. The BER performance of T-OFDM has been investigated in this work over AWGN, flat fading, and quasi-static fading channels models. Although, the issue of perfect knowledge of channel was considered, the effect of the mismatching among the coefficients of real and estimated channel on the BER performance of the proposed T-OFDM system should be investigated. Moreover, an optimal channel estimation technique that matches with the proposed system can be proposed. Independent sections of the T-transform can be utilised to investigate a new distributed manner for the pilot which may help to provide optimal channel coefficients estimation techniques either in Walsh-domain or in time-domain. Moreover, the hybrid scheme of channel estimation can be also investigated based on the pilot distributed either in Walsh-domain or in time-domain, and the channel estimation and compensation in frequency domain. Furthermore, the effect of time-variant channels on the performance of the T-OFDM system with relevant channel estimation techniques should be taken into consideration in the future work.

4. T-OFDM system performance is sensitive to the clipping distortion results from the HPA. Thus, T-transform can be considered with another distortion or distortionless schemes in order to achieve more PAPR reduction for the transmitted signal of the T-OFDM system. Although, it was shown that the T-OFDM system is minimally vulnerable to the in-band distortion cause by the clipping of HPAs working with relatively high input-backoff (IBO), future work should consider new schemes that can be used with such a system to obtain more PAPR and better BER, even in the presence of HPA working with low IBO, i.e. IBO $\simeq 0$.

5. Although, some traditional techniques of frequency offset compensation, such as maximum likelihood (ML), that already has been used with the conventional OFDM system can be used efficiently with the T-OFDM system, future work can be concentrated on the investigating of an optimal techniques that can be used to estimate and/or compensate for the fine and coarse frequency offset caused by either transceiver oscillators mismatch and/or Doppler shift.

Bibliography

[1] E. C. Ifeachor and B. W. Jervis, *Digital Signal Processing: A Practical Approach.* England: Prentice Hall, 2002.

[2] S. Boussakta and A. G. J. Holt, "Fast algorithm for calculation of both Walsh-Hadamard and Fourier transforms (FWFTs)," *IEE Electron. Lett.*, vol. 25, no. 20, pp. 1352–1354, Sep. 1989.

[3] S. Boussakta, *Algorithms and Development of the Number theoretic and Related Fast Transforms with applications.* PhD thesis, Newcastle University, UK, 1990.

[4] L. Hanzo, M. Munster, B. J. Choi, and T. Keller, *OFDM and MC-CDMA for broadband multi-user communications WLANs and broadcasting.* England: John Willey and Sons Ltd, 2003.

[5] F. Khan, *LTE for 4G mobile broadband air interface technologies and performance.* UK: Cambridge University Press, 2009.

[6] R. V. Nee and R. Prasad, *OFDM for wireless multimedia communications.* London: Artech House, 2000.

[7] E. T. H. M. L. Doelz and D. L. Martin, "Binary transmission techniques for linear systems," *Proc. Inst. Radio Eng. (IRE)*, vol. 45, pp. 656–661, May 1957.

[8] G. A. Franco and G. Lachs, "An orthogonal coding technique for communications," *Proc. Inst. Radio Eng. (IRE)*, vol. 9, pp. 126–133, 1961.

[9] S. B. Weinstein and P. M. Ebert, "Data transmission by frequency-division multiplexing using the discrete Fourier transform," *IEEE Trans. Commun. Technol.*, vol. 19, pp. 628–634, Oct. 1971.

[10] J. G. Andrews, A. Ghosh, and R. Muhamed, *Fundamentals of WiMAX, understanding broadband wireless networking.* USA: Prentice Hall, 2007.

[11] P. S. Chow, J. C. Tu, and J. M. Cioffi, "Performance evaluation of a multichannel transceiver system for ADSL and VHDSL services," *IEEE J. Sel. Areas Commun.*, vol. 9, no. 6, pp. 909–919, Aug. 1991.

[12] ——, "A discrete multitone transceiver system for HDSL applications,," *IEEE J. Sel. Areas Commun.*, vol. 9, no. 6, pp. 895–908, Aug. 1991.

[13] H. Liu and G. Li, *OFDM-based broadband wireless networks; Design and optimization.* New Jersey, USA: John Wiley and Sons, Inc., 2005.

[14] J. G. Proakis and M. Salehi, *Digital communication.* 5th Ed. New York, USA: McGraw-Hill, 2008.

[15] H. Bogucka, "BER of OFDM systems impaired by carrier frequency offset in multipath fading channels," *IEEE Trans. Wireless Commun.*, vol. 4, no. 5, pp. 2279–2288, Sep. 2005.

[16] *Guidelines for the evaluation of radio transmission technologies for IMT-2000.* Recommendation ITU-R M.1225, 1997.

[17] H. V. Poor, *An introduction to signal detection and estimation.* USA: Springer-Verlag, 1994.

[18] S. Hara and R. Prasad, *Multicarrier Techniques for 4G Mobile Communications.* Boston, London: Artech House, 2003.

[19] M. Ghosh, "Analysis of the effect of impulsive noise on multicarrier and single QAM systems," *IEEE Trans. Commun.*, vol. 44, no. 2, pp. 145–147, Feb. 1996.

[20] S. V. Zhidkov, "Analysis and comparison of several simple impulsive noise mitigation schemes for OFDM receivers," *IEEE Trans. Commun.*, vol. 56, no. 1, pp. 5–9, Jan. 2008.

[21] J. W. Cooley and J. W. Tukey, "An algorithm for the machine calculation of complex Fourier series," *Mathematics of Computation*, vol. 19, pp. 297–301, 1965.

[22] S. S. Kelkar, L. L. Grigsby, and J. Langsnery, "An extension of parseval's theorem and its use in calculating transient energy in the frequency domain," *IEEE Trans. on Industrial Electronics,*, vol. IE-30, no. 1, pp. 42–45, Feb. 1983.

[23] M. S. Correngton, *Advanced analytical and signal processing techniques.* ASTIA Document No. AD-277942, April 1962.

[24] F. E. Weiser, *Walsh function analysis of instantaneous nonlinear stochastic problems.* PhD thesis, Polytechnic Institute of New York, 1964.

[25] N. Ahmed, *Orthogonal Transforms for Digital Signal Processing.* New York: Springer-Verlag, 1975.

[26] A. C. Andrews, *Computer Techniques in Image Processing.* New York: Academic Press, 1970.

[27] G. Robinson, "Logical convolution and discrete walsh and fourier power spectra," *IEEE Trans. Audio Electroacoust.*, vol. 20, no. 4, pp. 271–280, Oct. 1972.

[28] M. Maqusi, *Applied Walsh Analysis.* London: Heyden and Son Ltd, 1981.

[29] E. Chu and A. George, *Inside The FFT Black Box, Serial and Parallel Fast Fourier Transform Algorithm.* CRC Press, 2000.

[30] Q. Wen, Y. Xiao, P. Cheng, C. Zhang, and S. Li, "S-PTS for PAPR reduction in OFDM systems," in *in Proc. IEEE WiCOM*, 2008, pp. 1–4.

[31] R. J. Baxley and J. T. Zhou, "Comparing selected mapping and partial transmit sequence for PAPR reduction," *IEEE Trans. Broadcast.*, vol. 53, no. 4, pp. 737–803, Dec. 2007.

[32] L. Yang, K. K. Soo, Y. M. Siu, and S. Q. Li, "A low complexity selected mapping scheme by use of time domain sequence superposition technique for PAPR reduction in OFDMsystem," *IEEE Trans. Broadcast.*, vol. 54, no. 4, pp. 821–824, Dec. 2008.

[33] D. Dardari and V. Tralli, "High-speed indoor wireless communications at 60 GHz with coded OFDM," *IEEE Trans. Commun.*, vol. 47, pp. 1736–1746, Nov. 1999.

[34] C. Snow, L. Lampe, and R. Schober, "Error rate analysis for coded multicarrier systems over quasi-static fading channels," *IEEE Trans. Commun.*, vol. 55, no. 9, pp. 1736–1746, Sep. 2007.

[35] H. Wang, J. Belzile, and C. L. Despins, "64-QAM OFDM with TCM coding and waveform shaping in a time-selective Rician fading channel," in *in Proc. Int. Zurich Seminar Broadband Communications*, Verdun, QC, Canada, 2000, pp. 257–261.

[36] L. Lin, L. J. Cimini, and J. C.-I. Chuang, "Comparison of convolutional and turbo codes for OFDM with antenna diversity in high-bit-rate wireless applications," *IEEE Commun. Lett.*, vol. 4, no. 9, pp. 277–279, Sep. 2000.

[37] R. G. Gallager, *Low-Density Parity-Check Codes*. Cambridge, MA: MIT Press, 1963.

[38] S.-Y. Chung, G. D. Forney, T. J. Richardson, and R. L. Urbanke, "On the design of low-density parity-check codes within 0.0045 db of the shannon limit," *IEEE Commun. Lett.*, vol. 5, no. 2, pp. 58–60, Feb. 2001.

[39] H. Pishro-Nik, N. Rahnavard, and F. Fekri, "Non-uniform error correction using low-density parity-check codes," *IEEE Trans. Inf. Theory*, vol. 51, pp. 2702–2714, July 2005.

[40] M. R. Chari, F. Ling, A. Mantravadi, R. Krishnamoorthi, R. Vijayan, G. K. Walker, and R. Chandhok, "FLO physical layer: an overview," *IEEE Trans. Broadcast.*, vol. 53, no. 1, pp. 145–160, March 2007.

[41] S. Papaharalabos, M. Papaleo, P. T. Mathiopoulos, M. Neri, A. Vanelli-Coralli, and G. E. Corazza, "DVB-S2 LDPC decoding using robust check node update

approximations," *IEEE Trans. Broadcast.*, vol. 54, no. 1, pp. 120–126, March 2008.

[42] M.-S. Alouini and A. J. Goldsmith, "Capacity of Rayleigh fading channels under different adaptive transmission and diversity-combining techniques," *IEEE Trans. Veh. Technol.*, vol. 48, no. 4, pp. 1165–1181, July 1999.

[43] Y.-P. Lin and S.-M. Phoong, "BER minimized OFDM systems with channel independent precoders," *IEEE Trans. Signal Process.*, vol. 51, no. 9, pp. 2369–2380, Sep. 2003.

[44] X. Huang, "Diversity performance of precoded OFDM with MMSE equalization," in *7th Int. Symposium on Comm. and Inf. Tech. (ISCIT)*, Sydney, Oct. 2007, pp. 802–807.

[45] I. S. Raad and X. Huang, "Exploiting time diversity to improve block spread OFDM in a multipath environment," in *in Proc. IEEE Inf. and Comm. Tech. (ICTTA)*, 2006, pp. 2444–2449.

[46] J. Wu and S. D. Blostein, "High-rate diversity across time and frequency using linear dispersion," *IEEE Commun. Mag.*, vol. 56, no. 9, pp. 1469–1477, Sep. 2008.

[47] Y. Li, J. H. Winters, and N. R. Sollenberger, "MIMO-OFDM for wireless communications: signal detection with enhanced channel estimation," *IEEE Trans. Commun.*, vol. 50, no. 9, pp. 1471–1477, Sep. 2002.

[48] D. Divakaran, *OWSS and MIMO-STC-OFDM: Signaling systems for the next generation of high speed wireless LANs.* PhD thesis, University of South Florida, USA, 2008.

[49] P.-Y. Qin, Y. J. Guo, , and C.-H. Liang, "Effect of antenna polarization diversity on MIMO system capacity," *IEEE Antennas Wireless Propag. Lett.*, vol. 9, pp. 1092–1095, 2010.

[50] A. Kuhne and A. Klein, "Throughput analysis of multi-user OFDMA-systems using imperfect CQI feedback and diversity techniques," *IEEE J. Sel. Areas Commun.*, vol. 26, no. 8, pp. 1440–1450, Oct. 2008.

[51] A. Sendonaris, E. Erkip, and B. Aazhang, "User cooperation diversity Part I: System description," *IEEE Trans. Commun.*, vol. 51, no. 11, pp. 1927–1938, Nov. 2003.

[52] J. N. Laneman and G. W. Wornell, "Distributed space-time coded protocols for exploiting cooperative diversity in wireless networks," *IEEE Trans. Inf. Theory*, vol. 50, no. 12, pp. 3062–3080, Dec. 2004.

[53] A. Nosratinia, T. E. Hunter, and A. Hedayat, "Cooperative communication in wireless networks," *IEEE Commun. Mag.*, vol. 42, no. 10, pp. 74–80, Oct. 2004.

[54] Z. Lei, Y. Wu, C. K. Ho, S. Sun, P. He, and Y. Li, "Iterative detection for Walsh-Hadamard transformed OFDM," in *in Proc. IEEE Vehicular technology conference (VTC)*, April 2003, pp. 637–640.

[55] S. Wang, S. Zhu, and G. Zhang, "Walsh-Hadamard coded spectral efficient full frequency diversity OFDM system," *IEEE Trans. Commun.*, vol. 58, no. 1, pp. 28–34, Jan. 2010.

[56] Z. Dlugaszewski and K. Wesolowski, "WHT/OFDM- an improved OFDM transmission method for selective fading channels," in *in Proc. IEEE Symposium on commun. and vehicular techn. (SCVT)*, Oct. 2000, pp. 144–149.

[57] X. Huang, "Diversity performance of precoded OFDM with MMSE equalization," in *in Proc. IEEE Inter. symp. commun. and infor. techn. (ISCIT)*, Oct. 2007, pp. 802–807.

[58] B. Gaffney and A. D. Fagan, "Walsh Hadamard transform precoded MB-OFDM: An improved high data rate ultra wideband system," in *in Proc. IEEE 17th inter. symp. on personal, indoor and mobile radio commun.*, Sep. 2006, pp. 1–5.

[59] M. S. Ahmed, S. Boussakta, B. Sharif, and C. C. Tsimenidis, "OFDM based new transform with BER performance improvement across multipath transmission," in *in Proc. IEEE Inter. Conf. on Comm. (ICC)*, June 2010, pp. 1–5.

[60] ——, "OFDM based on low complexity transform to increase multipath resilience and reduce PAPR," *IEEE Trans. Signal Process.*, vol. 3, no. 6, pp. 2013–2018, Nov. 2011.

[61] G. Robinson, "Logical convolution and discrete Walsh and Fourier power spectra," *IEEE Trans. Audio Electroacoust.*, vol. AU-20, no. 4, Oct. 1972.

[62] P. Banelli, "Theoretical analysis and performance of OFDM signals in nonlinear fading channels," *IEEE Trans. Wireless Commun.*, vol. 2, no. 2, pp. 284–293, March 2003.

[63] C. Snow, L. Lampe, and R. Schober, "Error rate analysis for coded multicarrier systems over quasi-static fading channels," *IEEE Trans. Commun.*, vol. 55, no. 9, pp. 1736–1746, Sep. 2007.

[64] ——, "Impact of WiMAX interference on MB-OFDM UWB systems: analysis and mitigation," *IEEE Trans. Commun.*, vol. 57, no. 9, pp. 2818–2827, Sep. 2009.

[65] A. Nasri and R. Schober, "Performance of BICM-SC and BICM-OFDM systems with diversity reception in non-Gaussian noise and interference," *IEEE Trans. Commun.*, vol. 57, no. 11, pp. 3316–3327, Nov. 2009.

[66] S. Lijun, T. Youxi, and L. Shaoqian, "BER performance of differential demodulation OFDM system in multipath fading channels," in *Proc. IEEE GLOBECOM*, China, 2003, pp. 1–5.

[67] K. Sathananthan and C. Tellambura, "Probability of error calculation of OFDM systems with frequency offset," *IEEE Trans. Commun.*, vol. 49, no. 11, pp. 1884–1888, Nov. 2001.

[68] H. A. Ahmed, A. I. Sulyman, and H. S. Hassanein, "BER performance of OFDM system with channel impairments," in *9th IEEE Int. Workshop on Wireless Local Net. (WLN)*, Switzerland, Oct. 2009.

[69] B. Muquet, Z. Wang, G. B. Giannakis, M. de Courville, and P. Duhamel, "Cyclic prefixing or zero padding for wireless multicarrier transmissions," *IEEE Trans. Commun.*, vol. 50, no. 12, pp. 2136–2148, Dec. 2002.

[70] X.-G. Xia, "Precoded and vector OFDM robust to channel spectral nulls and with reduced cyclic prefix length in single transmit antenna systems," *IEEE Trans. Commun.*, vol. 49, no. 8, pp. 1363–1374, Aug. 2001.

[71] E. J. P. K. Bae, J. G. Andrews, "Quantifying an iterative clipping and filtering technique for reducing PAR in OFDM," *IEEE Trans. Wireless Commun.*, vol. 9, no. 5, pp. 1558–1563, May 2010.

[72] J. Armstrong, "Peak-to-average power reduction for OFDM by repeated clipping and frequency domain filtering," *IEEE Elect. Lett.*, vol. 38, no. 5, pp. 246–247, Feb. 2002.

[73] T. Jiang, W. Xiang, P. C. Richardson, D. Qu, and G. Zhu, "On the nonlinear companding transform for reduction in PAPR of MCM signals,," *IEEE Trans. Wireless Commun.*, vol. 6, no. 6, pp. 2017–2021, June 2007.

[74] S. S. Yoo, S. Yoon, S. Y. Kim, and I. Song, "A novel PAPR reduction scheme for OFDM systems: Selective mapping of partial tones (SMOPT)," *IEEE Trans. Consum. Electron.*, vol. 52, no. 1, pp. 40–43, Feb. 2006.

[75] K. Yang and S. Chang, "Peak-to-average power control in OFDM using standard arrays of linear block codes," *IEEE Commun. Lett.*, vol. 7, no. 4, pp. 174–176, Apr. 2003.

[76] L. Yang, K. K. Soo, Y. M. Siu, and S. Q. Li, "A low complexity selected mapping scheme by use of time domain sequence superposition technique for PAPR reduction in OFDM system," *IEEE Trans. Broadcast.*, vol. 54, no. 4, pp. 821–824, Dec. 2008.

[77] D.-W. Lim, J.-S. No, C.-W. Lim, and H. Chung, "A new SLM OFDM scheme with low complexity for PAPR reduction," *IEEE Signal Process. Lett.*, vol. 12, no. 2, pp. 93–96, Feb. 2005.

[78] S. J. Heo, H. S. Noh, J. S. No, and D. J. Shin, "A modified SLM scheme with low complexity for PAPR reduction of OFDM systems," *IEEE Trans. Broadcast.*, vol. 53, no. 4, pp. 804–808, Dec. 2007.

[79] C.-P. Li, S.-H. Wang, and C.-L. Wang, "Novel low-complexity SLM schemes for PAPR reduction in OFDM systems," *IEEE Trans. Signal Process.*, vol. 58, no. 5, pp. 2916–2921, May 2010.

[80] C.-L. Wang and S.-J. Ku, "Novel conversion matrices for simplifying the IFFT computation of an SLM-based PAPR reduction scheme for OFDM systems," *IEEE Trans. Commun.*, vol. 57, no. 7, pp. 1903–1907, Jul. 2009.

[81] C.-L. Wang and Y. Ouyang, "Low-complexity selected mapping schemes for peak-to-average power ratio reduction in OFDM systems," *IEEE Trans. Signal Process.*, vol. 53, no. 12, pp. 4652–4660, Dec. 2005.

[82] A. Ghassemi and T. A. Gulliver, "PAPR reduction of OFDM using PTS and error-correcting code subblocking," *IEEE Trans. Wireless Commun.*, vol. 9, no. 3, pp. 980–989, Mar. 2010.

[83] S.-J. Ku, C.-L. Wang, and C.-H. Chen, "A reduced-complexity PTS-based PAPR reduction scheme for OFDM systems," *IEEE Trans. Wireless Commun.*, vol. 9, no. 8, pp. 2455–2460, Aug. 2010.

[84] Y. Wang, W. Chen, and C. Tellambura, "PAPR reduction method based on parametric minimum cross entropy for OFDM signals," *IEEE Commun. Lett.*, vol. 14, no. 6, pp. 563–565, Jun. 2010.

[85] H. Chen and H. Liang, "PAPR reduction of OFDM signals using partial transmit sequences and Reed-Muller codes," *IEEE Commun. Lett.*, vol. 11, no. 6, pp. 528–530, Jun. 2007.

[86] L. Yang, R. S. Chen, Y. M. Siu, and K. K. Soo, "PAPR reduction of an OFDM signal by use of PTS with low computational complexity," *IEEE Trans. Broadcast.*, vol. 52, no. 1, pp. 83–86, Mar. 2006.

[87] S. Y. L. Goff, S. S. Al-Samahi, B. K. Khoo, C. C. Tsimenidis, and B. S. Sharif, "Selected mapping without side information for PAPR reduction in OFDM," *IEEE Trans. Wireless Commun.*, vol. 8, no. 9, pp. 3320–3325, Jul. 2009.

[88] A. D. S. Tayalath and C. Tellambura, "SLM and PTS peak-power reduction of OFDM signals without side information," *IEEE Trans. Wireless Commun.*, vol. 4, no. 5, pp. 2006–2013, Dec. 2005.

[89] M. F. Naeiny and F. Marvasti, "Selected mapping algorithm for PAPR reduction of space-frequency coded OFDM systems without side information," *IEEE Trans. Veh. Technol.*, vol. 60, no. 3, pp. 1211–1216, 2011.

[90] S. Kim, J. Chung, and H. Ryu, "PAPR reduction of OFDM signal by the SLM-based WHT and DSI method," in *in Proc. IEEE TENCON*, Region 10 conf., Nov. 2006, pp. 1–4.

[91] M. Park, H. Jun, J. Cho, N. Cho, D.Hong, and C. Kang, "PAPR reduction in OFDM transmission using Hadamard transform," in *in Proc. IEEE ICC*, New Orleans, LA, USA, June 2000, pp. 430–433.

[92] L. Wang, *Peak-to-average power ratio reduction in OFDM systems.* PhD thesis, University of Alberta, Canada, Spring, 2008.

[93] D. Dardari, V. Tralli, and A. Vaccari, "A theoretical characterization of nonlinear distortion effects in OFDM systems," *IEEE Trans. Commun.*, vol. 48, no. 10, pp. 1755–1764, Oct. 2000.

[94] E. Costa and S. Pupolin, "M-QAM-OFDM system performance in the presence of a nonlinear amplifier and phase noise," *IEEE Trans. Commun.*, vol. 50, no. 3, pp. 462–472, March 2002.

[95] T. Jiang and Y. Wu, "An overview: peak-to-average power ratio reduction techniques for OFDM signals," *IEEE Trans. Broadcast.*, vol. 54, no. 2, pp. 257–268, June 2008.

[96] M.-O. P. K. D. Wong and H. V. Poor, "The continuous-time peak-to-average power ratio of OFDM signals using modulation schemes," *IEEE Trans. Commun.*, vol. 56, no. 9, pp. 1390–1393, Sep. 2008.

[97] M. S. Ahmed, S. Boussakta, B. Sharif, and C. C. Tsimenidis, "Performance enhancement and computational complexity reduction of SLM and PTS schemes," *Submitted to IEEE Trans. in Broadcast.*, Apr. 2012.

[98] Z. Hu and H. Wan, "A novel generic fast Fourier transform pruning technique and complexity analysis," *IEEE Trans. Signal Process.*, vol. 53, no. 1, pp. 274–282, Jan. 2005.

[99] J. Hou, J. Ge, and J. Li, "Peak-to-average power ratio reduction of OFDM signals using PTS scheme with low computational complexity," *IEEE Trans. Broadcast.*, vol. 57, no. 1, pp. 143–148, Mar. 2011.

[100] P. Tan and N. C. Beaulieu, "A comparison of DCT-based OFDM and DFT-based OFDM in frequency offset and fading channels," *IEEE Trans. Commun.*, vol. 54, no. 11, pp. 2113–2125, Nov. 2006.

[101] R. Pighi, M. Franceschini, G. Ferrari, and R. Raheli, "Fundamental performance limits of communications systems impaired by impulsive noise," *IEEE Trans. Commun.*, vol. 57, no. 1, pp. 171–182, Jan. 2009.

[102] Y. H. Ma, P. L. So, and E. Gunawan, "Performance analysis of OFDM systems for broadband power line communications under impulsive noise and multipath effects," *IEEE Trans. Power Del.*, vol. 20, no. 2, pp. 674–682, Apr. 2005.

[103] P. Amirshahi, S. M. Navidpour, and M. Kavehrad, "Performance analysis of uncoded and coded OFDM broadband transmission over low voltage power-line channels with impulsive noise," *IEEE Trans. Power Del.*, vol. 21, no. 4, pp. 1927–1934, Oct. 2006.

[104] S. V. Zhidkov, "Performance analysis and optimization of OFDM receiver with blanking nonlinearity in impulsive noise environment," *IEEE Trans. Veh. Technol.*, vol. 55, no. 1, pp. 234–242, Jan. 2006.

[105] F. Abdelkefi, P. Duhamel, and F. Alberge, "Impulsive noise cancellation in multicarrier transmission," *IEEE Trans. Commun.*, vol. 53, no. 1, pp. 94–106, Jan. 2005.

[106] A. Al-Dweik, A. Hazmi, B. Sharif, and C. Tsimenidis, "Efficient interleaving technique for ofdm system over impulsive noise channels," in *in Proc. IEEE Personal Indoor and Mobile Radio Commun. (PIMRC)*, 2010, p. 167171.

[107] ——, "Novel multiple-access interference reduction technique for multiuser FH-OFDM networks," in *in Proc. IEEE Int. Conf. Commun. Sys. (ICCS)*, 2010, p. 488492.

[108] H. Bogucka, "On the impact of the impulsive noise on the WHT/OFDM transmission," *IEEE Commun. Lett.*, vol. 9, no. 1, pp. 37–39, Jan. 2005.

[109] M. S. Ahmed, S. Boussakta, B. Sharif, and C. C. Tsimenidis, "The impact of impulsive noise on T-OFDM system performance and its suppression," *Submitted to IEEE Trans. in Commun.*, Apr. 2012.